Université d'Ottawa · University of Ottawa

"Công cha như núi Thái Sơn
Nghĩa mẹ như nước trong nguồn chảy ra..."

Abstract

A central composite design was employed to methodically investigate anaerobic treatment of aircraft deicing fluid (ADF) in bench-scale Upflow Anaerobic Sludge Blanket (UASB) reactors. A total of 23 runs at 17 different operating conditions were conducted in continuous mode. The development of four empirical models describing process responses (i.e., chemical oxygen demand (COD) removal efficiency, biomass specific acetoclastic activity, methane production rate, and methane production potential) as functions of ADF concentration, hydraulic retention time (HRT), and biomass concentration is presented. Model verification indicated that predicted responses (COD removal efficiencies, biomass specific acetoclastic activity, and methane production rates and potential) were in good agreement with experimental results.

Biomass specific acetoclastic activity was improved by almost two-fold during ADF treatment in UASB reactors. For the design window, COD removal efficiencies were higher than 90%. Predicted methane production potentials were close to theoretical values, and methane production rates increased as the organic loading rate (OLR) was increased. ADF toxicity effects were evident for 1.6% ADF at medium specific organic loadings (SOLR above 0.5 g COD/g VSS/d). In contrast, good reactor stability and excellent removal efficiencies were achieved at 1.2% ADF for reactor loadings approaching that of highly loaded systems (0.73 g COD/g VSS/d). Acclimation to ADF resulted in an initial reduction in the biomass settling velocity.

The fate of ADF additives was also investigated. There was minimal sorption of benzotriazole (BT), 5-methyl-1 H-benzotriazole (MeBT), and 5,6-dimethyl-1 H-benzotriazole (DiMeBT) to anaerobic granules. A higher sorption capacity was measured for NP. Active transport may be one of the mechanisms for NP sorption. Ethylene glycol degradation experiments indicated that BT, MeBT, DiMeBT, and the nonionic

surfactant Tergitol NP-4 had no significant effects on acidogenesis and methanogenesis at the concentration levels studied. A significant inhibition of acetoclastic activity was observed for NP at 100 mg/L, with acetic acid consumption rate at 38% of that for controls. No evidence for anaerobic degradation of benzotriazole and its derivatives was observed; however, both batch and continuous experiments suggested that anaerobic degradation of NP occurred.

Kinetic analysis of operational data obtained for the anaerobic treatment of ADF in UASB reactors indicated that the substrate utilization rate was independent of the reactor biomass concentration. The maximum rate of substrate utilization and the half-velocity constants for ADF treatment were 28.4 g COD/L/d and 648 mg COD/L, respectively. For 1.2% ADF, the biomass yield and endogenous decay coefficients were 0.027 g VSS/g COD and 0.012 d^{-1}, respectively.

Résumé

Un design expérimental statistique a été employé pour vérifier méthodiquement la capacité de traitement anaérobique du fluide de dégivrage pour avion (FDA) par un réacteur de Boues Anaérobique avec Débit Ascendant (BADA) à l'échelle de laboratoire. Un total de 23 tests à 17 conditions d'opération différentes ont été réalisés en mode continu. Le développement de quatre modèles décrivant les réponses du processus (ex: l'efficacité de la réduction en demande chimique d'oxygène (DCO), l'activité acétoclastique spécifique de la biomasse, le taux de production de méthane et le potentiel de production de méthane) en fonction de la concentration en FDA, le temps de rétention hydraulique et la concentration de biomasse est présenté. La vérification du modèle a indiqué que les réponses prédites (l'efficacité de la réduction en DCO, l'activité acétoclastique spécifique de la biomasse, le taux de production de méthane et le potentiel de production de méthane) étaient en bon accord avec les résultats expérimentaux.

L'activité acétoclastique spécifique de la biomasse a été améliorée par presque un facteur de deux pendant le traitement du FDA par les réacteurs BADA. Dans la plage du design, les efficacités de réduction en DCO étaient plus de 90 %. Les potentiels de production de méthane prédits étaient près des valeurs théoriques, et les taux de production ont augmenté avec des taux de chargement organique (TCO) augmentant. Les effets de toxicité du FDA étaient évidents pour 1,6 % FDA avec des charges organique moyennes (TCO spécifique de 0,5 g DCO/g matière suspendue volatile/d ou plus). Au contraire, une bonne stabilité du réacteur et de excellentes réductions en DCO ont été produites à 1,2 % FDA pour des charges approchant celles des réacteurs fortement chargés (0,73 g DCO/g MSV/d). L'acclimatation au FDA a eu comme résultat de réduire initialement la vitesse de dépôt de la biomasse.

Le sort des additifs de l'ADF a aussi été étudié. Il y a eu une sorption minimale du benzotriazole (BT), 5-methyl-1 H-benzotriazole (MeBT), et du 5,6-dimethyl-1 H-benzotriazole (DiMeBT) aux granules anaérobiques. Une capacité de sorption plus élevée a été mesurée pour le nonylphénol (NP). Le transport actif pourrait être un des mécanismes pour la sorption du NP. Les expériences de dégradation du glycol d'éthylène ont indiqué que le BT, MeBT, DiMeBT, et le surfactant non-ionique Tergitol NP-4 n'ont pas d'effet significatifs sur l'acidogénèse et la méthanogénèse aux nivaux de concentration étudiés. Une inhibition significative de l'activité acétoclastique a été observée pour NP a 100 mg/L, avec un taux de consommation de l'acide acétique à 38% de celui des contrôles. Aucune indication de la dégradation anaérobique du benzotriazole et ses dérivées a été observée; par contre, les résultats en batch et en continu suggèrent que la dégradation anaérobique du NP c'est produite.

Les analyses cinétiques des données opérationnelles obtenues pour le traitement anaérobique du FDA par les réacteurs BADA indiquent que le taux de capture du substrat est indépendant de la concentration en biomasse du réacteur. Le taux maximum de capture du substrat et les constantes de demi-vitesses pour le traitement du FDA sont 28.4 g DCO/L/d et 648 mg DCO/L, respectivement. Pour 1.2% FDA, les coefficients de rendement de biomasse et de dégradation endogène sont de 0.027 g MSV/g DCO et 0.012 d^{-1}, respectivement.

Acknowledgements

First of all I would like thank Dr. Kevin J. Kennedy for giving me the opportunity to work in an environment where everyone is a friend rather than a colleague, a relaxed and intellectually stimulating environment where creativity is encouraged and nurtured. Without his continuous guidance, support, encouragement, and patience, I would not have reached this far.

A big thank you is extended to Francisco for his help and friendship. Without his dedication and support, I would still be in the laboratory trying to fix those pumps and machines, rather than writing up this thesis. A special thank you is extended to Micha for providing a French translation of the abstract. To the support staff of the departments of chemical and civil engineering, thank you for all your help and advice. To the faculty staff of both science and engineering faculties, their guidance and encouragement are much appreciated. To all past and present fellow workers, thank you for your help, friendship and understanding. The numerous group outings and gatherings have made graduate studies much more than just books and beakers.

Last but not least, I thank my family for their endless support and encouragement. I am grateful that my late father has instilled in me the thirst for education and my mother's selfless support has made this journey possible. The support and understanding of my husband has made this journey less bumpy. And thanks to my son for reminding me to sleep.

Nomenclature

Ac	acetate
ADAF	aircraft deicing/anti-icing fluid
ADF	aircraft deicing fluid
AEA	Association of European Airlines
AFBR	anaerobic fluidized bed reactor
ANOVA	analysis of variance
ATA	anaerobic toxicity assay
ATPase	adenosine triphosphorylase
BOD	biochemical oxygen demand
BT	benzotriazole
$CBOD_5$	carbonaceous biochemical oxygen demand (after five day incubation)
CEPA	Canadian Environmental Protection Act
COD	chemical oxygen demand
conc.	concentration
DiMeBT	dimethylbenzotriazole
EC_{50}	concentration for 50% effect
EG	ethylene glycol
FAA	Federal Aviation Administration
GC	gas chromatography
H	height
HPLC	high pressure liquid chromatography
HRT	hydraulic retention time
IC_{50}	concentration for 50% inhibition
ISO	International Standards Organization
ID	internal diameter
LC_{50}	median lethal concentration
MeBT	methylbenzotriazole
MLSS	mixed liquor suspended solids
NP	nonylphenol
NPnEC	nonylphenol polyethoxy carboxylate

NPnEO	nonylphenol ethoxylate
OLR	organic loading rate
ppb	parts per billion (by volume)
ppm	parts per million (by volume)
rpm	revolutions per minute
RT	retention time
SAE	Society of Automotive Engineers
SOLR	specific organic loading rate
SRT	solids retention time
STP	standard temperature and pressure
TSS	total suspended solids
UASB	upflow anaerobic sludge blanket
VFA	volatile fatty acid
VSS	volatile suspended solids

c_{eq}	equilibrium concentration of sorbate in solution, mg/L
f	washout factor
H_0	null hypothesis
k	maximum specific rate of substrate utilization, g COD/g VSS/d
k'	maximum rate of substrate utilization, g COD/L/d
K, n	Freundlich constants
k_d	endogenous decay coefficient, d^{-1}
K_s	half-velocity constant, g COD/L
LFR	lack of fit to pure error ratio
log K_{OC}	coefficient of adsorption onto organic carbon from water
p	probability of committing a Type I error when testing the null hypothesis
Q	flow rate, L/d
q	sorbate concentration associated with biomass, mg/g VSS
r^2, R^2	coefficient of determination, a regression statistic
r_g	rate of bacterial growth, g VSS/L/d
r_{SU}	rate of substrate utilization, g COD/L/d
S	growth-limiting substrate concentration, g COD/L
t	time

U	specific rate of substrate utilization, g COD/g VSS/d
v_{50}	upflow velocity resulting in 50% biomass washout, m/h
V_r	reactor volume, L
X	biomass concentration, g VSS/L
X_0	biomass concentration in the feed, g VSS/L
x_1	coded variable for ADF concentration
x_2	coded variable for HRT
x_3	coded variable for biomass concentration
$\hat{y}$	predicted process response
y	process response
Y	cell yield coefficient, g VSS/g COD
α	coded operating variable level for star portion of central composite design
$\hat{\beta}$	parameter estimate
β	operating parameter
μ	population mean
μ_{max}	maximum specific growth rate, d^{-1}
θ_c	solids retention time (SRT), d^{-1}
$\hat{\rho}$	estimated correlation
$\hat{\sigma}^2$	estimate of the pure error variance

Table of Contents

List of Tables

List of Figures

1 Introduction

Air travel has become an essential part of today's global society. Ensuring flight safety is an absolute necessity since its absence or failure can lead to the loss of human lives. This is of particular importance during the winter months when ice and snow conditions interfere with the normal operation of aircraft. Disastrous consequences can occur as demonstrated by the crash of USAir Flight 407 on takeoff at New York's LaGuardia Airport during a winter storm in March, 1992. The accident resulted in the death of 27 passengers and crew. This prompted the U.S. Federal Aviation Administration (FAA) to increase the margin of safety by imposing more stringent requirements for deicing activities during snow and ice conditions. Consequently, greater quantities of aircraft deicing/anti-icing fluids (ADAF) are used by U.S. airlines and airports.

Large quantities of glycol-based deicing products are also used at Canadian airports each winter. It has been estimated that 4,700 – 5,800 tonnes of ethylene glycol (EG), diethylene glycol, and propylene glycol are used annually at Canadian federal airports (Environment Canada, 1994). As a result, large quantities of glycol-based deicing fluids are carried into airport storm water systems. For example, total glycol concentrations above 15,000 mg/L in storm water drains have been detected at some Canadian airports (MacDonald *et al.*, 1993).

Glycol-based deicing fluids are known to exert an extremely high biochemical oxygen demand (BOD). Furthermore, aircraft deicing/anti-icing fluids contain additives (*e.g.*, ethoxylated secondary alcohols, organic amine bases, aryl triazoles, and other proprietary compounds) that may be responsible for their higher toxicity as compared to pure aqueous ethylene or propylene glycol solutions (Jank *et al.*, 1973; Hartwell *et al.*, 1993; MacDonald *et al.*, 1993; Novak *et al.*, 2000). Thus, there is a need for effective

means to remove the glycol and additive contaminants from these runoffs since large untreated discharges of these chemicals can cause adverse effects on the environment. However, to date there are no comprehensive studies of EG-based ADF treatment under anaerobic conditions, which fully characterize process responses as functions of operating variables. Furthermore, the influence or effects of ADF additives on the anaerobic degradation process are unknown due to the proprietary nature of additive formulations.

1.1 Rationale for Project

As mentioned above, aircraft deicing/anti-icing fluids are known to exert extremely high BODs. There are technologies presently available for glycol recovery and recycling; however, end-of-pipe technologies are also required to deal with the remaining ADF that is not recoverable. According to LGL–Love (1979), this amount could account for 51% of the glycol used. Thus, this research focused on an end-of-pipe technology for ADF contaminated discharges.

Biodegradation of aircraft deicing fluid has been investigated under both aerobic and anaerobic conditions. Operational difficulties were encountered in aerobic treatment systems (Kilroy and Gray, 1992; Jank *et al.*, 1973). Aerobic biodegradation in soil was successful; however, the wastewater strength was quite low (Klečka, 1993). Anaerobic technologies have good potential for medium and high strength ADF treatment (Mulligan *et al.*, 1997; Darlington and Kennedy, 1998). However, to our knowledge only cursory EG-based ADF treatment studies have been performed thus far (i.e., the effects of important operating variables such as ADF concentration, biomass concentration, and HRT on process performance were not fully characterized).

In this study, anaerobic treatment of ADF was investigated in a methodical manner. Experimental run conditions were carefully planned in accordance with

statistical experimental design protocols. Three operating variables: HRT, biomass inventory, and ADF concentration, were considered. The effects of these three operating variables were assessed through rigorous examination of the data collected. Empirical models generated could also be used for process optimization purposes.

Furthermore, additives may be contributing to the higher toxicity associated with ADF as compared to pure aqueous ethylene or propylene glycol solutions (*vide infra*); their presence may be toxic or inhibitory to the anaerobic biodegradation process. Two very important classes of additives found in ADF are nonionic surfactants and corrosion inhibitors. Tolyltriazoles were recently identified as corrosion inhibitors in ADF (Cancilla *et al.*, 1997). Nonylphenol ethoxylates (NPnEOs, where n indicates the number of ethoxy units) have been widely used as nonionic surfactants for over 40 years (Naylor, 1995). Thus, it is of great scientific and practical interest to determine the fate of these additives during anaerobic treatment of ADF, as well as the effects of these additives on the treatment process.

Though much is known about the fate of NPnEO under aerobic, and to some extent anaerobic conditions (*vide infra*); there are no reports on the effects of NPnEO and NP on anaerobic degradation of ADF or EG. The effects of tolyltriazole on mesophilic anaerobic co-digestion of wastewater sludge and propylene glycol were studied by Gruden *et al.* (2001). Tolyltriazole concentrations above 300 mg/L resulted in a significant decrease in methanogenic activity; however, the study was carried out in microcosms.

In this study, the fate of aryl triazoles and NPnEO (and its metabolite NP) during anaerobic biodegradation of ADF in UASB reactors was monitored. Batch experiments were also performed to determine the fate and effects of aryl triazoles (benzotriazole, 5-methyl-1 H-benzotriazole, 5,6-dimethyl-1 H-benzotriazole), NP, and NPnEO (average n = 9 ethoxy units) during methanogenesis of EG. This finding would provide a better

understanding of the biodegradation process, as applied to known additives in the ADF contaminated wastewater.

1.2 Research Objectives

The main objectives of this study were: (1) to evaluate the treatment of ADF in UASB reactors and (2) to determine the effects or role of aryl triazoles and NPnEO/NP in the treatment process. The specific objectives of this study were to:

- Determine the optimum operating conditions for ADF treatment in UASB reactors;
- Derive an empirical model to describe the effects of ADF concentration, HRT, and biomass concentration on:
    a. COD removal efficiencies,
    b. Biomass specific acetoclastic activity,
    c. Methane production rates, and
    d. Methane production potential;
- Determine the fate of tolyltriazole and NP in UASB reactors;
- Evaluate changes in the characteristics of anaerobic granular biomass during ADF treatment;
- Determine kinetic constants such as biomass yield and substrate utilization rates for anaerobic treatment of ADF in UASB reactors;
- Determine sorption isotherms for benzotriazole, 5-methyl-1 H-benzotriazole, 5,6-dimethyl-1 H-benzotriazole, and NP;
- Evaluate the importance of biological activity in NP sorption;
- Determine the effects of benzotriazole, 5-methyl-1 H-benzotriazole, 5,6-dimethyl-1 H-benzotriazole, NP, and Tergitol NP-4 (NPnEO) on EG degradation; and
- Determine the fate of benzotriazole, 5-methyl-1 H-benzotriazole, 5,6-dimethyl-1 H-benzotriazole, and NP during anaerobic degradation of EG.

Two types of experiments were carried out to achieve these objectives. Batch experiments using serum bottles were conducted to characterize the effects of aryl triazoles and NPnEO/NP on the anaerobic treatment process. Anaerobic treatment of ADF was done in continuous mode using bench-scale UASB reactors, and run conditions were determined based on central composite design.

2 Background and Literature Review

2.1 Causes and Effects of Ice, Snow, and Frost on Aircraft Surfaces

Ice, snow, and frost can form and accumulate on aircraft surfaces, while the aircraft is on the ground as well as when it is in flight. On the ground, this can occur if the aircraft is exposed to frozen precipitation such as snow or sleet. There is also a risk if the outside air temperature is below 10°C and there is moisture, slush, or snow on ramps, taxiways, and runways. During flight, an aircraft can encounter atmospheric conditions that are conducive to ice formation on its surface. These conditions include super-cooled clouds (clouds containing water droplets at temperatures below freezing point), ice crystal clouds (clouds containing ice crystals), mixed conditions (clouds containing both super-cooled water droplets and ice crystals), and frozen precipitation (Duncan, 1995a).

The presence of ice, snow, and frost on aircraft surfaces can have adverse effects on flight safety. For example, wing lift can decrease by 30% while wing drag can increase by 40% if the leading edge and upper surfaces of wings are covered with snow, ice, or frost, having thickness and surface roughness of medium or coarse sandpaper (Duncan, 1995a). Such changes in lift and drag can greatly affect stall speed, as well as controllability and flight handling characteristics. In addition, the presence of ice, snow, and frost can cause mechanical interference that restricts movement of flight controls and landing gear mechanisms. Engine damage or failure can also occur if ice dislodges and is ingested by a turbine engine. Thus, it is crucial that aircraft surfaces and components are free of ice, snow, and frost prior to takeoff.

2.2 Aircraft Deicing/Anti-icing Fluids

There are three principle methods for removing ice, snow, and frost from parked aircraft surfaces: the use of heat, chemicals, or mechanical means. It is impractical to

employ any of the methods by itself because heating alone would require a special building to house the aircraft in order to prevent heat loss to the environment. Employment of chemicals that are safe for use on aircraft surfaces would be too expensive, considering the need to melt large accumulations of ice and snow. Mechanical means can cause damage to the aircraft due to the bonding of ice to the surface. Thus, all three methods are often combined in practice, where a heated solution of deicing chemicals is sprayed onto the aircraft to break the surface bonding of the ice, and the ice is removed mechanically by the force of the spray.

Currently, mixtures of glycols and water are generally used to remove and/or prevent frozen deposits of ice, snow, and frost on parked aircraft surfaces. These glycol-based fluids are classified into two main types. Type I fluids have deicing attributes and are not shear sensitive (Newtonian), while Type II fluids contain thickening agents which make them more viscous and shear sensitive. The higher viscosity of Type II fluids implies that a thicker film on the aircraft surface can be obtained which would result in a higher holdover time (period of time when ice, snow, and frost are prevented from adhering to the protected surface). Thus, Type II fluids are often referred to as anti-icing fluids.

Commercial deicing/anti-icing fluids (ADAF) currently available are formulated in accordance to fluid specifications established by such organizations as the Society of Automotive Engineers (SAE), the Association of European Airlines (AEA), and the International Standards Organization (ISO) (Mudd, 1993). As such, these fluids are more appropriately referred to by their fluid specification identifier (for example, SAE Type I, AEA Type II, ISO Type I, and so on).

2.2.1 Glycols and Chemical/Biochemical Oxygen Demand

The glycol component of ADAF usually comprises ethylene glycol ($HOCH_2CH_2OH$), propylene glycol ($CH_3CH(OH)CH_2OH$), and/or diethylene glycol ($HOCH_2CH_2OCH_2CH_2OH$). Concentrated Type I fluids contain a minimum of 80% glycol and are diluted to approximately 50% glycol before use, while Type II fluids contain a minimum of 50% glycol (Duncan, 1995b). In Europe, glycols used in ADAF are mostly diethylene glycol and propylene glycol; whereas those used in North America are predominantly EG and propylene glycol (Holmgren and Forsling, 1995).

Often, Type I fluids are EG-based and Type II fluids are propylene glycol-based. However, during the winter of 1994, the United States received a large amount of ice and snow that resulted in a national shortage of EG. This event led to the use of propylene glycol deicers to fill the EG deicer shortage. Since then, propylene glycol deicers have become increasingly popular in the United States since they were found to be less toxic than their EG counterparts (USAF, 1996). In fact, propylene glycol-based deicers are the only ADAF approved for purchase by the United States Air Force (PRO-ACT, 1995; McCarty and Willis, 1996). In contrast, EG-based deicers are still used predominantly in Canada (Simpson, 1997; Novak *et al.*, 2000).

Both ethylene and propylene glycol deicers are considered environmentally hazardous since they exert a very high BOD. For example, propylene glycol-based deicers have been reported to have a five-day carbonaceous biochemical oxygen demand ($CBOD_5$) approaching 1,000,000 mg/L; while EG-based deicers have been reported to have $CBOD_5$ values in the range of 400,000 – 800,000 mg/L. The actual BOD associated with various deicers has been known to vary, depending on the make (manufacturer) as well as type of fluid under study. However, both propylene glycol-based and EG-based deicers were found to exert a $CBOD_5$ higher than 300,000 mg/L (Limno-Tech Services, 2002). For example, Union Carbide UCAR XL 54 ADF (a Type I fluid) has been

reported to exert a BOD of 523,000 mg/L (Mulligan *et al.*, 1997). In terms of COD, our laboratory testing conducted on UCAR XL 54 ADF (54% EG content) resulted in COD values in the range of 700,000 – 800,000 mg/L.

The high BOD and COD associated with ADAF are of particular concern to surface and ground water environments. It has been reported that EG, propylene glycol, and diethylene glycol have very low coefficients of adsorption onto organic carbon from water (log K_{OC} in the range of –2.14 to –0.52); thus, they are not likely retained by soil (MacDonald *et al.*, 1993). This behavior also suggested that glycol contaminants cannot be easily contained, and leaching of these contaminants into ground and surface waters is of major concern. Since the vapor pressures of these glycols are very low (<0.2 mm Hg), volatilization is an unlikely mechanism for glycol reduction in contaminated waters (MacDonald *et al.*, 1993). Consequently, glycol removal from contaminated waters relies mostly on bacterial activities and partially on photo-oxidation by sunlight. Since aerobic biodegradation is the most important process affecting these glycols in surface water, the high BOD associated with ADAF can deplete the dissolved oxygen content of the water, resulting in an environment that is unsuitable for aquatic life.

2.2.2 Additives and Toxicity

Both Type I and Type II fluids contain small amounts of additives such as wetting agents, corrosion inhibitors, and pH modifiers (USAF, 1996; Holmgren and Forsling, 1995). The exact composition of these additives is often not readily obtainable since formulations are subject to change and the manufacturers consider them to be proprietary information. In general, fatty alcohols and/or alkoxylated fatty alcohols (e.g., NPnEOs; Figure 2–1) are employed as non-ionic surfactants (USAF, 1996). Corrosion inhibitors may include phosphates (H_3PO_4 or K_3PO_4), silicates (Na_2SiO_3 or K_2SiO_3), and amines (triethanolamine) (USAF, 1996; Holmgren and Forsling, 1995). Often inorganic bases

(KOH or NaOH) are employed as pH modifiers (USAF, 1996; Holmgren and Forsling, 1995). In addition, a silver chelating agent such as benzotriazole or tolyltriazole (Figure 2–2) may be added to reduce the hazards of EG decomposition to a very flammable ethylene oxide on silver-covered copper electrodes (Downs, 1968). Furthermore, a dye may be present to help identify various solutions and to reduce misapplication of a product.

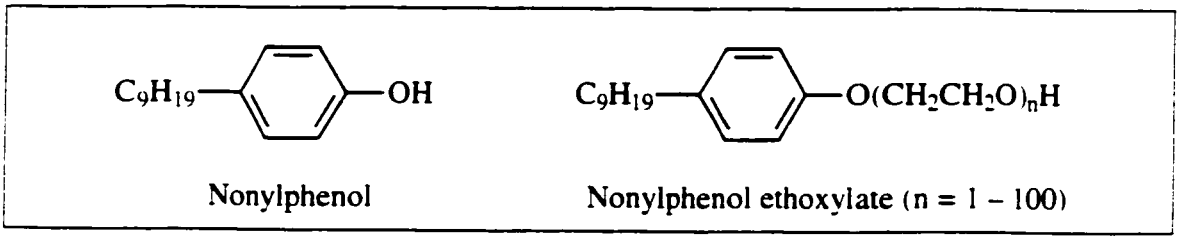

Figure 2–1 Chemical structure of NP and NPnEO. The nonyl chain is branched.

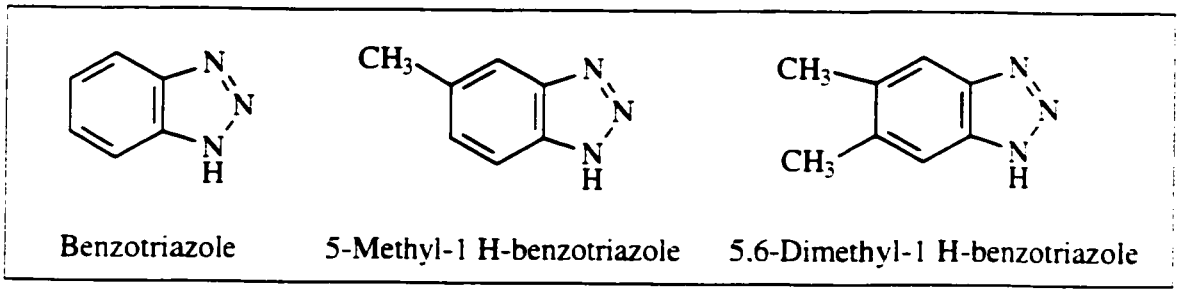

Figure 2–2 Chemical structure of benzotriazole and its derivatives.

In addition to the above-mentioned additives, Type II fluids also contain a thickener system. This thickening system consists of a proprietary crosslinker copolymer and a crosslinked polymer, forming a crosslinked network that gives the fluid its pseudoplastic flow behavior (Holmgren and Forsling, 1995). A crosslinked polymer such as crosslinked polyacrylic acid and its derivatives may be used in formulating Type II fluids (USAF, 1996). Different corrosion inhibitors and surfactants are also used in Type

II fluids to ensure proper thickener performance (Hartwell *et al.*, 1993). This difference in formulation may also account for higher toxicities associated with Type II anti-icers as compared to Type I deicers (Hartwell *et al.*, 1993).

It has been shown that the additives in ADAF contribute to the higher toxicity found for ADAF as compared to that for aqueous solutions of pure ethylene or propylene glycol. For example, Jank *et al.* (1973) conducted bioassays on juvenile rainbow trout to determine the acute toxicity of treated and untreated Dow and UCAR aircraft deicers. From the studies conducted, it was established that the 96-hour lethal concentration for 50% mortality of the fish (96-hr LC_{50}) for UCAR deicer was in the range of 5,700 – 6,750 mg/L and that for Dow deicer was between 8,900 – 12,000 mg/L. These authors also indicated that the observed toxicity could not be attributed to the glycols present since aeration of both deicers resulted in a reduction in toxicity, while glycol concentrations remained essentially unchanged. In addition, bioassays on pure EG resulted in a 96-hr LC_{50} value that was much larger (greater than 18,500 mg/L) than that for the two deicers. As for propylene glycol, very large 96-hr LC_{50} values (greater than 45,600 mg/L) for rainbow trout have also been reported (MacDonald *et al.*, 1993).

Hartwell *et al.* (1993) also reported higher toxicity for ADAF as compared to the parent glycol component. Toxicity assays conducted on Microtox® bioluminescent bacteria (*Photobacterium phosphoreum*), juvenile fathead minnows (*Pimephales promelas*), and three species of zooplantkton (*Daphnia magna*, *Daphnia pulex*, and *Ceriodaphnia dubia*) indicated that aircraft anti-icing fluid (propylene glycol based) was about two magnitudes more toxic than the EG-based deicing fluid. The 96-hr LC_{50} values for the multicellular organisms tested were 33 – 480 mg/L for anti-icing fluid and 3,300 – 14,800 mg/L for deicing fluid. Hartwell *et al.* (1993) also observed acute and chronic toxic effects for water samples collected from a tributary of a creek that receives

runoffs directly from the holding ponds of Baltimore-Washington International Airport after a storm event. The water samples collected contained 2,100 mg/L EG.

Pillard *et al.* (2001) reported that an isomeric mixture of tolyltriazole made up 0.5 – 0.6% of total ADF volume. This mixture is made up of 45% (by mass) of 4-methyl-1 H-benzotriazole (4-MeBT) and 55% 5-methyl-1 H-benzotriazole (5-MeBT). These authors compared toxicity effects of benzotriazole and its methyl derivatives on Microtox® bacteria (*Vibrio fischeri*), fathead minnow (*Pimephales promelas*), and water flea (*Ceriodaphnia dubia*). They observed that 5-MeBT was consistently more toxic than 4-MeTB to all three test organisms. The Microtox® 15-min median effective concentration causing a 50% reduction in light production by the bacteria (EC_{50}) of 4-MeBT and 5-MeBT were 21 mg/L and 8.7 mg/L, respectively. The 48-hr LC_{50} values for the water flea were 118 mg/L for 4-MeBT and 79 mg/L for 5-MeBT. Assays on fathead minnows gave a 96-hr LC_{50} of 63 mg/L for 4-MeBT and 22 mg/L for 5-MeBT. These authors also observed that the toxicities of the isomeric mixture of 4-MeBT and 5-MeBT for the water flea and the fathead minnow were approximately equal to the geometric mean of the toxicity of the individual isomers.

Alkylphenol (nonylphenol and octylphenol) ethoxylates are widely used as nonionic surfactants. They are found in both industrial and domestic applications such as detergents, emulsifiers, and wetting dispersing agents. Alkylphenol ethoxylates are also used as spermicides in contraceptive products (Nimrod and Benson, 1996). NPnEOs account for about 80% of the estimated 600,000 metric tonnes total alkylphenol ethoxylates volume produced annually (Naylor, 1995; Cox, 1996).

Toxicity data on NPnEOs indicated that toxicity depends on the ethoxy chain length. Higher toxicities are associated with lower oligomers, with the NP moiety about 10 times more toxic than the ethoxylated form (Yoshimura, 1986; Naylor, 1995). Sensitivity of different fish, invertebrates and algae to acute toxicity assays vary by

orders of magnitude (e.g., all fish LC_{50} acute range is 130 – 1,400 µg/L, all invertebrates LC_{50} acute range is 20 – 1,590 µg/L, and all algae LC_{50} acute range is 25 – 750 µg/L) (Naylor, 1995). Toxicity assays on the Japanese killifish (*Oryzias laptipse*) indicated that the 48-hr LC_{50} values are 1.4 mg/L for NP, 11.2 – 14.0 mg/L for NP9EO, and 8.9 – 9.6 mg/L for the carboxylic acid forms of NP1EO and NPE2EO (NP1EC and NP2EC) (Yoshimura, 1986). However, NP is considered to pose low bioaccumulation risks to fish as indicated by a bioaccumulation factor of 350 for fathead minnows (ratio of concentration in organism to that in water; there is low risk for bioaccumulation if this value is below 1000; Naylor, 1995).

Alkylphenols and alkylphenol ethoxylates have been designated as members of the endocrine disrupters or modulators, affecting growth and reproductive health of many species. Direct human exposure to alkylphenol ethoxylates occurs through the use of spermicides. This has great ramifications since exogenous estrogenic compounds such as nonsteroidal estrogen diethylstilbestol (DES; prescribed in the 1950s and 1960s to pregnant women to prevent miscarriage) was found to have adverse effects on human offspring exposed *in utero* (Nimrod and Benson, 1996). However, it cannot be clearly determined that NPnEO pose a major risk to human reproduction due to the paucity of data available on NPnEO estrogenic effects (Nimrod and Benson, 1996).

Exposure to sublethal levels of 4-nonylphenol (Baldwin *et al.*, 1997) and prolonged exposure to NPnEO at concentrations near acutely lethal levels (Baldwin *et al.*, 1998) affected the metabolic elimination of testosterone by water fleas. The 48-hr LC_{50} of NPnEO for *Daphnia magna* was 8.6 mg/L, and failure to produce offspring occurred after a 3-week exposure to 5.0 mg/L NPnEO (Baldwin *et al.*, 1998).

Hughes *et al.* (2000) reported NP may disrupt male reproductive development by inhibiting the endoplasmic reticulum Ca^{2+} pumps. Very low IC_{50} (concentration causing 50% inhibition) values for the inhibition of Ca^{2+}-ATPase activity (0.3 – 0.4 µM) and

Ca^{2+}-uptake (4 – 6 μM) in microsomes of rat testis were found for NP. Disruption of cellular Ca^{2+} homeostasis also resulted in higher intracellular concentrations of Ca^{2+} in mouse TM4 cells (a Sertoli cell line), which lead to decreased cell viability at NP concentrations higher than 20 μM. ATPase inhibition by alkyphenol ethoxylate was also observed, but at lower potency (IC_{50} of 57 – 65 μM Triton X100).

Estrogenic activity of NP was evident in *in vivo* studies using rainbow trout. Lech *et al.* (1996) reported vitellogenin protein induction (indicative of estrogenic activity) by NP at levels below LC_{50} levels. It was observed that estrogenic activity occurred at an effective concentration (EC_{50}) range of 6.4 – 31.5 ppb, as compared to an LC_{50} of 193.65 ppb. The effect of NP was not permanent as suggested by the reduction in vitellogenin production after 48-hr post-transfer of the rainbow trout to fresh water.

Kubota *et al.* (2000) also reported *in vitro* estrogenic activity of NP. Their report suggested that *p*-nonylphenol interacted with the estrogen receptor, suppressing 92 kDa gelatinase secretion by human peripheral lymphocytes. The enzyme 92 kDa gelatinase is one of four types of enzymes which are important in the regulation of cell-extracellular matrix interactions.

NP also inhibited respiration and reproduction of the fungus *Neurospora crassa* and the diploid yeast *Candida albicans* (Karley *et al.*, 1997). At 25 μM, NP affected the cell yield of the fungus by a 10-fold decrease. Abnormal cell shape was also observed. Almost complete inhibition of asexual yeast reproduction resulted at 100 μM NP exposure level.

Cardellini and Ometto (2001) reported that alcohol ethoxylates exhibit both teratogenic and toxicity effects in embryos and tadpoles of the clawed frog *Xenopus laevis*. The epithelial tissue, particularly that of the gills, was affected most. This observation was expected since the gills are the principle sites for surfactant uptake. Similarly, NP was reported to cause structural changes in three fish epidermal cell

cultures (Lamche and Burkhardt-Holm, 2000) and in the skin of rainbow trout (Burkhardt-Holm *et al.*, 2000).

2.3 Canadian Water Quality Guidelines

As mentioned previously, the extremely high BOD associated with the glycols in ADAF can cause a substantial reduction in the dissolved oxygen of the receiving waters, which can be detrimental to aquatic life. Furthermore, high concentrations of glycols, and particularly ADAF, can be toxic to fish and aquatic life that rely on the contaminated water for survival. Based on toxicity data reported by various researchers, Transport Canada has recommended the interim water quality guidelines for the protection of freshwater aquatic life as follows: 3 mg/L EG, 31 mg/L diethylene glycol, and 74 mg/L propylene glycol (MacDonald *et al.*, 1993). There were insufficient data to establish the guidelines for the protection of marine and estuarine aquatic life.

Canadian airports are major contributors to the total glycol released into the environment (MacDonald *et al.*, 1993). For example, in 1985, the reported average EG concentration in storm water at Ottawa International Airport was 1,814 mg/L, with a maximum value being 19,800 mg/L (MacDonald *et al.*, 1993). Total glycol concentrations as high as 16,400 mg/L in storm water drains have also been detected during the 1989/90 winter at Halifax International Airport (MacDonald *et al.*, 1993).

To ensure that highly contaminated storm waters are not discharged untreated into the environment, the Canadian Environmental Protection Act (CEPA) has set a limit of 100 mg/L total glycol that can be discharged into receiving waters (Simpson, 1997). Consequently, the spent ADAF produced annually by various airports must be dealt with (recovery or degradation of the glycol component), before they can be discharged into the environment.

2.4 Glycol Recovery

Recovery of the valuable glycol component in ADAF is an option that is both economically and environmentally sound. Currently, this practice is implemented mainly in Europe (Munich, Germany, Oslo, Norway and Lulea, Sweden) where Type I fluids are recovered and the recycled glycol is reused in aircraft deicer formulations (Holmgren and Forsling, 1995; Bremer, 1993). Although some recovery of glycols from spent ADAF does take place in North America, the recycled glycols are considered inappropriate for reuse in formulating new aircraft deicers (McDonald and Hales, 1997).

In general, not all of the glycol used can be recycled. According to LGL-Love (1979) about 16% of the deicers used adhered to the aircraft, and this material sloughed off during taxiing and liftoff. Another 35% is carried away by wind and deposited in the airport vicinity; thus, at best only 49% of the glycol used would be available for recovery. Consequently, there is a need for glycol treatment prior to discharge of contaminated airport runoffs if the CEPA's 100 mg/L total glycol limit is to be met.

2.5 Biological Treatment

Various researchers have investigated the biodegradation of glycols under both aerobic and anaerobic conditions, while the literature on ADAF treatment is quite limited. Most of the work reported on glycol biodegradation can be classified into two main categories: (1) isolation and use of pure cultures to elucidate the metabolic pathway(s) for glycol degradation, or (2) evaluation of the treatability of glycols by mixed cultures. Studies on the biodegradation of aircraft deicing/anti-icing fluids generally fall into the latter category.

2.5.1 Aerobic Biodegradation

To date, most of the available literature on glycol biodegradation has dealt with aerobic systems. Batch studies indicated that EG was readily biodegraded aerobically at

both 8 and 20°C, whereas degradation of higher molecular weight glycols such as diethylene glycol required higher temperatures (20°C; Evans and David, 1974) or if the sludge was acclimated to the test chemical (Cox, 1978). Studies on pure cultures isolated from soil, fresh water, or salt water have indicated that the aerobic bacteria capable of utilizing glycols as the sole carbon source are generally Gram-negative rods (Gonzalez *et al.*, 1972; Haines and Alexander, 1975; Child and Willetts, 1978; Pearce and Heydeman, 1980).

Pilot plant studies of EG treatment by activated sludge were investigated by Kilroy and Gray (1992). EG was co-treated with a pharmaceutical wastewater, which contained trace organic solvents and pharmaceutical compounds. The range of specific organic loading rate (SOLR) was 0.4 – 0.6 kg BOD/kg MLSS/d and the solids retention time (SRT) was in excess of 20 days. Sludge deterioration and scum formation were observed when EG concentration in the wastewater feed was greater than 0.25%. It was thus recommended that full-scale operations should be kept at 0.1% EG to preserve floc structure and avoid scum formation.

Biodegradation of aircraft deicing fluid by activated sludge has also been investigated. Tests conducted at a temperature range of 2 – 22°C indicated that biodegradation rates were faster at higher test temperatures (Jank *et al.*, 1973; Sabeh and Narasiah, 1992). In addition, operational problems such as filamentous bulking and scum formation were encountered when ADF was co-treated with raw sewage (mixture of industrial and domestic wastewater) at 10°C, with organic loadings greater than 0.15 kg BOD/kg mixed liquor suspended solids (MLSS)/day (Jank *et al.*, 1973). The glycol component of the ADF used was EG and propylene glycol.

Biodegradation of low concentrations of different types of ADF in soil at a temperature range of –2 to 25°C were studied by Klečka *et al.* (1993). Experiments were conducted by adding ADF to soil at levels ranging from 0.05 to 0.5% (v/w), giving glycol

concentrations of 392 – 5,278 mg/kg soil. Glycol biodegradation rates were temperature dependent. Rates at 25°C (66.3 – 93.3 mg/kg/d) were three times higher than those at 8°C (19.7 – 27.0 mg/kg/d). Biodegradation also occurred at –2°C, though at a much lower rate (2.3 – 4.5 mg/kg/d). Initial glycol concentration determined the time required for complete mineralization of the glycol present. At 8°C, an excess of 111 days was required for complete degradation in soil containing 0.5% ADF. Different types of ADF were studied and glycol composition included EG, propylene glycol, and diethylene glycol, present as a single component or as mixtures of two components. The glycol levels tested exerted no inhibitory effects, suggesting that residual glycol levels at airports can be removed by the surrounding soil microcosms if ample time is provided.

The above indicated that aerobic treatment of ADF could be effectuated at low ADF concentrations. Since ADF concentrations in airport storm water drains can reach quite high during heavy snowfalls (*vide ante*), dilution of the wastewater would be required. High operational costs could result with the additional pumping requirements. High strength wastewaters have been known to be effectively treated by anaerobic systems (Speece, 1996); thus, it was of interest to investigate the applicability and feasibility of this treatment system for ADF wastewaters.

2.5.2 Anaerobic Biodegradation

There is less literature available on anaerobic biodegradation of glycols, although studies in the early 1950's have shown anaerobic systems were more successful in degrading compounds such as diethylene glycol, triethylene glycol, and polyethylene glycol with a molecular weight of 400 than aerobic systems (Cox, 1978). To date, some attempts to elucidate the metabolic pathway for the anaerobic degradation of EG and polyethylene glycol have been done.

Schink and Stieb (1983) isolated pure cultures from mud sample enrichments containing strictly anaerobic, Gram-negative, nonsporeforming, rod-shaped bacteria that were capable of fermentative degradation of polyethylene glycols. Unlike their aerobic counterparts, these strains did not excrete extracellular depolymerizing enzymes and they could not degrade EG. Rather, they were inhibited by EG. A different bacterium capable of fermentative degradation of EG was isolated from the same mud enrichments.

Dwyer and Tiedje (1983) reported biodegradation of EG and polyethylene glycol by methanogenic enrichments from municipal anaerobic digester sludge. Based on degradation products detected by gas chromatography, the authors suggested that EG was initially dismutated to acetate and ethanol. Ethanol was subsequently consumed with concomitant production of acetate and methane. No production of methane from acetate was reported.

Fewer reports on anaerobic systems for ADF treatment are available. High removal efficiencies for propylene glycol-based ADF were achieved at the Albany International Airport, New York, using a 700–L anaerobic fluidized bed reactor (AFBR) (Switzenbaum *et al.*, 1999). COD removals greater than 95% were obtained for influent COD of 5,000 mg/L at an organic loading rate (OLR) of 15 kg COD/m^3/d. An average of 82% COD removal was obtained when operated at 25 kg COD/m^3/d.

Mulligan *et al.* (1997) reported that pilot plant scale multiplate reactors have been used successfully to anaerobically treat EG-based Union Carbide UCAR XL 54 aircraft deicing fluid at 39°C. It was reported that a COD reduction of 90% was obtained at an OLR of 16.5 kg COD/m^3 reactor/day (13 kg BOD/m^3 reactor/day), with an influent COD of 8,500 mg/L. Since 18.7 kg of biomass was used in the 900–L reactor, this OLR corresponded to a specific organic loading rate (SOLR) of 0.79 kg COD/kg biomass/day (0.63 kg BOD/m^3 reactor/day). Mulligan *et al.* (1997) did not report any operational

problems such as sludge deterioration and scum formation that were encountered by activated sludge treatment of ADF.

Darlington and Kennedy (1998) investigated the mesophilic treatment of medium to high strength EG-based ADF wastewater (5 – 20 g/L COD) in UASB reactors. COD removal efficiencies in the range of 70 – 98% for OLR reaching as high as 38.7 kg COD/m^3 reactor/day were obtained. This suggested that UASB reactors have good potential for effective treatment of high strength EG-based ADF containing wastewaters. However, no data were provided for granular biomass activity and settling velocities.

Most of the studies on anaerobic treatment of EG-based ADF were preliminary investigations. There are no comprehensive studies on the effects of important operating variables such as ADF concentration, HRT, and biomass concentration on process performance. Additionally, no studies have addressed the issue of fate or effects of ADF additives during the anaerobic treatment of ADF.

2.6 Biodegradation of Aircraft Deicing Additives

2.6.1 Nonylphenol and nonylphenol ethoxylates

Aerobic degradation of NP and particularly NPnEO under both laboratory and field conditions has been studied by several investigators. These reports indicated that NPnEOs are biodegradable; however, there is much controversy over the extent of degradation observed. Maki *et al.* (1996) investigated the degradation of NPnEO by river microbial consortia. They identified nonylphenolacetate (NP1EC) as the major and final biodegradation product of NPnEO. In contrast, Field and Reed (1996) reported that nonylphenol diethoxy carboxylate (NP2EC) was the dominant species among the nonylphenol polyethoxy carboxylate (NPnEC) oligomers found in river water and effluents from paper mills and sewage treatment plants in the U.S. Of the eight U.S. rivers tested, NP1EC and NP2EC were the only species found in five of the rivers, with a

total NPnEC concentration range of below detection to 13.8 µg/L. Higher NPnEC concentrations were detected for municipal sewage effluents (140 to 270 µg/L) and paper mill effluents (below detection to 1,300 µg/L). All six municipal sewage effluents contained NPnEC (n = 1 – 4), whereas, over half of the 15 paper mill effluents contained only NP1EC and NP2EC.

Results of a treatability study involving 11 full-scale sewage treatment plants in the Glatt Valley, Switzerland, carried out from 1983 to 1985, were reported by Ahel *et al.* (1994a). NPnEO concentration ranges in primary and secondary effluents were 1090 – 2060 µg/L and 240 – 270 µg/L, respectively. NPnEOs (n = 3 – 20) were the dominant nonylphenolic compounds in primary effluent (82.4%). However, secondary effluents were dominated by NPnEO metabolites (46.1% NP1EC + NP2EC, 21.8% NP1EO + NP2EO, and 3.9% NP). Average percentage NPnEO elimination efficiencies were 70 ± 15% (weight basis) and 59 ± 18% (molar basis). Low removal efficiencies were believed to be due to the generation of NPnEC (n = 1 – 2) in the activated sludge process (concentrations in secondary effluents 2.1 – 7.6 times higher than in primary effluent). Higher elimination efficiencies were obtained for systems operating at low loading rates and nitrifying conditions. Based on mass balances, it was suggested that 60 – 65% of the total NP/NPnEO entering the treatment plants were released into the environment (25% NP, 19% NPnEC, 11% NP1EO and NP2EO, and 8% untransformed NPnEO). Of the total NP released into the environment, greater than 90% was in anaerobically digested sludge. Similarly, Brunner *et al.* (1988) calculated that about 50% (molar basis) of NPnEO in raw sewage was transferred to anaerobically digested sludge as NP.

Evidence of large amounts of NP/NPnEO released into the environment was reflected in the NP/NPnEO levels found in the Glatt River, Switzerland during the 1983 – 1986 period (Ahel *et al.*, 1994b). This river is located in a densely populated area (240,000 inhabitants, 260 km^2). Considerable amounts of municipal sewage treatment

effluents were discharged into the river. Being a small river (discharge of 3 – 9 m^3/s), some reaches of the river can have up to 15 – 20% of the river flow as treated sewage effluents. Of the eight sampling sites along this river, NP, NPnEC (n = 1 – 2) and NPnEO (n = 1 – 5) were the only species detected. The most abundant nonylphenolic compounds were NP1EC (<1 – 45 µg/L) and NP2EC (2 – 71 µg/L). The second most abundant species were NP1EO (<3 – 69 µg/L) and NP2EO (<0.3 – 30 µg/L). Levels of NP (<0.3 – 45 µg/L, with one result above 10 µg/L and 84% of samples higher than 1 µg/L) in river water were lower than those in sediments (0.19 – 13.1 mg/kg dry matter). NPnEO (n = 3 – 5) were present in less than 1 µg/L range. A biodegradation efficiency of only 24% was obtained for the 35 km long river based on mass balances. It was thus concluded that lower oligomers of NPnEO were refractory to microbial transformations.

In contrast, much higher treatabilities (92.5 – 99.8% removal) were reported for NP/NPnEO at seven wastewater treatment plants in the U.S. (Naylor, 1995). Influent NP (up to 978 µg/L) and NPnEO (up to 33,700 µg/L) concentrations were reduced to effluent concentrations of <1 – 15 µg/L NP and <5 – 260 µg/L NPnEO (n = 1 – 17). Very little NP was found in the digested sludge measured at two of the seven plants (0.1% and 1.7% of the total NP/NPnEO). This indicated that digested sludge was not a major sink for NP. Also, a much smaller fraction of the NP/NPnEO entering the wastewater treatment plants (about 3% for a plant operating at an influent NPnEO flux of 557 kg/d, primary influent total NPnEO of 34,200 µg/L) was released into the environment. The inability of the treatment process to operate at 100% efficiency was considered to be the reason for the presence of lower oligomers of NPnEO in effluents, rather than the refractory nature of these compounds.

High NPnEO removal efficiencies obtained by wastewater treatment plants were reflected by low NPnEO levels in 30 U.S. rivers surveyed (Naylor, 1995). Over half of the river water contained NP and NPnEO below detection levels. The highest values

found for NP, NP1EO, and NP2EO in water were about 1 µg/L. The highest composite total of NPnEO (n = 3 – 17) was 15 µg/L. Higher concentrations were found in river sediments. Highest concentrations for NP and NPnEO were 3,000 µg/kg sediment and 175 µg/kg sediment, respectively. These values were smaller than those reported by Ahel *et al.* (1994b) and were believed to be indicative that lower oligomers of NPnEO were not refractory.

Evidence for complete mineralization of NPnEO under aerobic conditions was also reported by Hughes *et al.* (1996). Biodegradation of NPnEO in soil was carried out at a concentration of 15 mg/50 g soil. Carbon dioxide measurements suggested that biodegradation efficiency greater than 50% was accomplished. Quantification of the aromatic ring by high performance liquid chromatography (HPLC) showed a decrease, suggesting degradation of the aromatic ring after 63 days.

Evidence for aerobic degradation of NP was also reported. Ekelund *et al.* (1993) investigated the biodegradation of 4-nonylphenol by seawater and sediment, using NP with a ^{14}C-labelled phenolic moiety. Experiments were carried out at 11°C. Evidence for NP degradation was indicated by a 50% transfer of radioactivity to the recovered CO_2 fraction after 58 d of incubation. In addition, Tanghe *et al.* (1999) isolated a bacterial strain from activated sludge that was able to utilize branched NP as the sole carbon source. They suggested that fission of the aromatic ring was the first step in biodegradation since NP was the only aromatic compound detected by HPLC. Results also indicated that *para* substitution was preferred (over 98% removal of *p*-nonylphenol compared to 30 – 60% removal of *o*-nonylphenol).

Under anaerobic conditions, NP has been reported as the ultimate biodegradation product of NPnEO. Ejlertsson *et al.* (1999) investigated batch-scale mesophilic anaerobic biodegradation of NP1EO and NP2EO by digester sludge, landfilled municipal solid waste, and landfilled sludge. NP was the only biodegradation metabolite detected.

In addition, no radioactivity was found in the CO_2 and methane fraction of bottles amended with NP1EO and NP2EO having a ^{14}C-labelled phenolic group. This suggested that the aromatic ring remained intact during the biodegradation process. Substantial radioactivity was found associated with the solid phase, suggesting that there was sorption of NP and NPnEO (n = 1 – 2) to organic matter. This is in agreement with earlier findings where large concentrations of NP (around 1 g/kg) were found associated with anaerobically digested sewage sludge and these levels corresponded to the NP1EO and NP2EO content of undigested sludge (Giger *et al.*, 1984; Brunner *et al.*, 1988). Further studies were still needed since the experiments performed by Ejlertsson *et al.* (1999) were batch-scale. Continuously operated reactors, such as those used in this study, should provide conditions that are more favorable for the degradation of recalcitrant compounds such as NP.

2.6.2 Aryl triazoles

There is very little information regarding the biodegradation of aryl triazoles, especially in anaerobic treatment processes. Environmentally significant levels of benzotriazole (126 mg/L) and tolyltriazole (198 mg/L) were found in groundwater 5 m below a major international airport (Cancilla *et al.*, 1998). These concentrations were higher than the acute toxicity values reported by Pillard *et al.* (2001) (*vide ante*). Thus, it is important to address the issue of fate of aryl triazole during anaerobic treatment as well as the effects or role of these additives in the treatment process.

Recently, evidence for aerobic biodegradation of tolyltriazole (5-methyl-1 H-benzotriazole) was reported in microcosms of soil amended with tolyltriazole and/or propylene glycol based on respiration rates measured (Johnson, 1997; Baron, 1999). In addition to increased respiration rates, these authors reported a significant drop in the amount of tolyltriazole recovered from soil after a 14-d respiration study period. For

high clay soil amended with tolyltriazole at 25 mg/kg and 250 mg/kg, only 36 – 40% of the amended tolyltriazole was recovered after 14 d as compared to 85 – 90% recovered from fresh samples (Jonhson, 1997). At tolyltriazole concentrations of 25 – 1,000 mg /kg, 18 – 60% of the amended tolyltriazole was recovered after 14 d as compared to 90 – 99% recovered from fresh samples (Baron, 1999). Biodegradation was suggested since biosorption alone could not account for the observed decrease.

Kellner (1999) observed the appearance of an unknown peak accompanied by a decrease in 5-methyl-1 H-benzotriazole during HPLC analysis of soil samples exposed to 5-methyl-1 H-benzotriazole for 14 d. The retention time for this unknown peak was higher than that of 4-methyl-1 H-benzotriazole and 5-methyl-1 H-benzotriazole. It was believed that aerobic degradation of 5-methyl-1 H-benzotriazole occurred, and this unknown peak corresponded to a possible degradation product of this process. The mechanism for the aerobic generation of this compound was not known.

There is no report on the anaerobic degradation of benzotriazole and its derivatives during anaerobic treatment of ADF. In a recent paper, Gruden *et al.* (2001) conducted small-scale studies of mesophilic anaerobic co-digestion of wastewater sludge and propylene glycol spiked with the 4- and 5- isomers of tolyltriazole (100 – 1000 mg/L). The microcosms were maintained at an OLR of 6,950 – 7,500 mg COD/L/d and an SRT of 15 d. It was observed that tolyltriazole concentrations above 300 mg/L resulted in a significant decrease in methanogenic activity and volatile solids production. No degradation products of either isomers of tolyltriazole in the microcosms were detected by HPLC over an 18-month period. Further studies were still needed since these experiments were carried out in microcosms. Larger scale experiments using continuously operated reactors should provide conditions that are more favorable for the degradation of aryl triazoles.

2.7 Anaerobic Digestion

Anaerobic digestion is the cellular conversion of organic materials into carbon dioxide and methane gas, in the absence of molecular oxygen. This is a very complex process, which involves many classes of bacteria. As depicted in Figure 2–3, complex organic substrates are first hydrolyzed into simple organics in the liquefaction phase. The simple organics are converted to fatty acids by acidogenic bacteria. Acetogenic bacteria then convert organic acids having more than two carbons into acetic acid and hydrogen gas. Finally, methanogenesis occurs whereby acetic acid, hydrogen gas, and carbon dioxide are converted to methane. Two classes of methanogenic bacteria are involved. Methane generation from acetic acid involves acetoclastic methanogens, and hydrogen-utilizing methanogens produce methane from hydrogen and carbon dioxide gas.

There are two classes of methanogens that metabolize acetate. *Methanosaeta* (also known as *Methanothrix*) grows as short rods while *Methanosarcina* (referred to as *M. mazei*) grows as clumps of four or more cells (Speece, 1996). These two classes differ in their affinity for acetate (K_s) and their maximum specific utilization rates (k). *Methanosaeta* has a high substrate affinity (K_s = 20 mg/L), but a low k of 2 – 4 g COD/g volatile suspended solids (VSS)/d. In contrast, *Methanosarcina* has a low affinity for acetate (K_s = 400 mg/L), but the maximum specific utilization rate is much higher (k = 6 – 10 g COD/g VSS/d) (Speece, 1996). Photomicrographs of anaerobic reactor biomass indicated that *Methanosaeta* dominates at acetate concentrations below 70 mg/L, while *Methanosarcina* predominates above this concentration level. However, *Methanosaeta* still predominates at acetate levels above 1,000 mg/L if the bioavailability of specific trace metals such as iron, cobalt, and nickel is not satisfied (Speece, 1996).

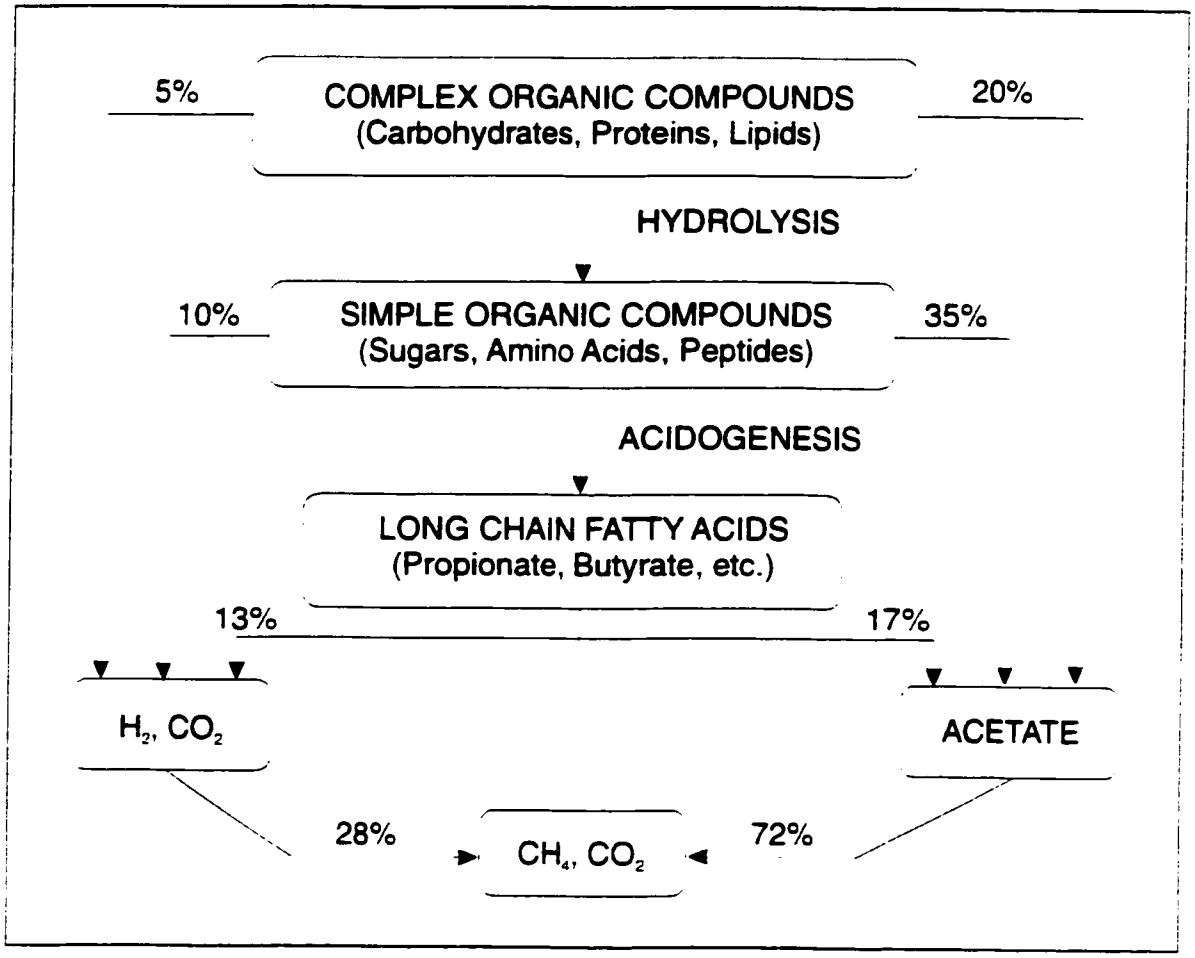

Figure 2–3 Anaerobic biotransformation of organic substances (Speece, 1996)

The success of the overall anaerobic biotransformation process is dependent on the performance of all the bacterial classes responsible for the various metabolic pathways. Methanogenesis of complex organics involves a series of metabolic steps, thus its rate is dictated by the rate-limiting step. An accumulation of a certain metabolic intermediate is reflective of the health of the bacterial class responsible for its biotransformation. In general, the acidogenesis step is much faster than the acetic and propionic acid transformation steps.

Care must often be taken to provide conditions for optimum activities of the acetic and propionic acid utilizers to ensure optimum anaerobic process performance. As

shown in Figure 2–3, about two thirds of the methane comes from acetate and one third from H_2 and CO_2. Optimum performance of hydrogen-utilizing methanogens is of paramount importance in maintaining H_2 at low levels since propionic acid biotransformation is not thermodynamically possible at H_2 partial pressures higher than 100 ppm (except in biofilms and granules; Speece, 1996). Dire consequences may result if these organic acid utilizers are not able to consume the volatile fatty acids at the rate at which they are generated. A pH drop may occur if the accumulated fatty acids and dissolved carbon dioxide exhaust the system's bicarbonate alkalinity. Furthermore, methanogenesis may cease altogether if the pH drops too low (pH < 6.2).

2.7.1 Anaerobic Digestion of ADF

In this study, the anaerobic degradation of an EG-based ADF was studied. As mentioned above, ADF mixtures are composed mostly of glycols and water. Additives are present in relatively small proportions. Thus, an understanding of the chemical pathways involved in the anaerobic degradation of EG is warranted.

The degradation of EG by bacterial enrichments under anaerobic conditions was investigated by Dwyer and Tiedje (1983). Two main metabolic stages were observed in the degradation of EG. First, EG was dismutated to generate ethanol and acetate. Once EG was depleted, ethanol was consumed to generate methane and more acetate. Further transformation of acetate was not observed.

To account for early formation of ethanol, Dwyer and Tiedje (1983) suggested the involvement of an acetaldehyde as depicted in Figure 2–4. The stoichiometric equations and metabolic pathway depicted in Figure 2–4 indicated that methane came solely from hydrogenotrophic methanogenesis and there was an accumulation of acetic acid. This acetic acid accumulation can become inhibitory to methanogenesis. However, this should not occur in UASB reactors since anaerobic granules contain a consortium of

microorganisms that can metabolize a wide range of organic substrates. In fact, it was hoped that this complex consortium of microorganisms can also metabolize ADF additives.

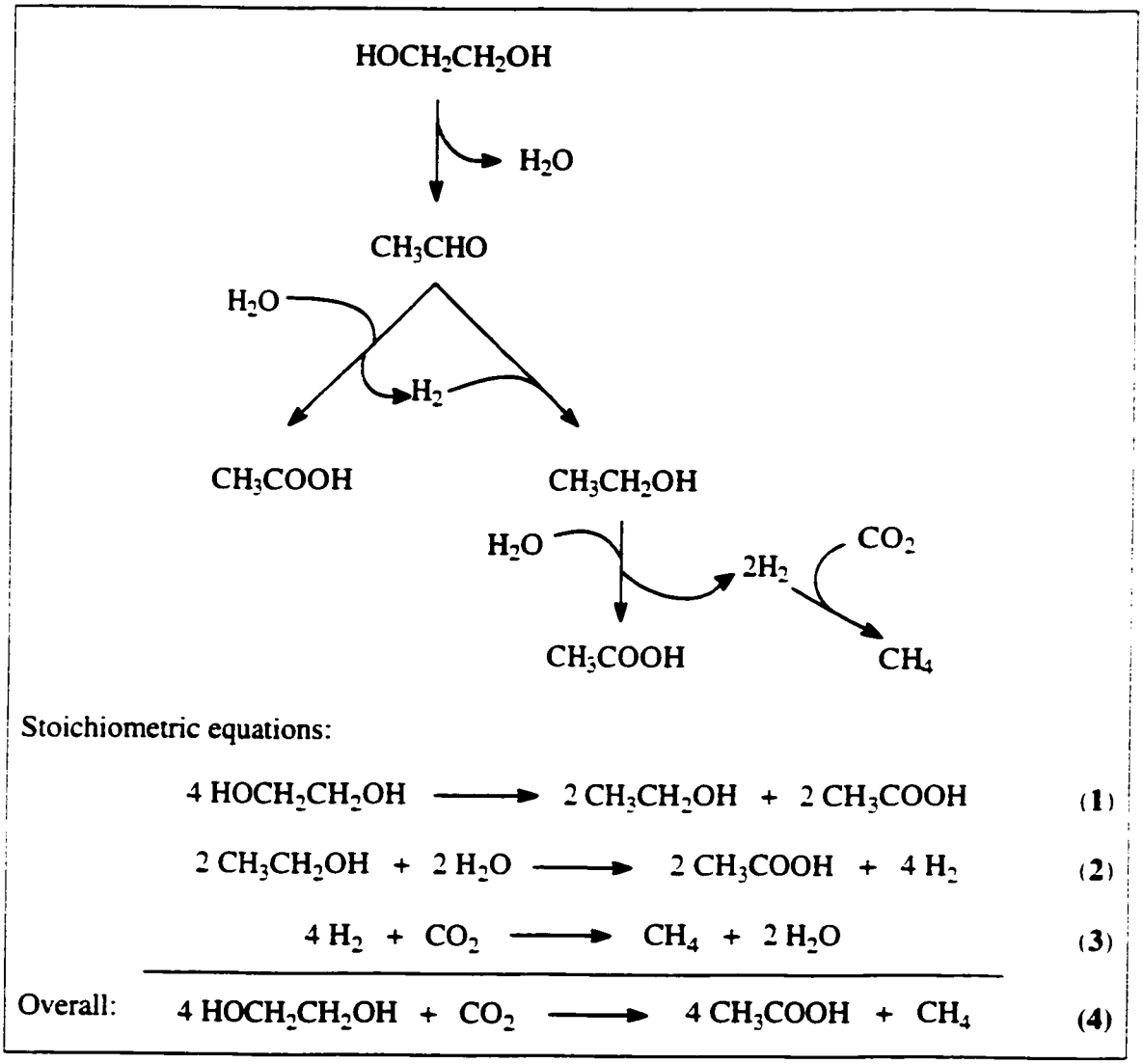

Figure 2–4 Proposed pathway and related stoichiometric equations for anaerobic degradation of EG (Dwyer and Tiedje, 1983).

The two classes of ADF additives studied in this investigation were the corrosion inhibitor aryl triazoles and the nonionic surfactant NPnEOs. There is no reported

literature on anaerobic biodegradation of benzotriazole and its derivatives. However, anaerobic degradation of tolyltriazole may be possible by initial fission of the triazole ring as depicted in Figure 2–5 (Baron, 1999). Deamination of the generated 3,4-diaminotoluene can occur at a *meta* or *para* position to give 4-aminotoluene or 3-aminotoluene, respectively. Demethylation or deamination of aminotoluene would generate aminobenzene and toluene, respectively. Biodegradation of toluene and aminobenzene is known (Rochkind-Dubinsky *et al.*, 1987).

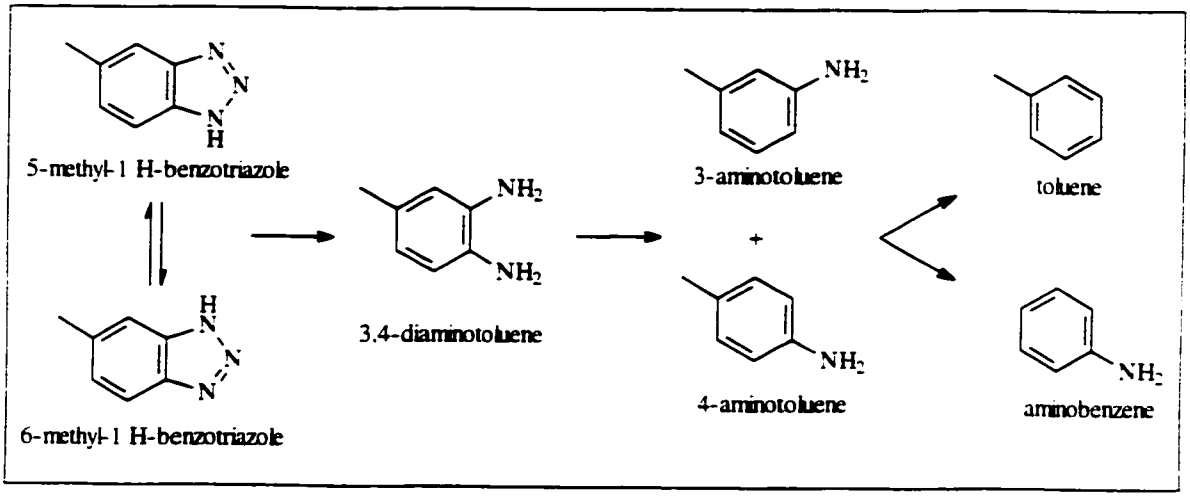

Figure 2–5 Proposed mechanism for anaerobic degradation of tolyltriazole (Baron, 1999).

NP was reported as the ultimate degradation product of NPnEO during anaerobic sewage sludge digestion (Giger *et al.*, 1984) and during batch-scale biodegradation of NPnEO (n = 1 – 2) by digester sludge, landfilled municipal solid waste, and landfilled sludge (Ejlertsson *et al.*, 1999). The actual mechanism for anaerobic degradation of NPnEO has not been reported. However, evidence for oxygen-independent acetaldehyde liberation during aerobic degradation of NPnEO by *Pseudomonas putida* was reported by John and White (1998). The proposed mechanism involved a shift of the terminal hydroxyl group, followed by hemiacetal decomposition to yield an acetaldehyde and an NPnEO homolog with one ethoxy group removed (Figure 2–6). NP2EO was the final

product of this process. It is possible that this mechanism may also take place during anaerobic degradation of NPnEO.

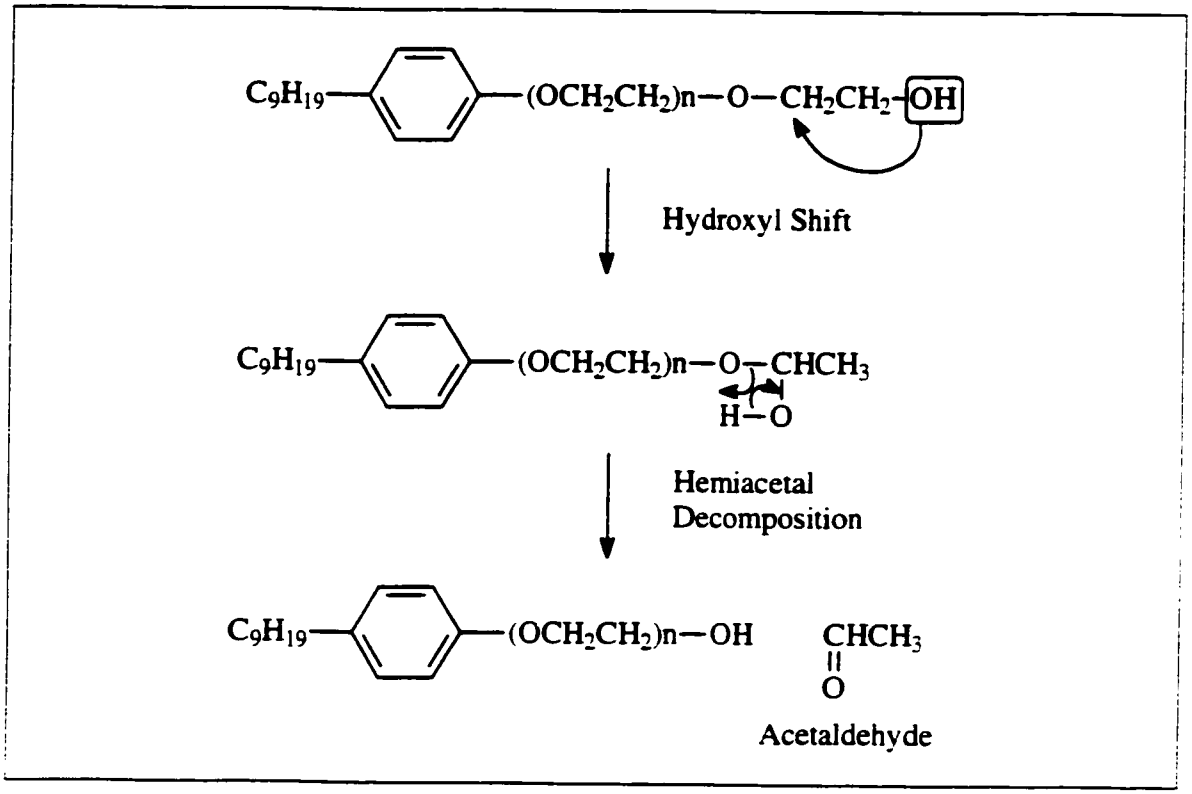

Figure 2–6 Proposed mechanism for oxygen-independent generation of acetaldehyde by *P. putida* (John and White, 1998).

Based on analogy to chlorinated phenol degradation in UASB reactors, anaerobic biodegradation of 4-nonylphenol may be difficult. Mohn and Kennedy (1992) investigated the anaerobic degradation of pentachlorophenol in UASB reactors. Complete mineralization was observed only for 2-chlorophenol. Both 3-chlorophenol and 4-chlorophenol were resistant to biodegradation. These findings suggested that dechlorination occurred preferentially at the *ortho* position.

2.7.2 Biosorption

As previously mentioned the lower homologs of NPnEO are lipophilic and may interact with anaerobic biomass through biosorption (Giger *et al.*, 1984; Ejlertsson *et al.*, 1999). In addition, sorption of tolyltriazole to soil (Keller, 1999) and to anaerobic digesting sludge (Gruden *et al.*, 2001) has been reported. It is thus important to determine the sorption capacity of anaerobic granular sludge for NP and aryl triazole.

The complexity of the biosorption process arises from the involvement of microbial cells acting as the biosorbent. Unlike sorption involving non-living materials, both the physical and biological characteristics of the biosorbent must be considered since cellular activities such as active transport may also be involved. In general, the surface area, chemical composition, lipid content, age, and species of microbes present may influence biosorption capacities. Biosorption of organic compounds has been correlated to the lipid contents of biosorbents used (Grimes and Morrison, 1975; Canton *et al.*, 1977). It was demonstrated that high biosorption capacities correspond to biosorbents having high lipid contents.

Irrespective of the mechanism involved in biosorption, the process has generally been described by the ***Freundlich equation:***

$$q = K \times c_{eq}^{\frac{1}{n}} \qquad (5)$$

where

q = sorbate concentration associated with biomass, mg/g VSS
K = Freundlich constant, L/g VSS (when $n = 1$)
c_{eq} = equilibrium concentration of sorbate in solution, mg/L
$1/n$ = exponent constant

A plot of the sorbate concentration associated with the biomass against that in solution on a log-log scale allows the determination of K and $1/n$ via linear regression.

Biosorption may play an important role in the removal of ADF additives during anaerobic treatment of ADF. It has been reported that NP interacted with anaerobic digester biomass through biosorption (Giger *et al.*, 1984; Ejlertsson *et al.*, 1999). This interaction was responsible for the high levels of NP associated with anaerobically digested sewage sludge (Brunner *et al.*, 1988; Ahel *et al.*, 1994a).

Gruden *et al.* (2001) reported significant sorption of tolyltriazole to anaerobic digesting sludge. For the tolyltriazole concentration range of 100 – 1000 mg/L and 1.5% total solids, 10 – 30% of the added tolyltriazole sorbed to the digesting sludge. The Freundlich constants for tolyltriazole biosorption to anaerobic digesting sludge at 37°C were n = 1.08 and K = 0.31. Thus, information on the sorption of ADF additives by anaerobic granules must be available to properly characterize the treatment process. To our knowledge, there are no ADF additive sorption data available for granular anaerobic biomass.

2.8 Advantages of Anaerobic Digestion

The treatability of ADF by an anaerobic system was studied since anaerobic biodegradation offers several advantages over aerobic digestion. An extensive discussion on the advantages and disadvantages of anaerobic technology is given by Speece (1996). Anaerobic digestion provides waste stabilization by transforming organic materials into carbon dioxide and methane gas. In general, microbial cell yields are only 5 – 20% of those for aerobic processes; thus, less biomass needs to be treated prior to disposal. In addition, nutrient requirements for anaerobic processes are 5 – 20% of those for aerobic processes, and there are no additional costs associated with aeration operations (500 – 2,000 kWh/1,000 kg COD for aerobic processes). As a bonus, the methane gas produced can be used as a fuel for heating or some other purpose since anaerobic digestion of one

gram of COD generates 0.35 L (STP) of methane gas (e.g., 1.000 mg/L COD consumed will increase the temperature of water by 3.3°C, assuming 100% heat transfer efficiency).

Air stripping of volatile organic pollutants from the wastewater is eliminated in anaerobic systems since there is no aeration involved. Oxygen transfer limitation is also not an issue in anaerobic systems. The substrate serves as both an electron donor and an electron acceptor allowing the treatment of high strength wastewater. With appropriate means for biomass retention, it is possible to maintain biomass concentrations 5 – 10 times that in aerobic systems (typically 3.500 mg/L MLSS for aerobic and 30.000 – 80.000 mg/L VSS for high rate anaerobic reactors). Consequently, volumetric loading rates can be 10 times higher in anaerobic treatment (5 – 10 $kg/m^3/d$ compared to 0.5 – 1 $kg/m^3/d$ for aerobic), and reactor volumes are significantly reduced. In addition, anaerobic biomass can be stored for months or years without significant deterioration in activity and are thus ideal for seasonal treatments. Furthermore, anaerobic systems have been shown to be more efficient than their aerobic counterparts in degrading certain organic contaminants such as chlorinated and surfactant wastewaters (Speece, 1996).

2.9 Upflow Anaerobic Sludge Bed Reactors

Advanced anaerobic digestion systems such as UASB reactors ensure high reactor biomass concentrations (30 – 80 g VSS/L) by making use of dense microbial granules with high settling velocities. They can operate efficiently at very high specific organic loading rates (SOLRs) and organic loading rates (OLRs) (1 – 2 kg BOD/kg MLSS/d or 20 – 60 kg $BOD/m^3/d$) and have been used successfully to treat a wide range of wastewaters.

UASB reactors were traditionally used for treatment of wastewaters from the food and related industries such as brewery, distillery, and food and fruit processing. Nowadays, UASB treatment is extended to include wastewaters from non-food related

industries such as pulp and paper, petrochemical and chemical, and sewage. It has been estimated that there are 772 full-scale UASB reactors built in the world (Macarie, 2000). Of the 772 UASB reactors, the largest percentage (21.9%) was applied to the treatment of wastewater from the brewery and malt industry. The second largest application of UASB treatment is for pulp and paper wastewater (9.7%). UASB treatment of sewage represented 7.5% of the total. Much success was also seen in the application of UASB reactors to treat petrochemical and chemical wastewaters. Some examples of full-scale UASB reactors treating high strength petrochemical and chemical wastewaters are presented in Table 2–1.

ADF wastewaters also contain high COD concentrations. In a limited study, Darlington and Kennedy (1998) demonstrated that UASB reactors can be used effectively to treat a synthetic wastewater containing ADF. It was thus of interest to perform a comprehensive study of this treatment process. A schematic diagram of a bench-scale UASB reactor is shown in Figure 3–1. As suggested by the name, an influent wastewater enters at the bottom of the reactor. Biotransformation of the organic matter occurs as the wastewater travels upward through a blanket of anaerobic granules. Plastic rings at the top of the reactor act as a gas-solids separator. Reactor mixing is provided by an internal recycle line and methane gas production. This setup is possible because the dense granules used have high settling velocities that minimize biomass washout, such that SRT is independent of HRT.

The UASB reactor is characterized as having three zones (Palns *et al.*, 1987):

1. Lower active zone – volatile acids are formed, with propionic acid reaching maximum levels at the higher boundary. High H_2 partial pressure and low pH are associated with this zone.
2. Upper active zone – H_2 partial pressure is low. COD, organic nitrogen, and volatile acids decrease to minimum levels, bringing the pH up to a stable level.

3. Upper inactive zone – there is virtually no growth: biomass is a surplus and it serves as a buffer for any changes in the loading rate.

The spatial configuration of the anaerobic granules in the UASB reactor allows the formation of microenvironments suitable for microbial activity even under unfavorable bulk conditions.

Table 2–1 Some examples of full-scale UASB reactors built worldwide for the treatment of petrochemical and chemical wastewater (Macarie, 2000).

Year of construction	Company and location	Industrial production generating the wastewater	Reactor volume m^3	Water COD g/L	Organic load kg COD/ $m^3 \cdot d$	COD removal %	Constructor
1986	DSM Chemicals Rotterdam, Netherlands	Phenol	1280	30.5	9–12	95	Biothane
1987	Shell Chemie Moerdijk, Netherlands	Methylstyrene and propene oxides	1430	20–45	10–20	80–95	Biothane
1991	Tuntex, Taiwan	Purified terephthalic acid	7000	6–13	10	55	Grontmij
1992	Bombay Dyeing Patalganga, India	dimethyl-terephthalate	1500	20	8	70	Paques
1992	Tonen Chemical Kawasaki, Japan	Maleic acid	100	13.6	17.8	90	Paques
1993	Petrocel, Mexico	dimethyl-terephthalate	2×2400	18.5	7.5	95	Biothane
1994	Akso-Nobel Emmen, Netherlands	Aramid fibers	1400	0.65	3.8	60	Paques
1996	Eastman Chemical Argentina	Polyethylene terephthalate	144	12	12	90–95	Biothane
1996	Rhône Poulec Chalampé, France	Nylon	990	16	8	80	Paques
1997	Catalana de polimers Spain	Polyethylene terephthalate	635	30	10	90	Arema

2.9.1 Anaerobic Granules

Microbial activity is responsible for the biotransformation of organic matter in wastewaters during biological treatment. High volumetric loading rates are possible if high biomass concentrations can be maintained in the reactors. In high rate UASB reactors, high biomass concentrations are achieved by using dense settleable microbial granules. These granules contain a consortium of anaerobic microorganisms in an optimal spatial configuration.

For UASB reactors treating high strength wastewaters, *Methanosarcina* is expected to dominate in the outer layers of the granules. *Methanosaeta* predominates in the interior of the granules where acetate concentrations are low (Speece, 1996). This layered structure offers great benefits to the degradation of hydrogen-producing substrates such as propionate and ethanol. The proximity of different classes of bacteria within the granules allows metabolites generated by one group to be consumed immediately by another group. This allows the formation of microenvironments within the granules where H_2 partial pressures are lower than 100 ppm. Consequently, propionate conversion can still proceed within the granules even if the bulk H_2 partial pressure is above 100 ppm. Evidence for predominance of propionate-degrading bacteria inside the granules was reported by Guiot *et al.* (1992).

2.9.2 Sludge Granulation and Settleability

Aggregation of a consortium of microorganisms to form densely packed granules with high settling velocity allows the SRT to be independent of HRT, a characteristic that is unique to high-rate anaerobic systems such as UASB reactors. Anaerobic granules with high settling velocity are desired since good biomass inventory can be maintained even at high volumetric loading rates. A high biomass inventory ensures good microbial activity, allowing high SOLR to be achieved while reactor volumes remain relatively small.

The settling velocity of anaerobic granules is known to be affected by the type of organic substrate present in the wastewater. In general, carbohydrate wastewaters generate anaerobic granules with high settling velocity, while protein and petrochemical wastewaters produce lower settleable granules (Speece, 1996). The phenomenon of anaerobic sludge granulation was investigated by Hulshoff Pol (1989). The microbial composition of the anaerobic granular sludge was affected by the volatile acid concentration (VFA). VFA (acetate, propionate, and butyrate) concentrations of 10,000 mg COD/L resulted in granules consisting mainly of undesirable *Methanosarcina*. Acetate concentrations below 150 mg/L were recommended for the development of *Methanosaeta* granules.

2.9.3 Kinetic Constants

The rate of bacterial growth in the UASB reactor can be defined based on the Monod substrate limited growth equation as

$$r_g = \frac{\mu_{max} XS}{K_S + S} \tag{6}$$

where r_g = rate of bacterial growth, g VSS/ L/d
μ_{max} = maximum specific growth rate, d^{-1}
X = active biomass concentration in the reactor, g VSS/L
S = growth-limiting substrate concentration, g COD/L
K_S = half-velocity constant, g COD/L.

This rate of bacterial growth is related to the rate of substrate utilization:

$$r_g = -Yr_{SU} \tag{7}$$

where r_{SU} = rate of substrate utilization, g COD/L/d
Y = cell yield coefficient, g VSS/g COD.

Substituting equation **6** into **7** gives

$$r_{SU} = -\frac{\mu_{max} XS}{Y(K_S + S)} \tag{8}$$

Equation **8** can be written as

$$r_{SU} = -\frac{kXS}{K_S + S} \tag{9}$$

or

$$r_{SU} = -\frac{k'S}{K_S + S} \tag{10}$$

where k = maximum specific rate of substrate utilization, g COD/g VSS/d
k' = maximum rate of substrate utilization, g COD/L/d.

Both equations **9** and **10** have been found to be applicable in a wide variety of wastewater treatment systems. The X term in equation **9** should be the actual active biomass concentration; however, it is more difficult to measure. Often, the X term is approximated by the VSS concentration. Under substrate limiting conditions, active biomass concentrations in reactors have been found to remain relatively constant, though the total biomass increases as the amount of solids in the reactor is increased. This makes the direct relation between VSS concentration and rate of substrate utilization less appropriate. Consequently, the kinetic model that best describes operational data should be used (Droste, 1997).

A mass balance performed on the reactor biomass incorporating endogenous decay gives the general equation

$$\frac{dX}{dt}V_r = QX_0 - QX_e + V_r(-Yr_{SU} - k_d X) \tag{11}$$

where V_r = reactor volume, L
Q = flow rate, L/d
X_0 = biomass concentration in the feed, g VSS/L
X_e = biomass concentration in the effluent, g VSS/L
k_d = endogenous decay coefficient, d^{-1}.

At steady state, dX/dt is zero. Since the biomass concentration in the feed is negligible, equation **11** can be simplified and rearranged to

$$\frac{QX_e}{V_r X} = \frac{1}{\theta_c} = -Y\frac{r_{SU}}{X} - k_d = YU - k_d \tag{12}$$

where θ_c = solids retention time (SRT), d

U = specific substrate utilization rate, g COD/g VSS/d.

The term $1/\theta_c$ refers to the net specific growth rate. The biomass yield coefficient Y and the endogenous decay coefficient k_d can be determined by plotting the net specific growth rate $1/\theta_c$ against the specific substrate utilization rate U.

In complete mixed systems, the SRT is equal to the HRT. Thus, the net specific growth rate is equal to HRT^{-1} or SRT^{-1}. For the UASB reactor, the granular anaerobic sludge has very high settling velocity. Thus, SRT is much larger than HRT and the specific growth rate is equal to SRT^{-1}. If sludge settleability remains relatively constant, a washout factor f can be used to relate SRT to HRT for different influent substrate concentrations:

$$f = \frac{\Delta HRT}{\Delta SRT} \tag{13}$$

The determination of the washout factor will allow reactor performance to be readily assessed by easily measured parameters such as HRT and SRT.

Graphical determination of the constants k (or k') and K_S, can be done by rearranging equations **9** and **10** to the linear Lineweaver-Burke form:

$$-\frac{X}{r_{SU}} = \frac{1}{U} = \frac{K_S}{k}\frac{1}{S} + \frac{1}{k}. \tag{14}$$

$$-\frac{1}{r_{SU}} = \frac{K_S}{k'}\frac{1}{S} + \frac{1}{k'}. \tag{15}$$

The slopes and intercepts of the Lineweaver-Burke plots ($1/U$ versus $1/S$ or $-1/r_{SU}$ versus $1/S$) define the constants. Once k (or k') and Y are known, the maximum growth rate μ_{max} for anaerobic granules treating ADF can be determined by

$$\mu_{max} = kY \quad \text{or} \quad \mu_{max} = k'XY. \tag{16}$$

The purpose of the above equations is to provide kinetic constants such as K_S and k, which are often reported for biological systems. It is not planned that these kinetic

constants be used in the development of mechanistic models to predict reactor performance. Empirical models predicting the effects of ADF concentration, HRT, and biomass concentration on reactor performance will be developed based on statistical experimental design.

2.10 Statistical Experimental Design

In UASB reactors, performance is affected by operating variables such as substrate concentration, HRT, and biomass concentration. One way to describe the effects of operating variables on a process response, y, is by a mathematical model. This can be accomplished through the use of statistical experimental design and response surface methodology.

2.10.1 Factorial Design

A 2^3 factorial design can be used to investigate the effects of three operating variables (ADF concentration, HRT, and biomass concentration) on the process response y (COD removal efficiency, biomass activity, and methane production rate and potential). The first-order linear model of the form:

$$y = \beta_0 + \beta_1 x_1 + \beta_2 x_2 + \beta_3 x_3 + \beta_{12} x_1 x_2 + \beta_{13} x_1 x_3 + \beta_{23} x_2 x_3 + \beta_{123} x_1 x_2 x_3 \qquad (17)$$

where β_i is a model parameter and x_i is a coded value of operating variable i, can be fitted to experimental data. Operating variables are coded to give x_i a value of -1, 0, or $+1$. The parameter β_i is indicative of the type of effect the corresponding operating variable has on the process response, while β_{ij} and β_{ijk} are indicative of interaction effects. A 2^3 factorial design, having eight experimental runs can be used to estimate the eight model parameters in equation **17**. However, center-point replicates ($x_i = 0$) are required for estimation of pure error variance and testing the model for lack of fit. Without the

center-point replicates the model will necessarily fit the data exactly. A typical 2^3 factorial design with four center replicates is shown in Table 2–2.

Table 2–2 A 2^3 factorial design in coded variables with center-point replicates*.

Runs	x_1	x_2	x_3	Runs	x_1	x_2	x_3
1	−1	−1	−1	7	−1	+1	+1
2	+1	−1	−1	8	+1	+1	+1
3	−1	+1	−1	9	0	0	0
4	+1	+1	−1	10	0	0	0
5	−1	−1	+1	11	0	0	0
6	+1	−1	+1	12	0	0	0

*Runs 9 – 12 represent center-point replicates.

The first-order linear model **17** can fitted to the results of the first eight runs in Table 2–2. From this model, the estimated parameter $\hat{\beta}_0$ can be compared with the average response of the four center-point replicates. If the two values are significantly different, this indicates that the response surface is nonlinear in the design region, and an extension of the model is required (*vide infra*). If, however, the two values are similar, the response surface is linear in the design region, and there is no need to extend the model further. A better fit of model **17** can be obtained by fitting it to all 12 run results (factorial design plus center-point replicates).

Since an estimate of the pure error variance is available, a $100(1 - \alpha)\%$ confidence interval for the estimated parameters can be determined. This exercise can also be used to eliminate any terms that contain a plausible value of zero in the confidence interval. The elimination of unnecessary terms is desirable since they cannot be said to have an effect on the response with any certainty, and the variance of model predictions will be unnecessarily inflated if left in the model. If terms can, in fact, be eliminated, then it is very important that the new model is checked for lack of fit. It must

also be remembered that the effects found to be insignificant may, in fact, have an effect on the response, but it is too small to be detected through the experimental error (noise).

To qualitatively test for lack of fit, an estimate of the pure error variance is required. For a design with four center-point replicates, an estimate of the pure error variance ($\hat{\sigma}^2$) with three degrees of freedom can be determined by

$$\hat{\sigma}^2 = \sum_{u=1}^{4} \frac{(y_u - \bar{y})}{4-1} \tag{18}$$

where y_u is the measured response value for an individual center point and $\bar{y}$ is the sample mean of all the measured response values at the center point. If multiple reactors are used, this estimate of pure error variance will give an indication of the degree of variation among the reactors and runs at the same conditions. If it is small then differences in response at other run conditions can be regarded as being reflective of the run conditions. On the other hand, if the variance is large, then the variation in reactor performance is significant and the confidence interval for the true value of the response will be large (true value of the response has a high degree of uncertainty). The latter case has a major drawback in that only large effects can be detected, whereas minor effects will be masked by random errors.

An overall measure of lack of fit is given by the residual (e_u) sum of squares for the fitted model, which has $(n - p)$ degrees of freedom and is given by

$$\sum_{u=1}^{n} e_u^2 = \sum_{u=1}^{n} (y_u - \hat{y}_u)^2 \tag{19}$$

where $\hat{y}_u$ is the model predicted response, n is the number of runs, and p is the number of parameters. Lack of fit can be evaluated by comparing the ratio of lack-of-fit variance to pure error variance (*LFR*), given by

$$LFR = \frac{\text{lack of fit}}{\text{pure error}} = \frac{\left(\sum_{u=1}^{4} e_u^2 - \nu_2 \hat{\sigma}^2 \right) \Big/ (n - p - \nu_2)}{\hat{\sigma}^2} \tag{20}$$

where $\nu_2 = m - 1$

with $F_{\nu_1,\nu_2,\alpha}$ where α is the probability level of the test. If *LFR* is larger than $F_{\nu_1,\nu_2,\alpha}$ then the lack of fit is significant. It must be noted that the number of degrees of freedom associated with the lack of fit term is only one. Thus, this quantitative test for lack of fit is not very sensitive.

To augment the quantitative lack of fit test, residual plots must be prepared. Lack of fit is indicated by trends in residual plots. A plot of the residual (e_u) against the predicted response should indicate the presence of outliers should they exist. Detection of time trends can be determined by examining the plot of residual against run order. Model deficiency can be detected by the presence of curvature in the plot of the residual against an operating variable.

If outliers are present, they can be discarded if, and only if, they can be explained in light of the laboratory records kept. The presence of time trends can be corrected by the addition of a term βt_u, where t_u is the time of observation. Model deficiency can be dealt with by adding more terms. In this case, second-order terms can be added to model **17** by extending the 2^3 factorial design to a central composite design.

2.10.2 Central Composite Design

Extension of the 2^3 factorial design with center points to a central composite design is accomplished by adding a star portion to the factorial design. The above empirical model **17** is extended to

$$y = \beta_0 + \beta_1 x_1 + \beta_2 x_2 + \beta_3 x_3 + \beta_{11} x_1^2 + \beta_{22} x_2^2 + \beta_{33} x_3^2 + \beta_{12} x_1 x_2 + \beta_{13} x_1 x_3 + \beta_{23} x_2 x_3 \qquad (21)$$

The star portion of the central composite design is normally arranged as "a one factor at a time experiment" where each factor (x_i) is tried in turn at both a high (α) and a low ($-\alpha$) level, while all other factors are kept at a central level (Hartley, 1959). The

value of α is chosen such that the design becomes *rotatable* and this condition occurs when

$$\alpha = \left(\frac{2kn_c}{n_s} \right)^{\frac{1}{4}} \tag{22}$$

where k is the number of factors in the design
n_c is the number of points in the factorial portion of the design
n_s is the number of points in the star portion of the design (Draper, 1982).

In this case, $k = 3$, $n_c = 8$, $n_s = 6$, and thus $\alpha = 1.682$. For a proper central composite design, the three operating variables under study must be carried out at a total of five levels ($\pm\alpha$, ± 1, and 0). The star portion of a typical central composite design is shown in Table 2–3.

Table 2–3 Star portion of a typical central composite design.

Run	x_1	x_2	x_3
1	−1.682	0	0
2	+1.682	0	0
3	0	−1.682	0
4	0	+1.682	0
5	0	0	−1.682
6	0	0	+1.682

The number of center points necessary for the central composite design has been suggested differently by several authors (Dykstra, 1960; Lucas, 1977; Draper, 1982). Different criteria are used to determine the number center points required, and later works indicate the need for fewer center points (Draper, 1982). Thus, extension of model **17** to model **21** by central composite design would only need three center-point replications as suggested by Draper (1982). This would introduce the possibility of increasing variability away from the center point. However, partial duplication of the factorial portion, or partial duplication of the star portion of the design as suggested by Dykstra (1960) would involve too many experimental runs. Furthermore, β_0 is the average

process response (percent COD removal) for the design conditions. Since the actual percent COD removal is of major importance, precision in β_0 is desired. With the addition of the star portion, the parameter estimates of the new model **21** are no longer uncorrelated like those of model **17** (see Appendix A). Model adequacy must again be evaluated as described for the factorial design.

3 Materials and Methods

Two types of experiments were conducted during the course of this study to investigate the continuous and batch anaerobic degradation of ADF. Different batch experiments were performed to determine the fate and effects of NP/NPnEO and aryl triazole during anaerobic degradation of ADF. Sorption experiments were conducted to account for any physical removal of these additives during the treatment process. Since EG is the main component of ADF, the effects of NP/NPnEO and aryl triazole on the degradation rates of EG and its metabolic intermediates were also investigated. Anaerobic treatment of ADF was evaluated by continuous operation of four bench-scale UASB reactors. A total of 23 experimental runs at 17 different run conditions were carried out.

3.1 Batch Experiments

Batch tests were carried out in the dark at 35°C in 160–mL glass serum bottles. EG (polymer grade) and Tergitol NP-4 (NPnEO, n = 1 – 16) were provided by Union Carbide Corporation (USA). Refer to Appendix C for the composition of Tergitol NP-4. Technical grade NP and reagent grade aryl triazoles (Sigma-Aldrich) were used as HPLC standards. Solvents used were HPLC grade (VWR Canlab).

3.1.1 Additive Stock Solutions

NP and Tergitol NP-4 standards were prepared by diluting known amounts in HPLC grade methanol. Benzotriazole (BT), 5-methyl-1 H-benzotriazole (MeBT), and 5,6-dimethyl-1 H-benzotriazole (DiMeBT) had low solubility in water. Consequently, EG was added to aid dissolution (250 g/L EG for BT and MeBT and 500 g/L EG for DiMeBT). Milli-Q water was used in the preparation of aryl triazole standards.

3.1.2 Biosorption Experiments

Biosorption experiments were carried out at 35°C with anaerobic granular biomass concentrations of approximately 3 g VSS/L. Biomass dilution was achieved by adding 0.01 N NaOH (pH 7.5). Appropriate amounts of additive stock solutions were added to 100 mL diluted biomass samples to give five different concentrations of test chemicals. Sample bottles were sealed with crimp caps containing Teflon-coated inserts and then shaken at 100 rpm for the length of time required for biosorption to reach equilibrium. The incubation time was 7 days for NP and one day for aryl triazole. For NP sorption, inhibited anaerobic granular biomass was also tested. Biomass inhibition was achieved by shaking the diluted granular biomass with 5% NaN_3 (sodium azide) overnight.

3.1.3 Ethylene Glycol Degradation

EG degradation experiments were conducted at 35°C. ADF-acclimated anaerobic granular biomass was diluted with defined medium (see Table 3–1) to give biomass concentrations of approximately 3 g VSS/L. Sample bottles containing 100 mg/L diluted biomass and 1.5 g/L EG were shaken at 100 rpm. Three different concentration levels for the additives (NP, NP-4, BT, MeBT, and DiMeBT) were added to investigate their effects on the degradation of 1.5 g/L EG.

3.1.4 Anaerobic Toxicity Assay (ATA)

Anaerobic toxicity assays were carried out by known procedures (Speece, 1996). Anaerobic granular sludge was diluted with defined medium (see Table 3–1) to give biomass concentrations of approximately 10 g VSS/L. The effect of ADF (up to 8%) on mesophilic (35°C) methanogenesis of acetate and propionate (3:1 mixture, approximately 2000 mg COD/L) by 50 mL diluted biomass was investigated. Samples were shaken at 100 rpm and biogas volumes were measured after 24 hours. Subsequent gas

measurements were carried out every other day until gas production slowed down. Evidence for inhibitory effects of the test substrate was reflected in the lower gas production by test bottles as compared to that of controls.

Table 3–1 Composition of aqueous defined medium for acetoclastic activity tests.

Component	Concentration (mg/L)
NaCl	500
$CaCl_2 \cdot 2H_2O$	100
NH_4Cl	1894
$MgCl_2 \cdot 6H_2O$	100
$(NH_4)_6Mo_7O_{24} \cdot 4H_2O$	10
$ZnSO_4 \cdot 7H_2O$	0.1
H_3BO_3	0.3
$FeCl_2 \cdot 4H_2O$	1.5
$CoCl_2 \cdot 6H_2O$	10
$MnCl_2 \cdot 4H_2O$	0.03
$NiCl_2 \cdot 6H_2O$	0.03
$AlK(SO_4)_2 \cdot 12H_2O$	0.1
Nicotinic acid	0.1
Cyanocobalamine	0.1
Thiamine	0.05
p-aminobenzoic acid	0.05
Pyridoxine	0.25
Pantothenic acid	0.025
KH_2PO_4	500
Resazurin	1.5
2-Methyl-*n*-butyric acid	102
$NaHCO_3$	3400

3.1.5 Analytical Methods

3.1.5.1 EG and EG Metabolic Intermediates

EG content of test bottles was determined by gas chromatography (GC). Two gas chromatographs were used in this study. Determination of EG and its metabolic

intermediates during EG degradation in the presence of additives (NP, NP-4, BT, MeBT, and DiMeBT) was carried out on the GC used for VFA determination (see section 3.2.4.2). Analyte quantification could not be performed based on the internal standard method since EG co-eluted with the internal standard isobutyric acid. Analysis was done using an external standard method (i.e., samples were centrifuged and the supernatant was injected without the addition of the internal standard). Analyte quantification was based on the data shown in Table 3–2.

Table 3–2 Calibration data for GC analysis of EG and its metabolic intermediates.

RT (min)	2.16	3.56	6.1	8.47	10.7
	Peak area				
mg/L	Ethanol	Acetic	Propionic	EG	Butyric
50	8960	4405	7186	4970	8408
100	17700	8528	14320	9832	16490
250	44250	21350	36630	25500	42020
500	89660	42730	71820	49960	80300
1000	177700	84820	139100	102500	160900
2000	347200	169500	279000	216800	314300
	Ethanol	Acetic	Propionic	EG	Butyric
Slope	0.005724	0.011791	0.007157	0.009357	0.006322
Deviation	0.000028	0.000011	0.000027	0.000111	0.000035
r^2	0.999770	0.999991	0.999863	0.998654	0.999714

For the analysis of EG and its metabolic intermediates in ATA test bottles, an internal standard method was used. Samples from test bottles were centrifuged at 5000 rpm for 5 min and the supernatant was diluted with Milli-Q water to give analyte concentrations below 500 mg/L. Equal volumes of an isobutyric acid internal standard (100 mg/L) were then added to the diluted samples prior to analysis. Sample analysis was performed on an Agilent 6090 gas chromatograph equipped with a model 7683 autosampler and a flame ionization detector. Analysis was done in splitless mode with a

temperature program: 40°C (hold 5 min) to 180°C at 35°C/min; hold at 180°C for 3 min. The total run time was 12 min. Injection temperature was 250°C and detector temperature was 300°C. Helium gas carrier passed through the HP-INNOWax capillary column (30 m × 0.25 mm, 0.50 µm film thickness) at a linear velocity of 36 cm/s. The injection volume was 1 µL.

3.1.5.2 Triazole Determination

Analysis of ADF additives was performed on a Hewlett-Packard 1100 liquid chromatograph. Analysis of aryl triazole additives was based on the method of Schmitt and Muzher (1981). Reverse phase high pressure liquid chromatography (HPLC) was carried out at isocratic conditions on an HP Zorbax® Eclipse XDB-C8 (4.6 × 150 mm) column. The mobile phase was composed of 40% methanol and 60% 0.08 M sodium acetate (pH 6). The analysis run time was 12 min and the mobile phase flow rate was 1.5 mL/min. Samples were filtered through 0.45 µm membrane filters (VWR Canlab) before injection. The detection limit was less than 1 mg/L and error of measurement was 0.1 mg/L for DiMeBT and 2 mg/L for MeBT and BT.

3.1.5.3 NP/NPnEO Determination

HPLC quantification of NP and NPnEO was based on the procedure by Varineau and Charminsky, (1995). Normal phase HPLC was carried out on a Supelcosil™ LC-NH_2 (25 cm × 4.6 mm) column. The elution profile used is presented in Table 3–3. An extractive steam distillation method outlined by Kubeck and Naylor (1990) was used to concentrate NP and NPnEO (n = 1 – 3) in the aqueous samples. Based on this method, up to 1 L of aqueous sample was refluxed with 2 mL of iso-octane (HPLC grade) for 1 h in a Nielson-Kryger apparatus (Ace Glass). The iso-octane fraction was injected directly, without further manipulation. The detection limit was 16 mg/L NP and the error of

measurement was 20 mg/L NP. Aqueous NP concentrations up to 500-fold lower than the detection limit can be measured using the extractive steam distillation method.

Table 3–3 Elution profile for HPLC analysis of NP and NPnEO.

Time (min)	% Hexane	% THF*	% Isopropanol	% Water	Flow (mL/min)
0	88	9	3	0	0.75
3	88	9	3	0	0.75
7	81.7	8.2	10.1	0.9	0.781
10	88	9	3	0	0.75
19	88	9	3	0	0.75

* THF = tetrahydrofuran

3.2 Continuous Experiments

The aircraft deicing fluid used in the study was UCAR XL 54 ADF (Union Carbide Canada Inc., Quebec). This deicing fluid was composed of 54% EG, 45.5% water, and 0.5% proprietary additives, and it exerted a COD in the range of 700 –800 g/L. Bicarbonate salt buffers (VWR Canlab) for feed synthesis were technical grade. All other chemicals used were reagent grade obtained from Sigma–Aldrich.

3.2.1 Apparatus

A total of four bench-scale UASB reactors (glass reactor with glass sealed top, ID = 12.5 cm, H = 57 cm, and a 6-L working volume) were operated in continuous mode during the course of the study. The reactors were seeded with various concentrations of anaerobic granular biomass obtained from Lake Utopia Paper (New Brunswick, Canada), a chemical thermal mechanical pulp treatment plant. Each reactor was equipped with an internal liquid recycling line at a 1:4 feed to recycling ratio. Plastic 2 cm Koch Flexi rings (72 g) were added to each reactor as solids/gas deflectors. As depicted by the schematic diagram presented in Figure 3–1, the wastewater feed for the four reactors was drawn from an insulated main feed circulation line. The wastewater flowed upward

through a bed of active anaerobic granular biomass and the treated effluent exited the reactor through the effluent overflow. Biogas production volumes were measured by wet tip gas meters installed at the top of the reactors. Gas, liquid, and solid samplings for analysis were done through various sampling ports located on the reactors.

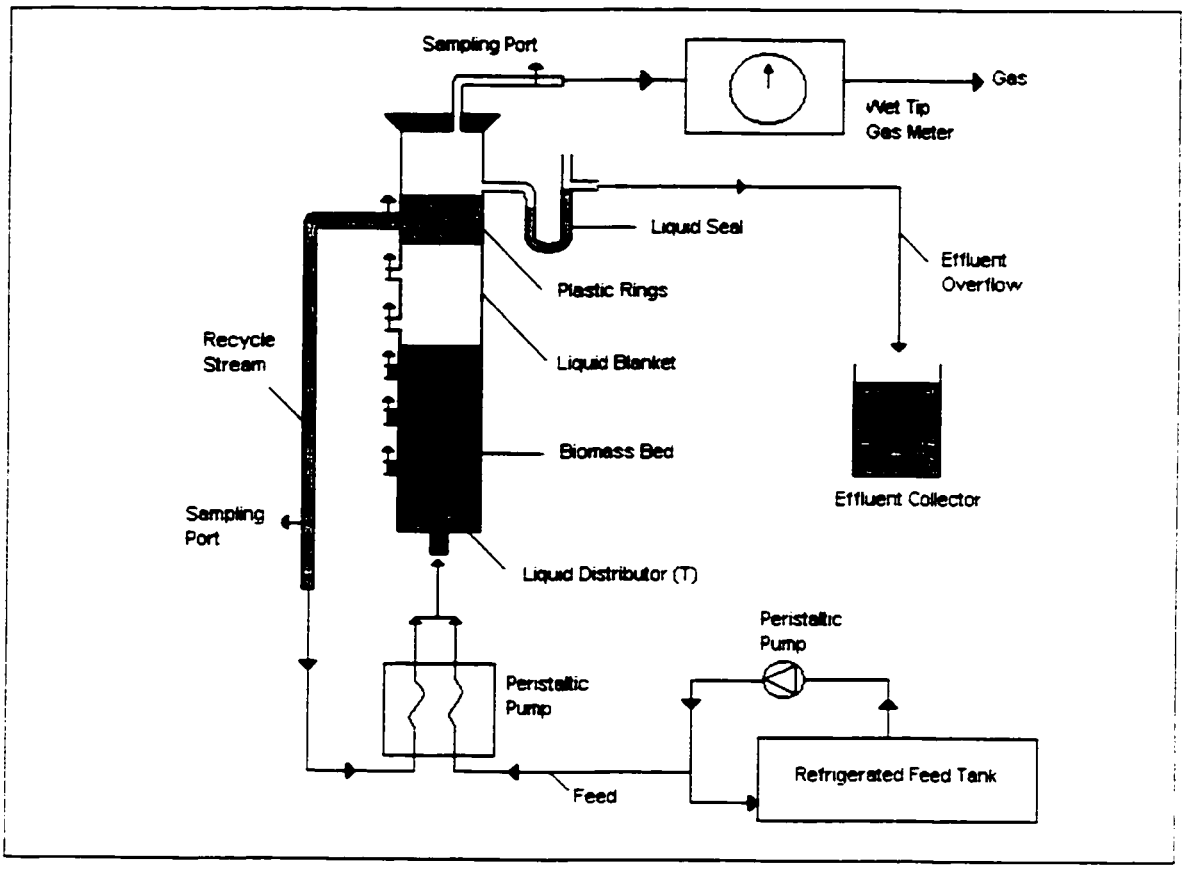

Figure 3–1 Schematic diagram of a bench-scale UASB reactor used in this study.

The four UASB reactors were mounted along one wall of a temperature controlled room (33 ± 2°C) as shown in Figure 3–2. The anaerobic treatment process did not produce any heat and acclimation of seed biomass to ADF feed was carried out prior to experimentation. The reactors were fed 1% ADF at low flow rates (6 d HRT) and gradually increased to a 2 d HRT in a period of two weeks. Reactor pH and volatile fatty acid (VFA) concentrations (>500 mg/L acetate) were closely monitored for signs of

reactor stress. In addition, a 23–L rectangular reactor seeded with 9 L granular biomass was setup where ADF feed was fed in semi-batch mode. The purpose of this fifth reactor was to provide a reserve of ADF-acclimated biomass. This biomass reserve could be used to replace washout biomass during the operation of the UASB reactors.

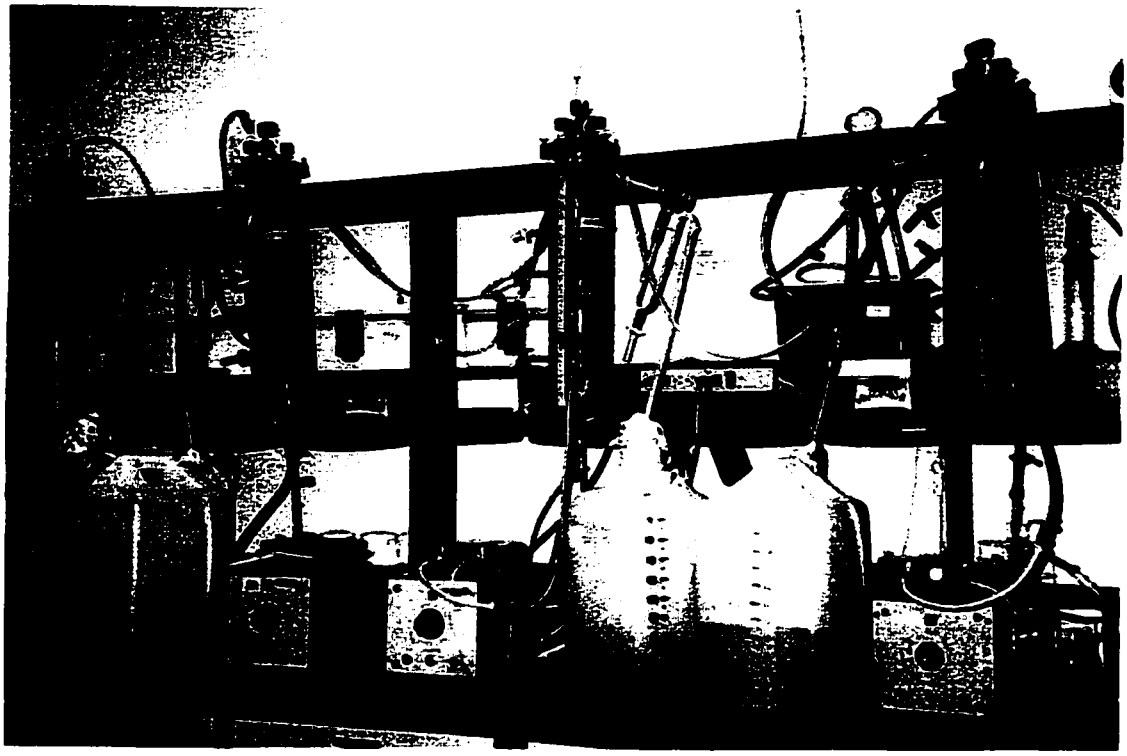

Figure 3–2 Photograph of the four bench-scale UASB reactors used in the ADF treatability study.

3.2.2 Experimental Program

It was of interest to determine how the ADF treatment process was affected by three operating variables: ADF concentration, HRT, and biomass concentration. Since the nature of the experiment required at least 4 – 5 weeks to complete a run (two weeks at steady state, plus time to reach steady state), it was important to minimize the number of runs and still retain important information. This was achieved through the use of the

statistical experimental design outlined in Chapter 3. A detailed discussion on run orders and run conditions followed in this study is described in Chapter 5.

During the course of the study, a total of 23 runs at 17 different run conditions were carried out. Reactors were operated continuously with minimum down-time between run conditions. Reactor performance was assessed based on measurements made during steady-state conditions. The reactor was considered to have reached steady state when VFA concentrations reached constant levels (changes not more than 50% since most of the time, VFA concentrations remained below 100 mg/L and the uncertainty associated with analytical method used was 50 mg/L; see Figure 4–32 for a sample of the VFA profile). Gradual transitions from low to high OLR were carried out to avoid reactor stress, as shown for reactor TP4 in Figure 3–3.

In general, the wastewater flow rate was increased by 5 – 10% each day at a constant ADF concentration, or the ADF concentration was increased by an increment of 0.1% ADF per day at a constant HRT. During these transition periods, the reactor VFA concentration and pH were carefully monitored. If VFA concentrations increased above 500 mg/L acetate, the feed flow rate was reduced. The reactor pH was measured on an hourly basis if the acetate concentration reached above 1000 mg/L. If the pH dropped below 7.0, the reactor was placed on complete recycling mode. Feeding was resumed at a lower rate of change of HRT when VFA concentrations decreased below 500 mg/L acetate and a neutral pH was re-established. Consequently, transition periods can be in the order of months (e.g., near the end of Figure 3–3) if pump failures occurred.

To ensure consistency in wastewater composition, ADF feed was synthesized every other day. Reactor HRTs were determined based on the amount of effluent collected daily. COD and suspended solid (SS) measurements for feed and effluent samples were taken only when the reactor reached steady state. The methane content of the reactor biogas was also determined for steady-state conditions.

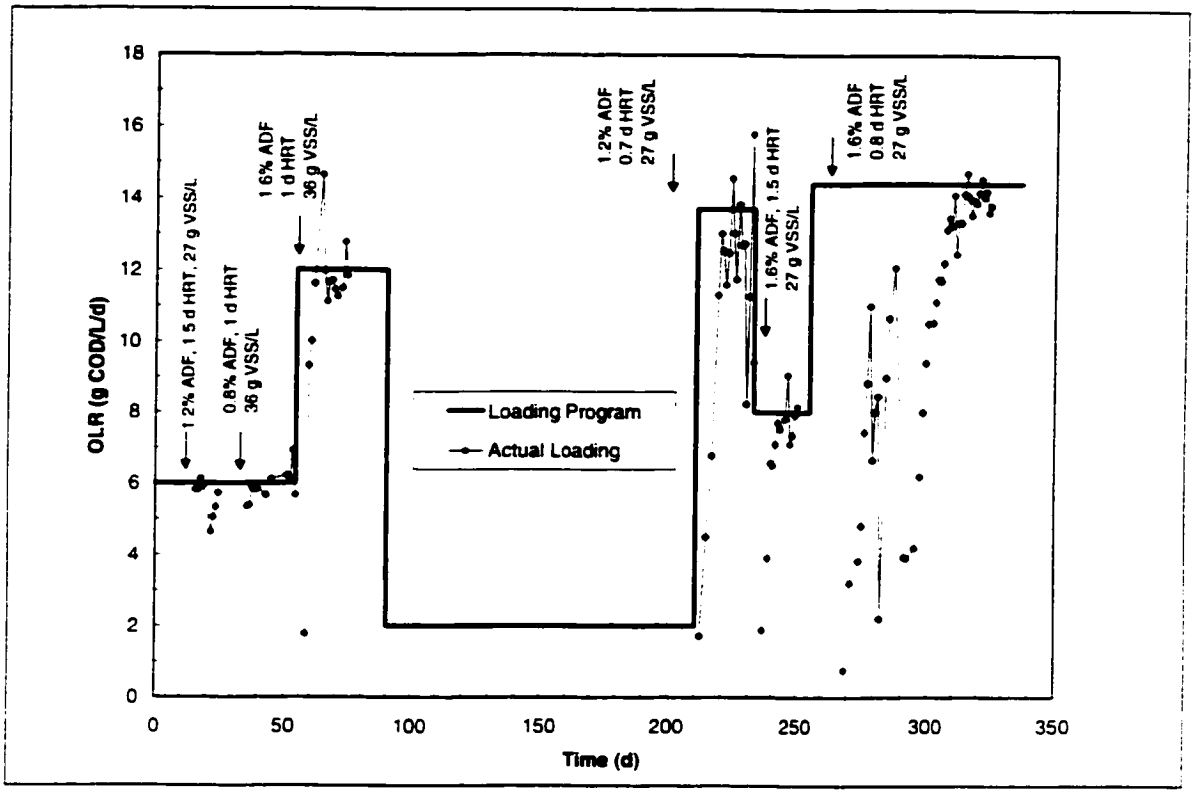

Figure 3–3 Organic loading program for reactor TP4 during the course of the study.

3.2.3 Feed Composition

The carbon source in the ADF wastewater was EG. The COD of concentrated UCAR XL 54 ADF was 700 – 800 g/L. Experiments were conducted at ADF concentrations of 0.8%, 1.2%, and 1.6% (v/v). This concentration range corresponded to feed COD levels of 6 – 12 g/L. Required nutrients and buffering capacities were added as shown in Table 3–4 to give a COD:N:P ratio of 102:5:1 (weight basis). Yeast extract was added to satisfy micronutrient requirements.

3.2.3.1 Acetoclastic Activity Tests

Biomass acetoclastic activity was also determined at the completion of each steady state, based on known procedures (Speece, 1996). Anaerobic granular biomass (10 mL) from UASB reactors were anaerobically transferred to 160–mL glass serum

bottles and diluted with 30 mL defined medium (see Table 3–1) to give a biomass concentration of approximately 10 g VSS/L. The sealed and capped serum bottles were shaken in the dark at 100 rpm and 35°C overnight. Acetic acid (0.2 mL, see Table 3–5) was injected into the bottles to give initial acetate concentrations in the range of 1200 – 1500 mg/L. Acetate consumption rates were determined by monitoring the change in acetate concentration over time.

Table 3–4 Composition of synthetic ADF feed for the treatability study.

	0.8% ADF	1.2% ADF	1.6% ADF
COD (g/L)	6.4	9.1	11.8
NH_4HCO_3 (g/L)	1.28	1.92	2.56
$NaHCO_3$ (g/L)	2.48	2.37	2.26
KH_2CO_3 (g/L)	2.98	2.61	2.32
$(NH_4)_2SO_4$ (g/L)	0.32	0.48	0.64
K_2HPO_4 (g/L)	0.17	0.25	0.33
KH_2PO_4 (g/L)	0.13	0.19	0.26
Yeast Extract (g/L)	0.06	0.10	0.13

Table 3–5 Acetic acid stock solution for acetoclastic activity tests.

Component	Concentration (g/L)
Ammonium acetate	31.3
Potassium acetate	41.4
Sodium acetate	46.2
Glacial acetic acid	16.8

3.2.4 Analytical Methods

3.2.4.1 Biogas Composition

The methane and carbon dioxide content of reactor biogas was determined by the GC method of van Huyssteen (1967), using a Hewlett-Packard 5710a gas chromatograph equipped with a thermal conductivity detector and a model 3380A integrator. A Porapak

T column (6.35 mm x 304.3 cm) was held at 70°C with a helium gas carrier flow rate of 40 mL/min. Biogas sample volumes of 0.5 mL were injected.

3.2.4.2 VFA Quantification

VFA quantification was determined by an internal standard method described by Ackman (1972), using a Hewlett-Packard 5840A gas chromatograph equipped with a flame ionization detector, an autosampler, a model 5840 integrator, and a Chromosorb 101 packed column (304.8 cm x 2 mm ID, 80/100 mesh size). The oven temperature was 180°C, and the injection temperature was 250°C. The detector temperature was maintained at 350°C. The flow rate of the formic acid saturated helium carrier gas was 15 mL/min. Samples were centrifuged at 5000 rpm for 5 min in a microcentrifuge, and the supernatant was diluted with an equal volume of an internal standard containing 1000 mg/L isobutyric acid prior to injection.

3.2.4.3 VSS and TSS Determination

Total and volatile suspended solids determination was based on procedures in Standard Methods (APHA, 1985). Biomass samples were dried in a 108°C oven overnight and the dry weight represented the TSS portion. The dried biomass was then ashed in a 550°C muffle furnace for 20 min and the difference between dry and ash weights represented the VSS portion. Effluent samples were filtered through GF/C glass filters (VWR Canlab) and the filters were dried and ashed for TSS and VSS determination.

3.2.4.4 COD Analysis

COD analysis was determined by a colorimetric technique (APHA, 1985). Light absorbance at 600 nm by samples was measured on a Perkin-Elmer spectrophotometer. Soluble COD of effluents was performed on filtrates obtained during TSS and VSS determination. Alternately, samples were centrifuged at 7500 rpm (10,000 g) for 20 min

and the supernatant used for soluble COD determination. For total COD determination, effluent samples were used directly without filtration or centrifugation. Unless otherwise stated, the COD concentrations reported in this thesis are soluble COD concentrations. Total COD determination was carried out in order to perform organic carbon balances on the UASB reactors during steady-state conditions.

4 Results and Discussion

4.1 Batch Experiments

Batch experiments were carried out to better understand the mechanisms involved in the removal of various organic species during anaerobic treatment of ADF. Possible ADF additives such as benzotriazole and its derivatives and NPnEOs (and its metabolite nonylphenol) are known to exhibit toxicity effects on a wide range of organisms (see section 2.2.2).

4.1.1 Biosorption of Aryl Triazole

One class of ADF additives considered in this study was the corrosion inhibitors. Since tolyltriazole was reported as an ADF additive (Cancilla *et al.*, 1998), it was thus decided that the benzotriazole family: benzotriazole (BT), 5-methyl-1 H-benzotriazole (MeBT), and 5,6-dimethyl-1 H-benzotriazole (DiMeBT) should be studied. Biosorption experiments described in section 3.1.2 were carried out for each additive. Analysis and quantification of these aryl triazoles were determined by HPLC. Variations in aryl triazole concentrations were monitored over time to establish the time required for equilibration. As presented in Table 4–1, aryl triazole concentrations in sample bottles containing biomass were slightly lower than those found in controls (no biomass). No degradation intermediates were detected during HPLC analysis of the samples, suggesting that this difference was due to biosorption. The biosorption process is believed to be very rapid since the difference was detected very early in the experiment, and BT and MeBT concentrations remained relatively constant over 131 days.

Results for DiMeBT indicated a significant drop in concentration after 131 days (from approximately 96 mg/L to less than 68 mg/L). However, evidence for DiMeBT biosorption or degradation was not seen in an experiment designed to evaluate the effects

of aryl triazoles on EG degradation. As shown in Table 4–2, DiMeBT levels remained constant over 15 days, suggesting that biodegradation (if any) occurred slowly. This observation is of importance since UASB reactors operate at very low HRTs. In this study, the UASB reactors were operated at HRTs less than three days. Consequently, only the sorbed DiMEBT would be degraded. Since, very little DiMeBT biosorption took place, the DiMeBT degradation in UASB reactors would be minimal. The large decrease in DiMeBT concentration observed after 131 days suggested that removal may be possible in lagoons and groundwater where both HRT and SRT are very high.

Table 4–1 Biosorption equilibrium data for aryl triazole additives at 35°C and 2.8 g VSS/L anaerobic granular biomass.

Sample*	Liquid phase concentrations (mg/L) at various times				
	0 h	3 h	6 h	1 d	131 d
BT	217±15	233±4	233±2	235±5	223±4
MeBT	209±15	222±9	220±6	220±5	215±7
DiMeBT	96±2	94±1	91±3	87±3	68±1
BT Control	240±6	246±1	242±3	244±3	243±3
MeBT Control	243±1	246±4	242±1	245±1	244±1
DiMeBT Control	103±1	102±1	102±2	100±4	102±2

*Test samples were done in triplicate. Controls (no biomass) were done in duplicate.

Results for the test triplicates were averaged over the test period to give aryl triazole levels in the liquid phase. Evidence for biosorption is indicated by the difference between aryl triazole concentration in controls and test bottles. Biosorption isotherms for the three aryl triazoles were determined based on the Freundlich equation **5**. Experimental results fitted well to this equation, as indicated by the general scattering of the data points about the linear lines presented in Figure 4–1. Biosorption results for BT and MeBT were very similar. Thus, the results were combined to produce one isotherm. It is not surprising that BT and MeBT behaved similarly. The addition of one methyl

group is not expected to have a large effect on the polarity of the whole molecule. Consequently, similar interactions with microbial biomass are expected for BT and MeBT.

Table 4–2 Aryl triazole concentrations measured during EG degradation by anaerobic granular biomass (2.8 g VSS/L) at 35°C.

Test*	Liquid phase concentrations (mg/L) at various times							
	0 h	3 h	6 h	1 d	2 d	3 d	4 d	15 d
B-50	47.6±1.3	47.7±1.0	47.5±0.9	46.6±1.3	46.2±1.3	4.46±0.9	42.3±2.1	45.7±1.2
B-100	92.6±1.4	94.4±0.1	93.1±1.3	92.5±0.1	91.8±0.8	91.9±0.6	86.5±1.2	91.3±0.1
B-150	144.2±0.2	143.8±0.5	142.9±0.7	140.7±2.4	141.5±0.2	140.7±0.2	134.0±0.4	140.3±0.2
M-50	46.1±0.5	47.1±0.1	46.8±0.1	46.0±0.4	46.3±0.4	47.1±0.4	46.8±0.1	47.2±0.2
M-100	91.1±0.6	92.8±2.1	92.9±1.3	90.7±1.5	91.3±1.3	92.3±1.5	92.7±1.4	93.8±1.6
M-150	139.3±2.0	138.5±0.5	139.5±0.1	137.2±0.3	136.7±0.1	138.4±0.4	138.6±0.3	141.3±0.9
D-0.5	0.40±0.00	0.43±0.01	0.44±0.00	0.40±0.01	0.41±0.01	0.42±0.01	0.34±0.13	0.42±0.00
D-1.0	0.81±0.04	0.86±0.02	0.87±0.04	0.82±0.03	0.83±0.01	0.84±0.03	0.69±0.04	0.84±0.02
D-1.5	1.30±0.00	1.36±0.04	1.34±0.03	1.27±0.02	1.29±0.02	1.31±0.02	1.25±0.06	1.31±0.00
B-50C	46.9±1.1				46.7±1.3		46.9±0.6	47.6±0.5
B-100C	94.3±0.5				96.1±0.7		95.2±0.7	94.0±4.1
B-150C	143.0±1.3				146.1±0.3		144.2±1.1	143.8±4.0
M-50C	48.3±1.6				47.2±0.7		46.9±0.6	44.6±0.4
M-100C	95.2±0.3				95.6±0.7		96.2±0.9	98.0±5.2
M-150C	141.9±0.1				143.3±0.8		144.0±2.6	148.2±5.8
D-0.5C	0.48±0.02				0.48±0.03		0.47±0.02	0.50±0.01
D-1.0C	0.98±0.04				0.95±0.02		0.99±0.04	0.99±0.02
D-1.5C	1.46±0.01				1.43±0.03		1.43±0.12	1.02±0.38

* Tests were done in duplicate. Letter indicates type of additive and number indicates concentration added in mg/L. The C indicates that the sample is a control. For example, B-50 contains 50 mg/L BT, M-50 contains 50 mg/L MeBT, D-0.5 contains 0.5 mg/L DiMeBT, and B-50C is a control containing 50 mg/L BT and no biomass, etc.

The presence of two methyl groups should make DiMeBT more lipophilic, thus, promoting its interaction with the biomass. Biosorption of DiMeBT was indeed higher than that of either BT or MeBT for the concentration range tested, as indicated by the

higher sorption capacity obtained for DiMeBT presented in Table 4–4 (e.g., for a liquid phase concentration of 10 mg/L, the calculated sorption capacities were 0.52 mg/g VSS for DiMeBT, and 0.013 mg/g VSS for MeBT and BT). Aryl triazole sorption capacities for the ADF-acclimated anaerobic granular biomass at various liquid phase concentrations were calculated based on the best-fit Freundlich sorption parameters presented in Table 4–3. Results presented in Table 4–4 suggested that for aryl triazole levels found in the environment (126 mg/L BT and 198 mg/L totyltriazole: Cancilla *et al.*, 1998), the sorption capacity for ADF-acclimated granular biomass is expected to be only 1 – 4 mg/g VSS.

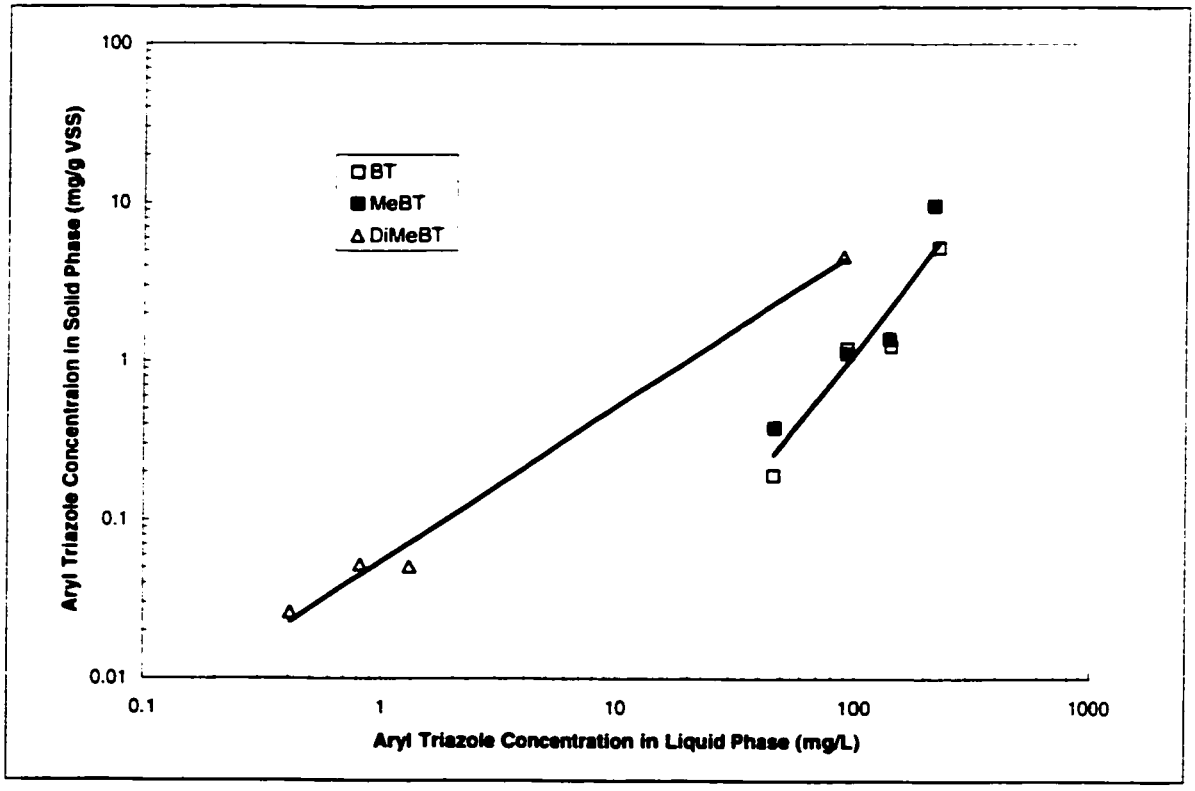

Figure 4–1 Biosorption of aryl triazole by ADF-acclimated biomass at 35°C.

Table 4–3 Freundlich parameters for biosorption of aryl triazole by active ADF-acclimated biomass at 35°C.

Additive	*K*	*n*	r^2
DiMeBT	0.055	1.02	0.991
BT/MeBT	0.00016	0.52	0.890

The Freundlich parameter *n* is a measure of the nonlinearity involved in the sorption process. It is also indicative of the mechanisms involved. For DiMeBT, *n* is near unity, suggesting that sorption of DiMeBT had no effect on anaerobic granular biomass characteristics. The attractiveness of the granular biomass for DiMeBT remained unchanged at all levels of sorption. On the other hand, $n = 0.52$ ($1/n = 1.93$) was obtained for BT and MeBT. This result suggested that the sorption of BT and MeBT might have modified the granular biomass surface which promoted further sorption.

Table 4–4 Aryl triazole sorption capacity for ADF-acclimated biomass at 35°C.

Additive	Sorption capacity (mg/g VSS) for liquid phase concentration of:			
	1 mg/L	10 mg/L	100 mg/L	200 mg/L
DiMeBT	0.055	0.52	4.9	9.7
BT/MeBT	0.00016	0.013	1.1	4.4

4.1.2 Biosorption of Nonylphenol

Biosorption of NP to anaerobic granular sludge was also investigated. Changes in liquid phase NP concentrations were monitored over time to determine the time required for biosorption to reach equilibrium. The results are presented in Figure 4–2. Liquid phase NP measurements showed a time-dependent decrease during the first few days. NP concentrations began to level off after seven days, suggesting that the biosorption process was slow. Based on these results, it was concluded that a week was required for the biosorption process to reach equilibrium. Consequently, sorption experiments involving NP were incubated for seven days prior to analysis.

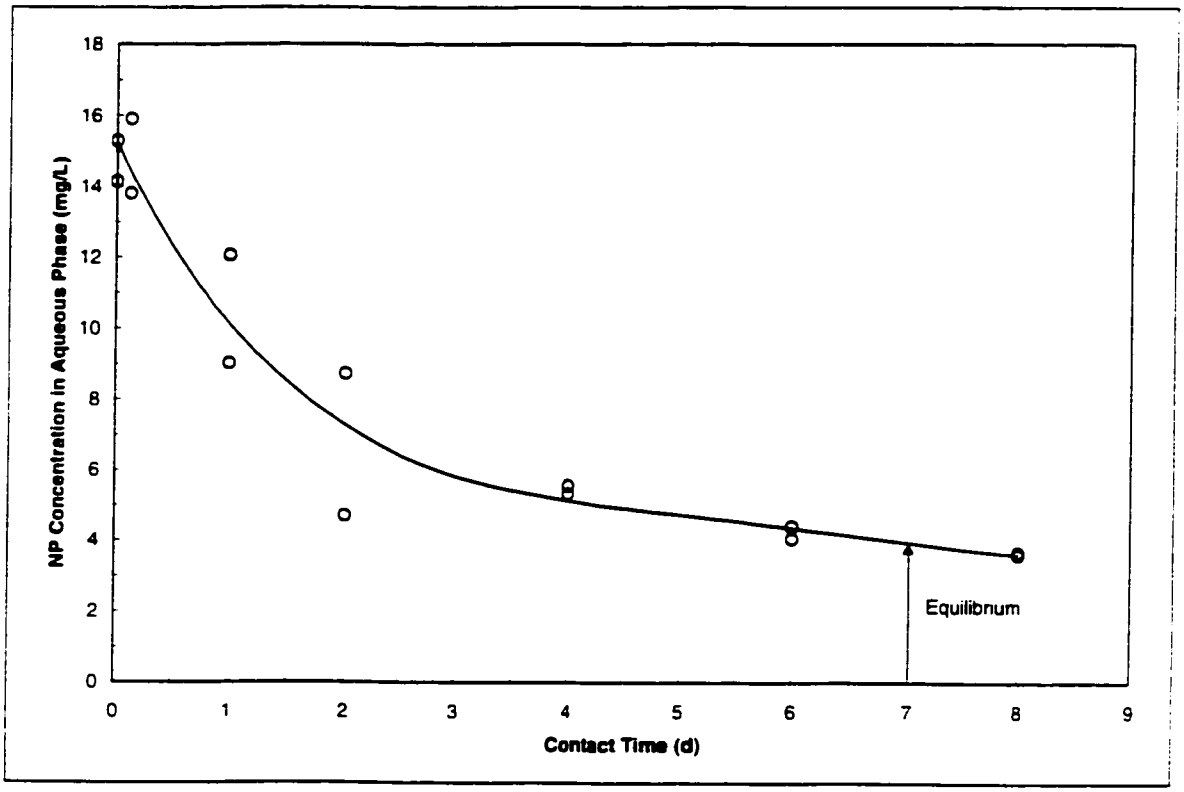

Figure 4–2 Time dependent liquid phase concentration of 25 mg/L NP in contact with 3 g/L anaerobic granular sludge at 35°C.

NP in aqueous samples was determined by an extractive steam distillation method outlined by Kubeck and Naylor (1990). As presented in Table 4–5. the recovery efficiency of this extraction process was 79 ± 11%. Thus. unknown NP concentrations in aqueous samples determined by this extraction method were corrected by this factor.

Table 4–5 NP recovery efficiency for the extractive steam distillation method.

NP added (mg/L)	NP measured after refluxing (mg/L)	Percentage recovered
40	33.0	83
50	33.0	66
50	41.2	82
80	65.4	82
160	152.2	95
320	215.5	67
	Average:	79±11

Results presented in Figure 4–2 suggested that biosorption played a major role in the removal of NP from the liquid phase. It was thus important to characterize the sorption process. Comparison of NP sorption capacities for active, dormant, and inactive anaerobic granular biomass can give insights into the sorption mechanisms involved (e.g., active versus inactive). ADF-acclimated anaerobic granular biomass from continuously fed UASB reactors was considered active, and seed granules stored at room temperature for four months were considered dormant. Inactivation by conventional means (autoclaving or drying) was not used since cell lysis can occur, which can release intracellular components that can interfere with biosorption. Thus, to keep the granules and microbial cells intact, inactivation of the biomass was carried out by the addition of inhibitors.

Sodium azide (NaN_3) is a reversible inhibitor of the cytochrome system. It has no effect on the cell structure, and a concentration of 3 mM was sufficient to inhibit microbial activity in slow sand filters (Weber-Shirk and Dick, 1997). A higher exposure level of 0.1% NaN_3 (15 mM) for two hours was required to inhibit acetic acid consumption by anaerobic granules (Klein, 1995). However, a 24 hour exposure to 0.1% NaN_3 did not inhibit EG metabolism by the ADF-acclimated granular biomass used in this study. It was thus required to determine the concentration of sodium azide that would inhibit EG degradation. As presented in Table 4–6, a sodium azide concentration of 5% was needed for complete inhibition of EG metabolism. This extremely high azide level was probably required to inhibit any residual activity of the microorganisms that are well shielded within the interior of the intact granules.

The Freundlich equation was fitted to NP biosorption data for the three types of anaerobic granular biomass (active, dormant, and inhibited). Sorption isotherms for these three types of granular biomass are presented in Figure 4–3. The general scattering of the

data points along the linear trend line suggested that the Freundlich model adequately described the biosorption process. All three types of granular biomass had higher sorption capacities for NP compared to aryl triazoles presented in section 4.1.1. At an equilibrium concentration of 10 mg/L NP in the liquid phase, the sorption capacity of active, dormant, and inhibited anaerobic granular sludge are 27, 13, and 3 mg/g VSS, respectively (compared to 0.5 and 0.01 mg/g VSS for MeDiBT and BT/MeBT, respectively). The high sorption capacity obtained for active biomass suggested that active transport may play an important role in the biosorption of nonylphenol. This was contrary to earlier findings for chlorinated phenols. Studies indicated that chlorinated phenol sorption by anaerobic granules was independent of physical properties (Pham and Kennedy, 1994) and biological activity (Klein, 1995). These opposing observations suggested that sorption mechanisms involved in anaerobic granular sludge are sorbate dependent.

Table 4–6 The effect of sodium azide on EG degradation by granular biomass at 35°C.

NaN_3 Concentration	Percentage EG converted after 24 hours
0.0%	100
0.1%	100
0.5%	87±17
1.0%	34±1
1.5%	14±7
2.0%	19±2
5.0%	1±1

The best-fit Freundlich parameters for the three isotherms for NP uptake by anaerobic granular sludge are presented in Table 4–7. Different values of n were obtained for the three types of granular biomass. For NaN_3 inhibited biomass, $n < 1$, suggesting that sorption of NP resulted in some modification of the biomass surface that promoted further sorption. Since NP contains a hydroxyl group, it may be possible that

hydrogen bonding is involved in promoting further sorption of NP molecules. In the case when active transport may be involved, n is expected to be greater than unity since there are a finite number of sites available for active transport. An n value near unity was obtained for active biomass. This suggested that both active and inactive mechanisms might have taken place during the biosorption of NP by active granular biomass. For dormant granular biomass, less active transport may be present and so n falls between those obtained for active and inhibited anaerobic granular biomass.

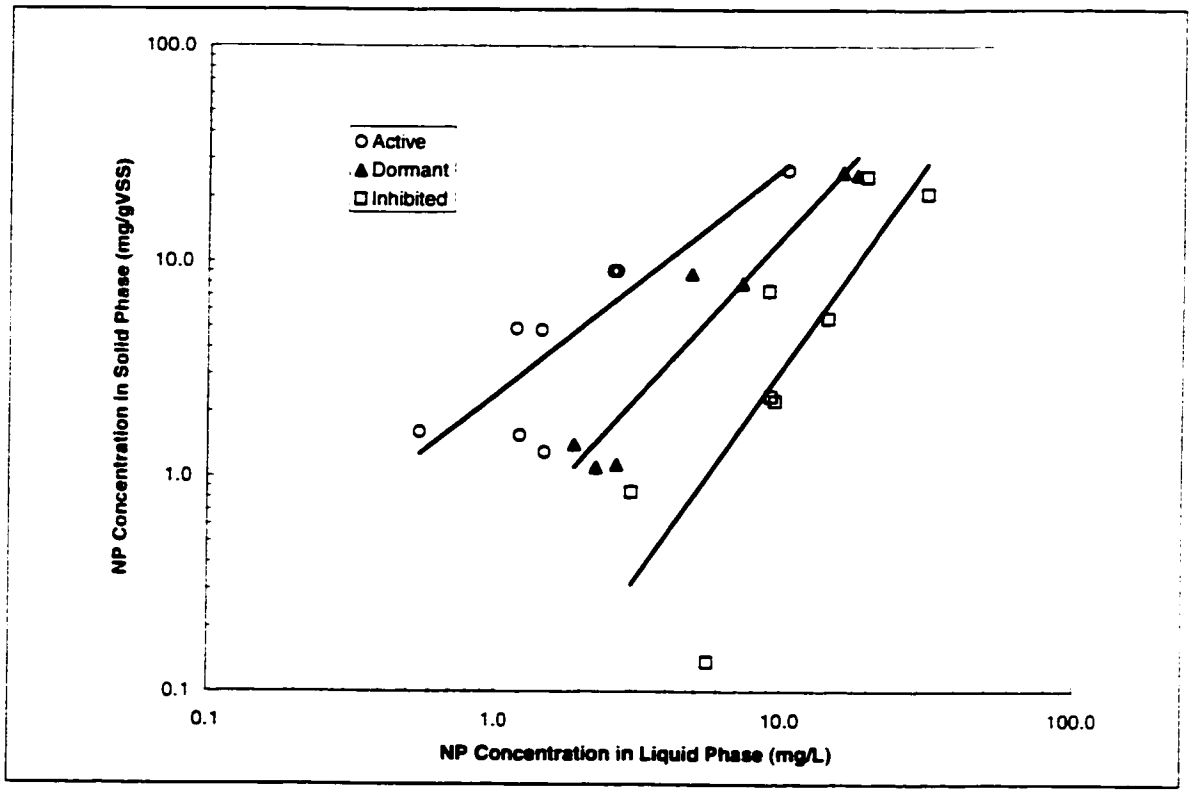

Figure 4–3 **Freundlich sorption isotherms for uptake of NP by active, dormant, and NaN_3 inhibited anaerobic granular biomass at 35°C.**

Table 4–7 **Freundlich parameters for biosorption of NP by active, dormant, and inhibited granular biomass at 35°C.**

Biomass	K	n	r^2
Active	2.38	0.95	0.732
Dormant	0.43	0.68	0.928
Inhibited	0.04	0.52	0.664

4.1.3 Effect of ADF Additives on EG Metabolism

The high COD associated with the ADF used was due to the EG fraction. Efficient removal of EG is of paramount importance in the treatment of ADF-contaminated wastewaters. It was thus important to determine the effects of the corrosion inhibitors and nonionic surfactants on the degradation of EG under anaerobic conditions.

Formation of metabolic intermediates during EG degradation was monitored by gas chromatography. Ethanol and acetic acid were the major metabolic intermediates generated. Propionic and butyric acid concentrations remained well below 10 mg/L for all samples. Thus, they are not included with the results presented in Figures 4–4 to 4–8. Average values for duplicate samples were plotted to minimize cluttering since concentrations of three different chemicals in four different samples are presented on each graph. Trend lines for EG consumption with concomitant production of ethanol and acetate for controls are included in all figures to serve as reference points for comparison purposes.

The results presented in Figures 4–4 to 4–8 indicated that EG degradation by anaerobic granular sludge (in the presence or absence of ADF additives) resulted in concomitant production of ethanol and acetic acid. EG consumption and ethanol/acetate production followed the same trend as that of controls for all test samples (data for test samples follow control trends closely). A larger deviation of data points from the control trend lines for acetate and ethanol consumption indicated that the additives had some effect on methanogenic activity.

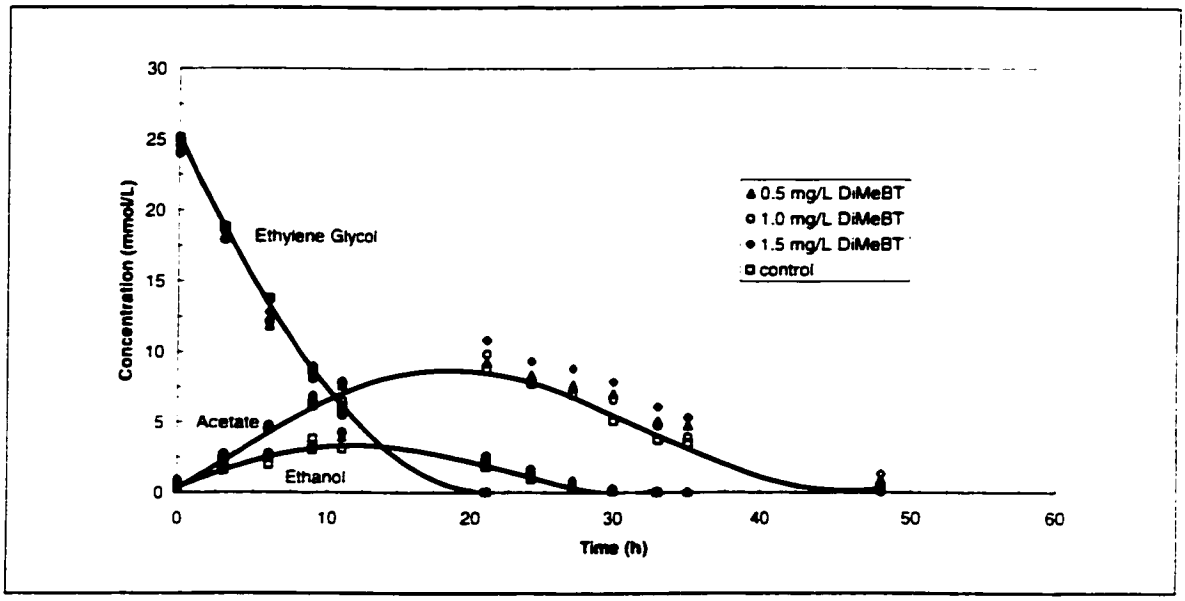

Figure 4–4 **Effect of 5,6-dimethyl-1 H-benzotriazole on EG metabolism by anaerobic granular sludge at 35°C. Data points are average values for duplicate samples. Trend lines are based on results for controls.**

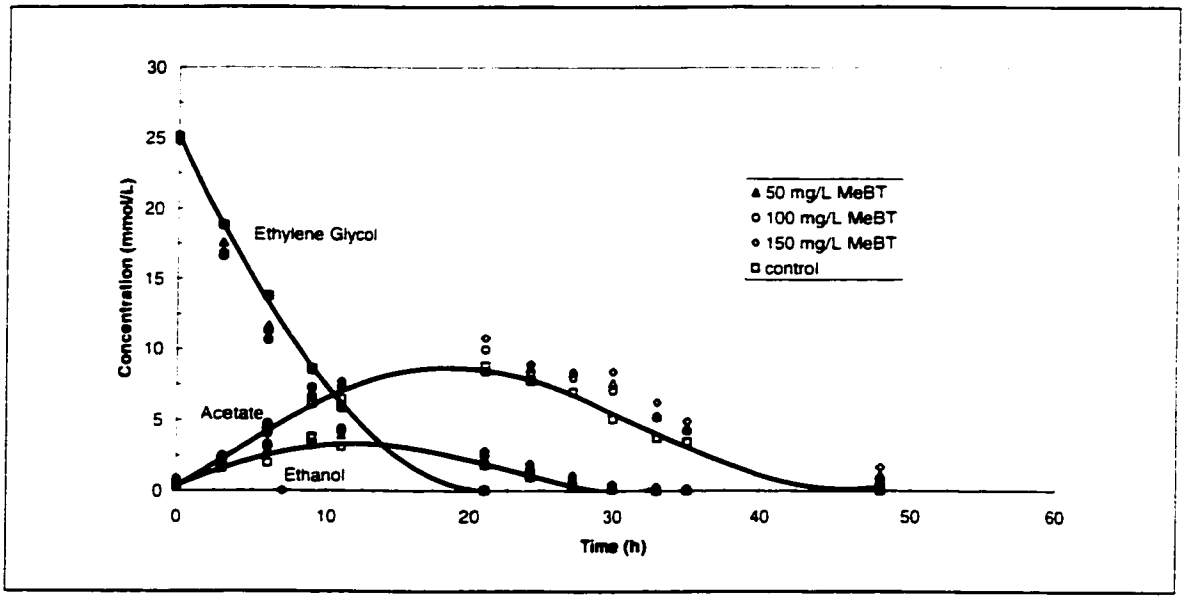

Figure 4–5 **Effect of 5-methyl-1 H-benzotriazole on EG metabolism by anaerobic granular sludge at 35°C. Data points are average values for duplicate samples. Trend lines are based on results for controls.**

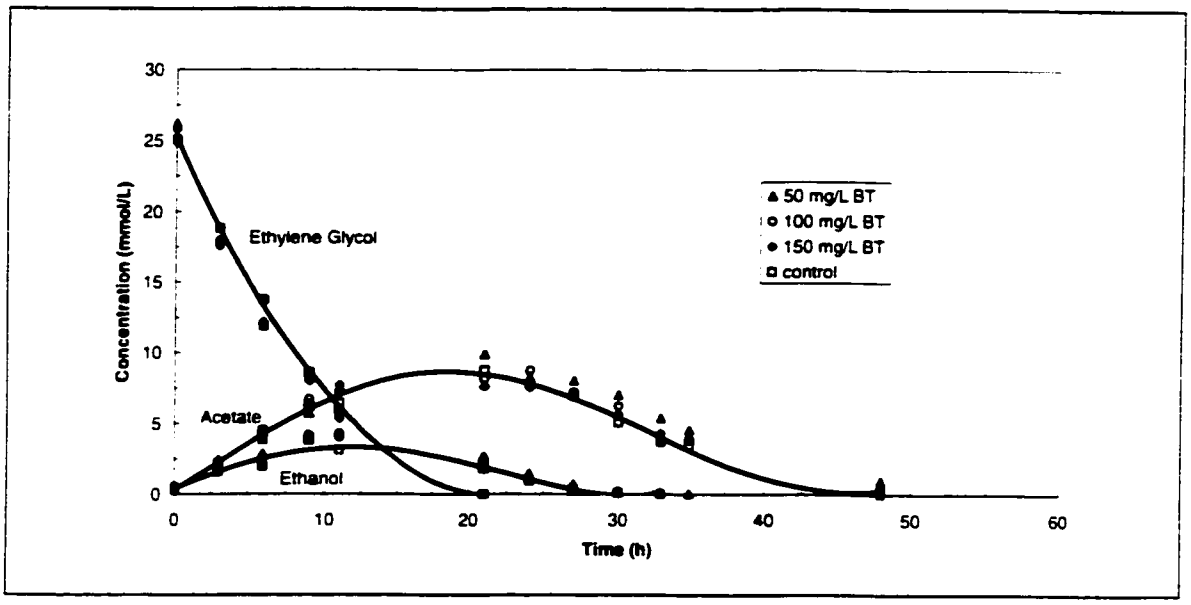

Figure 4–6 **Effect of benzotriazole on EG metabolism by anaerobic granular sludge at 35°C. Data points are average values for duplicate samples. Trend lines are based on results for controls.**

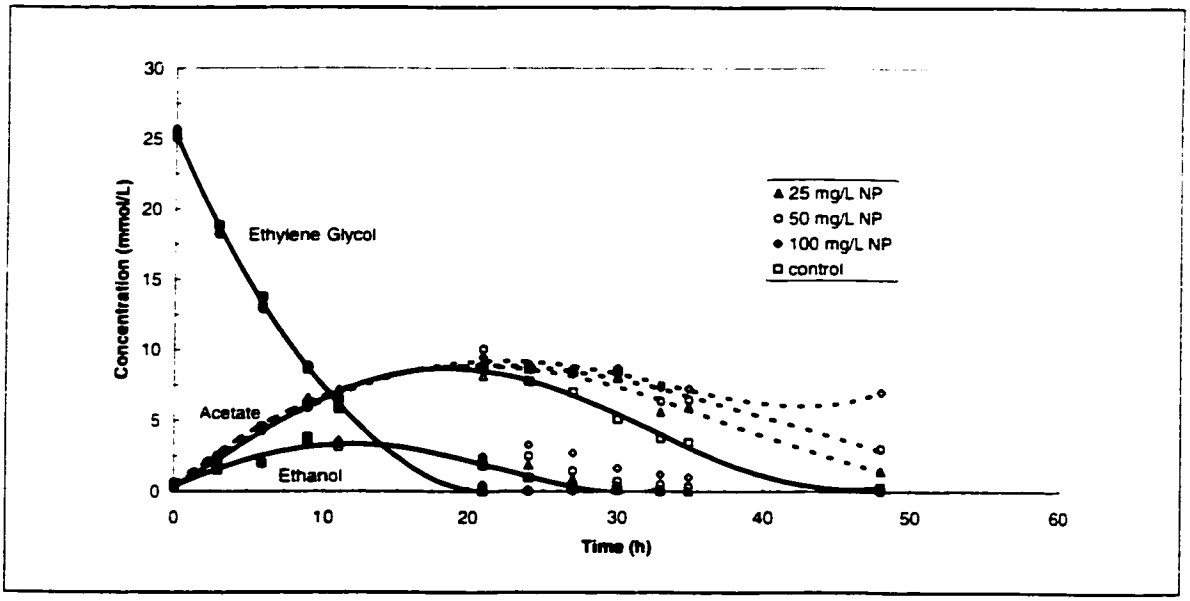

Figure 4–7 **Effect of NP on EG metabolism by anaerobic granular sludge at 35°C. Data points are average values for duplicate samples. Solid trend lines are based on results for controls.**

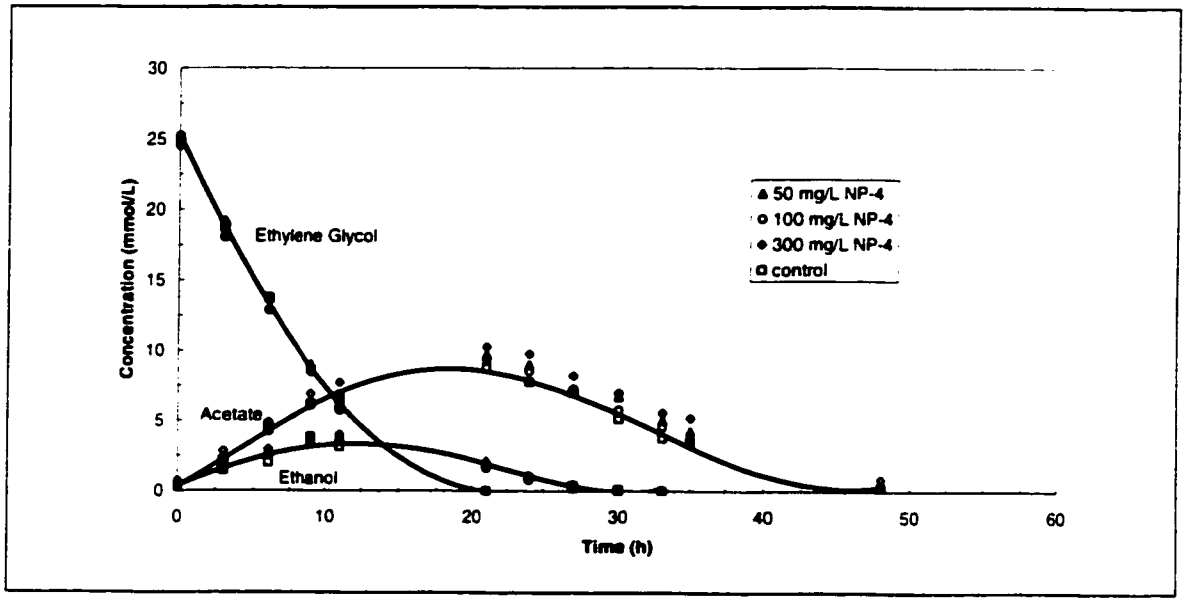

Figure 4–8 Effect of Tergitol NP-4 on EG metabolism by anaerobic granular sludge at 35°C. Data points are average values for duplicate samples. Trend lines are based on results for controls.

An analysis of variance (ANOVA) was performed on the metabolic rates presented in Table 4–8 to determine whether there is a significant difference between metabolic rates measured for controls and sample bottles. The probability (p) of committing a type I error where a true null hypothesis H_0: $\mu_1 = \mu_2 = \cdots = \mu_k$ is falsely rejected was determined. If p is less than 0.05, the null hypothesis is rejected. The results presented in Table 4–8 indicated that only the acetate consumption rates for test samples containing 100 mg/L NP were statistically different from that of controls ($p = 0.03$).

The specific EG and ethanol consumption rates presented in Table 4–8 indicated that acidogenic activities were not affected by the additives used in this study ($p > 0.7$ for null hypothesis H_0: $\mu_1 = \mu_2 = \cdots = \mu_k$). It is also likely that the levels of additives used in this study did not inhibit the activities of hydrogen utilizing methanogens since propionic acid levels in all test bottles remained below 10 mg/L at all sampling times. It is expected that an accumulation of H_2 would occur if the activities of the hydrogen utilizers

were inhibited. This would have resulted in an accumulation of propionic acid since propionic acid conversion is inhibited by high H_2 partial pressures.

Methanogenic activity was affected as indicated by lower acetate consumption rates for samples containing 100 mg/L NP (compared to controls). As depicted in Figure 4–7, acetic acid concentrations in samples containing NP were much higher than that of controls at 48 hours. The consumption rate for controls was 0.19 g acetate/g VSS/d as compared to 0.15, 0.12, and 0.07 g acetate/g VSS/d for 25, 50, and 100 mg/L NP, respectively (Table 4–8). However, only the difference between controls and samples containing 100 mg/L NP was found statistically significant by the Tukey test ($q < q_{0.05,15,16}$ for the null hypothesis H_0: $\mu_{control} = \mu_{test}$ for all but one test. For the null hypothesis H_0: $\mu_{control} = \mu_{100\ NP}$, $q = 6.13$ which is greater than $q_{0.05,15,16} = 5.72$ and thus H_0 is rejected). For NP concentration at 100 mg/L, the acetic acid consumption rate was 38% that of controls. This indicated that the acetoclastic activity of anaerobic granular sludge was inhibited by NP. The inhibition was statistically significant at an NP concentration of 100 mg/L.

Evidence for NP inhibition of methanogenic activity was further supported by biogas production results presented in Table 4–9. An ANOVA performed on the cumulative biogas production measured at 21 and 48 h indicated that the results for the tests were statistically different ($p < 0.05$ for null hypothesis H_0: $\mu_1 = \mu_2 = \cdots = \mu_k$). Based on the Tukey test, the cumulative gas production at 21 h for all three NP concentration levels tested (43.7, 44.4, and 41.5 mL biogas for 25, 50, and 100 mg/L NP, respectively) was lower than that of controls (52.4 mL). The test statistic q was 7.21, 6.63, and 9.04 for 25, 50, and 100 mg/L NP, respectively. These values were larger than $q_{0.05,15,16} = 5.72$ and thus H_0 was rejected.

Table 4–8 Effect of ADF additives on metabolic rates of anaerobic granular sludge at 35°C.

Sample*	Specific Rates (g/g VSS/d)				
	Ethanol Production	Acetate Production	Ethanol Consumption	Acetate Consumption	Ethylene Glycol Consumption
Control	0.10±0.02	0.27±0.02	0.07±0.01	0.19±0.02	0.82±0.04
0.5 ppm 5.6-Me_2BT	0.10±0.01	0.28±0.02	0.10±0.02	0.15±0.01	0.80±0.07
1.0 ppm 5.6-Me_2BT	0.11±0.01	0.30±0.02	0.09±0.01	0.18±0.02	0.79±0.05
1.5 ppm 5.6-Me_2BT	0.11±0.01	0.30±0.02	0.09±0.01	0.17±0.02	0.80±0.06
50 ppm 5-MeBT	0.11±0.01	0.30±0.02	0.10±0.01	0.16±0.02	0.81±0.08
100 ppm 5-MeBT	0.12±0.02	0.29±0.03	0.09±0.01	0.18±0.02	0.86±0.08
150 ppm 5-MeBT	0.12±0.01	0.29±0.03	0.09±0.02	0.15±0.02	0.79±0.08
50 ppm BT	0.13±0.01	0.28±0.02	0.09±0.03	0.15±0.02	0.85±0.10
100 ppm BT	0.13±0.01	0.29±0.02	0.08±0.01	0.16±0.02	0.84±0.08
150 ppm BT	0.12±0.02	0.30±0.02	0.07±0.01	0.14±0.01	0.82±0.06
25 ppm NP	0.11±0.01	0.28±0.02	0.08±0.01	0.15±0.01	0.83±0.05
50 ppm NP	0.10±0.01	0.26±0.02	0.07±0.01	0.12±0.01	0.81±0.07
100 ppm NP	0.10±0.01	0.26±0.02	0.08±0.01	0.07±0.02	0.79±0.06
50 ppm NP-4	0.11±0.01	0.25±0.04	0.08±0.01	0.18±0.02	0.81±0.04
100 ppm NP-4	0.11±0.01	0.27±0.02	0.06±0.02	0.19±0.03	0.80±0.07
300 ppm NP-4	0.12±0.01	0.30±0.02	0.08±0.01	0.18±0.02	0.83±0.05
ANOVA H_0: $\mu_1 = \mu_2 = \cdots = \mu_k$	Accept H_0 $p = 0.752$	Accept H_0 $p = 0.884$	Accept H_0 $p = 0.784$	Reject H_0 $p = 0.0322$	Accept H_0 $p > 0.999$
Tukey Test H_0: $\mu_{control} = \mu_{test}$ $q_{0.05,15,16} = 5.72$				$q = 6.13$ $\mu_{control} = \mu_{100\ NP}$	

* Tests were done in duplicates ($n = 2$). See Appendix G for ANOVA and Appendix F for Tukey Test procedures.

The null hypothesis H_0: $\mu_{control} = \mu_{100\ NP}$ was rejected for cumulative biogas production at 48 h, where $q = 6.13 > q_{0.05,15,16} = 5.72$. This effect was also observed for the data presented in Figure 4–9. Again, early biogas production was inhibited by NP (lower cumulative gas production for samples containing 50 mg/L NP between 30 and 100 h); however, the final cumulative biogas produced by all samples was the same. This

suggested that NP inhibited the rate of biogas production, which was consistent with NP inhibition on acetate consumption rate discussed above.

Table 4–9 Effect of ADF additives on biogas production by ADF-acclimated anaerobic granular biomass at 35°C.

Sample*	Cumulative Biogas Production (mL) at	
	21 h	48 h
Control	52.4±0.3	92.7±0.7
0.5 ppm 5,6-Me_2BT	51.5±0.7	91.4±2.3
1.0 ppm 5,6-Me_2BT	47.8±0.0	87.4±0.6
1.5 ppm 5,6-Me_2BT	48.1±2.7	88.9±3.8
50 ppm 5-MeBT	47.1±2.1	87.0±2.3
100 ppm 5-MeBT	47.1±0.4	87.1±1.0
150 ppm 5-MeBT	46.1±1.3	87.3±1.8
50 ppm BT	47.6±0.1	87.6±4.7
100 ppm BT	49.5±0.7	90.9±2.7
150 ppm BT	51.1±0.4	90.9±0.1
25 ppm NP	43.7±0.1	86.0±0.6
50 ppm NP	44.4±2.5	86.2±3.4
100 ppm NP	41.5±0.1	78.3±0.4
50 ppm NP-4	49.7±0.4	92.0±1.1
100 ppm NP-4	51.3±0.4	92.3±3.5
300 ppm NP-4	49.1±1.3	92.4±1.7
ANOVA	Reject H_0	Reject H_0
H_0: $\mu_1 = \mu_2 = \cdots = \mu_k$	$p = 0.00035$	$p = 0.0431$
Tukey Test	$q = 7.21$ ($\mu_{control} \neq \mu_{25\ NP}$)	
H_0: $\mu_{control} = \mu_{test}$	$q = 6.63$ ($\mu_{control} \neq \mu_{50\ NP}$)	$q = 6.13$ ($\mu_{control} \neq \mu_{100\ NP}$)
$q_{0\ 05.15.16} = 5.72$	$q = 9.04$ ($\mu_{control} \neq \mu_{100\ NP}$)	

* Tests were done in duplicates ($n = 2$). See Appendix G for ANOVA and Appendix F for Tukey Test procedures.

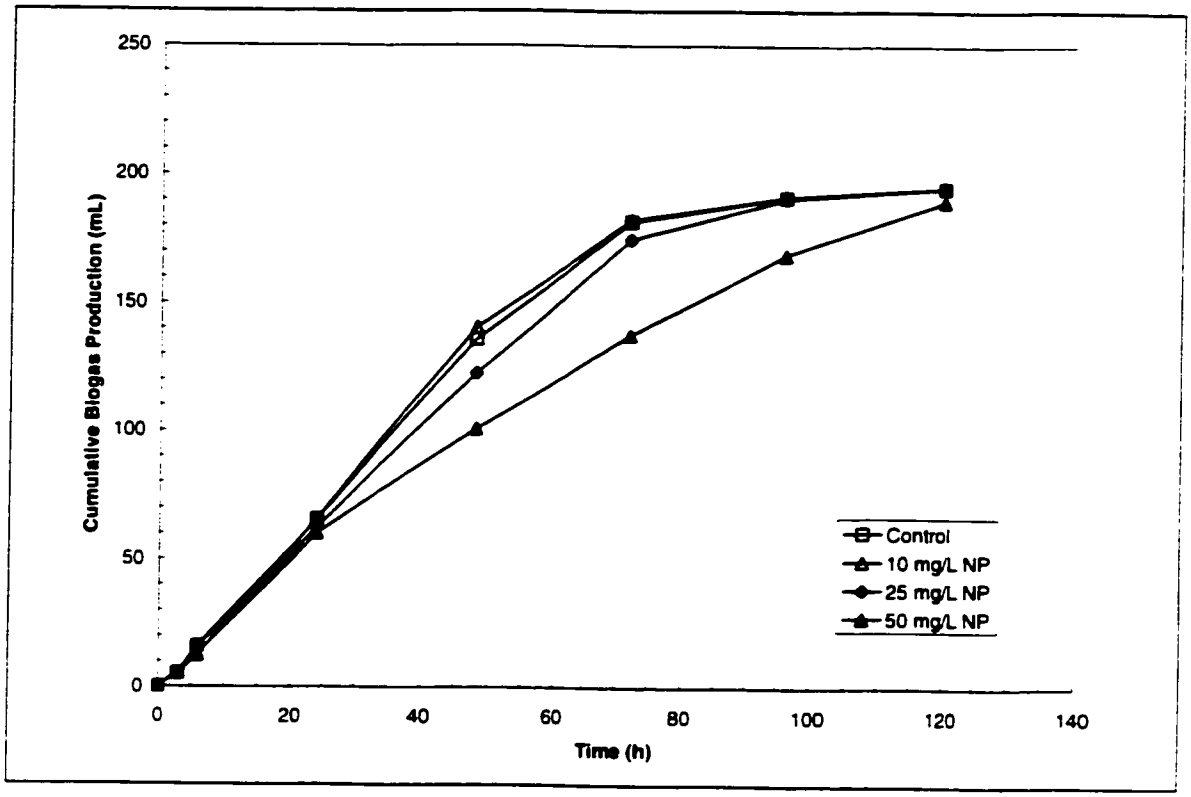

Figure 4–9 Effect of NP on biogas production during degradation of EG by ADF-acclimated anaerobic granular sludge at 35°C.

Similar to the findings of Dwyer and Tiedje (1983), concomitant production of ethanol and acetic acid suggested that EG was dismutated. However, a carbon balance indicated a continuous decrease in total moles of carbon in all samples (Appendix H). In addition, positive biogas readings were obtained at all sampling times (Figure 4–9). This indicated that methane production commenced as soon as ethanol and acetic acid were generated. This observation is different from the results reported by Dwyer and Tiedje (1983), where methane production occurred only after the depletion of EG.

In addition, Dwyer and Tiedje (1983) observed that there was an accumulation of acetic acid at the end of their experiments, and all of the methane produced came from the H_2 generated during conversion of ethanol into acetic acid. In contrast, the experiments in this study indicated that both ethanol and acetic acid were degraded to

form methane as the final product. Complete degradation of EG indicated that the anaerobic granules used in these experiments contained a wider range of microorganisms than the enrichment cultures used by Dwyer and Tiedje (1983).

4.1.4 Fate of ADF Additives

The complexity of the microbial consortium in anaerobic granules plays an important role in the transformation of organic substrates. Their microbial diversity has been used successfully in the degradation of recalcitrant chemicals such as chlorinated phenols. It was believed that ADF additives could be transformed by some microbial strains present in the anaerobic granules used in this study. Thus, the concentrations of the various additives (BT, MeBT, DiMeBT, and NP) were also monitored during EG degradation tests.

The results for benzotriazole and its methyl derivatives were presented in Table 4–2. A slight decrease in aryl triazole concentrations was observed during the EG degradation test period; however, this decrease was due to biosorption. In addition, no new peaks were detected by the HPLC methodology used, suggesting that benzotriazole and its methyl derivatives were not degraded by the anaerobic granules during batch degradation tests.

A different result was obtained for NP. A large decrease in NP concentration was observed at the end of the EG degradation experiment (t = 4d). Based on Freundlich parameters for NP sorption by active anaerobic granular sludge (n = 0.95 and K = 2.38), the concentration of NP sorbed to the biomass was calculated and the results presented in Table 4–10. The total NP measured is the sum of the NP in the liquid phase and that associated with the biomass. For the NP concentrations monitored (10, 25, and 50 mg/L), less than 40% of the amount added was accounted for (e.g., NP not detected for the 10 mg/L NP sample; only 9.2 and 18.2 mg/L measured for 25 and 50 mg/L NP samples.

respectively). This large difference in NP concentrations suggested that NP degradation by anaerobic granules may have taken place during EG degradation. It was thus believed that NP can be degraded during anaerobic treatment of ADF in UASB reactors.

Table 4–10 NP concentration during EG degradation by anaerobic granular sludge (3.8 g VSS/L) at 35°C.

NP added (mg/L)	NP measured[a] (mg/L)	NP sorbed[b] (mg/L)	Total NP measured (mg/L)	% of the NP added unaccounted for
10	not detected	–	–	>99%
25	0.9	8.3	9.2	63%
50	1.8	16.5	18.2	64%

[a] Liquid concentration measured at end of test (t = 4d).

[b] Calculated based on Freundlich parameters for active granular biomass. n = 0.95 and K = 2.38.

4.2 Continuous Experiments

It was intended that statistical experimental design would be used to investigate anaerobic biodegradation of ADF in bench-scale UASB reactors. However, information on the operational limits for the treatment of ADF wastewaters by an anaerobic process was not available at the beginning of this research project. Thus, information on operable HRTs and toxic ADF concentrations for the treatment system were required. As such, a series of batch tests and experimental runs were carried out to establish a workable window of operation for the treatment of ADF wastewater in bench-scale UASB reactors.

Since ADF is reported to be more toxic than aqueous solutions of ethylene or propylene glycol (Jank *et al.*, 1973; Hartwell *et al.*, 1993; MacDonald *et al.*, 1993; Novak *et al.*, 2000), an ATA described in section 3.1.4 was carried out to determine the maximum concentration of ADF that was not inhibitory to the anaerobic granules used in the UASB reactor system. As presented in Figure 4–10, ADF concentrations higher than 1% had significant inhibitory effects as indicated by the lower gas production for 2, 4, and 8% ADF, as compared to that for 1% ADF. Furthermore, granules exposed to 4 and

8% ADF were discolored, accompanied by a complete cessation of gas production (cell death) after day nine. The upper concentration limit of the experimental design was believed to be 2% ADF since a slight biomass activity was observed at the end of the test.

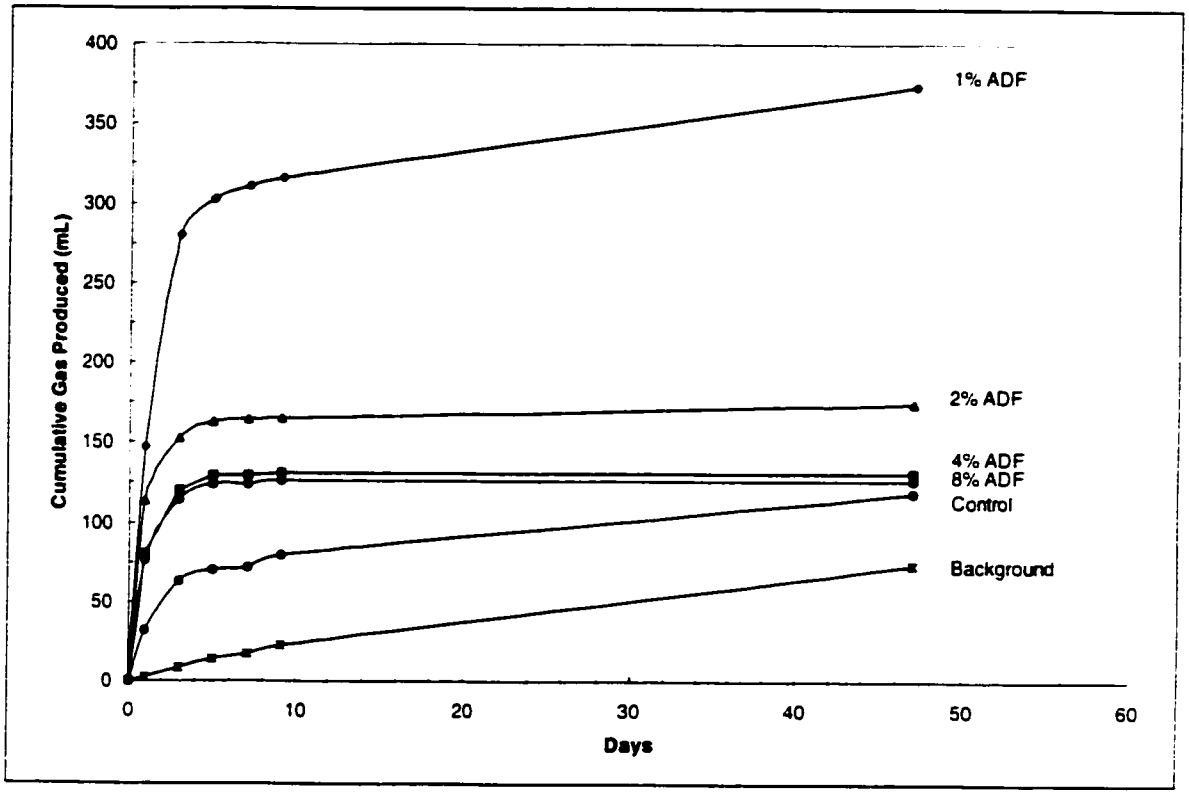

Figure 4–10 Anaerobic toxicity assay performed on unacclimated anaerobic granular sludge at 35°C.

An ADF concentration of 1% had no effect on biomass activity since the test sample behaved similarly to background and control samples (gas production trends were almost parallel after day nine, which was believed to be endogenous decay after depletion of substrate). Thus, a bench-scale UASB reactor containing 32 g VSS/L biomass was operated with 1% ADF for 41 days. The feed flow rates were varied to determine the workable window of operation for the reactor in terms of HRT. For the range of HRT (0.5 – 1.5 d) studied, a COD removal efficiency greater than 95% was obtained (Table 4–

11). The methane potential achieved (0.36 - 0.38 L CH4/g COD removed) was comparable to the theoretical value of 0.39 L CH4/g COD removed at 35°C. In addition, a stable SOLR as high as 0.63 kg COD/kg VSS/day (HRT of 0.5 d) could be obtained, suggesting that the UASB reactor behaved well under the operating conditions used. Thus an HRT of 12 h was believed to be the lower limit of the design window since different concentrations of granular biomass and higher concentrations of ADF would be studied.

Table 4-11 Summary of UASB reactor performance for the treatment of 1% ADF at 35°C.

HRT (d)	COD Removal (%)	CH_4/COD (L/g Removed)
1.5	98	0.36
1.0	97	0.38
0.5	98	0.37

4.2.1 Factorial Design

The efficiency of an anaerobic treatment process is greatly affected by operating variables such as temperature, biomass concentration, feed flow rate, and feed concentration. In this study, the effect of temperature on process response was not investigated because preliminary studies (results not shown) indicated that the ADF biodegradation rates were greatly reduced at temperatures lower than 30°C.

It is well known that anaerobic systems operate optimally at mesophilic (35°C) and thermophilic (55°C) temperatures. A mesophilic operating temperature was chosen for this investigation since deicing fluids are employed during the winter months and so the glycol-contaminated wastewater produced would be cold (~4°C). It was anticipated that the methane gas produced from the biodegradation process could be used to heat the wastewater to the desired 35°C temperature.

Operation at 55°C would no doubt provide interesting information since metabolic rates can be 50 – 100% above the rates at 35°C (Speece, 1996). However, after a startup period of almost six months, a UASB reactor failed to produce an acceptable level of methane at thermophilic conditions. This was not surprising since thermophilic startup periods are known to be slow, sometimes taking up to a year (Speece, 1996). It was thus decided that thermophilic treatment of ADF by UASB reactors could not be done within the time frame of this project. As a result, the effects of the following three operating variables on UASB reactor performance at 35°C were studied:

1. ADF concentration in the feed;
2. Feed flow rate in terms of HRT; and
3. Granular biomass concentration in each UASB reactor.

The ATA results presented in Figure 4–10 suggested that 2% ADF could be treated if the granular biomass were given adequate time to acclimate. Since it was of interest to treat the highest ADF concentration possible, 1.5% ADF was chosen as the central level for ADF concentration. Good reactor performance at 1.5% ADF was achieved within a few weeks; however, attempts to increase the feed concentration to 1.75% ADF were problematic. Daily reactor VFA levels were erratic, even after an acclimation period of two months (data not shown). Thus, lower ADF concentrations were considered to avoid reactor failure. The operating window for the statistical design was thus reconsidered.

For a 2^3 factorial design, each operating variable must be tested at three levels. These levels must be far enough apart to ensure that the effects are not masked by extraneous sources of variations. The three levels used for the three operating variables presented in Table 4–12 were coded as follows:

$$x_1 = (\%\ \text{ADF} - 1.2) \div 0.4$$

$$x_2 = (\text{HRT} - 36) \div 12$$

$$x_3 = (\text{Biomass conc.} - 26.64) \div 8.88$$

Table 4–12 Different levels for the three operating variables of the factorial design.

Operating variable	x	Levels		
		Low	Center	High
ADF concentration, %	x_1	0.8	1.2	1.6
HRT, h	x_2	24	36	48
Biomass concentration, g VSS/L	x_3	17.8	26.6	35.5
Coded		−1	0	+1

A difference of 0.4% between ADF concentration levels was considered adequate. HRT adjustments were based on the volume of effluent generated by the 6–L bench-scale UASB reactor used. To simplify the process of fine-tuning HRT values used, the three levels in Table 4–12 were used since they corresponded to 6, 4, and 3 L of effluent generated daily. In terms of biomass, full-scale UASB reactors are usually operated with the biomass bed occupying ½ of the reactor volume. Thus the biomass concentration levels were chosen to correspond to biomass bed heights of ⅓, ½, and ⅔ of the reactor volume.

A total of four 6–L bench-scale reactors seeded with granular sludge from Lake Utopia Paper were used in this experiment. The seed granular sludge had a specific acetoclastic activity of 0.23 g Ac/g VSS/d and a volatile solids concentration of 67.7 g VSS/L (Table 4–13). The variability among the reactors must be determined. This was required for differentiation between variations in process response due to the changes in the operating conditions and those due to reactor variability. Thus, the four center points presented in Table 2–2 were carried out first.

Table 4–13 Properties of anaerobic granular seed from Lake Utopia Paper (New Brunswick, Canada).

Specific acetoclastic activity (g Ac/g VSS/d)	VSS Content (g VSS/L)	Upflow Velocity, v_{SO} (m/h)
0.23±0.01	67.7±0.3	32±1

Based on Table 4–12, the center-point run condition corresponded to the treatment of 1.2% ADF at a 36 h HRT and 26.6 g VSS/L biomass concentration. At least five measurements were taken during steady-state conditions (duration of two weeks) for the determination of SOLR and process responses presented in Table 4–14. Comparison of the process responses (biomass acetoclastic activity of 0.40 – 0.43 g Ac/g VSS/d, percentage COD removal of 98.3 – 98.5%, methane production rate of 13.2 – 14.7 L/d, and methane production potential of 0.39 – 0.40 L/g COD reduced) for the four reactors presented in Table 4–14 indicated that reactor variability was small. Consequently, the four UASB reactors were treated as identical. Changes in process responses observed will be due to changes in the run conditions, rather than the reactor used.

Table 4–14 Reactor performance for the four center-point **runs of the factorial design where 1.2% ADF was treated at a 36 h HRT and 26.6 g VSS/L granular biomass concentration.**

Reactor	Run	SOLR* (g COD/g VSS/d)	Activity (g Ac/g VSS/d)	COD Removal* (%)	CH_4 Production* (L/d)	CH_4 Potential* (L/g COD)
TP1	1	0.19±0.01	0.42±0.02	98.3±0.1	14.7±0.4	0.39±0.01
TP2	2	0.18±0.01	0.40±0.02	98.4±0.3	14.3±0.5	0.40±0.02
TP3	3	0.17±0.01	0.43±0.02	98.4±0.3	13.5±0.5	0.39±0.02
TP4	4	0.16±0.02	0.42±0.01	98.5±0.3	13.2±1.0	0.39±0.01
Average:		0.18±0.02	0.42±0.01	98.4±0.2	14.0±0.9	0.39±0.02

*The reported values are average values of at least five measurements taken during steady-state conditions.

The ecological nature of the anaerobic process dictates that changes in operating conditions must be gradual. In addition, they must progress from a lower to a higher

level to avoid reactor stress. This constraint restricted the extent to which the experimental run orders of the 2^3 factorial design outlined in Table 2–2 could be randomized to spread the extraneous sources of variations. Since randomization of run order does not eliminate extraneous sources of variations, good laboratory practices were important in minimizing these sources of variations. One likely source of variation was the feed concentration. Thus, ADF feeds were synthesized on a regular basis to avoid feed deterioration due to biodegradation during storage. The COD content of the feed was checked regularly and if a significant variation was detected, a new batch of feed was made. In addition, all run conditions were maintained at steady state for two weeks (or at least 4 HRTs) and process responses were determined from at least five samplings taken during steady-state conditions.

To change the biomass concentration (biomass bed level), the reactors had to be opened and biomass was either added or removed. This process introduced a lot of air that put the biomass under stress. To ensure process responses measured after this change was not due to biomass being under stress, a period of 1 – 2 weeks was required for the biomass to recover. Consequently, the biomass concentrations of a reactor were kept at the same level for as long as possible.

The temperature controlled room used for experimentation was heated by a large heater installed on one side of the room. A fan was installed at the top corner of the room to improve air circulation. However, a temperature difference was observed for different parts of the room. Temperature readings were relatively constant along the wall where the four UASB reactors were mounted. But as a precaution, reactors containing low and high biomass levels were alternated to help spread variations resulting from any temperature difference that might occur. The biomass level of reactor TP1 was chosen randomly by a draw from a hat. The biomass levels (x_3) were thus low, high, low, and high for TP1,

TP2, TP3, and TP4, respectively. The run order and run condition used for the factorial design are presented in Table 4–15.

Table 4–15 Run order and run condition used for the 2^3 factorial design.

Run order	Reactor	Run	x_1 (%ADF)	x_2 (HRT)	x_3 (biomass conc.)
I	TP1	5	−1 (0.8%)	+1 (48 h)	−1 (17.8 g VSS/L)
	TP2	6	−1 (0.8%)	+1 (48 h)	+1 (35.5 g VSS/L)
	TP3	7	−1 (0.8%)	−1 (24 h)	−1 (17.8 g VSS/L)
	TP4	8	−1 (0.8%)	−1 (24 h)	+1 (35.5 g VSS/L)
II	TP1	9	+1 (1.6%)	+1 (48 h)	−1 (17.8 g VSS/L)
	TP2	10	+1 (1.6%)	+1 (48 h)	+1 (35.5 g VSS/L)
	TP3	11	+1 (1.6%)	−1 (24 h)	−1 (17.8 g VSS/L)
	TP4	12	+1 (1.6%)	−1 (24 h)	+1 (35.5 g VSS/L)

The synthetic feed used in the experiment had to be kept refrigerated to minimize changes in COD content due to biodegradation over time. Due to space limitation, it was more practical to use one feed concentration at any given time. Changes in ADF concentration (x_1) must be from low to high to avoid reactor stress. Thus, the first set of four runs was carried out at 0.8% ADF. The HRT levels (x_2) for each set of low-high biomass levels were randomly chosen. Once the appropriate HRT level for each reactor was established, no further adjustments were made. Progression from the first set of four runs to the second set was achieved by gradually increasing the ADF concentration in the feed.

A summary of the steady-state data for the factorial design with four center-point replicates (runs 1 – 12) is presented in Appendix I. The SOLR and the corresponding process responses (biomass activity, COD removal efficiency, and methane production and potential) for the factorial design (runs 5 – 8) are presented in Table 4–16. The reported SOLR was determined from measured rather than design values of COD concentration, HRT, and biomass concentration used.

Table 4–16 UASB reactor performance for the 2^3 factorial design

Run	SOLR (g COD/g VSS/d)	Activity (g Ac/g VSS/d)	COD removal (%)	CH_4 production (L/d)	CH_4 Potential (L/g COD)
5	0.17±0.02	0.46±0.01	98.3±0.3	6.5±0.2	0.39±0.02
6	0.09±0.01	0.44±0.03	98.0±0.3	6.5±0.2	0.36±0.02
7	0.36±0.04	0.55±0.03	98.3±0.5	13.4±0.9	0.37±0.01
8	0.18±0.01	0.50±0.02	98.1±0.3	15.3±0.5	0.44±0.03
9	0.29±0.02	0.41±0.01	98.7±0.1	12.9±0.4	0.39±0.02
10	0.15±0.01	0.42±0.02	98.7±0.1	12.5±0.3	0.36±0.01
11	0.57±0.02	0.39±0.01	82.0±5.4	19.9±2.2	0.36±0.02
12	0.29±0.02	0.38±0.01	98.2±0.1	29.4±0.8	0.43±0.02

For the SOLR range of 0.09 – 0.57 g COD/g VSS/d tested, the COD removal efficiency was greater than 82%. In fact, COD removal efficiencies in excess of 98% were obtained for 11 out of 12 runs conducted. In addition, the specific acetoclastic activity of the granular biomass (0.38 – 0.55 g Ac/g VSS/d) was approximately 2-fold higher than that of the seed sludge (0.23 g Ac/g VSS/d). The high COD removal efficiencies augmented by the improvement in biomass acetoclastic activity indicated that ADF can be treated successfully in UASB reactors.

Good process performance was also indicated by the similarity between measured (0.36 – 0.44 L/g COD removed) and theoretical (0.39 L/g COD removed at 35°C) methane production potentials. Different methane production rates were obtained for similar SOLRs. For example, at an SOLR of 0.29 g COD/g VSS/d (runs 9 and 12), the methane production rates were 12.9 and 29.4 L/d. This indicated that the individual operating variables (HRT, and biomass concentration) had significant influence on the process response. It was thus required to develop empirical models to describe the process responses (COD removal efficiency, biomass activity, and methane production and potential) as functions of ADF concentration, HRT, and biomass concentration.

Empirical model **17** was fitted to the four process responses obtained for the 12 experimental runs presented in Tables 4–14 and 4–16. Results for the center-point replicates (Table 4–14) were used to determine an estimate of the pure error variance for the different responses (equation **18**). A 95% confidence interval for the true value of each parameter β_i in equation **17** was calculated based on this estimate of the pure error variance. The parameter estimates ($\hat{\beta}_i$) and their 95% confidence intervals for the four process responses are presented in Table 4–17. The value of $\hat{\beta}_0$ for biomass activity, COD removal efficiency, methane potential, and methane production are 0.44 g Ac/g VSS/d, 98.4% COD removal, 0.39 L/g COD removed, and 14.4 L/d, respectively. Since β_0 represents the average process response for the design conditions, very high COD removal efficiencies were expected for ADF treatment in UASB reactors.

Table 4–17 Parameter estimates from the 2^3 factorial design for the four responses.

Parameter	95% confidence interval			
	Activity (g Ac/g VSS/d)	COD removal* (%)	CH_4 Potential (L/g COD removed)	CH_4 Production (L/d)
β_0	0.4351±0.0109	98.39±0.14	0.3907±0.0045	14.35±0.64
β_1	-0.0421±0.0134	0.22±0.19	-0.0019±0.0055	4.12±0.78
β_2	-0.0107±0.0134	0.04±0.19	-0.0119±0.0055	-4.94±0.78
β_3	-0.0087±0.0134	-0.14±0.19	0.0089±0.0055	1.36±0.78
β_{12}	0.0268±0.0134	0.05±0.19	0.0025±0.0055	-1.04±0.78
β_{13}	0.0073±0.0134	-0.01±0.19	0.0027±0.0055	0.90±0.78
β_{23}	0.0064±0.0134	0.09±0.19	-0.0249±0.0055	-1.46±0.78
β_{123}	0.0001±0.0134	0.08±0.19	-0.0009±0.0055	-1.00±0.78

* Run 11 ($x_1 = +1, x_2 = -1, x_3 = -1$) was excluded.

COD removal efficiency for run 11 ($x_1 = +1, x_2 = -1, x_3 = -1$) was excluded from the model fitting process. The fitted model displayed lack of fit, even after second-order terms were added (Appendix B). The residual plot presented in Figure 4–11 suggested that the data point for run 11 might possibly be an outlier.

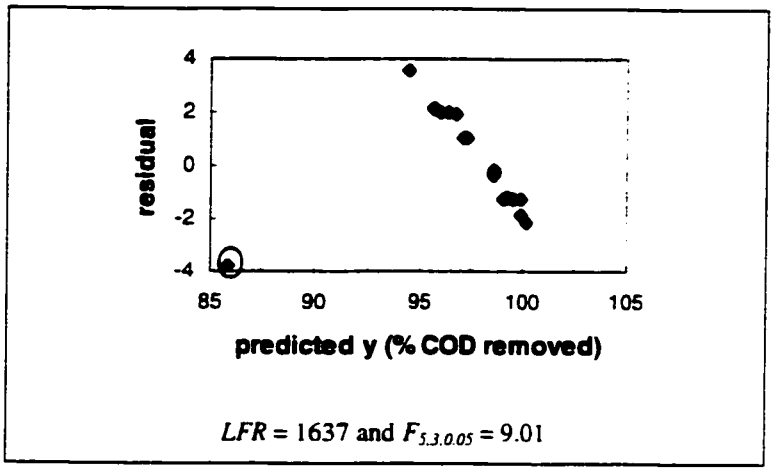

Figure 4–11 Residual plot for a fitted model from the central composite design, which included COD removal efficiency results for run 11.

Empirical models for COD removal efficiency, biomass activity, methane production, and methane potential as functions of the three coded variables (ADF concentration, HRT, and biomass concentration) are defined by the parameter estimates presented in Table 4–17. However, the 95% confidence intervals for the true value of each parameter β_i presented in Table 4–17 indicated that zero is a plausible value for some of the parameters and they can be discarded. Thus, the fitted empirical models based on a 2^3 factorial design can be reduced to the following:

$$\hat{y}_{activity} = 0.44 - 0.042x_1 + 0.027x_1x_2 \quad (23)$$

$$\hat{y}_{COD} = 98.39 + 0.22x_1 \quad (24)$$

$$\hat{y}_{CH_4\ potential} = 0.39 - 0.012x_2 + 0.0089x_3 - 0.025x_2x_3 \quad (25)$$

$$\hat{y}_{CH_4\ production} = 14.35 + 4.12x_1 - 4.94x_2 + 1.36x_3 - 1.04x_1x_2 + 0.90x_1x_3 - 1.46x_2x_3 - 1.00x_1x_2x_3 \quad (26)$$

The reduced fitted models must be tested for lack of fit. Lack of fit was checked by determining the lack of fit to pure error ratio, *LFR*, defined by equation **20**. The *LFR*

values and the respective $F_{\nu_1,\nu_2,\alpha}$ values for empirical models **23** to **26** are presented in Table 4–18. Lack of fit is not significant if $LFR < F_{\nu_1,\nu_2,\alpha}$. However, the sensitivity of this test is particularly dependent on ν_2 (the degrees of freedom associated with the estimate of the pure error variance, $\hat{\sigma}^2$). Since ν_2 was three, only gross inadequacies in the fitted models are detected. Thus, residual plots from the models are useful to confirm model fit and to diagnose the cause of the lack of fit.

The value of *LFR* is less than $F_{\nu_1,\nu_2,\alpha}$ for the fitted models **23** to **25** (activity, COD removal, and methane potential), residual plots for the fitted models **23** to **25** are presented in Figures 4–12 to 4–14. These residual plots should not show any particular trends for the data points presented. A plot of the residual ($y - \hat{y}$) against the predicted response ($\hat{y}$) can be used to identify possible outliers as in the case presented in Figure 4–11. The relatively random scattering of data points for the residual versus predicted response shown in Figures 4–12 to 4–14 suggested that there are no outliers present. As per methane production (model **26**), $LFR = 68.19 > F_{1,3,0.05} = 10.13$. This indicated that the fitted model **26** for methane production displayed lack of fit. Extension of the 2^3 factorial design to a central composite design will be required to improve model adequacy.

Table 4–18 ***LFR*** **values and respective** $F_{\nu_1,\nu_2,\alpha}$ **values for reduced models from the** 2^3 **factorial design.**

Response	ν_1	ν_2	α	*LFR*	$F_{\nu_1,\nu_2,\alpha}$	Lack of Fit
Activity	6	3	0.05	5.05	8.94	Not Significant
COD removal	6	3	0.05	5.60	8.94	Not Significant
CH_4 potential	5	3	0.05	2.12	9.01	Not Significant
CH_4 production	1	3	0.05	68.19	10.13	Significant

To identify the presence of time trend effects, the residual was plotted against run order. Residual versus run order plots in Figures 4–12 to 4–14 indicated that time trend

effects were significant for models **23** (biomass activity) and **25** (methane potential). This is not unexpected since all four reactors were operated in continuous mode, with minimal down time. Biomass used in the first set of runs was re-used in the next set of runs. Consequently, biomass in later runs should be different from those at the beginning, especially if chronic toxicities are involved.

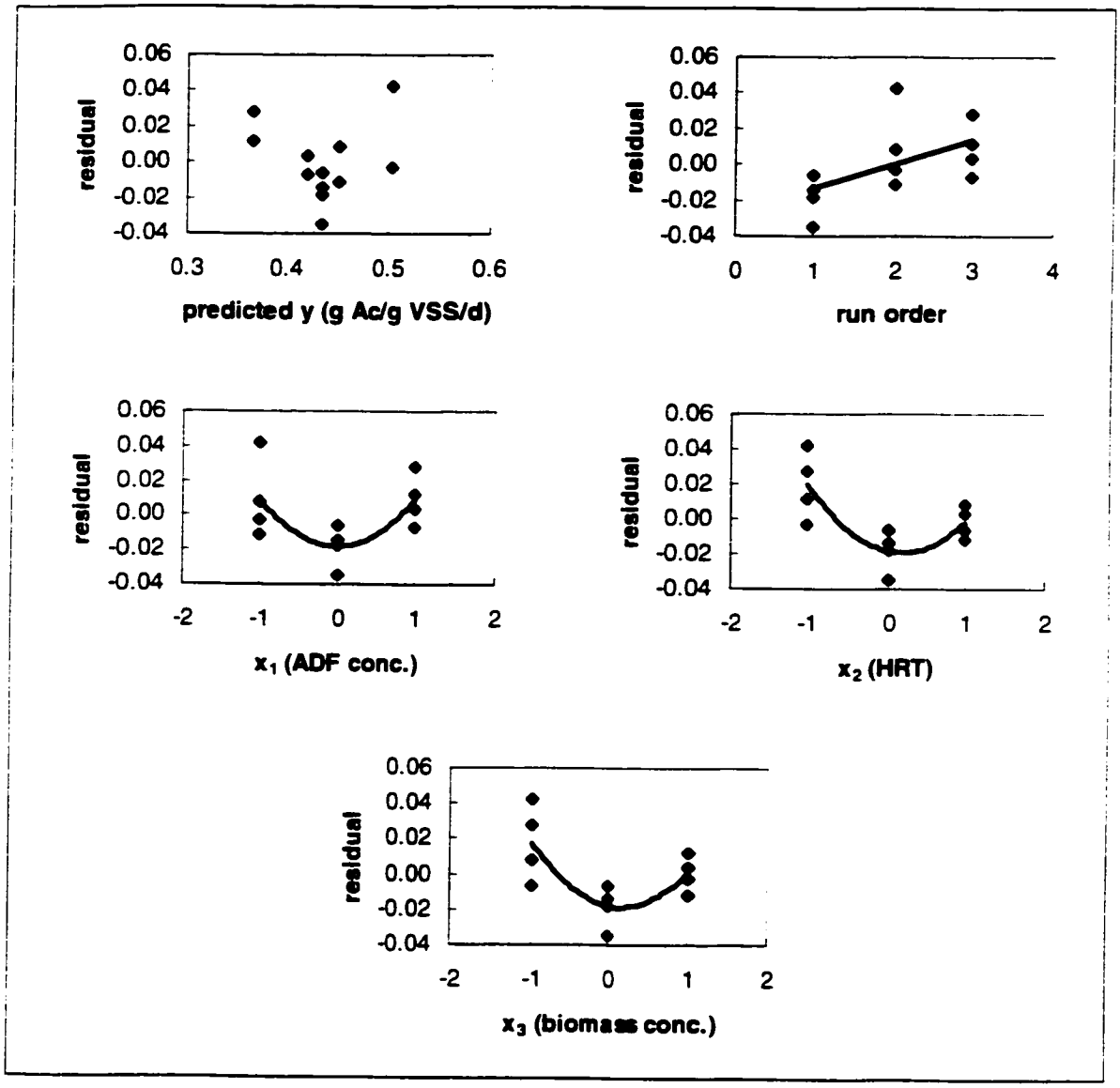

Figure 4–12 Residual plots for fitted model 23 (biomass activity) from the 2^3 factorial design.

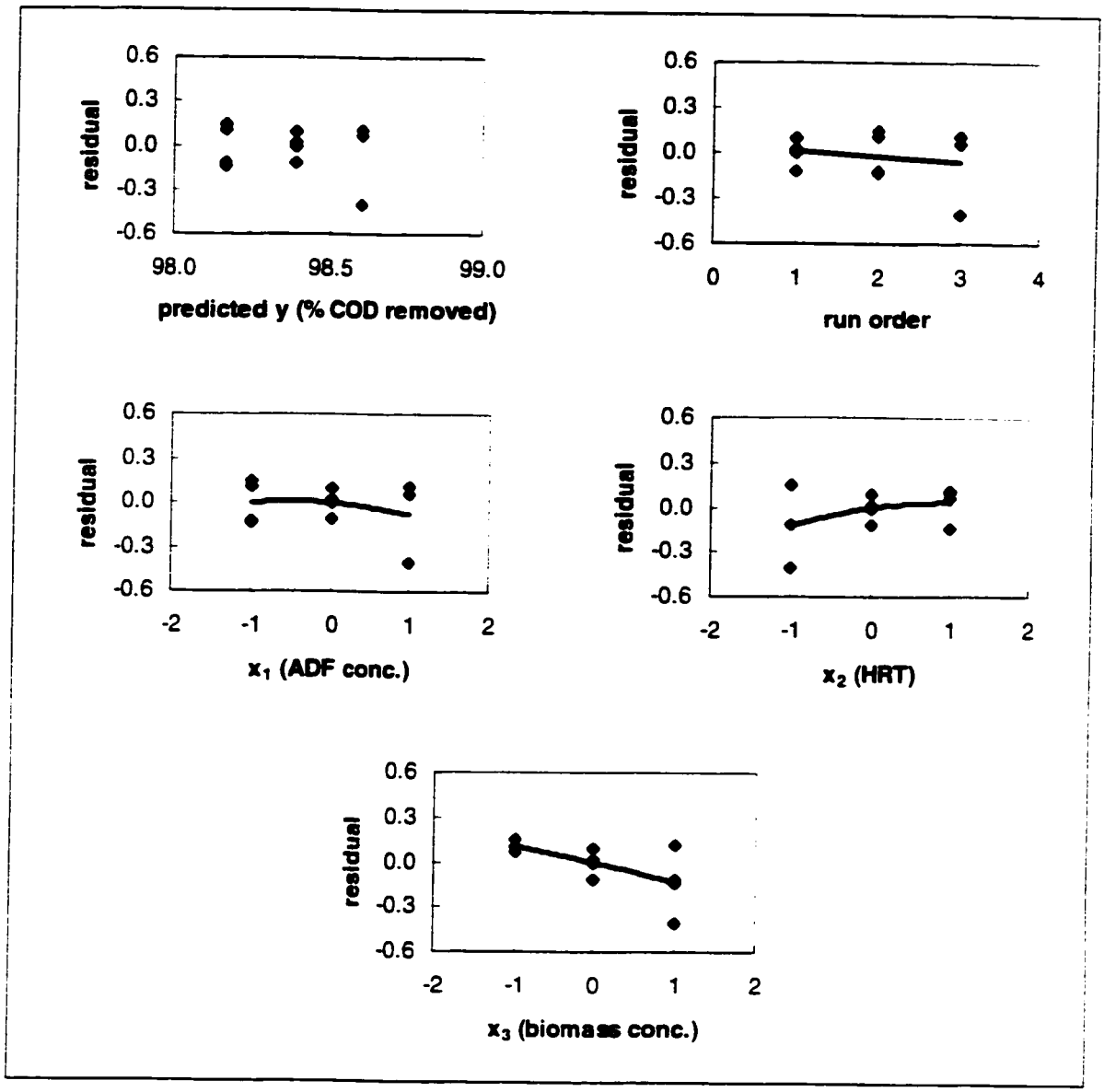

Figure 4–13 Residual plots for fitted model 24 **(COD removal) from the 2^3 factorial design.**

Time trend effects would probably be minimized if each run was seeded with new anaerobic granular biomass. This could be accomplished if a pilot-scale reactor were available to maintain at least 72 L of unacclimated granular biomass in a biologically active state (e.g., fed with a sucrose feed). Acclimation of this biomass reserve to ADF feed is not desirable since exposure to ADF may cause time dependent changes on the biomass since alcohols are known to cause changes in the structure of cell membranes

(Shuler and Kargi, 2002). Rather, acclimation of this sucrose-fed biomass to ADF must be carried out at the start of each run, using identical acclimation regimes to ensure identical starting points. However, this was not practical since several weeks would be required for each acclimation period. In addition, large volumes of active unacclimated granular biomass (at least 72 L) would be required and this biomass was not available from Lake Utopia Paper, New Brunswick.

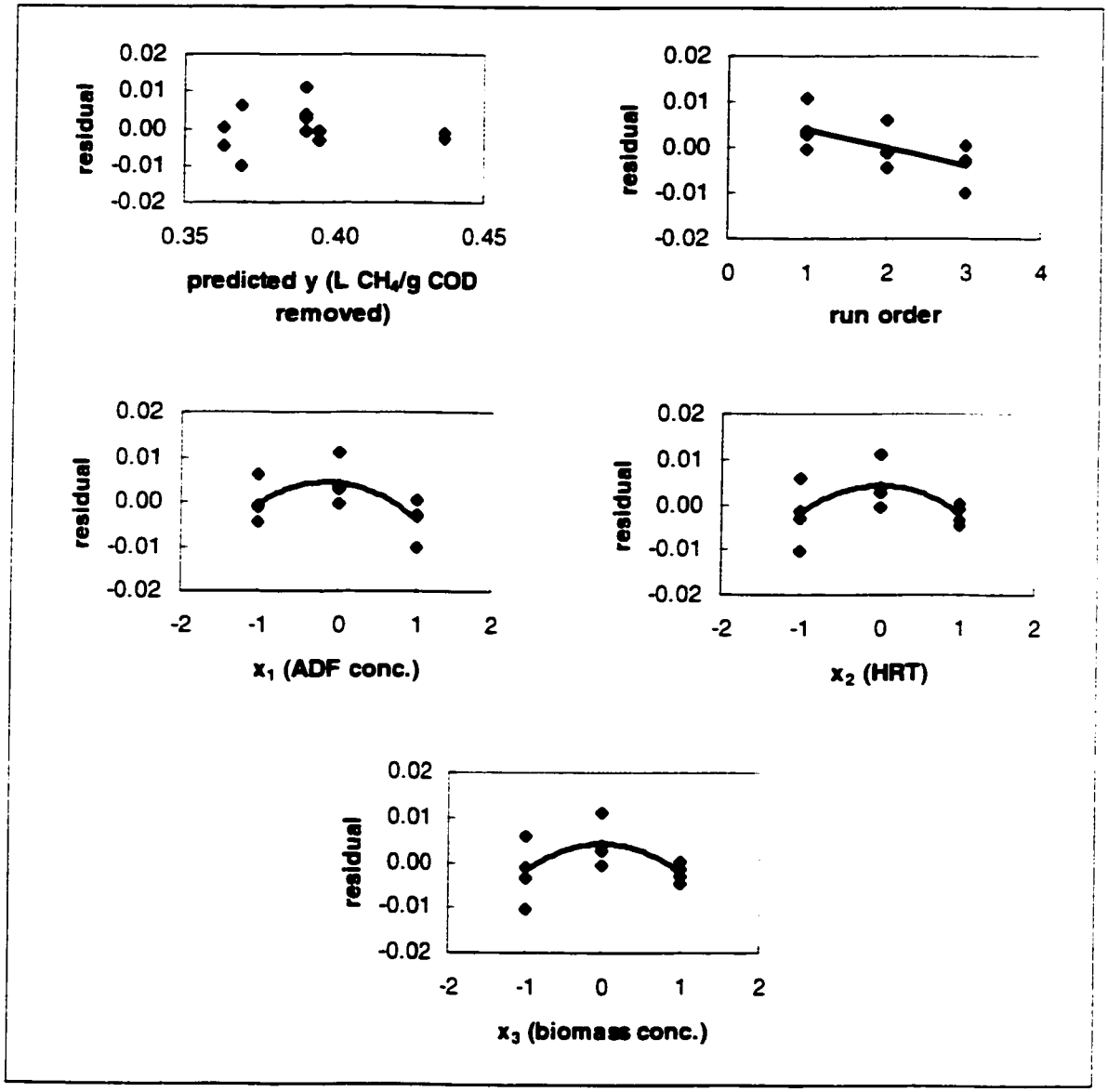

Figure 4–14 Residual plots for fitted model 25 (methane potential) from the 2^3 factorial design.

There was also the cost factor. At the lowest flow rate (48 h HRT), a total of 12 L of feed would be required for the four UASB reactors daily. For a two-week acclimation period, a total of 168 L of feed would be required. This would increase operation costs since chemicals must be added to the synthetic feed as nutrients and buffering capacity. Thus, elimination of time trend effects was not a viable option. Rather, model modification by the addition of extra terms to account for time trend effects were considered.

The need to modify the above reduced fitted empirical models (**23** to **25**) to include second-order terms was tested by plotting the residual against the three coded operating variables. Second-order terms are required if curvatures are present in these residual plots. From Figures 4–12 to 4–14, it was evident that second-order terms were required. Extension of the factorial design to a central composite design was thus required.

4.2.2 Central Composite Design

Extension of the 2^3 factorial design to the central composite design was achieved by adding six runs to make up the star portion of the design. The operating variables were coded as presented in Table 4–19. A typical star portion of the central composite design would involve trying each operating variable at $\pm\alpha$ (± 1.682) levels while keeping the other two variables at center level. However, $\pm\alpha$ levels for x_1 (ADF concentration) and x_3 (biomass concentration) could not be attained.

Only three levels of biomass concentration ($x_3 = -1, 0, +1$) were studied since these values represented 2, 3, and 4 L of biomass in a 6–L UASB reactor. Since biological treatment is a dynamic process where biomass is continuously being destroyed and generated, a quick determination of reactor biomass concentration at any given time must be based on the measurement of biomass bed height in the reactor. However,

methane is constantly being produced, resulting in an expansion of bed height, and so there would be a large uncertainty associated with a biomass volume difference of less than 1 L. Furthermore, using a biomass volume of less than 1 L would encounter the risk of washout effects (condition when the amount of biomass produced is less than the amount of biomass being washed out of the reactor and no waste stabilization takes place). On the other hand, biomass volumes of more than 4 L (more than ⅔ the reactor height) would also experience biomass washout due to bed expansion, so that the effective biomass volume in the reactor is less than the amount put in.

Table 4–19 Star portion of a the central composite design.

Reactor	Run	x_1 (%ADF)	x_2 (HRT)	x_3 (biomass conc.)
TP1	13	0 (1.2%)	0 (36 h)	−1 (17.8 g VSS/L)
TP2	14	0 (1.2%)	0 (36 h)	+1 (35.5 g VSS/L)
TP3	15	0 (1.2%)	+1.682 (56.1 h)	0 (26.6 g VSS/L)
TP4	16	0 (1.2%)	−1.682 (15.8 h)	0 (26.6 g VSS/L)
TP3	17	−1 (0.8%)	0 (36 h)	0 (26.6 g VSS/L)
TP4	18	+1 (1.6%)	0 (36 h)	0 (26.6 g VSS/L)

As per ADF concentration, an $x_1 = +\alpha$ would correspond to 1.9% ADF. It was believed that this concentration would be extremely inhibitory to the anaerobic biomass since operational problems were encountered for 1.6% ADF at a high SOLR. This was confirmed by the large inhibitory effects of 2% ADF observed in the ATA results for ADF-acclimated biomass presented in Figure 4–31. Consequently, $x_1 = +1$ (1.6% ADF) was taken as the upper limit for anaerobic ADF treatment in UASB reactors.

Reactor performances for the six runs of the star portion of the central composite deign are presented in Table 4–20. Steady-state data for these runs (run 13 – 18) can be found in Appendix I. Again, very high COD removal efficiencies (97.8 – 98.3%) were obtained. The methane potentials (0.32 – 0.37 L/g COD removed) were lower than those

obtained for the factorial portion (0.36 – 0.44 L/g COD removed); however, they were still similar to the theoretical value (0.39 L/g COD removed at 35°C). Biomass acetoclastic activities (0.28 – 0.46 g Ac/g VSS/d) were higher than that of the seed biomass (0.23 g Ac/g VSS/d), but they were lower than those obtained for the factorial portion (0.38 – 0.55 g Ac/g VSS/d).

Table 4–20 Reactor performance for the star portion of the central composite design.

Run	SOLR (g COD/g VSS/d)	Activity (g Ac/g VSS/d)	COD removal (%)	CH_4 production (L/d)	CH_4 Potential (L/g COD)
13	0.33±0.04	0.28±0.02	98.0±0.4	12.4±0.8	0.34±0.05
14	0.17±0.01	0.35±0.01	97.9±0.2	11.3±0.7	0.32±0.04
15	0.14±0.02	0.34±0.02	98.1±0.2	7.3±0.4	0.33±0.03
16	0.45±0.07	0.34±0.01	97.8±0.7	26.1±1.5	0.35±0.03
17	0.17±0.01	0.46±0.01	98.1±0.7	8.1±0.5	0.37±0.02
18	0.34±0.03	0.35±0.02	98.3±0.5	15.4±0.8	0.35±0.02

The results for the star portion of the central composite design were combined with those of the 2^3 factorial design (Tables 4–14 and 4–16) and fitted to model **21**. A 95% confidence interval for the true value of each parameter β_i in equation **21** was calculated based on the estimate of pure error variance obtained from center-point replicates. The parameter estimates and their 95% confidence intervals for the four process responses (biomass activity, COD removal efficiency, methane production, and methane potential) are presented in Table 4–21.

The value of $\hat{\beta}_0$ for biomass activity, COD removal efficiency, methane potential, and methane production are 0.38 g Ac/g VSS/d, 98.2% COD removal, 0.39 L/g COD removed, and 13.1 L/d, respectively (compared to 0.44 g Ac/g VSS/d, 98.4% COD removal, 0.39 L/g COD removed, and 14.4 L/d, respectively for the factorial portion). A

lower $\hat{\beta}_0$ was obtained for the new biomass activity empirical model since lower biomass acetoclastic activities were obtained for the star portion.

Table 4–21 Parameter estimates from the central composite design for the four process responses.

Parameter	95% confidence interval			
	Activity (g Ac/g VSS/d)	COD removal* (%)	CH_4 Potential (L/g COD removed)	CH_4 Production (L/d)
β_0	0.3823±0.0161	98.25±0.12	0.3920±0.0066	13.13±0.94
β_1	-0.0441±0.0120	0.12±0.10	-0.0019±0.0049	4.05±0.70
β_2	-0.0067±0.0102	0.11±0.08	-0.0107±0.0042	-5.23±0.60
β_3	0.0007±0.0120	-0.04±0.10	0.0043±0.0049	0.95±0.70
β_{11}	0.0735±0.0215	0.15±0.16	0.0180±0.0088	-0.30±1.26
β_{22}	-0.0074±0.0103	-0.07±0.07	-0.0072±0.0042	1.39±0.60
β_{33}	-0.0170±0.0215	-0.08±0.16	-0.0026±0.0088	0.05±1.26
β_{12}	0.0268±0.0134	0.15±0.12	0.0025±0.0055	-1.04±0.78
β_{13}	0.0073±0.0134	0.09±0.12	0.0027±0.0055	0.90±0.78
β_{23}	0.0064±0.0134	-0.01±0.12	-0.0249±0.0055	-1.46±0.78

* Run 11 ($x_1 = +1, x_2 = -1, x_3 = -1$) was excluded.

Based on the results presented in Table 4–21, operating parameters containing zero as a plausible value were eliminated from the fitted models. The reduced empirical models from the central composite design are as follows:

$$\hat{y}_{activity} = 0.38 - 0.044x_1 + 0.074x_1^2 + 0.027x_1x_2 \quad (27)$$

$$\hat{y}_{COD} = 98.25 + 0.12x_1 + 0.11x_2 + 0.15x_1x_2 \quad (28)$$

$$\hat{y}_{CH_4\ potential} = 0.37 - 0.011x_2 + 0.018x_1^2 - 0.0072x_2^2 - 0.025x_2x_3 \quad (29)$$

$$\hat{y}_{CH_4\ production} = 13.13 + 4.05x_1 - 5.23x_2 + 0.95x_3 + 1.39x_2^2 - 1.04x_1x_2 + 0.90x_1x_3 - 1.46x_2x_3 \quad (30)$$

Model lack of fit was again tested by determining the lack of fit to pure error ratio *LFR* using equation **20**. The *LFR* values and the respective $F_{\nu_1,\nu_2,\alpha}$ values for equations **27** to **30** are presented in Table 4–22. Comparison of the ratio *LFR* to the corresponding

$F_{\nu_1,\nu_2,\alpha}$ value indicated that the reduced fitted models for biomass activity (model **27**) and methane potential (model **29**) displayed lack of fit ($LFR > F_{\nu_1,\nu_2,\alpha}$). Lack of fit was not significant for COD removal efficiency (model **28**, $LFR = 7.26 < F_{10,3,0.05} = 8.79$) and methane production (model **30**, $LFR = 7.77 < F_{7,3,0.05} = 8.89$). Again, residual plots are required for confirmation of model adequacy. Plots of the residual ($y - \hat{y}$) against run order for the four responses are presented in Figure 4–15. Linear trends were observed, indicating that time trend effects were significant for all four models.

Table 4–22 ***LFR*** **values and respective** $F_{\nu_1,\nu_2,\alpha}$ **values for reduced empirical models from the central composite design.**

Response	ν_1	ν_2	α	*LFR*	$F_{\nu_1,\nu_2,\alpha}$	Lack of Fit
Activity	11	3	0.05	18.59	8.76	Significant
COD removal	10	3	0.05	7.26	8.79	Not Significant
CH_4 potential	10	3	0.05	37.07	8.79	Significant
CH_4 production	7	3	0.05	7.77	8.89	Not Significant

It is likely that the time trend effects seen in Figure 4–15 was due to the fact that the star portion of the design was carried out several months after completion of the 2^3 factorial design. A blocking variable *B* was thus added to account for the difference in biomass properties before and after this storage period. This blocking variable was coded as follows:

B = −1 for the factorial portion (active biomass before storage)

B = +1 for the star portion (active biomass after storage for 4 months)

Process responses from the central composite design were thus refitted to the following blocked model:

$$y = \beta_0 + \beta_1 x_1 + \beta_2 x_2 + \beta_3 x_3 + \beta_{11} x_1^2 + \beta_{22} x_2^2 + \beta_{33} x_3^2 + \beta_{12} x_1 x_2 + \beta_{13} x_1 x_3 + \beta_{23} x_2 x_3 + \beta_B B \quad (31)$$

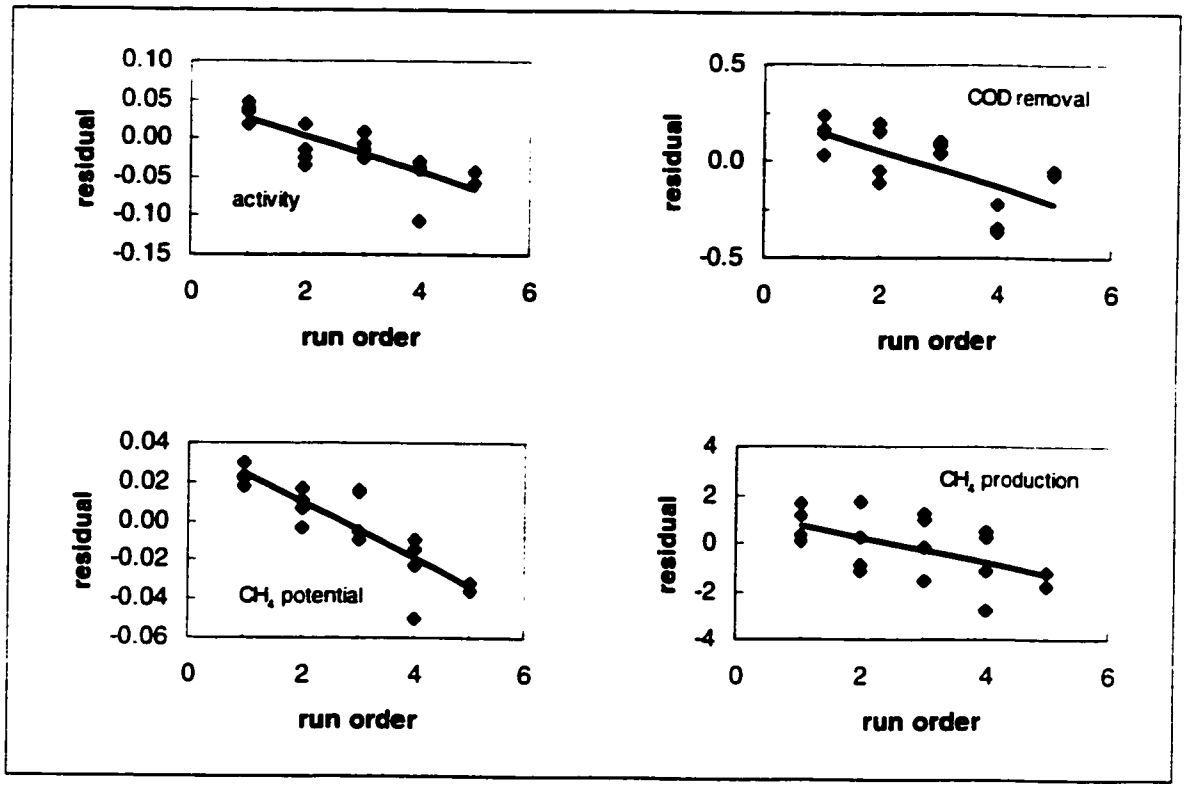

Figure 4–15 Residual plots for fitted models from the central composite deign.

The parameter estimates and their 95% confidence intervals for the four process responses based on blocked model **31** are presented in Table 4–23. Similar values for the parameter estimate $\hat{\beta}_0$ were obtained for biomass activity, COD removal efficiency, methane potential, and methane production (0.38 g Ac/g VSS/d, 98.2% COD removal, 0.37 L/g COD removed, and 13.1 L/d compared to 0.38 g Ac/g VSS/d, 98.2% COD removal, 0.37 L/g COD removed, and 13.1 L/d for central composite design without blocking variable). Elimination of operating parameters which contain zero as a plausible value resulted in the final reduced fitted models presented in Table 4–24.

Test for lack of fit was performed on the reduced models from the blocked central composite design (Table 4–24) and the results are presented in Table 4–25. Based on this test, the lack of fit ratio *LFR* was not significant ($LFR < F_{\nu_1,\nu_2,\alpha}$) for all four responses

(models **32** to **35**). The residual plots for these four reduced fitted models are presented in Figures 4–16 to 4–19.

Table 4–23 Parameter estimates from the blocked central composite design for the four responses.

Parameter	95% confidence interval			
	Activity (g Ac/g VSS/d)	COD removal* (%)	CH_4 Potential (L/g COD removed)	CH_4 Production (L/d)
β_0	0.3812±0.0161	98.235±0.117	0.3713±0.0066	13.10±0.94
β_1	-0.0441±0.0120	0.143±0.104	-0.0019±0.0049	4.05±0.70
β_2	-0.0067±0.0102	0.097±0.085	-0.0107±0.0042	-5.23±0.60
β_3	0.0007±0.0120	-0.066±0.104	0.0043±0.0049	0.95±0.70
β_{11}	0.0593±0.0219	0.102±0.161	0.0086±0.0090	-0.63±1.28
β_{22}	-0.0008±0.0105	-0.043±0.077	-0.0028±0.0043	1.54±0.61
β_{33}	-0.0312±0.0219	-0.132±0.161	-0.0120±0.0090	-0.28±1.28
β_{12}	0.0269±0.0134	0.124±0.121	0.0025±0.0055	-1.04±0.78
β_{13}	0.0074±0.0134	0.063±0.121	0.0027±0.0055	0.90±0.78
β_{23}	0.0065±0.0134	-0.015±0.121	-0.0249±0.0055	-1.46±0.78
B_B	-0.0357±0.0103	-0.153±0.076	-0.0236±0.0042	-0.83±0.60

* Run 11 ($x_1 = +1, x_2 = -1, x_3 = -1$) was excluded.

Table 4–24 Reduced fitted models from the blocked central composite design.

$$\hat{y}_{activity} = 0.381 - 0.044x_1 + 0.059x_1^2 - 0.031x_3^2 + 0.027x_1x_2 - 0.036B \quad (32)$$

$$\hat{y}_{COD} = 98.24 + 0.14x_1 + 0.097x_2 + 0.12x_1x_2 - 0.15B \quad (33)$$

$$\hat{y}_{CH_4\ potential} = 0.371 - 0.011x_2 - 0.012x_3^2 - 0.025x_2x_3 - 0.024B \quad (34)$$

$$\hat{y}_{CH_4\ production} = 13.10 + 4.05x_1 - 5.23x_2 + 0.95x_3 + 1.54x_2^2 - 1.04x_1x_2 + 0.90x_1x_3 - 1.46x_2x_3 - 0.83B \quad (35)$$

Table 4–25 *LFR* values and respective $F_{\nu_1,\nu_2,\alpha}$ values for reduced empirical models from the blocked central composite design.

Response	ν_1	ν_2	α	*LFR*	$F_{\nu_1,\nu_2,\alpha}$	Lack of Fit
Activity	9	3	0.05	4.29	8.81	Not Significant
COD removal	9	3	0.05	3.10	8.81	Not Significant
CH_4 potential	10	3	0.05	7.34	8.79	Not Significant
CH_4 production	6	3	0.05	8.27	8.94	Not Significant

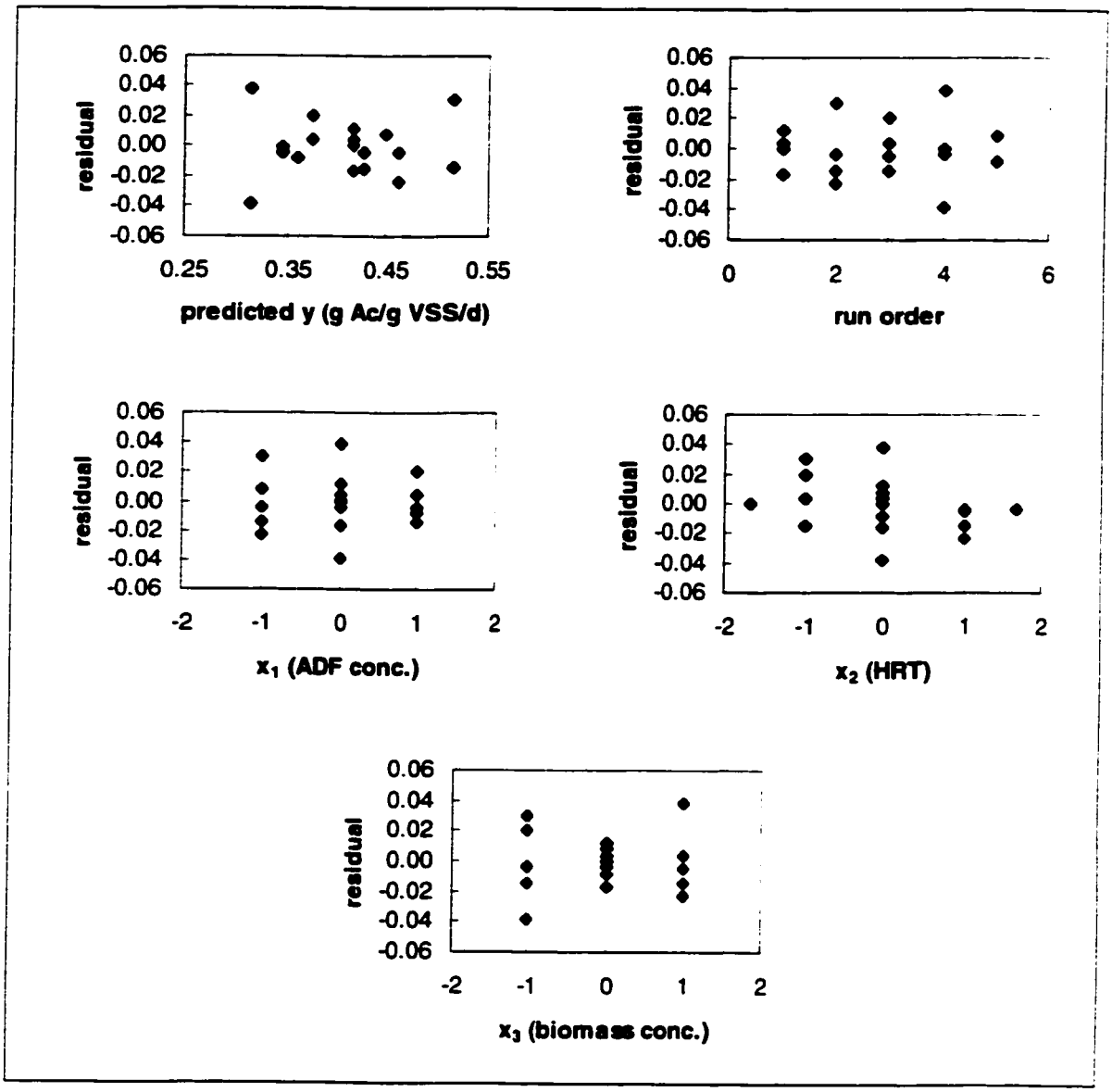

Figure 4–16 Residual plots for specific acetoclastic activity model from the blocked central composite design.

In general, the data points are randomly scattered and time trend effects are no longer evident in any of the plots presented in Figures 4–16 to 4–19. Curvature trends are no longer observed in the residual versus operating variable plots. Hence, trend lines are not included in any of the residual plots presented in Figures 4–16 to 4–19.

Additionally, it can be said that the reduced fitted models from the blocked central composite design presented in Table 4–24 revealed no evidence for lack of fit.

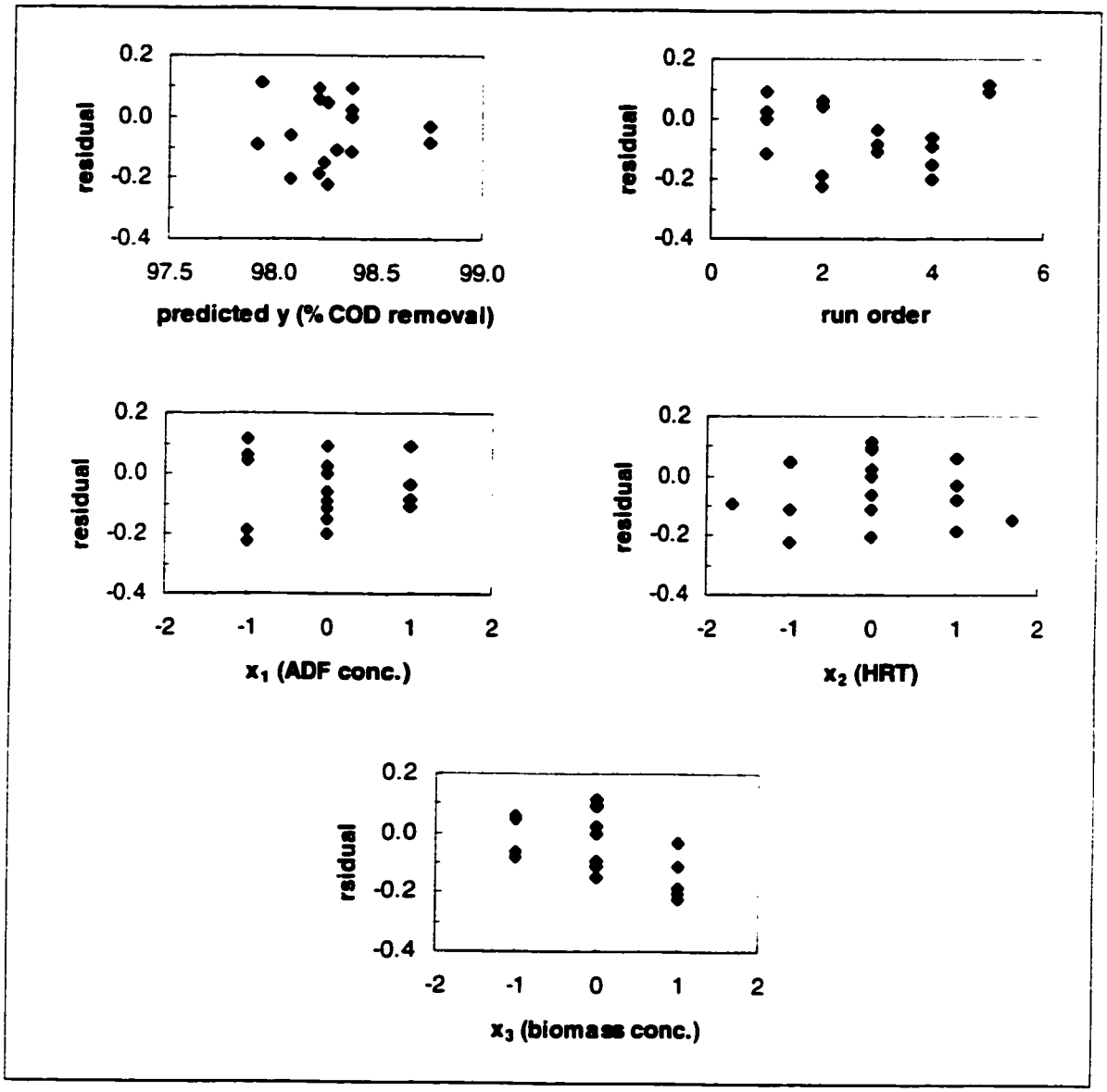

Figure 4–17 Residual plots for COD removal model from the blocked central composite design.

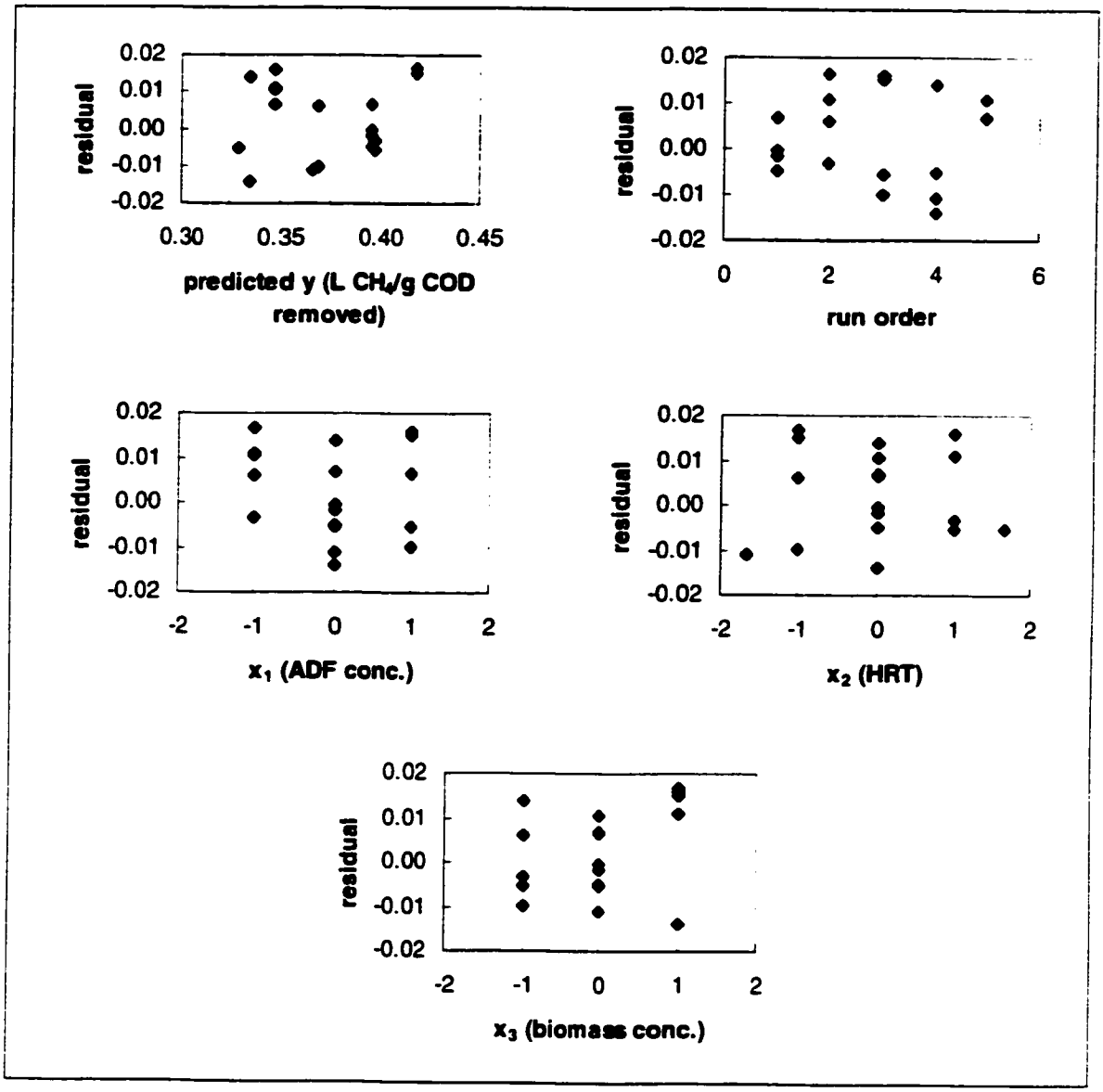

Figure 4–18 Residual plots for methane potential model from the blocked central composite design.

The parameter estimates for the reduced fitted models (**32** to **35**) from the blocked central composite design are no longer uncorrelated as the parameters obtained from the 2^3 factorial design (see Appendix A). This means that the observed effects are no longer independent of each other. A change in one effect (parameter) will change another effect. For example, a positive correlation between effect *a* and effect *b* means that if the value of *a* is increased, the value of *b* will also be increased. A negative correlation indicates at

an increase in the value of one effect will result in a decrease in the value of the other effect. Correlations make the optimization process more difficult since operating variables and their effects must be considered together.

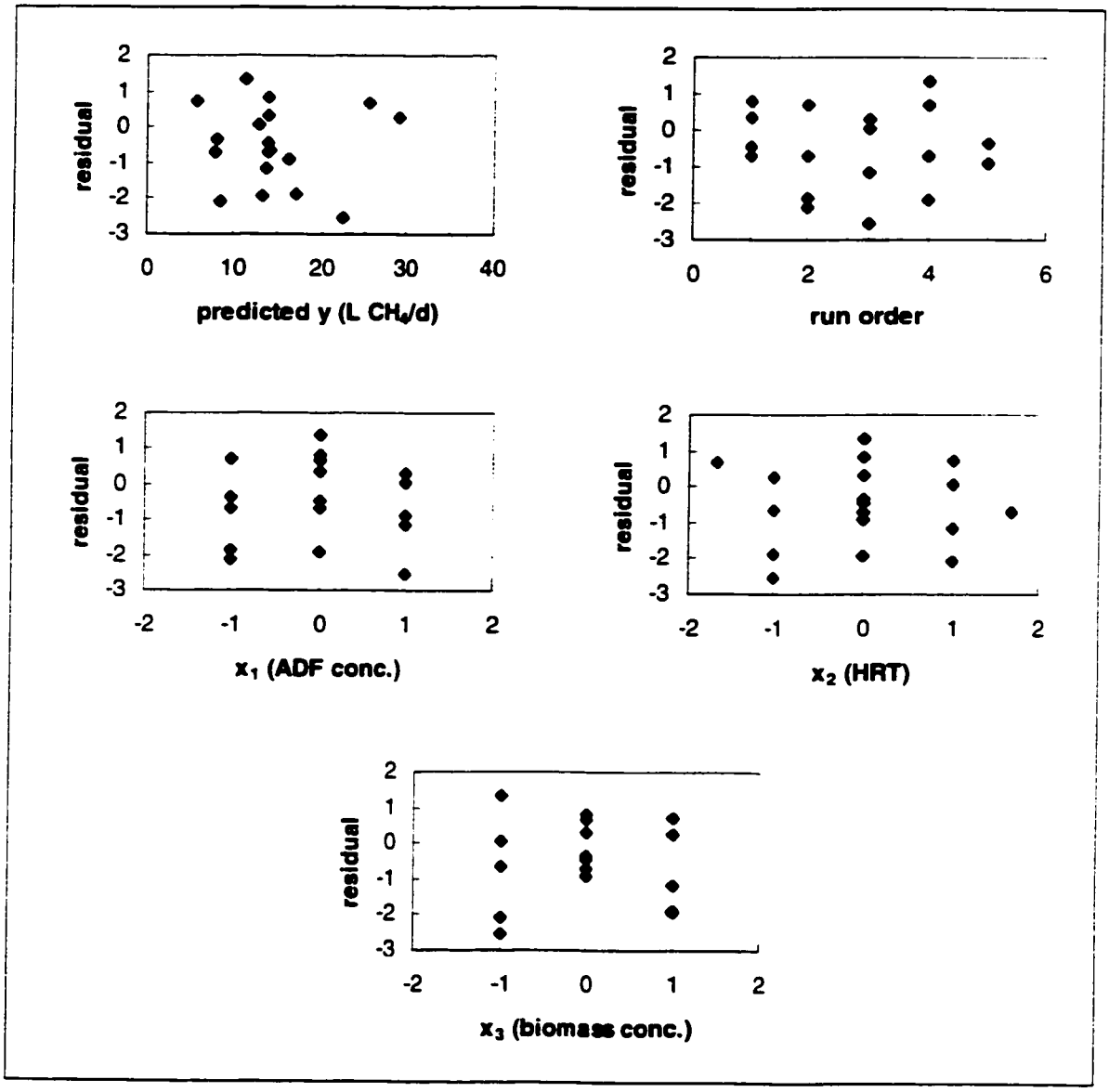

Figure 4–19 Residual plots for methane production model from the blocked central composite design.

The estimated correlations $\hat{\rho}(\hat{\beta}_i, \hat{\beta}_j)$ between $\hat{\beta}_i$ and $\hat{\beta}_j$ for the reduced models **32. 34.** and **35** are presented in Table 4–26. Since correlation values must lie between –1 and +1. there was a significant negative linear correlation between $\hat{\beta}_0$ and the estimated parameters of the second-order terms ($\hat{\beta}_{ii}$). The estimated correlation between $\hat{\beta}_{11}$ (ADF concentration squared term) and $\hat{\beta}_{33}$ (biomass concentration squared term) was also significant. There was less correlation between $\hat{\beta}_{22}$ (HRT squared term) and $\hat{\beta}_{ii}$. and most of the correlations involving the block variable *B* were positive.

Table 4–26 Summary of the non-zero estimated correlation between the parameter estimates of the fitted models for biomass activity and methane production and potential obtained from the blocked central composite design.

	$\hat{\beta}_0$	$\hat{\beta}_{11}$	$\hat{\beta}_{22}$	$\hat{\beta}_{33}$
$\hat{\beta}_{11}$	–0.31	–	–0.06	–0.49
$\hat{\beta}_{22}$	–0.44	–0.06	–	–0.06
$\hat{\beta}_{33}$	–0.31	–0.49	–0.06	–
$\hat{\beta}_B$	+0.02	+0.19	–0.18	+0.19

For the reduced fitted COD model (**33**). one experimental run (run 11) was excluded from the model fitting process. As a result. all terms in the $(\mathbf{X}^T\mathbf{X})^{-1}$ matrix were non-zero (Appendix A). As such. all parameter estimates for this fitted model were correlated. Optimization will be difficult since it is difficult to discern which effect produced the observed response. All operating variables and their effects must be dealt with as an integrated unit. A summary of the correlation estimates for the reduced fitted model **33** is presented in Table 4–27. Correlations involving $\hat{\beta}_0$ were much less than those involving first-order effects and their interactions.

Table 4–27 Summary of the non-zero estimated correlation between the parameter estimates of the reduced fitted model for COD removal efficiency from the blocked central composite design.

	$\hat{\beta}_0$	$\hat{\beta}_1$	$\hat{\beta}_2$	$\hat{\beta}_{12}$
$\hat{\beta}_1$	–0.07	–	–0.27	–0.33
$\hat{\beta}_2$	+0.06	–0.27	–	+0.29
$\hat{\beta}_{12}$	+0.08	–0.33	+0.29	–
$\hat{\beta}_B$	+0.05	–0.11	+0.10	+0.12

The reduced fitted models (**32** to **35**) can be expressed in terms of the original (uncoded) operating variables as presented in Table 4–28. For all four models (**36** to **39**), the effect of the blocking variable was negative. This was expected since the biomass was less active after a four-month storage period. Anaerobic granules are known to be resilient and can be stored for long periods of time without significant loss in activity (Speece, 1996). In this case, some of the biomass (reactor TP3 operating at $x_1 = +1$, $x_2 = -1$, $x_3 = -1$) was under stress when it was taken off-line. The granules from all four UASB reactors were pooled prior to running the star portion of the design. Better retention of activity might have resulted if the biomass was in its prime condition when it was placed into storage.

The reduced fitted model **36** suggested that the specific acetoclastic activity of the biomass was largely affected by ADF concentration. An increase in ADF concentration would result in a large decrease in biomass acetoclastic activity. This model prediction is in agreement with ATA results (Figures 4–10 and 4–31) which indicated that high ADF concentrations were toxic to the anaerobic granular biomass used.

Table 4–28 Reduced fitted empirical models from the blocked central composite design in original (uncoded) variables*.

Predicted Specific Activity = 1.01 – 1.20 (%ADF) – 0.0067 (HRT) + 0.021 [Biomass] + 0.37 (%ADF)^2 – 0.00040 [Biomass]^2 + 0.0056 (%ADF) (HRT) – 0.036 B	**(36)**
Predicted COD Removal = 98.63 – 0.57 (%ADF) – 0.023 (HRT) + 0.026 (%ADF) (HRT) – 0.15 B	**(37)**
Predicted CH_4 Potential = 0.071 + 0.0053 (HRT) + 0.017 [Biomass] – 0.00015 [Biomass]^2 – 0.00023 (HRT) [Biomass] – 0.024 B	**(38)**
Predicted CH_4 Production = 13.21 + 11.19 (%ADF) – 0.58 (HRT)+ 0.30 [Biomass] + 0.011 (HRT)^2 – 0.22 (%ADF) (HRT) + 0.25 (%ADF) [Biomass] – 0.014 (HRT) [Biomass] – 0.83 B	**(39)**

* %ADF is percentage ADF, HRT is in hours, [Biomass] is biomass concentration in g VSS/L, B is –1 if the biomass is active, and B is +1 if the biomass came from storage.

A graphical representation of model **36** is required to facilitate model interpretation. A plot can be done only if a response is a function of one or two operating variables. Thus, for B = –1 and biomass concentration of 27 gVSS/L (biomass level at ½ reactor volume), model **36** is simplified to

$$\text{Predicted Specific Activity} = 1.32 - 1.20\,(\%\text{ADF}) - 0.0067\,(\text{HRT}) + 0.37\,(\%\text{ADF})^2 + 0.0056\,(\%\text{ADF})\,(\text{HRT}) \quad \textbf{(40)}$$

For B = –1 and biomass level at ⅓ or ⅔ reactor volume (18 or 36 g VSS/L), model **36** is simplified to

$$\text{Predicted Specific Activity} = 1.29 - 1.20\,(\%\text{ADF}) - 0.0067\,(\text{HRT}) + 0.37\,(\%\text{ADF})^2 + 0.0056\,(\%\text{ADF})\,(\text{HRT}) \quad \textbf{(41)}$$

The predicted response surfaces for specific acetoclastic activity (models **40** and **41**) are similar in structure (Figure 4–20). The plot of model **40** (Figure 4–20A) is of interest since full-scale UASB reactors are usually operated with biomass levels at ½ full. Contour plots of the predicted response surfaces are also presented for better clarity.

As expected, better biomass specific acetoclastic activity was predicted for low HRT and low ADF concentration. As mentioned earlier, high ADF levels were toxic to

the biomass. In addition, it is reasonable that a decrease in HRT should accompany a decrease in ADF concentration. For optimum activity, the carbon source should not be limited. If the COD concentration in the feed is reduced, then the HRT must be decreased to maintain a certain level of OLR. If the ADF concentration of the wastewater is 1% ADF, the specific acetoclastic activity of the biomass is expected to be 0.45 - 0.50 g Ac/g VSS/d. This value is 2-fold greater than that of the seed granular sludge from Lake Utopia Paper (0.23 g Ac/g VSS/d).

A plot of the predicted response surface for COD removal efficiency (model **37**) where B = −1 is presented in Figure 4–21. Better COD removal efficiencies were predicted for higher ADF concentrations at longer HRTs. This is likely related to substrate limitations at long HRT and low ADF levels. For example, for the lowest biomass concentration used (18 g VSS/L), the SOLR would only be 0.08 g COD/g VSS/d for 0.5% ADF operated at an HRT of 72 h. In addition, COD removal efficiencies were based on the difference between influent and effluent COD content. The lowest effluent COD obtained during the course of the study was above 100 mg/L. Consequently, decreasing influent COD content would result in a decrease in removal efficiency.

At shorter HRTs, Figure 4–21 predicted better COD removal efficiencies for low ADF levels. This was expected since the SOLR is large for shorter HRT and high ADF levels. In addition, ADF toxicity effects may also become important at short HRTs. Better COD removal efficiencies were also predicted for longer HRT and high ADF levels; however, it is of little interest to operate at long HRTs in high-rate UASB reactors.

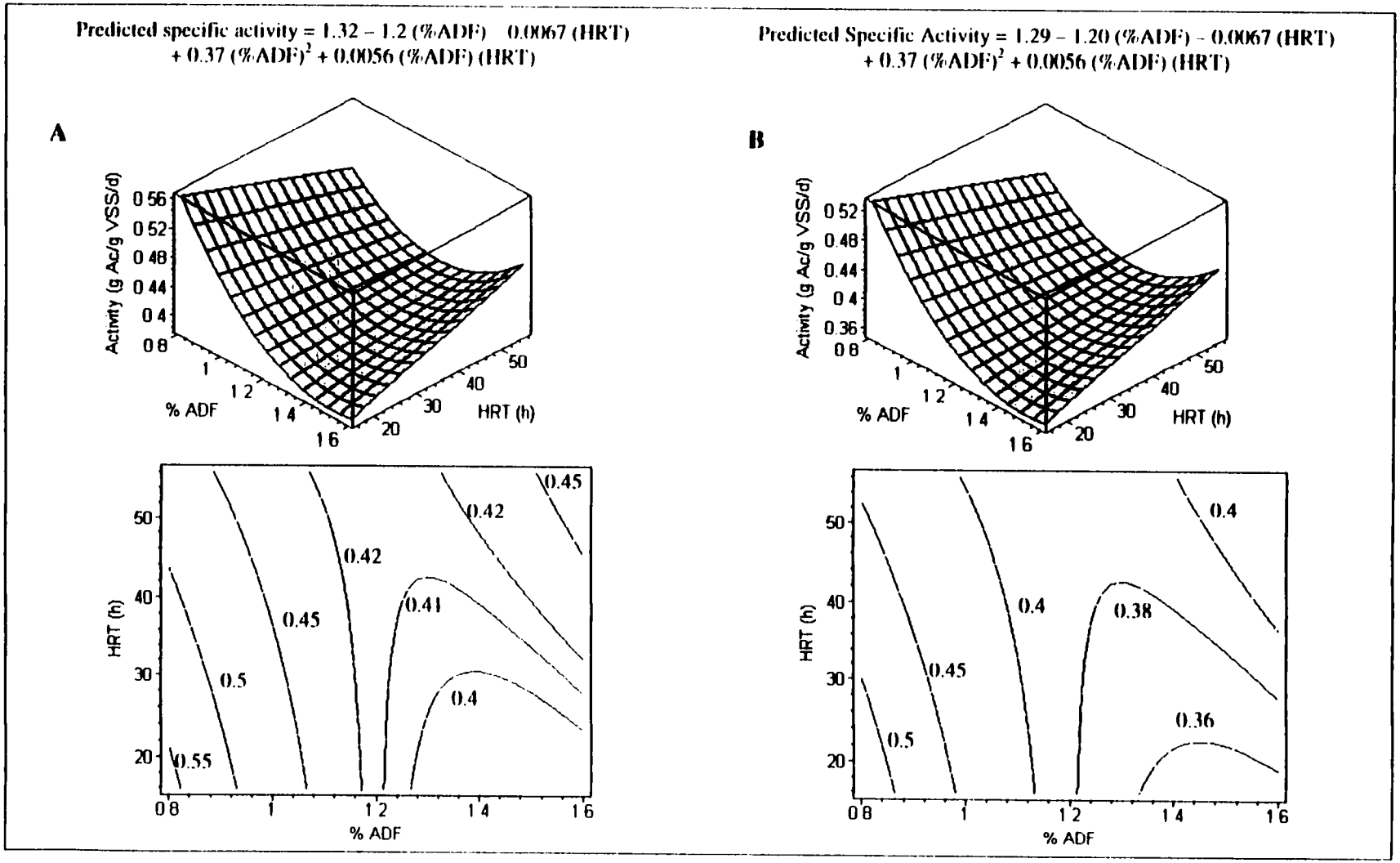

Figure 4–20 Predicted biomass specific acetoclastic activity for ADF treatment at 35°C and biomass concentration of: (A) 27 g VSS/L (reactor biomass volume at ½ full) and (B) 18 or 36 g VSS/L (biomass level at ⅓ or ⅔ reactor volume).

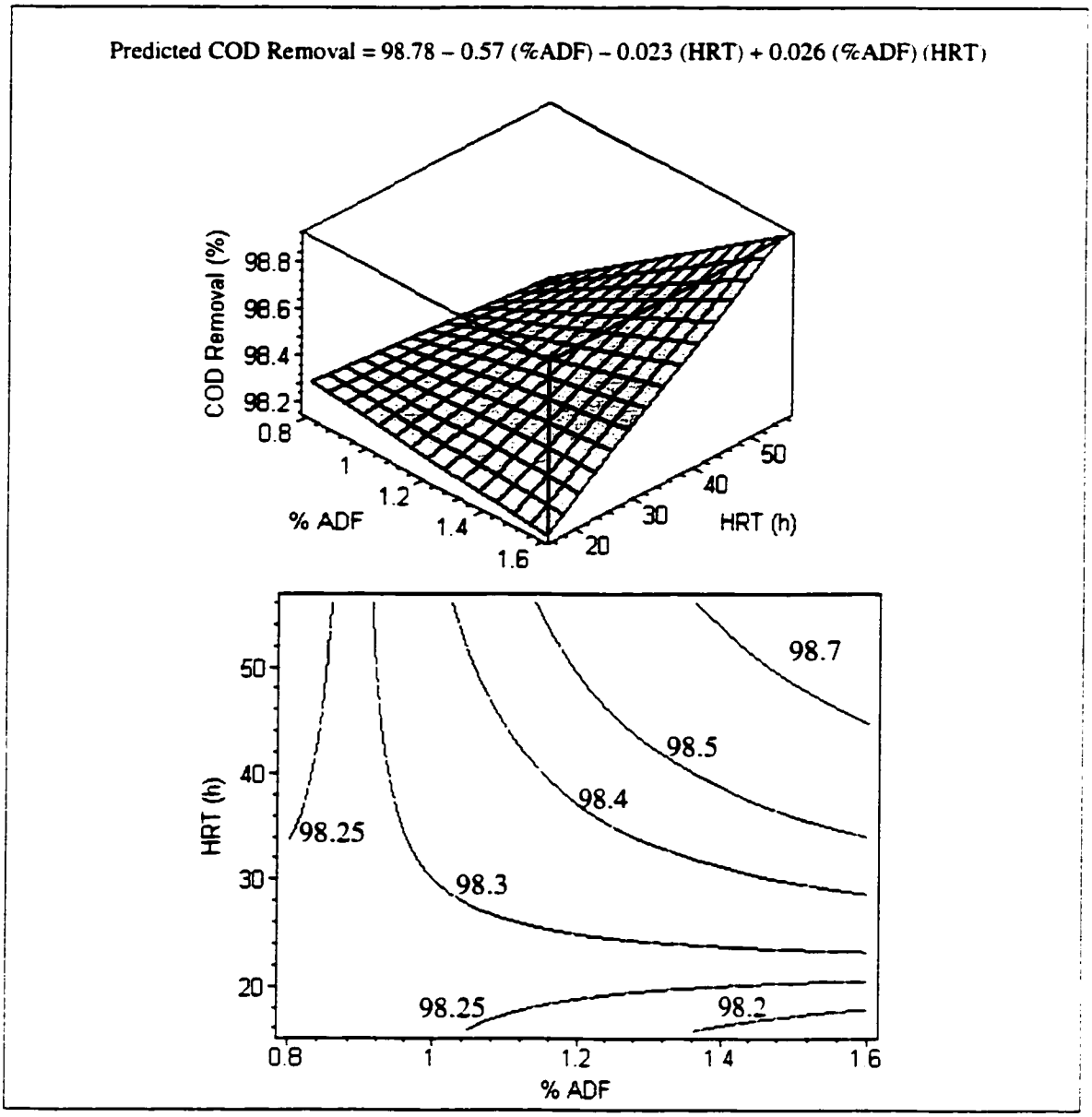

Figure 4–21 Predicted COD removal efficiency for ADF treatment at 35°C.

A plot of the predicted response surface for methane production potential (model **38**) where B = –1 is presented in Figure 4–22. The theoretical value of 0.39 L CH_4/g COD removed at 35°C was predicted for a biomass concentration of 27 g VSS/L (reactor biomass volume at ½ full) for the plotted HRT range of 3 – 72 h. Endogenous decay was probably the reason for predicted methane potentials higher than 0.39 L CH_4/g COD

removed for high biomass concentrations at short HRT levels. The SOLR is high for low biomass concentration at short HRT levels. Thus, it was likely that substrate inhibition of the methanogens might be involved. Impediment of methanogenesis would lead to lower methane content in the biogas, and ultimately a lower methane potential.

Simplification of the reduced fitted model for methane production (**39**) was required before a plot of the predicted response surface can be made. For B = −1 and biomass level at ⅓ reactor volume (18 g VSS/L), model **39** is simplified to

$$\text{Predicted } CH_4 \text{ Production} = 19.33 + 15.69\,(\%ADF) - 0.82\,(HRT) + 0.011\,(HRT)^2 - 0.22\,(\%ADF)\,(HRT) \quad (42)$$

For B = −1 and biomass level at ½ reactor volume (27 g VSS/L), model **39** is reduced to

$$\text{Predicted } CH_4 \text{ Production} = 21.97 + 17.93\,(\%ADF) - 0.95\,(HRT) + 0.011\,(HRT)^2 - 0.22\,(\%ADF)\,(HRT) \quad (43)$$

For B = −1 and biomass level at ⅔ reactor volume (36 g VSS/L), model **39** is reduced to

$$\text{Predicted } CH_4 \text{ Production} = 24.61 + 20.18\,(\%ADF) - 1.07\,(HRT) + 0.011\,(HRT)^2 - 0.22\,(\%ADF)\,(HRT) \quad (44)$$

Graphical representations of the above models are presented in Figure 4–23.

As expected, higher methane production was predicted for higher OLRs (short HRT and high ADF concentration). At high OLRs, more substrates are available for conversion to methane. Higher methane production rates should result even if the conversion efficiency is reduced as a result of extremely high OLRs.

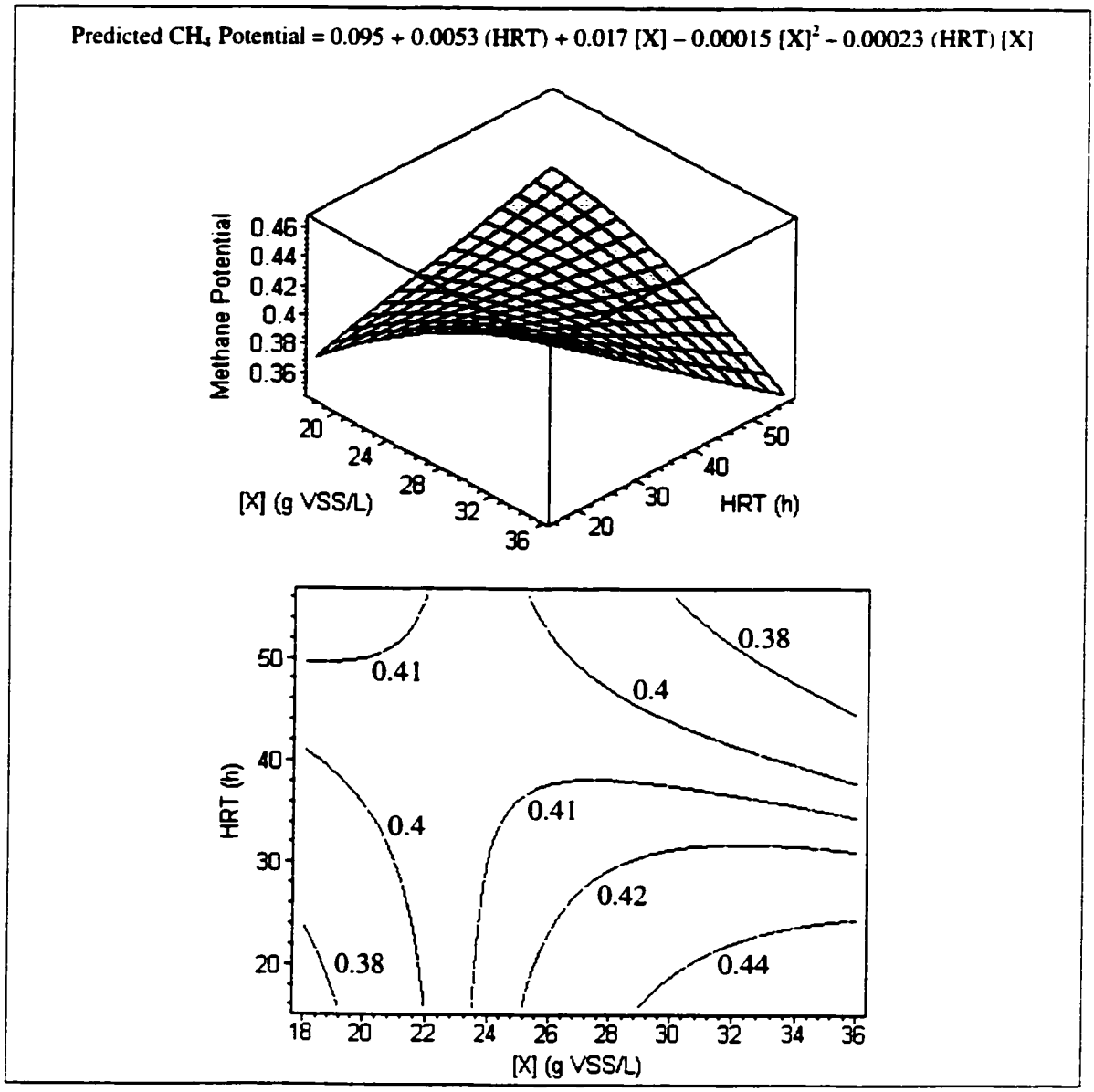

Figure 4–22 Predicted methane potential for ADF treatment at 35°C.

For the same level of OLR, the SOLR is decreased as the biomass concentration is increased. Methane conversion efficiency is expected to increase as SOLR decreases, thus methane production rates should increase. This is in agreement with the response surface behavior depicted in Figure 4–23. At high ADF concentration and short HRT levels, the highest methane production rates were predicted for the highest reactor biomass concentration (Figure 4–23C).

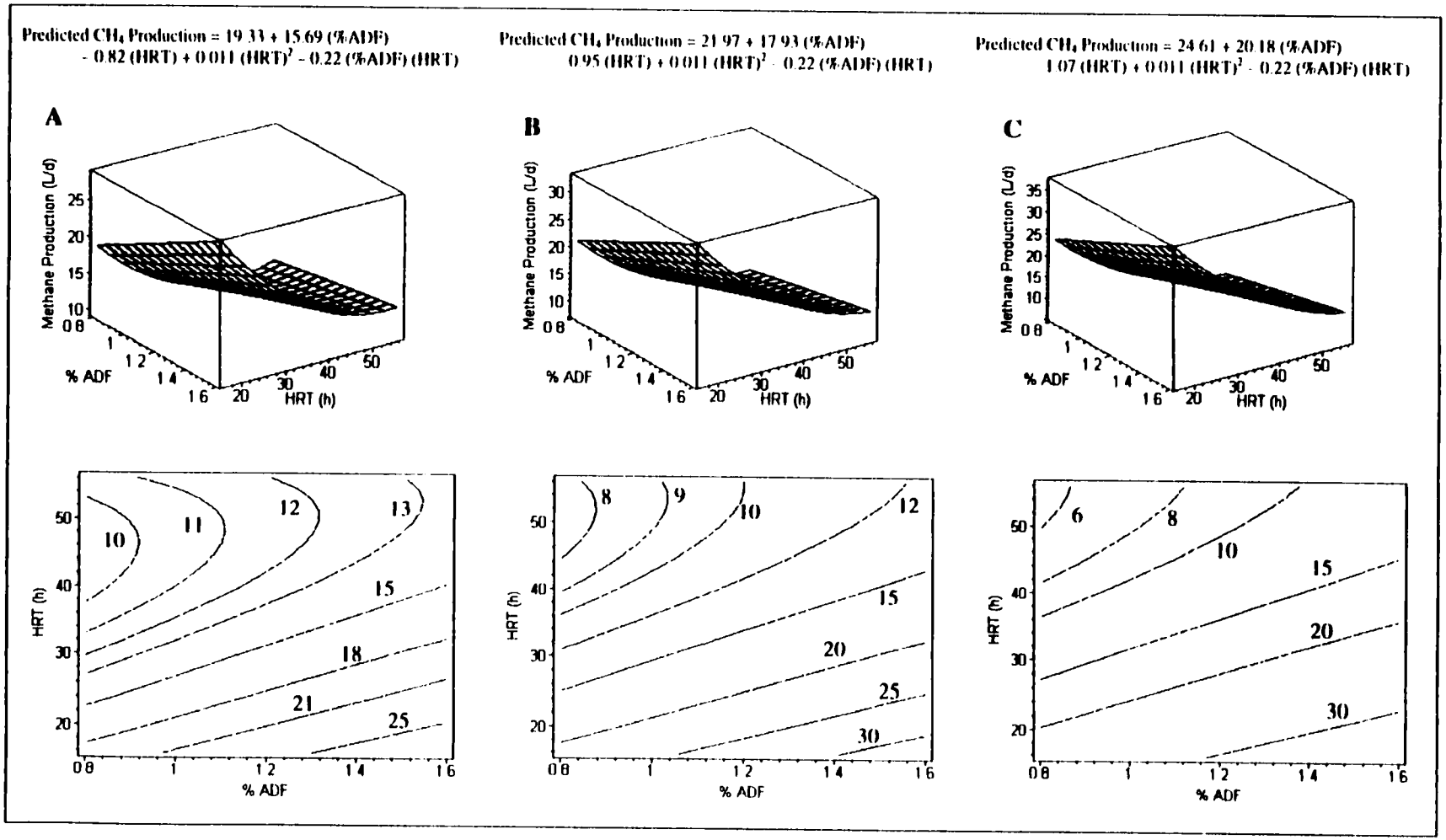

Figure 4–23 Predicted methane production rates for ADF treatment at 35°C and a biomass concentration of : (A) 18 g VSS/L (reactor biomass volume at ⅓ full), (B) 27 g VSS/L (reactor biomass volume at ½ full), and (C) 36 g VSS/L (reactor biomass volume at ⅔ full).

4.2.3 Model Verification

After the completion of the experimental runs for the star portion of the central composite design, five additional runs were carried out for model verification purposes. The results for these five runs are presented in Tables 4–29 to 4–32. The results presented in Table 4–29 indicated that biomass acetoclastic activities measured (0.23 – 0.31 g Ac/g VSS/d) were much lower than the predicted values (0.37 – 0.42 g AC/g VSS/d) for all five runs. This suggested that the biomass might have been altered after prolonged exposure to ADF that they became sensitive to environmental changes and oxygen exposure: for example, alcohol exposure can change cell membrane structure (Shuler and Kargi, 2002). Preparation of serum bottles for activity assays resulted in some oxygen exposure, which placed the biomass under stress. Discrepancies between actual and batch test measured activities are not uncommon.

Table 4–29 Comparison of biomass specific acetoclastic activity to predicted values.

Run	%ADF	HRT (h)	[Biomass] (g VSS/L)	SOLR (g COD/g VSS/d)	Activity (g Ac/g VSS/d)	
					Predicted	Measured
19	1.2	36	27	0.22±0.01	0.42±0.01	0.25±0.01
20	1.2	36	27	0.23±0.02	0.42±0.01	0.23±0.01
21	1.6	20	27	0.50±0.03	0.40±0.02	0.24±0.01
22	1.2	12	27	0.73±0.04	0.42±0.01	0.31±0.03
23	1.6	24	18	0.61±0.03	0.37±0.05	0.28±0.01

Experimental runs 19 and 20 (center-point conditions) were carried out to determine whether there was any variability in reactor performance for experiments conducted at different times during the course of the study. Results presented in Tables 4–30 to 4–32 indicated that the measured values for COD removal efficiency (98.3 – 98.4%), methane potential (0.34 – 0.35 L/g COD removed), and methane production (11.2 – 12.7 L/d) were similar to predicted values (98.4% COD removal, 0.39 L/g COD

removed, and 13.9 L/d). This suggested that the variability in process performance due to time differences was quite small. In addition, the high COD removal efficiency obtained suggested that retention of good reactor performance was possible over long periods of operation.

Table 4–30 Comparison of COD removal efficiency to predicted values.

Run	%ADF	HRT (h)	[Biomass] (g VSS/L)	SOLR (g COD/g VSS/d)	COD Removal (%)	
					Predicted	Measured
19	1.2	36	27	0.22±0.01	98.39±0.04	98.4±0.3
20	1.2	36	27	0.23±0.02	98.39±0.04	98.3±0.2
21	1.6	20	27	0.50±0.03	98.24±0.13	94.9±1.9
22	1.2	12	27	0.73±0.04	98.19±0.13	94.5±2.2
23	1.6	24	18	0.61±0.03	98.31±0.06	96.0±1.2

Table 4–31 Comparison of methane potential to predicted values.

Run	%ADF	HRT (h)	[Biomass] (g VSS/L)	SOLR (g COD/g VSS/d)	Methane Potential (L/g COD removed)	
					Predicted	Measured
19	1.2	36	27	0.22±0.01	0.395±0.002	0.34±0.02
20	1.2	36	27	0.23±0.02	0.395±0.002	0.35±0.02
21	1.6	20	27	0.50±0.03	0.409±0.003	0.36±0.01
22	1.2	12	27	0.73±0.04	0.416±0.006	0.30±0.03
23	1.6	24	18	0.61±0.03	0.369±0.013	0.38±0.01

Table 4–32 Comparison of measured methane production rates to predicted values.

Run	%ADF	HRT (h)	[Biomass] (g VSS/L)	SOLR (g COD/g VSS/d)	Methane Production (L/d)	
					Predicted	Measured
19	1.2	36	27	0.22±0.01	13.9±0.3	11.2±0.2
20	1.2	36	27	0.23±0.02	13.9±0.3	12.7±0.5
21	1.6	20	27	0.50±0.03	29.1±0.3	26.4±0.8
22	1.2	12	27	0.73±0.04	30.6±1.6	32.5±1.7
23	1.6	24	18	0.61±0.03	22.5±0.4	23.3±1.5

Higher discrepancies between measured and predicted values were obtained for COD removal efficiency of runs 21 – 23. This suggested a deficiency in the fitted model **37** to predict COD removal for run conditions away from the design center. This is not surprising since stable COD removal efficiencies could not be achieved for either run 11 or run 23. Consequently, model **37** was derived based on only the results for 17 out of 18 runs.

In general, there was good agreement between measured and predicted values for methane potential and methane production rates. This indicated that the predicted models **38** and **39** were adequate. Comparison of results for runs 21 and 22 indicated that better performance was achieved for lower ADF levels, even at a higher SOLR level. Thus for good reactor performance, low ADF levels should be treated. Required OLRs can be achieved by shortening the HRT.

4.3 Fate of Additives in UASB Reactors

4.3.1 Fate of Nonylphenol

Feed and effluent samples collected during the treatability study were also analyzed periodically by HPLC for NP and NPnEO. Extractive steam distillation of feed samples indicated the presence of NP (RT ~ 5 – 6 minutes), NP1EO (RT ~ 7 minutes), NP2EO (RT ~ 8 minutes), and NP3EO (RT ~ 9 minutes) as shown in Figure 4–24 (see Appendix C for discussion on peak identification and quantification). A summary of the NP content of 0.8%, 1.2%, and 1.6% ADF is presented in Table 4–33. Total NP was determined by converting NPnEO (n = 1 – 3) into NP equivalents, and multiple NP peaks were obtained because the nonyl chain is branched. The NP content of the three ADF concentrations was in the range of 2.49 – 5.45 mg/L. This NP concentration range was much lower than the acute anaerobic toxicity concentration (100 mg/L NP) observed in

batch experiments: thus, any toxicity effects observed in the continuous process were likely due to long term exposure (chronic effects).

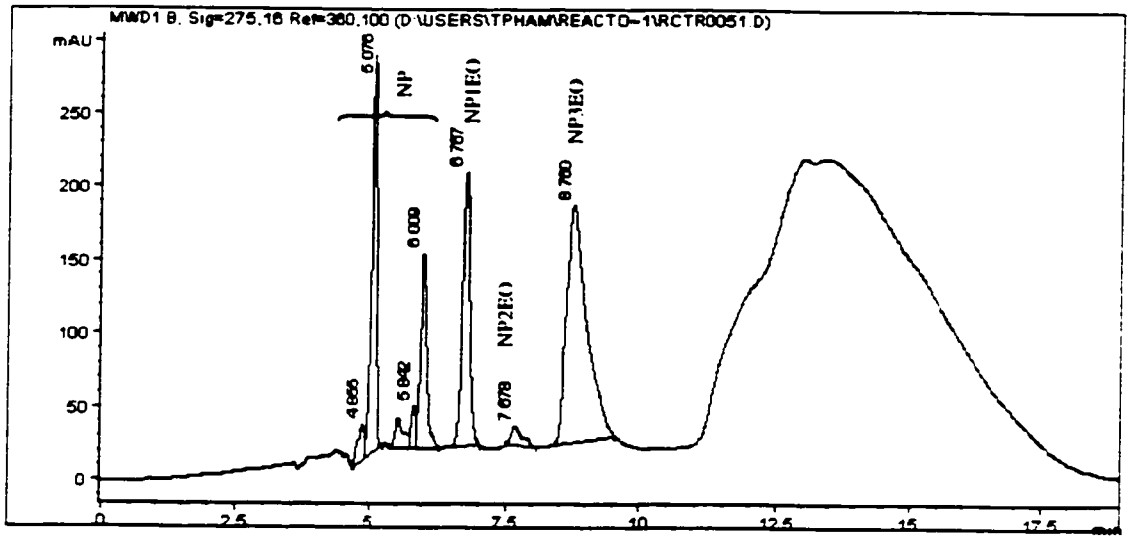

Figure 4–24 A representative chromatogram of 1.6% ADF feed sample after extractive steam distillation.

Table 4–33 Concentration of NP and NPnEO in 0.8%, 1.2%, and 1.6% ADF feed samples.

ADF	Concentration measured by HPLC (mg/L)				Total NP
	NP	NP1EO	NP2EO	NP3EO	(mg/L)
0.8%	2.19	0.19		0.22	2.49
1.2%	2.57	1.15			3.53
1.6%	1.98	1.90	0.10	2.90	5.45

Analysis of UASB effluent samples indicated that half of the samples contained NP and NPnEO below detectable levels (Table 4–34). For samples containing NP and NP1EO (Figure 4–25), the range of NP concentrations detected in the effluent was 0.012 – 0.076 mg/L. A mass balance on NP was carried out by determining the concentration of NP associated with the granular biomass for the measured effluent NP, using

Freundlich sorption parameters for active anaerobic granular biomass (n = 0.95 and K = 2.38).

Table 4–34 Mass balances on NP for the 23 continuous UASB experiments conducted at 35°C.

	Design conditions				Conc. in effluent (mg/L)					
Run	ADF (%)	HRT (h)	[Biomass] (g VSS/L)	Feed NP (mg/L)	NP[a]	NP1EO	Total NP[b]	NP Sorbed[c] (mg/L)	Total NP measured[d] (mg/L)	NP not accounted for[e] (%)
1	1.2	36	27	3.53	0.013	nd	0.013	0.838	0.851	75.9
2	1.2	36	27	3.53	0.012	nd	0.012	0.784	0.796	77.4
3	1.2	36	27	3.53	0.024	nd	0.024	1.570	1.594	54.8
4	1.2	36	27	3.53	0.023	nd	0.023	1.534	1.557	55.9
5	0.8	48	18	2.49	nd	nd	–	–	–	>99.9
6	0.8	48	36	2.49	nd	nd	–	–	–	>99.9
7	0.8	24	18	2.49	nd	nd	–	–	–	>99.9
8	0.8	24	36	2.49	nd	nd	–	–	–	>99.9
9	1.6	48	18	5.45	nd	nd	–	–	–	>99.9
10	1.6	48	36	5.45	nd	nd	–	–	–	>99.9
11	1.6	24	18	5.45	nd	nd	–	–	–	>99.9
12	1.6	24	36	5.45	nd	nd	–	–	–	>99.9
13	1.2	36	18	3.53	0.058	0.021	0.075	2.765	2.840	19.5
14	1.2	36	36	3.53	0.070	nd	0.070	4.868	4.934	-39.8
15	1.2	56.1	27	3.53	0.052	nd	0.052	2.849	2.901	17.8
16	1.2	15.8	27	3.53	nd	nd	–	–	–	>99.9
17	0.8	36	27	2.49	0.042	nd	0.042	2.272	2.314	6.9
18	1.6	36	27	5.45	0.021	0.037	0.051	2.814	2.865	47.4
19	1.2	36	27	3.53	nd	nd	–	–	–	>99.9
20	1.2	36	27	3.53	nd	nd	–	–	–	>99.9
21	1.6	20	27	5.45	0.068	nd	0.068	3.679	3.747	31.2
22	1.2	12	27	3.53	0.022	nd	0.022	1.104	1.126	68.1
23	1.6	24	18	5.45	0.020	0.035	0.049	1.730	1.779	67.3

[a] nd = not detected.

[b] Total NP (effluent) = NP measured + NP equivalent for NP1EO measured.

[c] Calculated based on Freundlich parameters for active granular biomass. n = 0.95 and K = 2.38.

[d] Total NP measured = Effluent total NP + Sorbed NP.

[e] % NP not accounted for = 100% × [(Feed NP – Total NP measured) / Feed NP]

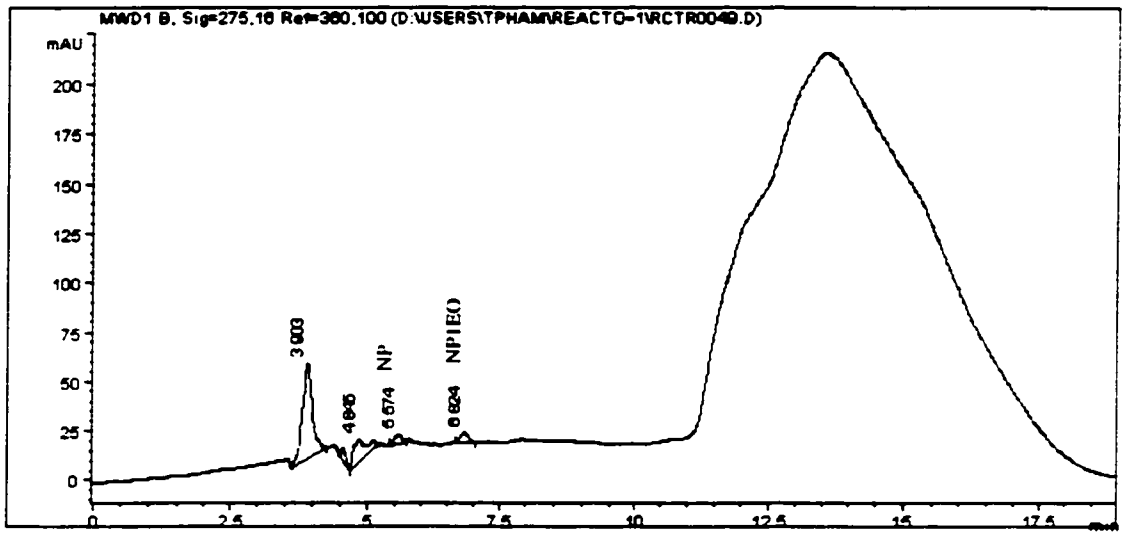

Figure 4–25 Chromatogram of an effluent sample from UASB reactor treating 1.6% ADF at 24 h HRT and 18 g VSS/L biomass concentration (run 23) after extractive steam distillation.

The data presented in Table 4–34 suggested that degradation of NP occurred since the measured NP (effluent plus sorbed) was less than that in the feed. For 21 out of 23 experimental runs conducted, greater than 17% (17.8% to >99.9%) of the NP in the feed was not accounted for. However, on one occasion (run 14) the effluent and sorbed NP measured was larger than the concentration measured in the feed. This may have resulted from desorption processes or an experimental anomaly.

The NP mass balance presented in Table 4–34 was carried out by assuming that the granular biomass in each run had maximum sorption capacity (similar to virgin biomass which had not come into contact with NP). If sorption occurred without any biodegradation, an accumulation of NP would be expected since new feed containing NP was continuously fed to the USAB reactor. This accumulation over time should lead to higher NP concentrations in the effluent approaching those in the feed. However, effluent NP concentrations were still two orders of magnitude below those in the feed at the end of the study period (run 23, after one year of operation). Since the UASB reactors were operated in continuous mode, NP removal can be determined based on

soluble NP concentrations entering and leaving the treatment system. As presented in Table 4–35, NP removal efficiencies were in excess of 97% (97.9% to >99.9%) for all 23 experimental runs conducted. This high NP removal efficiency is similar to those reported by Naylor (1995) for aerobic treatment of wastewaters containing NP/NPnEO at seven wastewater treatment plants in the U.S.

Table 4–35 NP removal efficiencies for the 23 continuous UASB experiments conducted at 35°C.

	Design conditions			Feed	Effluent	NP
Run	ADF (%)	HRT (h)	[Biomass] (g VSS/L)	NP (mg/L)	NP (mg/L)	Removal (%)
1	1.2	36	27	3.53	0.013	99.6
2	1.2	36	27	3.53	0.012	99.7
3	1.2	36	27	3.53	0.024	99.3
4	1.2	36	27	3.53	0.023	99.3
5	0.8	48	18	2.49	–	>99.9
6	0.8	48	36	2.49	–	>99.9
7	0.8	24	18	2.49	–	>99.9
8	0.8	24	36	2.49	–	>99.9
9	1.6	48	18	5.45	–	>99.9
10	1.6	48	36	5.45	–	>99.9
11	1.6	24	18	5.45	–	>99.9
12	1.6	24	36	5.45	–	>99.9
13	1.2	36	18	3.53	0.075	97.9
14	1.2	36	36	3.53	0.070	98.1
15	1.2	56.1	27	3.53	0.052	98.5
16	1.2	15.8	27	3.53	–	>99.9
17	0.8	36	27	2.49	0.042	98.3
18	1.6	36	27	5.45	0.051	99.1
19	1.2	36	27	3.53	–	>99.9
20	1.2	36	27	3.53	–	>99.9
21	1.6	20	27	5.45	0.068	98.7
22	1.2	12	27	3.53	0.022	99.4
23	1.6	24	18	5.45	0.049	99.1

Similar to batch studies. NP mass balances indicated that anaerobic degradation of NP occurred. Phenol is a possible degradation intermediate of NP; however, it was not detected in any of the batch tests and UASB samples analyzed. Thus, further experiments are required to confirm whether NP was degraded. Radioactive labeling the phenol moiety would provide information on whether or not the aromatic ring was cleaved.

4.3.2 Fate of Tolyltriazole

Effluent samples from UASB reactors were also analyzed for aryl triazole. A comparison of the retention times obtained to those of authentic samples indicated that tolyltriazole was the corrosion inhibitor in the ADF studied. Similar to that reported by Cancilla *et al.* (1998), the double peaks eluting at 5 minutes retention time shown in Figure 4–26 indicated that the tolyltriazole present was a mixture of two isomers.

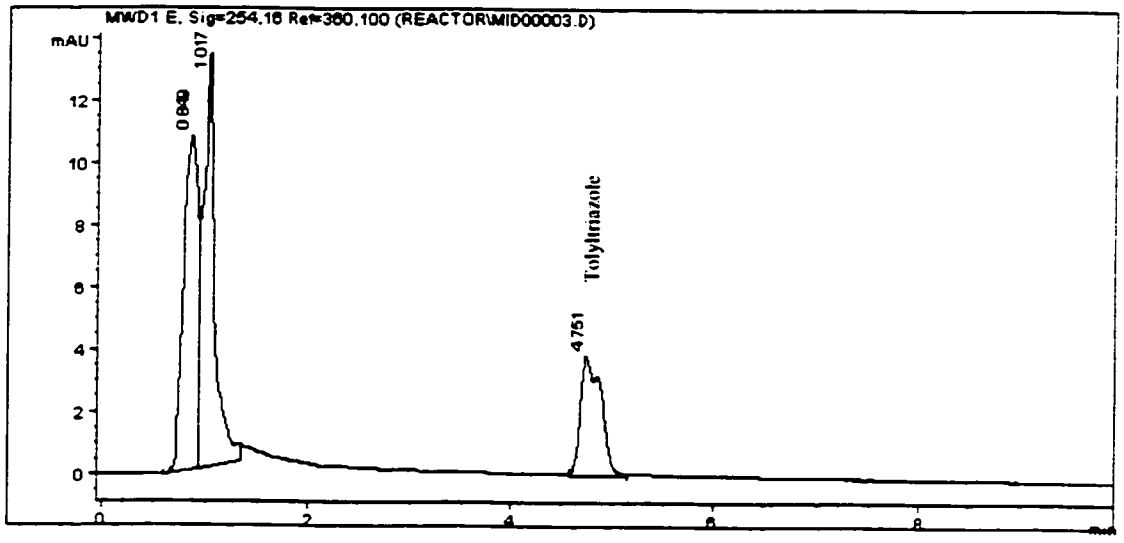

Figure 4–26 Tolyltriazole in an effluent sample collected from a UASB reactor treating 1.2% ADF at 36 h HRT and 27 g VSS/L biomass concentration (run 3).

Tolyltriazole concentration levels in feed and effluent samples taken for the 18 central composite runs are presented in Table 4–36. The tolyltriazole concentration range in the effluent was 2.6 – 4.8 mg/L. Comparison of feed and effluent tolyltriazole content measured indicated that there was very little difference between the two. A two-tailed paired-sample *t* test of the difference between feed and effluent concentrations indicated that the difference was not significant (see Appendix D for details).

Table 4–36 Tolyltriazole levels in feed and effluent samples from the central composite design

	Design Conditions			Tolyltriazole Concentration (mg/L)	
Run	ADF (%)	HRT (h)	[Biomass] (g VSS/L)	Feed	Effluent
1	1.2	36	27	3.68±0.06	3.61±0.01
2	1.2	36	27		3.62±0.07
3	1.2	36	27		3.63±0.04
4	1.2	36	27		3.58±0.02
5	0.8	48	18	2.54±0.09	2.64±0.05
6	0.8	48	36		2.63±0.16
7	0.8	24	18		2.63±0.01
8	0.8	24	36		2.60±0.05
9	1.6	48	18	4.61±0.26	4.66±0.07
10	1.6	48	36		4.55±0.09
11	1.6	24	18		4.75±0.03
12	1.6	24	36		4.66±0.07
13	1.2	36	18	3.51±0.44	3.59±0.01
14	1.2	36	36		3.60±0.04
15	1.2	56.1	27		3.55±0.02
16	1.2	15.8	27		3.70±0.03
17	0.8	36	27	2.60±0.06	2.57±0.02
18	1.6	36	27	4.85±0.02	4.84±0.01

It was not unexpected that effluent and feed tolyltriazole concentrations were similar since biosorption experiments indicated that very little tolyltriazole interacted with the biomass (Table 4–4). A liquid phase concentration of 5 mg/L (highest level

measured) would be in equilibrium with 0.0035 mg/g VSS. For the highest reactor biomass concentration of 36 g VSS/L, this would correspond to a decrease of only 0.13 mg/L due to biosorption. This small difference can easily be masked by experimental errors.

4.4 Biomass Characterization.

4.4.1 Biomass Settling Characteristics

Excellent granular settling characteristics were of paramount importance in ensuring good performance in high rate reactors. Consequently, changes in biomass settling characteristics were regularly monitored during the continuous operation of the UASB reactors. A total of 23 experimental runs were carried out in the ADF treatment study. Settling tests were performed on biomass taken from the top and bottom part of the reactor sludge bed immediately after the completion of each of the 23 runs. A typical settling curve is presented in Figure 4–27.

Examination of settling curves can only provide qualitative comparisons. To perform a quantitative comparison of the results, upflow velocities that would result in a 50% washout of the biomass (v_{50}) were interpolated based on linear regression of the linear portion of the settling curves (see Figure 4–27). Duplicate settling tests were carried out for seed granular sludge originally obtained from Lake Utopia Paper, New Brunswick (v_{50} of 31.7 m/h, see Figure 4–27). Single settling tests were performed on UASB granular sludge sampled at the end of each of the 23 run conditions. Since both the top and bottom layers of the UASB granular sludge bed were sampled, 46 different settling tests were conducted on UASB granular sludge. As a result, a total of 48 settling tests were conducted during the ADF treatment study. A summary of the v_{50} values for the 23 run conditions is presented in Table 4–37.

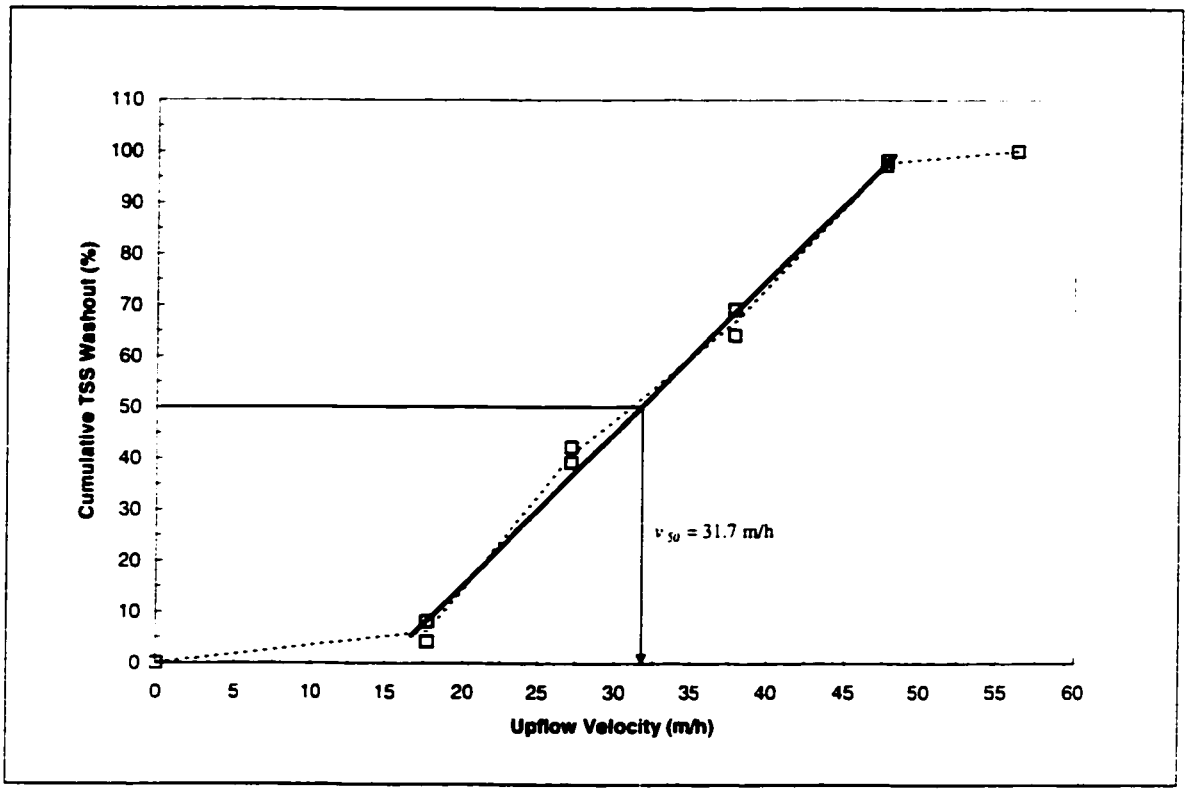

Figure 4–27 Settling curve for seed granular anaerobic sludge obtained from Lake Utopia Paper.

A two-tailed paired-sample *t* test (as described in Appendix D) was carried out to determine whether there was a difference between the settling velocity for biomass at the top and bottom of the reactor, for each run. As presented in Table 4–37, the difference was found to be significant, with generally higher settling velocities measured for biomass taken from the bottom layer of the biomass bed. This was expected since the feed flowed upward inside the UASB reactor, thus, it was reasonable that heavier granules would dominate the bottom biomass layer. This two-tailed paired-sample *t* test performed only indicated that there was a significant difference between the settling velocity of biomass from the top and bottom of the reactor. To characterize the effects of operating conditions on settling velocity, empirical model **31** was fitted to the settling data for the first 18 runs presented in Table 4–37. The parameter estimates and their 95%

confidence intervals of the fitted models for the biomass from the bottom and top of the reactor are presented in Table 4–38.

Table 4–37 Settling velocity (v_{50}) for granular biomass after completion of an experimental run.

	Design Conditions			Biomass v_{50}[a]		
Run	ADF (%)	HRT (h)	[Biomass] (g VSS/L)	Top (m/h)	Bottom (m/h)	Difference, d (m/h)
1	1.2	36	27	24.2	23.6	-0.6
2	1.2	36	27	23.8	23.6	-0.2
3	1.2	36	27	22.1	22.7	0.6
4	1.2	36	27	24.1	24.0	-0.1
5	0.8	48	18	21.2	23.0	1.8
6	0.8	48	36	22.0	22.3	0.3
7	0.8	24	18	23.5	22.4	-1.1
8	0.8	24	36	21.6	23.4	1.8
9	1.6	48	18	20.0	20.8	0.8
10	1.6	48	36	19.5	21.5	2.0
11	1.6	24	18	22.7	22.4	-0.3
12	1.6	24	36	21.5	22.8	1.3
13	1.2	36	18	18.6	26.6	8.0
14	1.2	36	36	24.1	26.7	2.6
15	1.2	56.1	27	21.6	23.8	2.2
16	1.2	15.8	27	23.4	26.4	3.0
17	0.8	36	27	23.6	24.1	0.5
18	1.6	36	27	21.5	23.2	1.7
19	1.2	36	27	17.9	24.1	6.2
20	1.2	36	27	21.7	26.8	5.1
21	1.6	20	27	23.1	23.9	0.8
22	1.2	12	27	21.8	27.4	5.6
23	1.6	24	18	22.5	24.4	1.9

For two-tailed paired sample *t* test.

$$t = \frac{|\bar{d}|}{s_{\bar{d}}} = \frac{1.9087}{\sqrt{5.408/23}} = 3.936 \quad > \quad t_{0.05(2),22} = 2.074 \quad (p = 0.00107)$$

Reject H_0

[a] Biomass settling velocity determined at the end of each steady-state run: Top and Bottom designates biomass sampled from the top and bottom portion of the reactor sludge bed, respectively.

Table 4–38 Parameter estimates from the blocked central composite design for settling velocity.

Parameter	95% confidence interval	
	v_{50} for Biomass from Top of Reactor (m/h)	v_{50} for Biomass from Bottom of Reactor (m/h)
β_0	23.23±1.33	24.55±0.74
β_1	-0.67±0.99	-0.45±0.55
β_2	-0.71±0.85	-0.57±0.47
β_3	0.27±0.99	0.15±0.55
β_{11}	-0.35±1.81	-1.98±1.01
β_{22}	-0.14±0.86	-0.19±0.48
β_{33}	-1.55±1.81	1.02±1.01
β_{12}	-0.35±1.10	-0.30±0.62
β_{13}	-0.08±1.10	0.10±0.62
β_{23}	0.42±1.10	-0.18±0.62
B_B	-0.32±0.85	1.08±0.48

For biomass taken from the top layer of the biomass bed, all parameters were found to be insignificant (95% confidence intervals indicated that zero was a plausible value for all parameters, except $\hat{\beta}_0$). It was, however, unlikely that the operating variables (ADF concentration, HRT, and biomass concentration) had no effects on biomass settling velocity, since ADF exposure resulted in settling velocities (17.9 – 27.4 m/h, Table 4–37) which were lower than that of seed biomass (32 m/h). It was more likely that the effects were masked by the experimental error or noise associated with settling velocity measurements. The sample variances for the v_{50} values at center-point run conditions (runs 1-4) were 0.96 and 0.30 for top and bottom of the biomass bed, respectively.

The reduced fitted model for settling velocity of biomass taken from the bottom of the reactor is

$$\hat{y}_{v_{50},\text{Bottom}} = 24.55 - 0.57x_2 - 1.98x_1^2 + 1.02x_2^2 + 1.08B \qquad (45)$$

Lack of fit was tested for this reduced fitted model **45** by calculating the *LFR* term defined in equation **20**. This quantitative test indicated that lack of fit was not significant ($LFR = 1.68 < F_{10,3,0.05} = 8.79$). Lack of trends in the residual plots presented in Figure 4–28 also indicated that lack of fit was not significant. It was interesting to note that a positive value was obtained for the blocking term. This was the opposite of what was found for the four process responses presented in Table 4–24 (negative effect for blocking term). The positive value obtained for the blocking term of model **45** suggested that there was a time-dependent increase in the settling velocity. This increase was probably due to the secretion of the grayish-white extracellular material, which was observed on some granules after a few months of exposure to ADF. This extracellular material might have contributed to an increase in granular density. Since the presence of this material was time-dependent, a positive blocking effect was required.

The reduced fitted model **45** can be expressed in terms of the original (uncoded) operating variables as

$$\text{Predicted } v_{50,\text{Bottom}} = 17.60 + 29.71\,(\%\text{ADF}) - 0.047\,(\text{HRT}) - 0.69\,[\text{Biomass}] - 12.38\,(\%\text{ADF})^2 + 1.08\,B \qquad (46)$$

where %ADF is a percentage value, HRT is in hours, [Biomass] is biomass concentration in g VSS/L, and $B = -1$ for first 12 runs, and $B = +1$ for the last 6 runs of the central composite design. A plot of the response surface was needed to better visualize how each individual operating variable affected settling velocity. Model **46** had to be simplified to include only two of the three operating variables. For $B = -1$ and biomass concentration of 27 g VSS/L (biomass level at ½ reactor volume), model **46** is simplified to

$$\text{Predicted } v_{50,\text{Bottom}} = 7.35 + 29.17\,(\%\text{ADF}) - 0.047\,(\text{HRT}) - 12.38\,(\%\text{ADF})^2 \qquad (47)$$

For B = -1 and biomass level at ⅓ or ⅔ reactor volume (18 or 36 g VSS/L), model **46** is simplified to

Predicted $v_{50,\text{Bottom}} = 8.37 + 29.17\ (\%\text{ADF}) - 0.047\ (\text{HRT}) - 12.38\ (\%\text{ADF})^2$ (**48**)

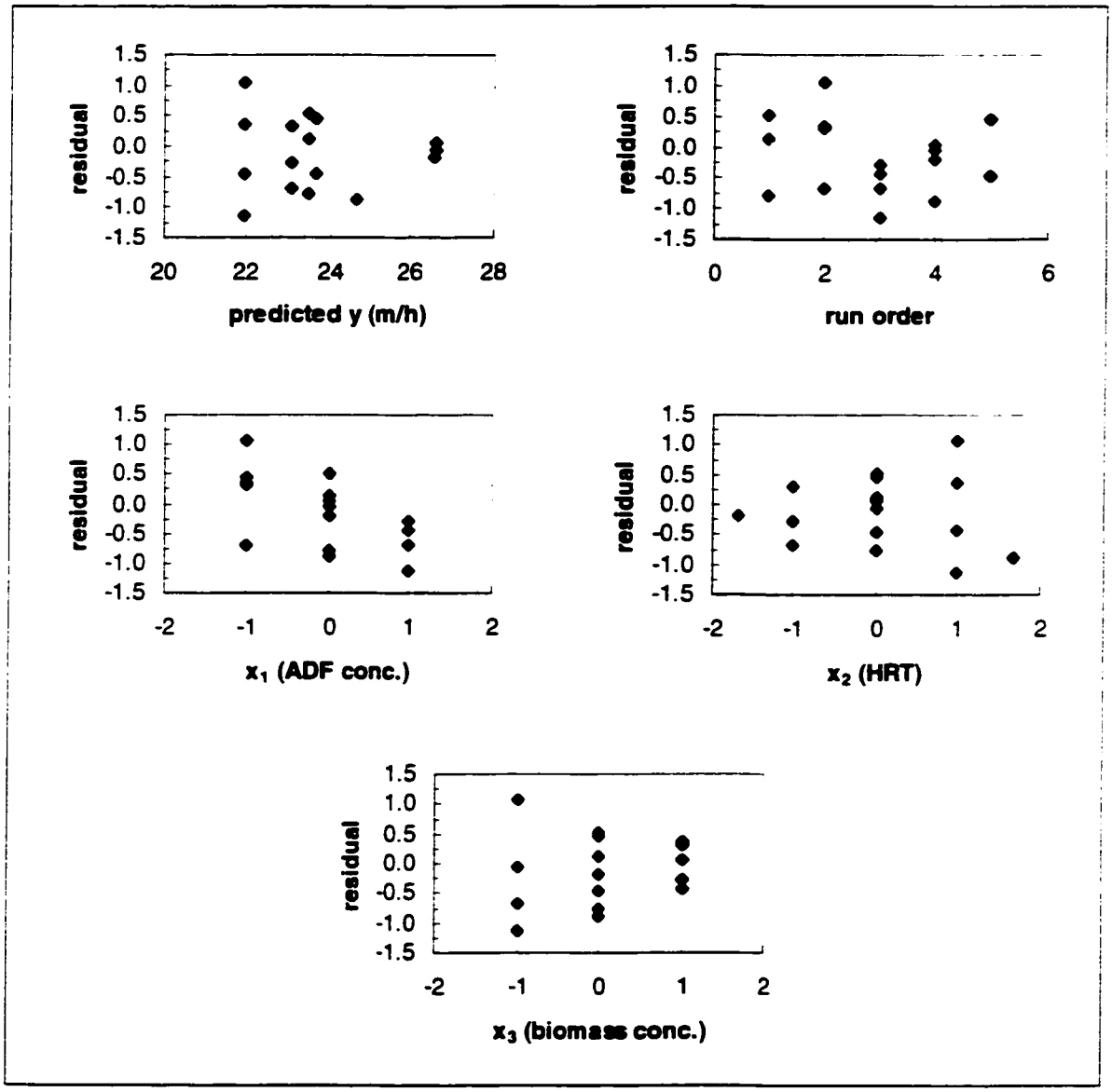

Figure 4–28 Residual plots for fitted model 45 (v_{50} **for biomass from bottom of reactor).**

The predicted response surfaces for settling velocity of biomass at the bottom of the reactor (models **47** and **48**) are presented in Figure 4–29. For both models **47** and **48**, highest settling velocities were predicted for 1.2% ADF. A decrease in settling velocity was predicted for ADF concentrations which deviated from the 1.2%. This was probably due to the fact that the first 4 runs were carried out at center-point conditions (1.2% ADF). It was likely that the biomass was acclimated to the 1.2% ADF. A change in ADF concentration to either 0.8 or 1.6% ADF might have caused a slight decrease in settling velocity. This change in settling velocity due to changes in substrate composition and concentration is known (Speece, 1996).

4.4.2 Biomass Granule Size Distribution

The separation of granular biomass during settling tests was based on density and size. Biomass fractions obtained at lower upflow velocities contained small granules, while fractions with larger granules were obtained at high upflow velocities. A photograph of the five fractions of a typical biomass sample taken from reactor TP2 after completion of run 20 (1.2% ADF, 36 h HRT, and 27 g VSS/L biomass concentration) is shown in Figure 4–30. The typical size range of the five biomass fractions in the photograph was observed for all samples taken from the UASB reactors during ADF treatment. The average size distribution for seed biomass (Lake Utopia Paper) and biomass samples taken from the top and bottom of the UASB reactors after completion of each of the 23 ADF treatment runs is shown in Table 4–39.

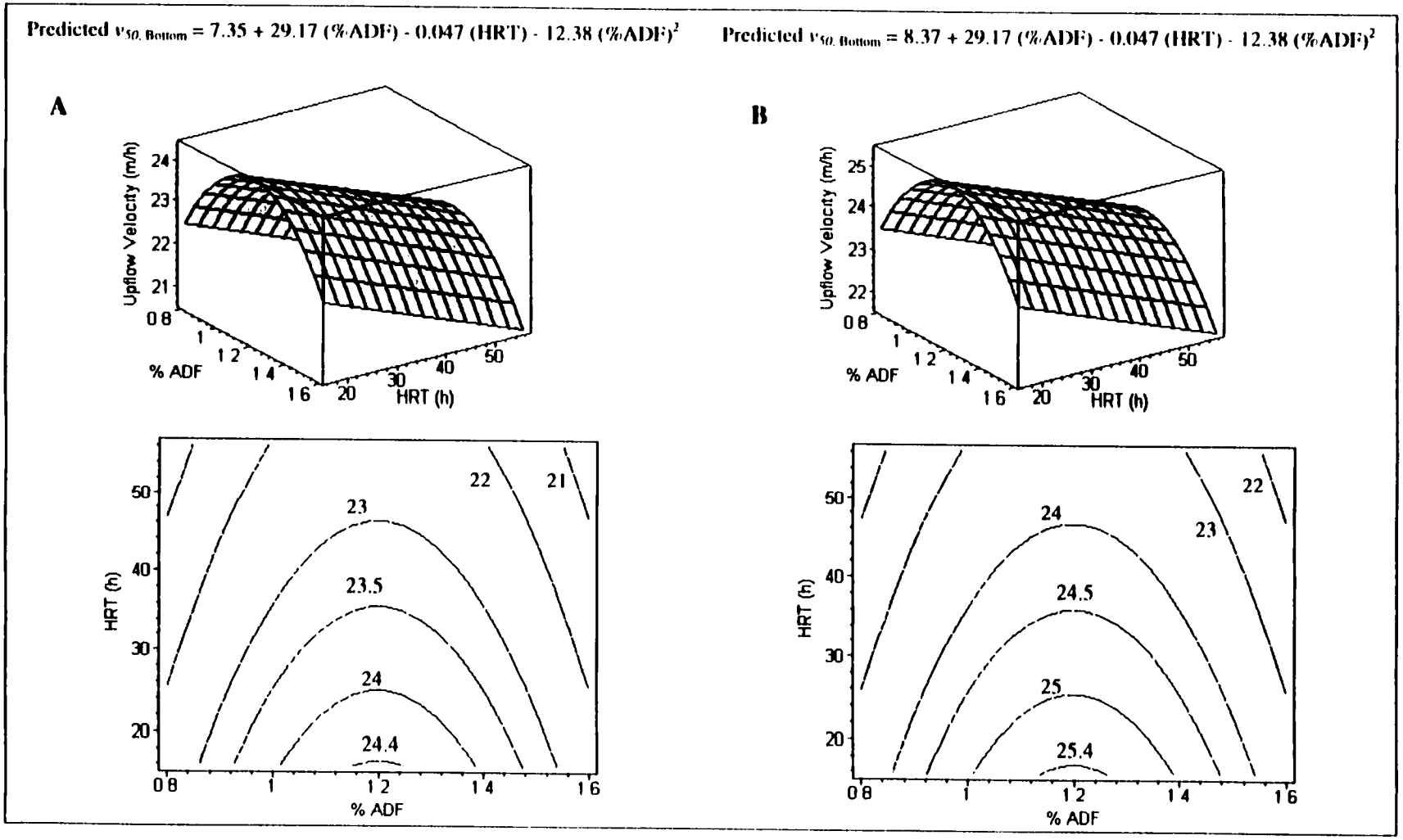

Figure 4–29 Predicted v_{50} for biomass at the botoom of the reactor during ADF treatment at 35°C and biomass concentration of: (A) 27 g VSS/L (reactor biomass volume at ½ full) and (B) 18 or 36 g VSS/L (biomass level at ⅓ or ⅔ reactor volume).

129

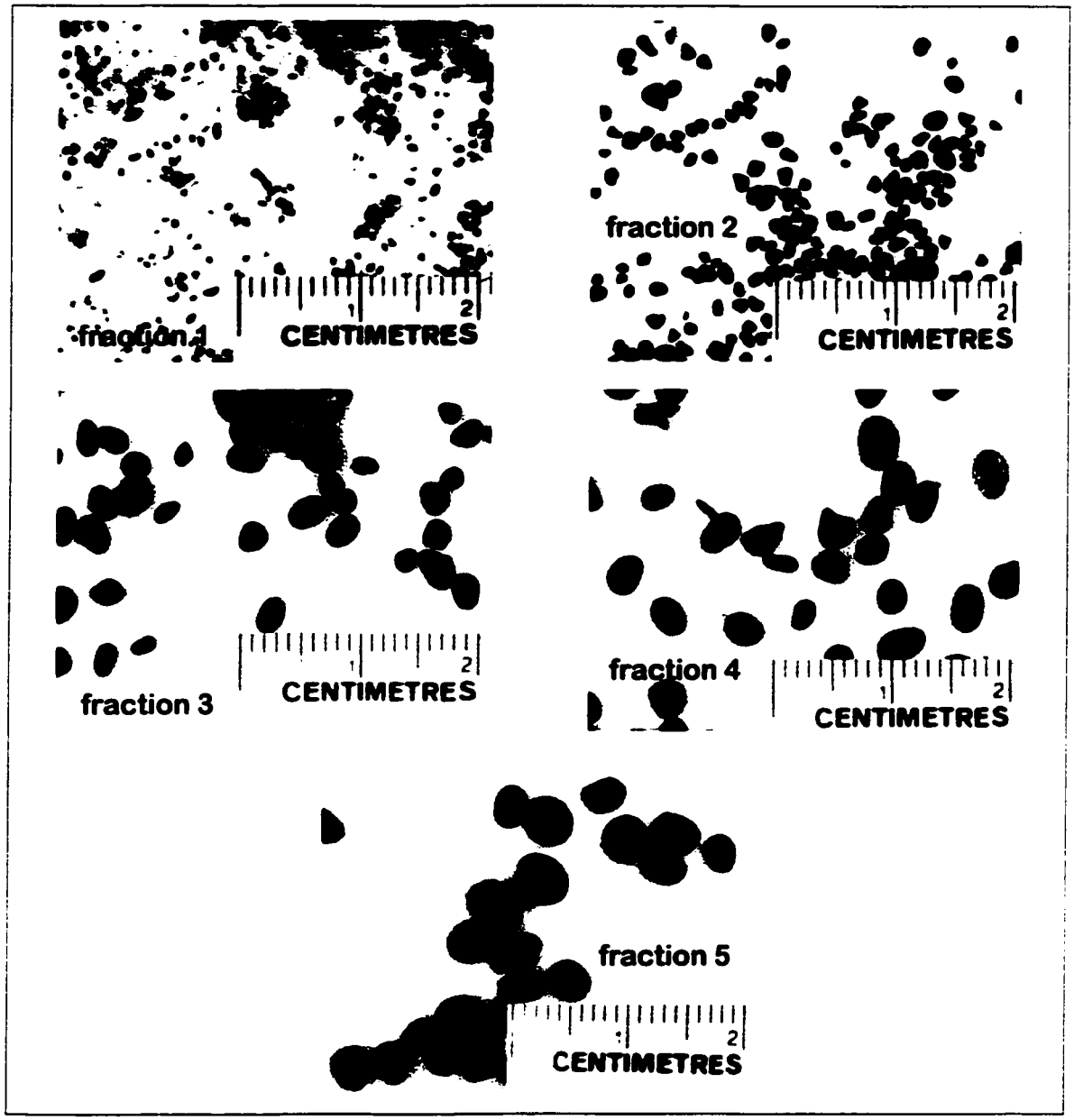

Figure 4–30 Photograph of different fractions of a biomass sample taken from reactor TP2 after completion of run 20 (281 days).

Seed biomass (33%) contained more large granules (D ≤ 2.5 mm) than samples taken from the top (6%) and bottom (9%) of the UASB reactor sludge bed. This was consistent with the above mentioned observation where large granules were lost from

UASB reactors due to flotation problems. A considerable fraction of the biomass samples taken from the top (36%) and bottom (29%) of the UASB reactor sludge bed had average diameters less than 1.5 mm. This fraction was likely composed of newly formed and/or disintegrated granules since only 6% of the seed biomass was this small. It is expected that a considerable fraction of the biomass samples from UASB reactors should consist of small granules since new biomass was being produced.

Table 4–39 The size distribution of typical granular biomass samples obtained from various sources.

Fraction	Upflow Velocity (m/h)	Average Diameter (mm)	Percentage of total biomass sample		
			Seed Biomass[a]	UASB Reactor Top[b]	UASB Reactor Bottom[b]
1	8.6	$D \leq 1.0$	–	8±6	5±3
2	17.7	$0.5 \leq D \leq 1.5$	6±3	28±6	22±9
3	27.2	$1.0 \leq D \leq 2.5$	35±1	37±4	40±5
4	37.9	$2.0 \leq D \leq 3.5$	26±1	21±5	24±8
5	47.7	$2.5 \leq D \leq 4.5$	31±3	6±3	9±5
6	56.2	$D \geq 4.5$	2±1	–	–

[a] Seed granular sludge obtained from Lake Utopia Paper

[b] Results from settling tests performed on biomass taken from the top or bottom part of the sludge bed for the 23 experimental runs conducted in this study were combined.

It was also observed that some of the larger granules from the UASB reactors were covered with a grayish slime material after exposure to feed ADF concentrations above 1.2%. Secretion of extracellular polypeptides is known to occur when there is a nitrogen deficiency or due to toxicity effects (Speece, 1996). It was likely that ADF toxicity was the cause since the feed contained an abundance of nitrogen (COD:N:P ratio of 102:5:1 on a weight basis).

4.4.3 Biomass Acclimation and ADF Toxicity

The anaerobic toxicity assay (ATA) performed on seed granular biomass obtained from Lake Utopia Paper indicated that ADF concentrations higher than 2% were toxic to the biomass. The lack of any further gas production after day nine (horizontal gas production curve), accompanied by the discoloration of the granules suggested that cell death occurred (see Figure 4–10). It was thus of interest to determine whether acclimation would reduce the toxicity effects of ADF.

ATA results presented in Figure 4–31 indicated that acclimation helped retain some microbial activity after 14 days at ADF concentrations higher than 2% (some gas production still occurring at 14 days). However, ADF inhibition of initial biogas production was more pronounced in acclimated biomass. Initial biogas production for samples containing ADF (1 – 8%) was higher than that of controls for unacclimated biomass (Figure 4–10). For ADF-acclimated biomass, the initial biogas production for controls was higher than that for samples containing ADF higher than 1%. Alcohols are known to cause changes in cell membranes (Shuler and Kargi, 2002). Since ADF-acclimated granular has been exposed to 1.6% ADF (9000 mg/L EG), some changes in the microbial cell membrane might have taken place. This might have caused the granular biomass to become more sensitive to the high EG concentrations of the test bottles (5500 – 52,000 mg/L EG for 1 – 8% ADF).

Gas chromatographic results presented in Table 4–40 indicated that high levels of ethanol and volatile fatty acids were present in bottles containing high ADF concentrations. At the termination of the test (14 d), ethanol (3100 – 4100 mg/L) and acetate (1900 – 4900 mg/L) were measured in bottles containing 2, 4, and 8% ADF. The EG concentration for samples containing 4 and 8% ADF were in excess of 15,000 mg/L. A higher final level of EG was measured as compared to the amount added for the 8%

ADF sample bottle. This was likely due to dilution errors, since the sample was diluted by 333-fold prior to analysis.

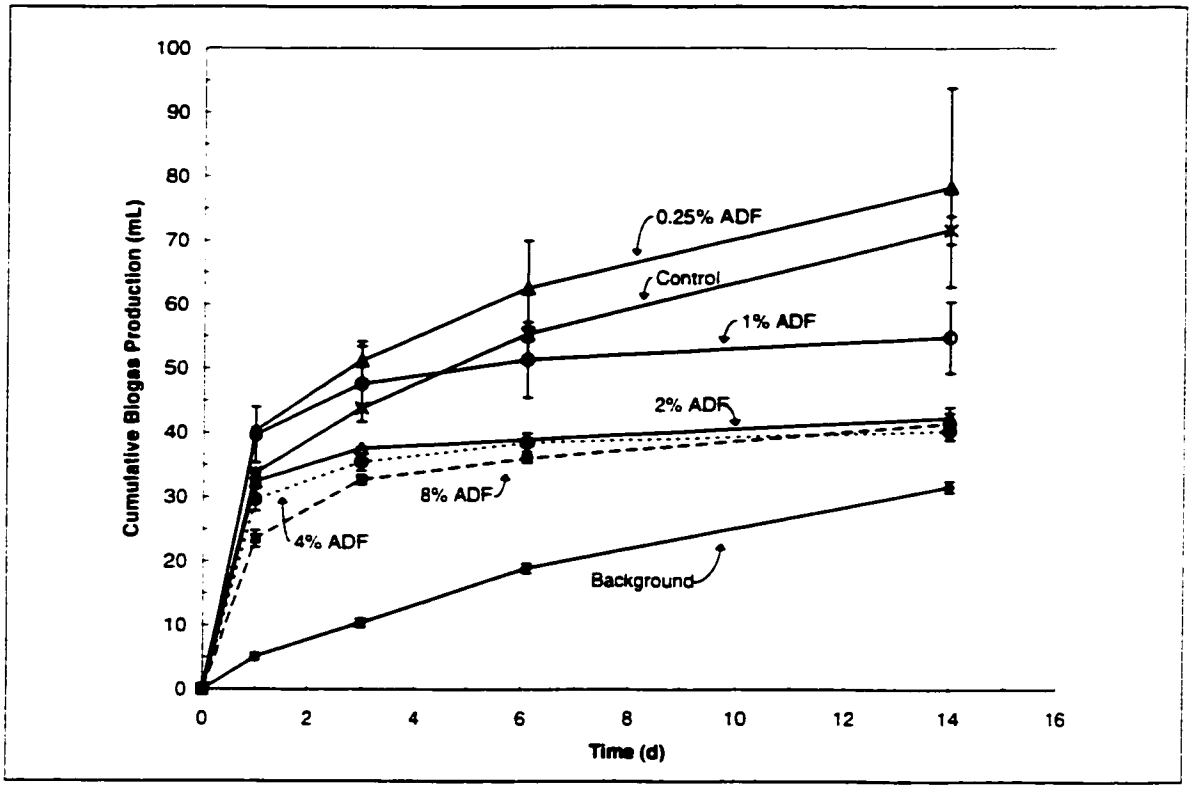

Figure 4–31 Anaerobic toxicity assay at 35°C performed on ADF-acclimated biomass taken from reactor TP2 after completion of run 20.

Propionate and butyrate concentrations measured were less than 500 mg/L. These volatile acids were not detected in samples containing 4 and 8% ADF. This was very unlikely to be the case since samples containing high ADF concentrations should also contain high concentrations of volatile acids. These volatile acids were likely diluted to below detection levels due to the large dilution factors required for EG quantification.

The inhibitory effects observed in Figure 4–31 were likely due several factors. In addition to higher concentrations of additives, EG concentrations also increased as the ADF concentrations are increased. The presence of high concentrations of EG after 14

days of incubation indicated that EG exerted some inhibitory effects, since acidogenic activities are known to be fast. Furthermore, acetic acid levels (more than 3000 mg/L) in bottles containing ADF above 2% were at inhibitory levels.

Table 4–40 GC analysis of serum bottle content from the ATA performed on ADF-acclimated biomass taken form reactor TP2 after completion of run 20.

Sample*	EG added (mg/L)	Final measured concentrations (mg/L)				
		Ethanol	Acetate	Propionate	Butyrate	EG
Background	0	16	5	0	0	0
Control	0	9	1	0	0	0
0.25% ADF	1300	0	0	0	0	0
1% ADF	5500	10	590	80	120	60
2% ADF	13000	3400	3000	300	400	300
4% ADF	26000	4100	4900	0	0	16000
8% ADF	52000	3100	1900	0	0	62000

*Samples were done in duplicates.

4.5 Reactor Characterization

4.5.1 VFA Content

During the course of the ADF treatment study, a total of four bench-scale UASB reactors were operated in continuous mode. A total of 23 experimental runs at 17 different run conditions were conducted (see Appendix I for steady-state data and run conditions). Changes in OLR were often required to progress from one run to the next. To avoid putting the reactors into stress, reactor response to changes in OLR was monitored by regularly measuring the reactor VFA concentration. A typical time course profile of reactor TP2's VFA concentration is presented in Figure 4–32. The sharp rise in acetate levels following an abrupt change in the SOLR indicated that reactor VFA levels can be used as a reliable tool for monitoring reactor stability.

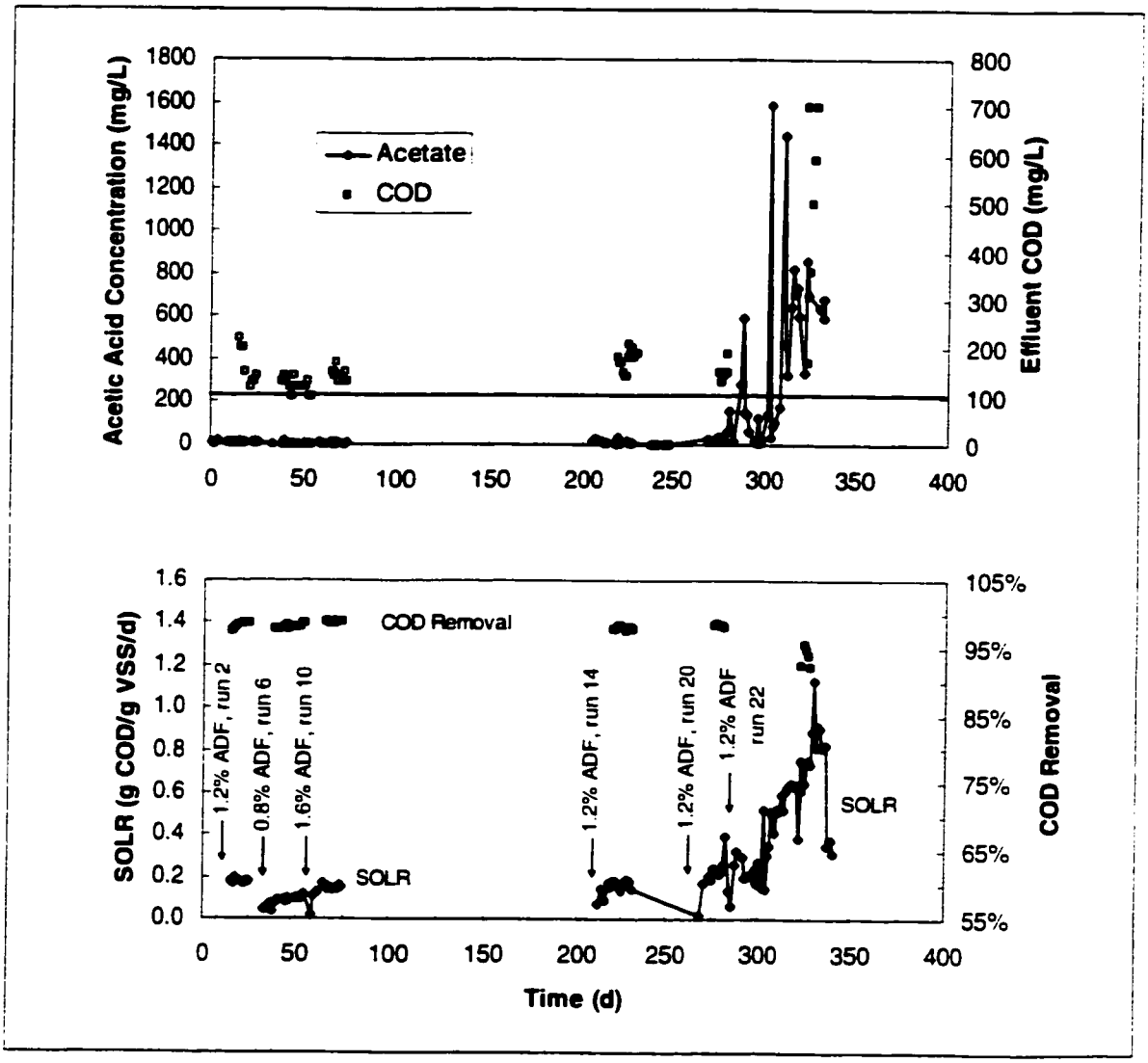

Figure 4–32 COD removal efficiency and reactor acetate content in response to various specific organic loading rates used for reactor TP2 during the course of the study.

Comparison between Figures 4–32 and 4–33 indicated that better reactor stability was achieved at high SOLRs for lower ADF concentrations. At 1.2% ADF (see Figure 4–32), reactor acetate levels were easily maintained below 1000 mg/L with good COD removal efficiencies for an SOLR close to 0.8 g COD/g VSS/d. For 1.6% ADF feed (see Figure 4–33), reactor acetate concentrations could not be maintained at stable levels, even though the SOLR was much lower (near 0.6 g COD/g VSS/d).

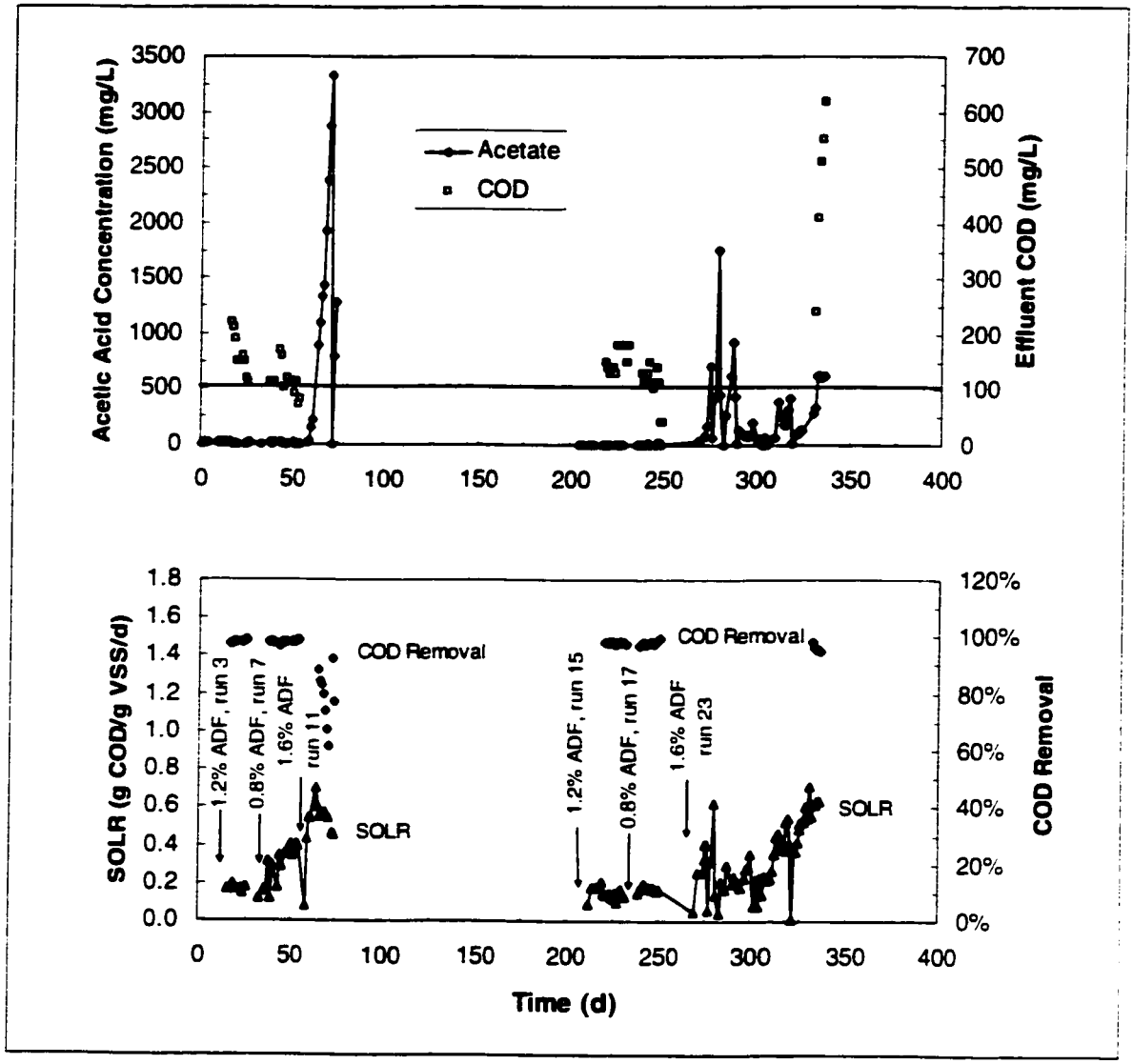

Figure 4–33 COD removal efficiency and reactor acetate content in response to various specific organic loading rates used for reactor TP3 during the course of the study. Effluent COD (920 – 4290 mg/L) for run 11 (day 61 – 72) is not plotted, since the range is too large.

Effluent COD concentrations for all for reactors (Figures 4–32 and 4–33 and Appendix I) were mostly above 100 mg/L (average of 400 ± 100 mg/L). Thus, a polishing unit will be required to meet the discharge limit of 25 mg/L COD. For the reactor treating 1.6% ADF at high SOLR (Figure 4–33), effluent COD concentrations

were in excess of 300 mg/L. The effluent COD range of run 11 (day 61 – 72) and run 23 (day 332 – 336) were 920 – 4290 mg/L and 240 – 620 mg/L, respectively. The run conditions for runs 11 and 23 were the same. However, a longer time (2 months) was employed for the transition from run 17 to run 23, while a period of only 1 week was employed to change from run 7 to run 11. This indicated that gradual transitions from low to high SOLR are very important in influencing reactor stability, especially in the treatment of 1.6% ADF.

4.5.2 Methane Quality

Methane concentration in reactor biogas produced during the ADF treatment was measured on a weekly basis. An average of the results obtained for all 23 runs (Appendix I) indicated that the biogas was composed of 62% ± 3% methane and 37% ± 3% carbon dioxide, on a volume basis. These values are comparable to typical values for anaerobic processes (Droste, 1997). The theoretical carbon dioxide to methane ratio is 3/5 = 0.6, based on the stoichiometric conversion of EG below:

$$4\,HOCH_2CH_2OH \longrightarrow 5\,CH_4 + 3\,CO_2 + 2\,H_2O \qquad (49)$$

A ratio of $^{62\%}/_{37\%} = 0.59$ was obtained for the UASB reactors. This suggested that reactor methane came primarily from EG degradation. This was expected since EG is the main carbon source in the ADF used in the study.

4.5.3 Chemical Oxygen Demand Balance

Mass balances give additional support for experimental data by acting as cross-check mechanisms. Thus COD balances were performed on steady-state data (Appendix I) for the 23 experimental runs carried out in this study. Based on the first law of thermodynamics, the total COD entering the UASB reactor is equal to the total COD leaving the reactor. Thus the theoretical ratio of COD in to COD out is unity. The results

presented in Table 4–41 indicated that experimental data were reliable since the range for the measured ratio of COD in to COD out for the 23 experimental runs was 0.89 – 1.22. Ten of the 23 runs (43%) had measured COD in to COD out ratio of 1.00 ± 0.05 (0.96 – 1.05).

The large uncertainties associated with the COD in to COD out ratios presented in Table 4–41 were likely due to uncertainties in biogas measurements rather than COD measurements. Biogas readings were measured using battery operated wet tip meters. Deviations in the measured gas volumes can result if the battery is near the end of its life. Fewer clicks would be registered on the rotary counter. This can easily go unnoticed until gross discrepancies in day to day biogas volumes are measured. The uncertainty in the ratio of COD in to COD out is affected by the uncertainty in the biogas volume measurement since the total COD leaving the reactor is directly influenced by the biogas (methane) production.

The uncertainties in the reported effluent total COD concentrations were high (can be as high as 50% as for run 23); however, these deviations were due to changes in the day to day COD concentrations measured during the designated steady-state conditions. Changes in effluent COD concentrations would result in appropriate changes in methane production (i.e., less methane gas would be produced if the effluent COD is increased). The total COD leaving the reactors were calculated individually for all measurements taken during each steady state, and the average of these values are reported for each run. Thus, the uncertainties associated with the ratio of COD in to COD out due to uncertainties in effluent COD concentrations should be relatively small.

Table 4–41 Mass balances on COD for the 23 continuous UASB experiments conducted[a].

Run	Flow Rate (L/d)	Influent COD_t[b] (g/L)	Effluent COD_t[b] (mg/L)	CH_4 Produced (L/d)	COD In[c] (g COD/d)	COD Out[d] (g COD/d)	COD In : Out Ratio
1	4.1±0.1	9.2±0.2	250±44	14.7±0.4	38.1±1.1	38.3±1.4	1.00±0.07
2	4.0±0.1	9.1±0.2	260±60	14.3±0.5	36.1±1.9	37.1±1.6	0.97±0.09
3	3.9±0.2	9.0±0.2	281±79	13.5±0.5	35.2±2.5	35.8±1.5	0.98±0.11
4	3.6±0.3	9.1±0.2	255±54	13.2±1.0	32.8±3.0	33.6±3.3	0.98±0.18
5	2.7±0.1	6.2±0.3	139±40	6.5±0.2	16.9±0.9	17.2±0.5	0.98±0.08
6	3.0±0.1	6.2±0.3	183±43	6.5±0.2	18.7±1.5	17.4±0.7	1.08±0.13
7	5.8±0.5	6.3±0.3	157±22	13.4±0.9	36.4±2.6	35.4±2.5	1.03±0.14
8	5.9±0.2	6.2±0.3	198±40	15.3±0.5	35.9±2.3	40.4±1.5	0.89±0.09
9	2.9±0.1	11.4±0.5	259±22	12.9±0.4	33.4±1.8	33.7±1.2	0.99±0.09
10	3.1±0.1	11.4±0.5	238±60	12.5±0.3	34.8±1.4	32.7±0.9	1.07±0.07
11	6.0±0.1	11.3±0.4	2082±638	19.9±2.2	67.7±2.2	63.5±9.4	1.06±0.19
12	6.1±0.1	11.4±0.5	318±31	29.4±0.8	69.1±2.9	77.0±2.3	0.90±0.06
13	4.3±0.3	8.4±0.6	280±84	12.4±0.8	35.7±3.9	32.9±2.4	1.09±0.20
14	4.3±0.3	8.3±0.6	305±51	11.3±0.7	35.5±3.2	29.9±2.7	1.19±0.22
15	2.7±0.3	8.3±0.6	257±42	7.3±0.4	22.1±2.9	18.6±2.4	1.19±0.31
16	8.8±1.5	8.3±0.6	333±81	26.1±1.5	72.6±11.7	67.4±11.2	1.08±0.35
17	4.1±0.1	5.5±0.4	214±71	8.1±0.5	22.5±1.4	22.1±1.4	1.02±0.13
18	3.9±0.2	11.4±1.0	476±179	15.4±0.8	44.5±4.3	41.3±2.8	1.08±0.18
19	3.7±0.1	9.0±0.2	252±58	11.2±0.2	33.6±1.2	29.7±0.7	1.13±0.07
20	4.1±0.2	9.0±0.2	302±125	12.7±0.5	36.6±2.6	33.7±1.8	1.08±0.14
21	7.1±0.3	10.9±0.3	845±189	26.4±0.8	77.2±4.1	73.5±3.4	1.05±0.10
22	12.5±0.3	9.1±0.5	778±200	32.5±1.7	113.4±6.2	93.2±7.0	1.22±0.16
23	5.4±0.3	11.7±0.2	1160±565	23.3±1.5	63.1±3.1	66.0±7.0	0.96±0.15

[a] There was no biomass accumulation; thus, COD in = effluent total COD + methane COD

[b] COD_t is total COD.

[c] COD In = Influent COD_t × Flow Rate.

[d] COD Out = Effluent COD_t + (CH_4 Produced ÷ 0.394) + (0.032 × Flow Rate ÷ 0.394),
where 0.394 L/g COD is the methane potential at 35°C,
and 0.032 L CH_4/L effluent is the methane solubility at 35°C (Switzenbaum, 1978).

4.5.4 Kinetic Constants for ADF Treatment in UASB Reactors

Maintenance of a high biomass inventory in UASB reactors is of paramount importance in ensuring good reactor performance. Thus, it was of interest to determine the washout factor for the wastewater treatment process. A plot of SRT (Appendix I) as a function of HRT was carried out to determine the washout factor for the three influent COD concentrations used during ADF treatment in bench-scale UASB reactors. Based on equation **13**, the washout factor f is equal to the inverse of the slope of the lines presented in Figure 4–34.

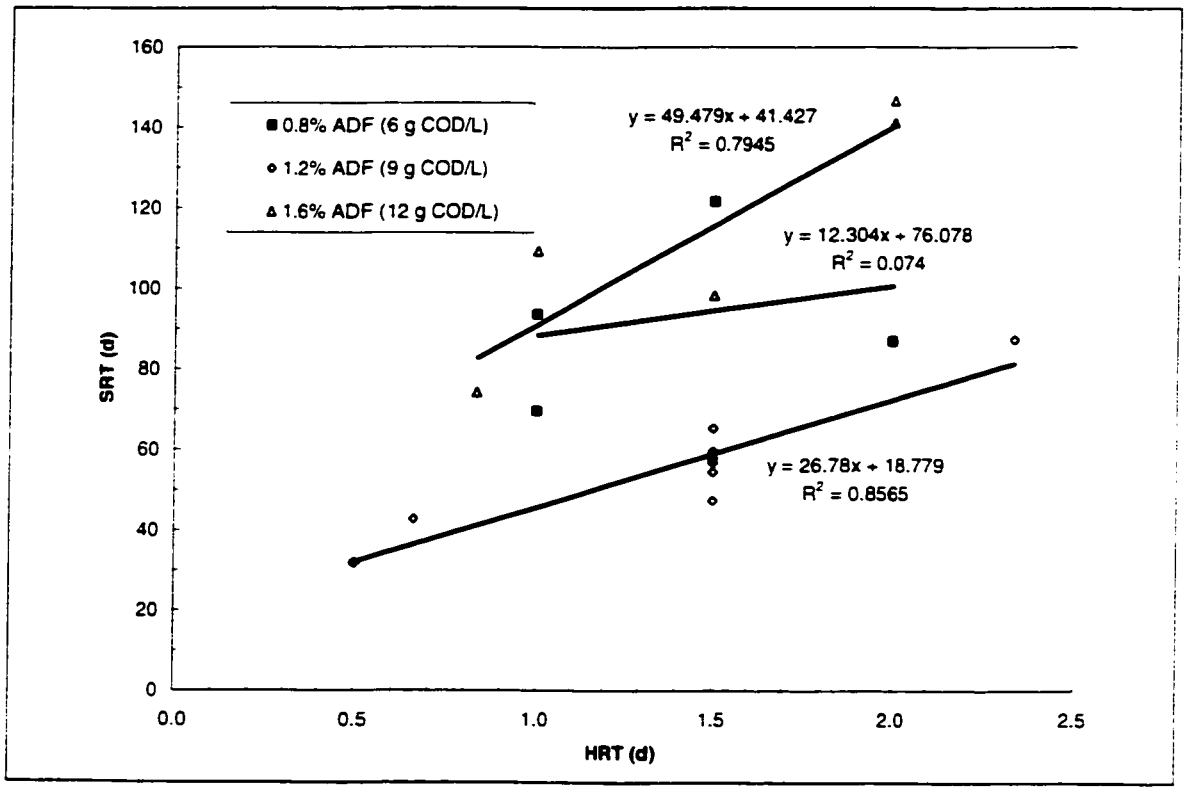

Figure 4–34 A plot of SRT as a function of HRT for ADF treatment in bench-scale UASB reactors.

The values of f were 0.081, 0.037, and 0.020 for 0.8, 1.2, and 1.6% ADF, respectively. From the results presented in Figure 4–35, a linear relationship between f

and the influent COD concentration S_0 (g COD/L) for the range of ADF concentration used in this study was:

$$f = -0.011 S_0 + 0.15 \quad (50)$$

The results suggested that more biomass washout occurred for lower influent COD concentrations as reflected by the negative slope in equation **50**. This was contrary to reported results for anaerobic downflow stationary fixed film reactors (Kennedy, 1985) and fixed film activated sludge processes (Droste, 1997). This difference can be accounted for by the difference in reactor configuration and flow pattern.

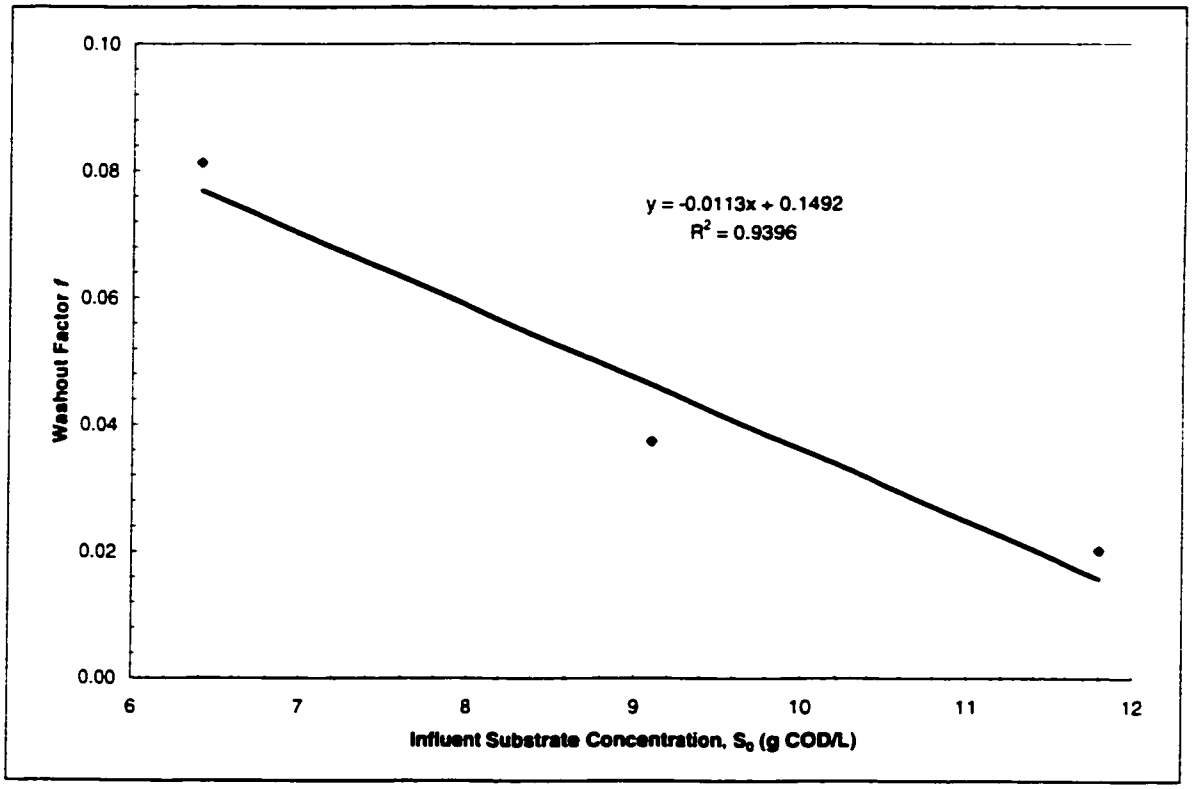

Figure 4–35 Washout factor *f* as a function of influent COD concentration.

Kinetic constants for ADF treatment in UASB reactors were also calculated. Based on equation **12**, the net specific growth rate was plotted against the specific substrate utilization rate U as shown in Figure 4–36. The results indicated that the

biomass yield coefficients were 0.015, 0.027, and 0.021 g VSS/g COD and the endogenous decay coefficients were 0.008, 0.012, and 0.003 d^{-1} for 0.8, 1.2, and 1.6% ADF, respectively.

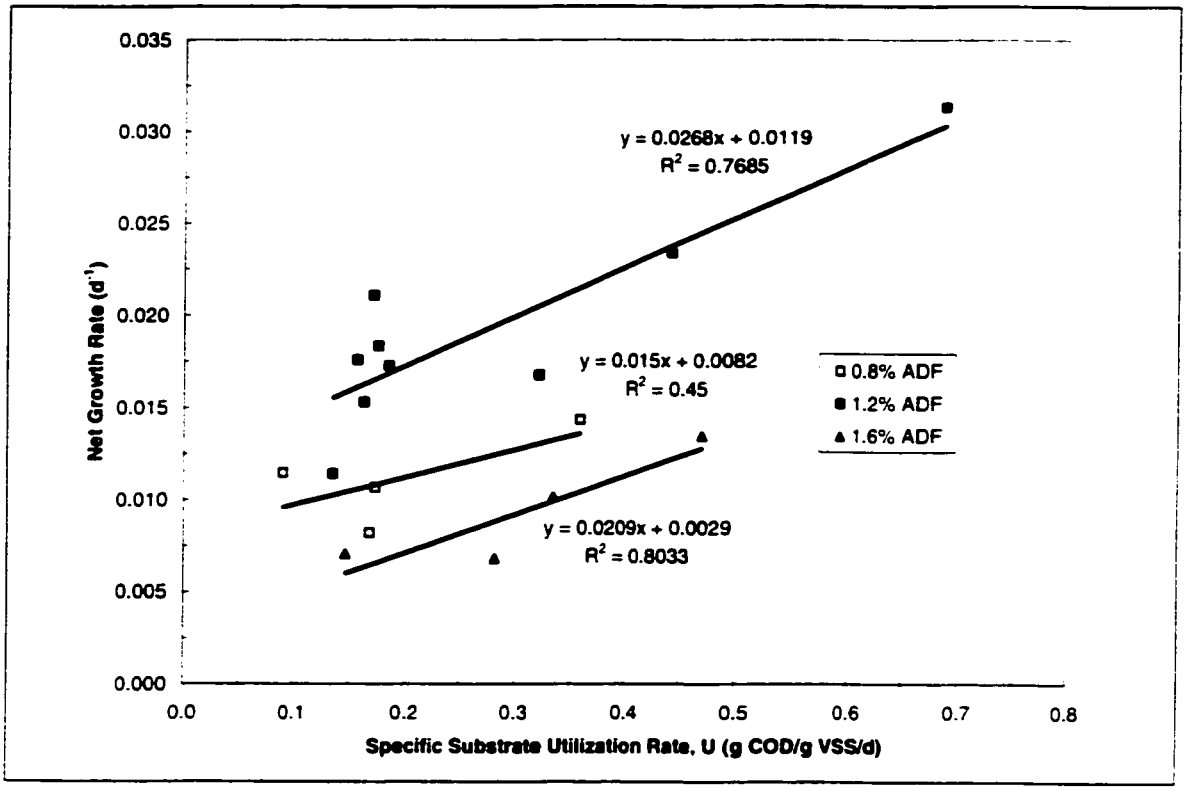

Figure 4-36 Net specific growth rate versus specific substrate utilization rate at 0.8%, 1.2%, and 1.6% ADF.

The biomass yields were determined based on washout biomass measurements. There was essentially no biomass accumulation detected in the reactors. This is expected to change over time since a slight increase in biomass settling velocities was observed near the end of the study. An increase in settling velocity would allow more biomass to be retained in the reactor. However, the net yield will be small since the biomass yield coefficients were small. On the other hand, the low endogenous decay coefficients obtained are desirable. With low decay coefficients, the biomass can be stored over long

periods of time without significant effects on its viability. This is ideal for ADF treatment which is seasonal in nature.

For mesophilic anaerobic treatment of acetic acid, the range for Y and k_d are in the range of 0.01 – 0.054 g VSS/g COD and 0.004 – 0.037 d^{-1} (Speece, 1996). Acidogenesis of EG in the UASB reactors during ADF treatment was very rapid since no EG was detected in any of the samples taken from the reactor recycling lines. Thus, it is reasonable that Y and k_d values similar to those for acetoclastic methanogenesis were obtained.

Substrate removal by biological treatment processes have been described by both models **9** and **10** (Droste, 1997). For ADF treatment in bench-scale UASB reactors, the r^2 values (0.38 for model **9** and 0.53 for model **10**) for the Lineweaver-Burke plots presented in Figure 4–37 indicated that the kinetic model **10** better represented the operational data obtained for this study. Although an r^2 of 0.53 is quite small, it is comparable to reported values for experimental data (Droste, 1997).

The maximum rate of substrate utilization k' and the half-velocity constant K_S were 28.4 g COD/L/d and 648 mg COD/L, respectively. At a reactor biomass concentration of 27 g VSS/L (biomass bed at ½ reactor volume), the maximum specific rate of substrate utilization k was 1.05 g COD/g VSS/d and the maximum specific growth rate μ_{max} for 0.8, 1.2, and 1.6% ADF were 0.016, 0.028, and 0.022 d^{-1}, respectively. ADF toxicity may be a contributing factor to the lower μ_{max} obtained for 1.6% ADF as compared to that for 1.2% ADF

A half-velocity constant of 648 mg COD/L indicated effluent COD concentrations will be high (above 100 mg COD/L). This is reasonable since influent COD concentrations were in the range of 6400 – 11,800 mg COD/L. If lower effluent COD concentrations are desired to meet discharge limits, polishing units will be required.

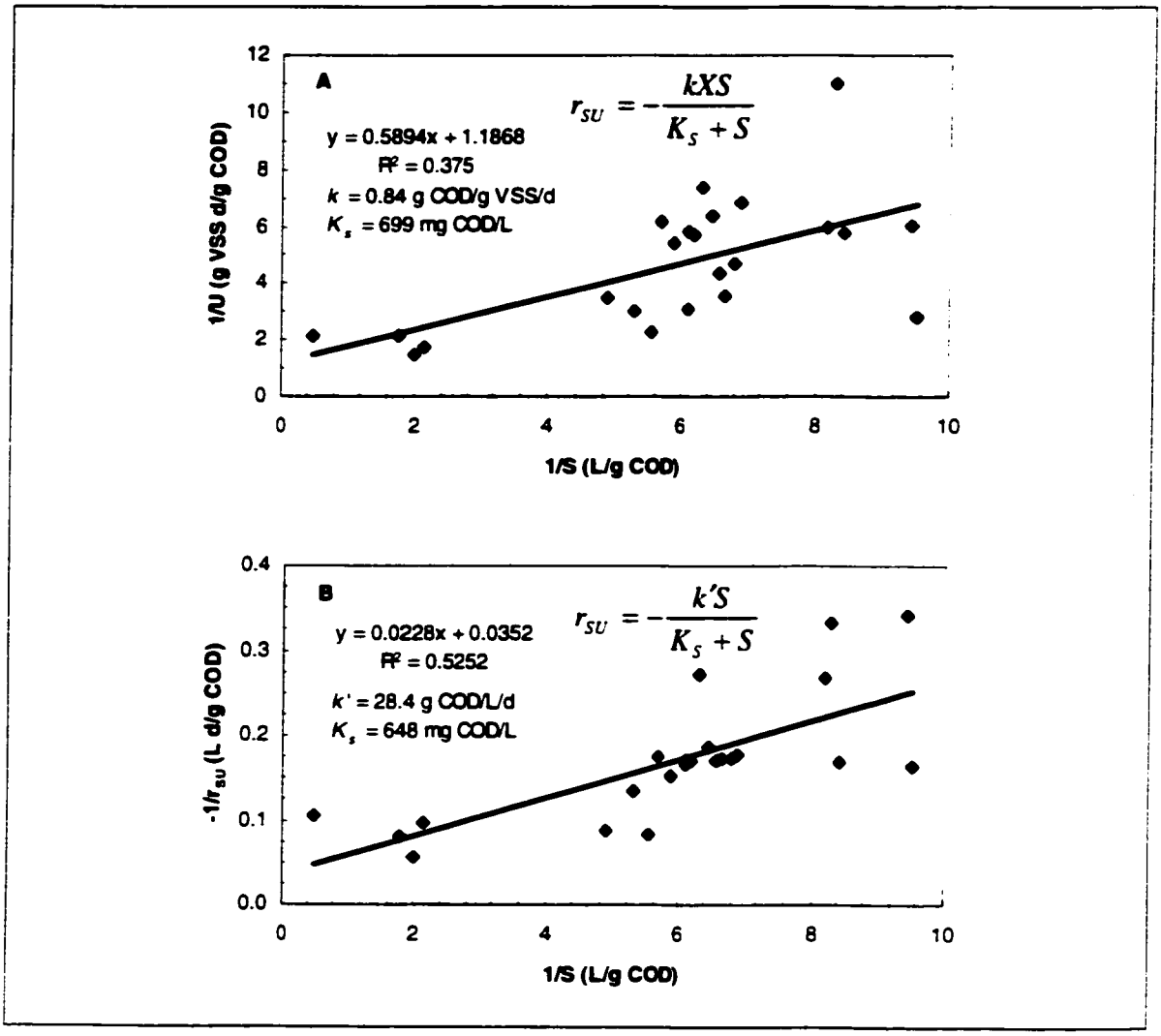

Figure 4-37 Lineweaver-Burke plots for Monod (A) kinetic model 9 and (B) kinetic model 10.

5 Conclusions

Empirical models were developed for COD removal efficiencies, biomass specific acetoclastic activity, methane production rates, and methane production potential as functions of ADF concentration, HRT, and biomass concentration. Time trend effects were found to be significant. The addition of a blocking variable was required to compensate for experiments being conducted in two blocks. Model verification indicated that predicted responses were in good agreement with experimental results.

Biomass specific acetoclastic activity was improved by almost two-fold during ADF treatment in UASB reactors. The reduced fitted empirical model indicated that specific acetoclastic activity was affected by all three operating variables tested. Better activities were predicted for biomass inventory at ½ reactor volume (biomass concentration of 27 g VSS/L). The effects of ADF concentration, HRT, and HRT – ADF concentration interactions were significant. For optimum specific acetoclastic activities, UASB reactors should be operated at low HRTs and ADF concentrations (1 – 1.2% ADF or 8 – 9 g COD/L).

For the range of run conditions tested, COD removal efficiency was independent of biomass concentration. Similar to biomass activity, better COD removal efficiencies were predicted for low HRT and ADF concentration levels. The response surface for the predicted empirical model was relatively flat, with predicted COD removals above 95% for the design window. This is of practical importance since very good COD removal efficiencies can be obtained for a wide range of operation conditions.

ADF toxicity effects were more pronounced at medium organic loadings (SOLR above 0.5 g COD/g VSS/d) for high ADF concentrations (1.6% ADF). For a lower ADF level (1.2% ADF), good reactor stability and excellent removal efficiencies (greater than

90% COD removal) were achieved for reactor loadings approaching that of highly loaded systems (0.73 g COD/g VSS/d).

Methane production potentials measured were close to the theoretical value of 0.39 L CH_4/g COD removed at 35°C. The reduced fitted empirical model indicated that methane production potential was affected by HRT and biomass concentration. For a biomass inventory at ½ reactor volume (27 g VSS/L), theoretical methane production potentials were predicted for all HRTs tested. On the other hand, the methane production rate was affected by all three operating variables. In general, methane production increased as the OLR is increased.

Toxicity effects of ADF were evident in the structure of the anaerobic granules. Some of the larger granules were covered with a grayish slime material after exposure to feed concentrations above 1.2% ADF. The ADF-acclimated biomass from the UASB reactors had lower settling velocities than seed biomass obtained from a pulp and paper mill treatment plant. However, settling velocities leveled off to a new steady state after this initial decrease. Thus, good biomass inventory in UASB reactors can be maintained for prolong periods of ADF treatment.

Freundlich sorption isotherms for BT, MeBT, and DiMEBT indicated that aryl triazole sorption to anaerobic granules was minimal. Higher sorption capacity was obtained for NP. For example, at a liquid phase concentration of 10 mg/L, the sorption capacity of active granular biomass for NP, DiMeBT, and BT/MeBT were 27 mg/g VSS, 0.53 mg/g VSS, and 0.013 mg/g VSS, respectively. There was also evidence for the involvement of active transport in NP sorption by anaerobic granular biomass, since dormant and NaN_3 inhibited biomass had lower sorption capacities (i.e., 13 mg/g VSS and 3.1 mg/g VSS for dormant and inhibited biomass, respectively).

EG degradation experiments indicated that BT, MeBT, DiMeBT, and Tergitol NP-4 (NPnEO) had no significant effects on acidogenesis and methanogenis at

concentration levels studied. A significant inhibition of acetoclastic activity was observed for NP at 100 mg/L. The acetic acid consumption rate at 100 mg/L NP was reduced to 38% of that for controls. Metabolic intermediates of these additives (NP, BT, MeBT, and DiMeBT) were not detected in either batch or continuous experiments. However, biosorption alone cannot account for the measured reduction in NP levels found during ADF treatment in UASB reactors and in batch EG degradation experiments. This suggested that anaerobic degradation occurred; however, further studies are required to better characterize the fate of NP in UASB reactors.

Organic carbon balances performed on the UASB reactors indicated that reliable experimental data were obtained for the 23 continuous runs conducted. Kinetic considerations indicated that substrate removal was independent of reactor biomass concentration. The maximum rate of substrate utilization k' and the half-velocity constant K_S for ADF treatment were 28.4 g COD/L/d and 648 mg COD/L, respectively. The biomass yield and endogenous decay coefficients for 1.2% ADF (9 g COD/L) wastewater were 0.027 g VSS/g COD and 0.012 d^{-1}, respectively. The high K_S value of 648 mg COD/L indicated that polishing units will be required to meet discharge limits.

6 Future Studies

The following topics are suggested as possible subjects for further investigations:

- Evaluate the treatability of a much more complex ADF wastewater collected from an airport, which also contains oil and other contaminants.
- Use radioactive labels to better characterize the fate of NP and elucidate the mechanism involved.
- Develop mechanistic models for ADF treatment in UASB reactors.
- Investigate the effects of micronutrient (Fe, Ni, Co) addition on biodegradation at high ADF concentrations.
- Investigate ADF treatment by a dual anaerobic/aerobic system, where an aeration chamber is used as a polishing unit. The effectiveness of this system for NP removal should also be evaluated since aerobic degradation of NP is known.
- Investigate the fate other possible ADF additives such as 2,4-dioxane (a known contaminant in ethylene glycols) and triethanolamine.
- Investigate the use of phase separation in ADF treatment, where acidogenesis is separated from methanogenesis.

References

Note that all referenced Web sites were last visited on January 2002 and they may change in the future.

Ackman, R.G. (1972) Porous polymer bead packing and formic acid vapour in GLC of volatile fatty acids. *J. Chromatogr. Sci.* **10**, 560–565.

Ahel, Marijan and Walter Giger (1985) Determination of nonionic surfactants of the alkylphenol polyethoxylate type by high-performance liquid chromatography. *Anal. Chem.* **57**, 2584–2590.

Ahel, Marijan, Walter Giger, and Markus Koch (1994a) Behaviour of alkylphenol polyethoxylate surfactants in the aquatic environment – I. Occurrence and transformation in sewage treatment. *Wat. Res.* **28**, 1131–1142.

Ahel, Marijan, Walter Giger, and Christian Schaffner (1994b) Behaviour of alkylphenol polyethoxylate surfactants in the aquatic environment – II. Occurrence and transformation in rivers. *Wat. Res.* **28**, 1143–1152.

Andras, E., K.J. Kennedy, and D.A. Richardson (1989) Test for characterizing settleability of anaerobic sludge. *Environ. Tech. Let.* **10**, 463–470.

Limno-Tech Services (2002) The deicing dilemma: balancing safety and environmental impact. Available from http://www.limno.com/services/air_envr.shtml

APHA (1985) *Standard methods for the examination of water and wastewater*. 16th Ed. American Public Health Association, Washington, D.C.

Baldwin, William S., Stephen E. Graham, Damian Shea, and Gerald A. LeBlanc (1997) Metabolic androgenization of female *Daphnia magna* by the xenoestrogen 4-nonylphenol. *Environ. Toxicol. Chem.* **161**, 1905–1911.

Baldwin, William S., Stephen E. Graham, Damian Shea, and Gerald A. LeBlanc (1998) Altered metabolic elimination of teresterone and associated toxicity following exposure of *Daphnia magna* to nonylphenol polyethoxylate. *Ecotoxicol. Environ. Saf.* **39**, 104–111.

Baron, Burke (1999) Biodegradation of aircraft deicing fluid components in soil. Report # AD-a361 762 AFIT/GEE/ENV/99-04. Air Force Inst. of Tech. Wright-Patterson AFB, OH. (Cornell, J.S. (1998) Aspects of the chemistry, toxicity and biodegradation of benzotriazole and its derivatives. Unpublished data. Air Force Inst. of Tech., University of Boulder Colorado.)

Bremer, K. (1993) The double deicing dilemma. Available from http://www.airportnet.org/depts/publicat/airmags/am91093/deicing.htm

Brunner, Paul H., Silvio Capri, Antonio Marcomini, and Walter Giger (1988) Occurrence and behaviour of linear alkylbenzenesulphonates, nonylphenol, nonylphenol mono- and nonylphenil diethoxylates in sewage and sewage sludge treatment. *Wat. Res.* **22**, 1465–1472.

Burkhardt-Holm, Patricia, Thomas Wahli, and Willy Meier (2000) Nonylphenol affects the granulation pattern of epidermal mucous cells in rainbow trout, *Oncorhynchus mykiss*. *Ecotoxicol. Environ. Saf.* **46**, 34–40.

Cancilla, Devon A., A. Holtkamp, L. Matassa, and X. Fang (1997) Isolation and characterization of microtox-active components from aircraft deicing/anti-icing fluids. *Environ. Toxicol. Chem.* **16**, 430–434.

Cancilla, Devon A., Jennifer Martinez, and Graham C. Van Aggelen (1998) Detection of aircraft deicing/antiicing fluid additives in a perched water monitoring well at an international airport. *Environ. Sci. Tech.* **32**, 3834–3835.

Canton, J.H., G.J. van Esch, P.A. Greve, and A.B.A.M. van Hellemond (1977) Accumulation and elimination of α-hexachlorocyclohexane (α-HCH) by a marine algae Chlamydomonas and Dunaliella. *Wat. Res.* **19**, 111.

Cardellini, Pietro and Lino Ometto (2001) Teratogenic and toxic effects of alcohol ethoxylates and alcohol ethoxy sulfate surfactants on *Xenopus laevis* embreos and tadpoles. *Ecotoxicol. Environ. Saf.* **48**, 170–177.

Child, J. and A.Willetts (1978) Microbial metabolism of aliphatic glycols, bacterial metabolism of ethylene glycol. *Biochim. Biophys. Acta* **538**, 316–327.

Cox, D.P. (1978) The biodegradation of polyethylene glycols. *Adv. Appl. Microbiol.* **23**, 173–194.

Cox, C. (1996) Masculinity at risk, pesticides and male fertility. *J. Pestic. Reform* **16**, 2–7.

Darlington, C. and K J. Kennedy (1998) Biodegradation of aircraft deicing fluid in an Upflow Anaerobic Sludge Blanket (UASB) reactor. *J. Environ. Sci. Health* **A33(3)**, 339–351.

Downs, W.R. (1968) Chemically induced ignition in aircraft and spacecraft electrical circuitry by glycol/water solutions. *NASA Technical Note.* NASA TN D–4327.

Draper, N.R. (1982) Center points in second-order response surface designs. *Technometrics* **24**, 127–133.

Droste, Ronald L. (1997) *Theory and practice of water and wastewater treatment.* John Wiley & Sons, Inc., Toronto.

Duncan, P.–A. (1995a) The clean aircraft concept, part one. *FAA Aviation News.* Available from http://www.faa.gov/avr/news/Clean.htm

Duncan, P.–A. (1995b) The clean aircraft concept, part two. *FAA Aviation News.* Available from http://www.faa.gov/avr/news/Clean2.htm

Dwyer, D.F.and J.M. Tiedje (1983) Degradation of ethylene glycol and polyethylene glycols by methanogenic consortia. *Appl. Environ. Microbiol.* **46**, 185–190.

Dykstra, O.Jr. (1960) Partial duplication of response surface designs. *Technometrics* **2**, 185–195.

Ejlertsson, Jörgen, Marie-Louise Nilsson, Henrik Kylin, Åke Bergman, Leif Karlson, Mats Öquist, and Bo H. Svensson (1999) Anaerobic degradation of nonylphenol mono- and diethoxylates in digester sludge, landfilled municipal solid waste, and landfilled sludge. *Environ. Sci. Tech.* **33**, 301–306.

Ekelund, R., A. Granmo, K. Magnusson, M. Berggren, and A. Bergman (1993) Biodegradation of 4-nonylphenol in seawater and sediment. *Environ. Microbiol. Pollut.* **79**, 59–61.

Environment Canada (1994) Glycol guidelines, p. 840–842. *In* Canada Gazette Part I. Environment Canada, Evaluation and Interpretation Branch, Ottawa.

Evans, W.H. and E.J. David (1974) Biodegradation of mono-, di-, and triethylene glycols in river waters under controlled laboratory conditions. *Wat. Res.* **8**, 97–100.

Field, Jennifer A., Ralph L. Reed (1996) Nonylphenol polyethoxy carboxylate metabolites of nonionic surfactants in U.S. paper mill effluents, municipal sewage treatment plant effluents, and river water. *Environ. Sci. Tech.* **30**, 3544–3550.

Giger, Walter, Paul H. Brunner, and Christian Schaffner (1984) 4-Nonylphenol in sewage sludge : accumulation of toxic metabolites from nonionic surfactants. *Science* **225**, 623–625.

Gonzalez, C.F., W.A. Taber, and M.A. Zeitoun (1972) Biodegradation of ethylene glycol by a salt-requiring bacterium. *Appl. Microbiol.* **24**, 911–919.

Grimes, D.J. and S.M. Morrison (1975) Bacterial bioconcentration of chlorinates hydrocarbon insecticides from aqueous systems. *Microbial Ecology* **2**, 43.

Gruden, Cyndee L., Sarahann M. Dow, and Mark T. Hernandaz (2001). Fate and toxicity of aircraft deicing fluid additives through anaerobic digestion. *Water Environ. Res.* **73**, 72–79.

Guiot, S.R., A. Pauss, and J.W. Corterton (1992) A structured model of the anaerobic granule consortium. *Wat. Sci. Tech.* **25**, 1–10.

Haines, J.R. and M. Alexander (1975) Microbial degradation of polyethylene glycols. *Appl. Microbiol.* **29**, 621–625.

Hartley, H.O. (1959) Smallest composite designs for quadratic response surfaces. *Biometrics* **15**, 611–624.

Hartwell, S. Ian, David M. Jordahl, and Eric B. May (1993) Toxicity of aircraft de-icer and anti-icer solutions to aquatic organisms. Maryland Department of Natural Resources. Tidewater Administration. May 1993.

Holmgren, A. and W. Forsling (1995) A prestudy of the recycling properties of aircraft de/anti-icing fluids. *Coldtech project no. 29/93.* Available from http://www.luth.se/depts/lib/coldtech/ct95-1.html

Hughes, Ami L., Jeff Fisher, and Ernie Brumbaugh (1996) Biodegradation of NPE in soil. In *Proceedings of the 4th CESIO World Surfactants Congress* **4**, reprinted in *the Alkylphenols and Alkyphenol Ethoxylates Review*, **1**, 17–23.

Hughes, P.J., H. McLellan, D.A. Lowes, S. Safar Khan, J.G. Bilmen, S.C. Tovey, R.E. Gadfrey, R.H. Michell, C.J. Kirk, and F. Michelangeli (2000) Estrogenic alkylphenols induce cell death by inhibiting testis endoplasmic reticulum Ca^{2+} pumps. *Biochem. Biophys. Res. Com.* **277**, 568–574.

Hulshoff Pol, L.W. (1989) *The phenomenon of granulation of anaerobic sludge.* Ph.D. Thesis, Wageningen Agricultural University, Wageningen, The Netherlands.

Jank, B. E., H. M. Guo, and V.W. Cairns (1973) Biological treatment of airport wastewater containing aircraft deicing fluids. *Wastewater Technology Center, Environmental Protection Service.* Report No. EPS 4–WP–73–5.

John, Dominic M.and Graham F. White (1998) Mechanism for biotransformation of nonylphenol polyethoxylates to xenoestrogens in *Pseudomonas putida. J. Bacteriol.* **180**, 4332–4338.

Johnson, Laura (1997) Evaluation of the natural biodegradation of aircraft deicing fluid. Report # AD-a334 350 AFIT/GEE/ENV/97D-12. Air Force Inst. of Tech. Wright-Patterson AFB, OH.

Karley, Alison J., Simon I. Powell, and Julia M. Davies (1997) Effect of nonylphenol on the growth of *Neurospora crassa* and *Candida albicans. Appl. Environ. Microbiol.* **63**, 1312–1317.

Keller, David (1999) Sorption of the aircraft deicing fluid component methyl-benzotriazole in soil. Report # AD-a374 457 AFIT/GEE/ENV/99M-11. Air Force Inst. of Tech. Wright-Patterson AFB, OH.

Kennedy, K.J. (1985) *Startup and steady state kinetics of anaerobic downflow stationary fixed film reactors.* Ph.D. Thesis, University of Ottawa, Canada.

Kilroy, A.C. and N.F. Gray (1992) Pilot plant investigation of the treatability of ethylene glycol by activated sludge. *Environ. Tech.* **13**, 293–300.

Klečka, G.M., C.L. Carpenter, and B.D. Landenberger (1993) Biodegradation of aircraft deicing fluids in soil at low temperatures. *Ecotoxicol. Environ. Saf.* **25**, 280–295.

Klein, Carmen M. (1995) *The effect of inhibitors on the biosorption of 2,4-dichlorophenol and 2,3,6-trichlorophenol by anaerobic granules.* B.A.Sc. Thesis. University of Ottawa, Canada.

Kubeck, Edmund and Carter G. Nayor (1990) Trace analysis of alkylphenol ethoxylates. *JAOCS* **67**, 400–405

Kubota, Shunichiro, Sachiko Ohara, Taeko Miyauchi, Tomomi Edo, Eiji Takayama, Kousuke Tomita, and Yousuke Seyama (2000) Effects of *para*-nonylphenol on 92 kDa gelatinase secretion by human peripheral lymphocytes and U937 cells *in vitro. Biochem. Biophys. Res. Com.* **279**, 270–274.

Lamche, Gisela and Patricia Burkhardt-Holm (2000) Nonylphenol provokes a vesiculation of the golgi apparatus in three fish epidermis cultures. *Ecotoxicol. Environ. Saf.* **47**, 137–148.

Lech, J. John, Steven K. Lewis, and Lifen Ren (1996) *In vivo* estrogenic activity of nonylphenol in rainbow trout. *Fundam. Appl. Toxixol.* **30**, 229–232.

LGL–Love (1979) Analysis of shrinkage in volume of glycol in de-icing fluid recovery systems. Report for the Department of Supply and Services, Quebec Region, Montreal, Quebec. DSS 09SDT 8200–8–8524.

Lucas, J.M. (1977) Design efficiencies for varying numbers of center points. *Biometrika* **64**, 145–147.

Macarie, H. (2000) Overview of the application of anaerobic treatment to chemical and petrochemical wastewaters. *Wat. Sci. Tech.* **42**, 201–214.

MacDonald, D.D., I.D. Cuthbert, P.M. Outridge, R.T. Ruthman, and S.L. Walker (1993) Canadian water quality guidelines for the protection of aquatic life for ethylene glycol, diethylene glycol, and propylene glycol. *Scientific Series Report.* Environmental Canada.

Maki, H., M. Fujita, and Y. Fujiwara (1996) Identification of final biodegradation product of nonylphenol ethoxylate (NPE) by river microbial consortia. *Bull. Environ. Contam. Toxicol.* **57**, 881–887.

McCarty, Brian D. and Roy T. Willis (1996) Technology assessment requirement analysis: de-icing final report. Department of the Air Force, USA Contract No. F33615–90–D–0652 / 0006

McDonald E.and M. Hales (1997) Survey of commercial technologies and research in deicing. Labat-Anderson, Inc.'s presentation at the AWMA's 90th Annual Meeting & Exhibition, June 8–13, Toronto, Ontario, Canada.

Mudd, Leonard E. (1993) Design of aircraft deicing facilities. Advisory Circular No: 150/5300–14. Available from: http://www.faa.gov/arp/pdf/5300-14.pdf

Mulligan, C., J. Chebib, and B. Safi (1997) Anaerobic treatment of aircraft de-icing agent using the SNC-Lavalin multiplate reactor. SNC Research Corp.'s presentation at the AWMA's 90th Annual Meeting & Exhibition, June 8–13, Toronto, Ontario, Canada.

Naylor, Cartor G. (1995) Environmental fate and safety of nonylphenol ethoxylates. *Textile Chem. Color* **27**, 29–33.

Nimrod, Alison C. and William H. Benson (1996) Environmental estrogenic effects of alkylphenol ethoxylates. *Crit. Rev. Toxicol.* **26**, 335–364.

Novak, Lesley J., Keith Holtze, Robert A. Kent, Catherine Jefferson, and Don Anderson (2000) Acute toxicity of storm water associated with de-icing/anti-icing activities at canadian airports. *Environ. Toxicol. Chem.* **19**, 1846–1855.

Palns, S.S., R.E. Loewenthal, P.L. Dold, and G.R. Marais (1987) Hypothesis for pelletisation in the upflow anaerobic sludge bed reactor. *Water SA* **13**, 69–80.

Pearce, B.A.and M.T. Heydeman (1980) Metabolism of di(ethylene glycol) [2-(2'-hydroxyethoxy)ethanol] and other short poly(ethylene glycol)s by Gram-negative bacteria. *J. Gen. Microbiol.* **118**, 21–27.

Pham, Thi Tham and Kevin J. Kennedy (1994) Biosorption of pentachlorophenol (PCP) by granular and dispersed anaerobic sludge. *J. Environ. Sci. Health* **A29(7)**, 1451–1469.

Pillard, David A., Jeffrey S. Cornell, Doree L. Dufresne, and Mark T Hernandez (2001) Toxicity of benzotriazole and benzotriazole derivatives to three aquatic species. *Wat. Res.* **35**, 557-560.

PRO-ACT (1995) Deicers currently approved by the Air Force. Available from http://chppm-meis.apgea.army.mil/pro-act/6159.txt

Rochkind-Dubinsky, Melissa L., Gary S. Salyler, and James W. Blackburn (1987). *Microbial decomposition of chlorinated aromatic compounds*. M. Dekker, New York.

Sabeh, Y. and K.S. Narasiah (1992) Degradation rate of aircraft deicing fluid in a sequential biological reactor. *Wat. Sci. Tech.* **26**, 2061–2064.

Schink B.and M. Stieb (1983) Fermentative degradation of polyethylene glycol by a strictly anaerobic, Gram-negative, nonsporeforming bacterium, *Pelobacter venetianus* sp. nov. *Appl. Environ. Microbiol.* **45**, 1905–1913.

Schmitt, Thomas M. and Ead S. Muzher (1981) Determination of 2-mercaptobenzothiazole, tolyltriazole and benzotriazole in coolant formulations by liquid chromatography. *Talanta* **28**, 777–779.

Shuler, Michael L. and Fikret Kargi (2002) *Bioprocess engineering: Basic concepts.* Second Edition. Prentice Hall, New Jersey.

Simpson, A. (1997) Aircraft deicing best management plans. Transport Canada's presentation at the AWMA's 90th Annual Meeting & Exhibition, June 8–13, Toronto, Ontario, Canada.

Speece, R.E. (1996) *Anaerobic technology for industrial wastewaters*. Archae Press, Tennessee.

Switzenbaum, Michael S. (1978) *The anaerobic attached film expanded bed reactor for the treatment of dilute organic wastes.* Ph.D. Thesis, Cornell University, USA.

Switzenbaum, Michael S., Dean Mericas, and Bryan Wagoner (1999) Best management practices for airport deicing stormwater. Water Resources Research Center, University of Massachusetts/Amherst. Publication No. 173, 57 pages.

Tanghe, Tom, Willem Dhooge, and Willy Verstraete (1999) Isolation of a bacterial strain able to degrade branched nonylphenol. *Appl. Environ. Microbiol.* **65**, 746–751.

USAF (1996) Technology assessment requirements analysis: deicing. *Department of the Air Force, USA.* Available from http://xre22.brooks.af.mil/detoc.htm

van Huyssteen, J.J. (1967) Gas chromatographic separation of anaerobic digester gases using porous polymer. *Wat. Res.* **1**, 237–242.

Varineau, P.T. and R.M. Charminski (1995) The synthesis of alkyl phenol ethoxylates (APE) and alkyl phenol carboxylates (APEC) for environmental fate studies. Project Report, Union Carbide Corporation, West Virginia.

Weber-shirk, Monroe L. and Richard I. Dick (1997) Biological mechanisms in slow sand filters. *Journal AWAW* **89**, 72–83.

Yoshimura, Kiochi (1986) Biodegradation and fish toxicity of nonionic surfactants. *J. Am. Oil Chem. Soc.* **63**, 1590–1596.

Zar, Jerrold H. (1999) *Biostatistical analysis*. Fourth Edition. Prentice-Hall Inc., New Jersey. Chapter 18, 360–375.

Appendix A Correlation Between Parameter Estimates

For the 2^3 factorial design with four center-point replicates used in this study, the **X** matrix in coded variables is

$$X = \begin{array}{c} \begin{matrix} x_0 & x_1 & x_2 & x_3 & x_1x_2 & x_1x_3 & x_2x_3 & x_1x_2x_3 \end{matrix} \\ \begin{bmatrix} 1 & 0 & 0 & 0 & 0 & 0 & 0 & 0 \\ 1 & 0 & 0 & 0 & 0 & 0 & 0 & 0 \\ 1 & 0 & 0 & 0 & 0 & 0 & 0 & 0 \\ 1 & 0 & 0 & 0 & 0 & 0 & 0 & 0 \\ 1 & -1 & 1 & -1 & -1 & 1 & -1 & 1 \\ 1 & -1 & 1 & 1 & -1 & -1 & 1 & -1 \\ 1 & -1 & -1 & -1 & 1 & 1 & 1 & -1 \\ 1 & -1 & -1 & 1 & 1 & -1 & -1 & 1 \\ 1 & 1 & 1 & -1 & 1 & -1 & -1 & -1 \\ 1 & 1 & 1 & 1 & 1 & 1 & 1 & 1 \\ 1 & 1 & -1 & -1 & -1 & -1 & 1 & 1 \\ 1 & 1 & -1 & 1 & -1 & 1 & -1 & -1 \end{bmatrix} \end{array}$$

and its corresponding $(\mathbf{X}^T\mathbf{X})^{-1}$ is

$$(\mathbf{X}^T\mathbf{X})^{-1} = \begin{bmatrix} \frac{1}{12} & 0 & 0 & 0 & 0 & 0 & 0 & 0 \\ 0 & \frac{1}{8} & 0 & 0 & 0 & 0 & 0 & 0 \\ 0 & 0 & \frac{1}{8} & 0 & 0 & 0 & 0 & 0 \\ 0 & 0 & 0 & \frac{1}{8} & 0 & 0 & 0 & 0 \\ 0 & 0 & 0 & 0 & \frac{1}{8} & 0 & 0 & 0 \\ 0 & 0 & 0 & 0 & 0 & \frac{1}{8} & 0 & 0 \\ 0 & 0 & 0 & 0 & 0 & 0 & \frac{1}{8} & 0 \\ 0 & 0 & 0 & 0 & 0 & 0 & 0 & \frac{1}{8} \end{bmatrix}$$

Because this $(\mathbf{X}^T\mathbf{X})^{-1}$ matrix is a diagonal matrix, the parameter estimates for the first-order linear model from the 2^3 factorial design are uncorrelated. The variance of $\hat{\beta}_0$ is smaller than that of other seven parameter estimates because replicates were done at the center point of the design.

For the blocked central composite design, the **X** matrix in coded variables is

$$
\mathbf{X} = \begin{array}{c}
\begin{array}{cccccccccccc} x_0 & x_1 & x_2 & x_3 & x_1^2 & x_2^2 & x_3^2 & x_1x_2 & x_1x_3 & x_2x_3 & \mathbf{B} \end{array} \\
\begin{bmatrix}
1 & 0 & 0 & 0 & 0 & 0 & 0 & 0 & 0 & 0 & -1 \\
1 & 0 & 0 & 0 & 0 & 0 & 0 & 0 & 0 & 0 & -1 \\
1 & 0 & 0 & 0 & 0 & 0 & 0 & 0 & 0 & 0 & -1 \\
1 & 0 & 0 & 0 & 0 & 0 & 0 & 0 & 0 & 0 & -1 \\
1 & -1 & 1 & -1 & 1 & 1 & 1 & -1 & 1 & -1 & -1 \\
1 & -1 & 1 & 1 & 1 & 1 & 1 & -1 & -1 & 1 & -1 \\
1 & -1 & -1 & -1 & 1 & 1 & 1 & 1 & 1 & 1 & -1 \\
1 & -1 & -1 & 1 & 1 & 1 & 1 & 1 & -1 & -1 & -1 \\
1 & 1 & 1 & -1 & 1 & 1 & 1 & 1 & -1 & -1 & -1 \\
1 & 1 & 1 & 1 & 1 & 1 & 1 & 1 & 1 & 1 & -1 \\
1 & 1 & -1 & -1 & 1 & 1 & 1 & -1 & -1 & 1 & -1 \\
1 & 1 & -1 & 1 & 1 & 1 & 1 & -1 & 1 & -1 & -1 \\
1 & 0 & 0 & -1 & 0 & 0 & 1 & 0 & 0 & 0 & 1 \\
1 & 0 & 0 & 1 & 0 & 0 & 1 & 0 & 0 & 0 & 1 \\
1 & 0 & -1.68 & 0 & 0 & 2.82 & 0 & 0 & 0 & 0 & 1 \\
1 & 0 & 1.68 & 0 & 0 & 2.82 & 0 & 0 & 0 & 0 & 1 \\
1 & -1 & 0 & 0 & 1 & 0 & 0 & 0 & 0 & 0 & 1 \\
1 & 1 & 0 & 0 & 1 & 0 & 0 & 0 & 0 & 0 & 1
\end{bmatrix}
\end{array}
$$

It can be determined that the $(\mathbf{X}^{\mathbf{T}}\mathbf{X})^{-1}$ is no longer a diagonal matrix as that of the 2^3 factorial design. For this case, the $(\mathbf{X}^{\mathbf{T}}\mathbf{X})^{-1}$ is

$$
(\mathbf{X}^{\mathbf{T}}\mathbf{X})^{-1} = \begin{bmatrix}
0.180 & 0 & 0 & 0 & -0.077 & -0.051 & -0.077 & 0 & 0 & 0 & 0.0020 \\
0 & 0.100 & 0 & 0 & 0 & 0 & 0 & 0 & 0 & 0 & 0 \\
0 & 0 & 0.073 & 0 & 0 & 0 & 0 & 0 & 0 & 0 & 0 \\
0 & 0 & 0 & 0.100 & 0 & 0 & 0 & 0 & 0 & 0 & 0 \\
-0.077 & 0 & 0 & 0 & 0.335 & -0.010 & -0.165 & 0 & 0 & 0 & 0.030 \\
-0.051 & 0 & 0 & 0 & -0.010 & 0.076 & -0.010 & 0 & 0 & 0 & -0.014 \\
-0.077 & 0 & 0 & 0 & -0.165 & -0.010 & 0.334 & 0 & 0 & 0 & 0.030 \\
0 & 0 & 0 & 0 & 0 & 0 & 0 & 0.125 & 0 & 0 & 0 \\
0 & 0 & 0 & 0 & 0 & 0 & 0 & 0 & 0.125 & 0 & 0 \\
0 & 0 & 0 & 0 & 0 & 0 & 0 & 0 & 0 & 0.125 & 0 \\
0.002 & 0 & 0 & 0 & 0.030 & -0.014 & 0.030 & 0 & 0 & 0 & 0.074
\end{bmatrix}
$$

Consequently, some of the parameter estimates will be correlated. The estimated correlation $\hat{\rho}(\hat{\beta}_i, \hat{\beta}_j)$ between $\hat{\beta}_i$ and $\hat{\beta}_j$ is

$$\hat{\rho}(\hat{\beta}_i, \hat{\beta}_j) = \frac{\text{Cov}(\hat{\beta}_i, \hat{\beta}_j)}{\left(\text{Var}(\hat{\beta}_i) \cdot \text{Var}(\hat{\beta}_j)\right)^{\frac{1}{2}}} \qquad \textbf{(A-I)}$$

But the estimated variance of $\hat{\beta}_i$ is $\hat{\sigma}^2 \cdot c_{ii}$ and the estimated covariance between $\hat{\beta}_i$ and $\hat{\beta}_j$ is $\hat{\sigma}^2 \cdot c_{ij}$. Thus,

$$\hat{\rho}(\hat{\beta}_i, \hat{\beta}_j) = \frac{\hat{\sigma}^2 c_{ij}}{(\hat{\sigma}^2 c_{ii} \hat{\sigma}^2 c_{jj})^{\frac{1}{2}}} = \frac{c_{ij}}{(c_{ii} c_{jj})^{\frac{1}{2}}} \qquad \textbf{(A-II)}$$

where c_{ii} and c_{ij} are the diagonal and off-diagonal element of the $(\mathbf{X}^T\mathbf{X})^{-1}$ matrix above, respectively. Based on equation **(A-II)**, the estimated correlation between the parameter estimates of the fitted models from the blocked central composite design can be determined.

In the case where the process response is COD removal efficiency, the result from one experimental run was excluded from the model fitting process. The $(\mathbf{X}^T\mathbf{X})^{-1}$ matrix for this case is

$$(\mathbf{X}^T\mathbf{X})^{-1} = \begin{bmatrix} 0.184 & -0.012 & 0.009 & 0.012 & -0.083 & -0.054 & -0.083 & 0.015 & 0.015 & -0.015 & 0.005 \\ -0.012 & 0.144 & -0.032 & -0.044 & 0.023 & 0.008 & 0.023 & -0.055 & -0.055 & 0.055 & -0.012 \\ 0.009 & -0.032 & 0.097 & 0.032 & -0.017 & -0.006 & -0.017 & 0.040 & 0.040 & -0.040 & 0.009 \\ 0.012 & -0.044 & 0.032 & 0.144 & -0.023 & -0.008 & -0.023 & 0.055 & 0.055 & -0.055 & 0.012 \\ -0.083 & 0.023 & -0.017 & -0.023 & 0.347 & -0.006 & -0.153 & -0.029 & -0.029 & 0.029 & 0.023 \\ -0.054 & 0.008 & -0.006 & -0.008 & -0.006 & 0.078 & -0.006 & -0.010 & -0.010 & 0.010 & -0.016 \\ -0.083 & 0.023 & -0.017 & -0.023 & -0.153 & -0.006 & 0.347 & -0.029 & -0.029 & 0.029 & 0.023 \\ 0.015 & -0.055 & 0.040 & 0.055 & -0.029 & -0.010 & -0.029 & 0.194 & 0.069 & -0.069 & 0.015 \\ 0.015 & -0.055 & 0.040 & 0.055 & -0.029 & -0.010 & -0.029 & 0.069 & 0.194 & -0.069 & 0.015 \\ -0.015 & 0.055 & -0.040 & -0.055 & 0.029 & 0.010 & 0.029 & -0.069 & -0.069 & 0.194 & -0.015 \\ 0.005 & -0.012 & 0.009 & 0.012 & 0.023 & -0.016 & 0.023 & 0.015 & 0.015 & -0.015 & 0.077 \end{bmatrix}$$

This $(\mathbf{X}^T\mathbf{X})^{-1}$ matrix indicated that all parameter estimates of the fitted model are correlated.

Appendix B Empirical Modeling for COD Removal

Model fitting the empirical model **21** for all COD removal results from the central composite design was carried out. Matrix calculations were performed using the software package, Maple 7. The Maple 7 generated results are as follows:

```
>restart;
>with(linalg):
>X:=matrix(18,10,[1,0,0,0,0,0,0,0,0,0,
>1,0,0,0,0,0,0,0,0,0,
>1,0,0,0,0,0,0,0,0,0,
>1,0,0,0,0,0,0,0,0,0,
>1,-1,1,-1,1,1,1,-1,1,-1,
>1,-1,1,1,1,1,1,-1,-1,1,
>1,-1,-1,-1,1,1,1,1,1,1,
>1,-1,-1,1,1,1,1,1,-1,-1,
>1,1,1,-1,1,1,1,1,-1,-1,
>1,1,1,1,1,1,1,1,1,1,
>1,1,-1,-1,1,1,1,-1,-1,1,
>1,1,-1,1,1,1,1,-1,1,-1,
>1,0,0,-1,0,0,1,0,0,0,
>1,0,0,1,0,0,1,0,0,0,
>1,0,1.68,0,0,2.8224,0,0,0,0,
>1,0,-1.68,0,0,2.8224,0,0,0,0,
>1,-1,0,0,1,0,0,0,0,0,
>1,1,0,0,1,0,0,0,0,0]);
```

$$X := \begin{bmatrix} 1 & 0 & 0 & 0 & 0 & 0 & 0 & 0 & 0 & 0 \\ 1 & 0 & 0 & 0 & 0 & 0 & 0 & 0 & 0 & 0 \\ 1 & 0 & 0 & 0 & 0 & 0 & 0 & 0 & 0 & 0 \\ 1 & 0 & 0 & 0 & 0 & 0 & 0 & 0 & 0 & 0 \\ 1 & -1 & 1 & -1 & 1 & 1 & 1 & -1 & 1 & -1 \\ 1 & -1 & 1 & 1 & 1 & 1 & 1 & -1 & -1 & 1 \\ 1 & -1 & -1 & -1 & 1 & 1 & 1 & 1 & 1 & 1 \\ 1 & -1 & -1 & 1 & 1 & 1 & 1 & 1 & -1 & -1 \\ 1 & 1 & 1 & -1 & 1 & 1 & 1 & 1 & -1 & -1 \\ 1 & 1 & 1 & 1 & 1 & 1 & 1 & 1 & 1 & 1 \\ 1 & 1 & -1 & -1 & 1 & 1 & 1 & -1 & -1 & 1 \\ 1 & 1 & -1 & 1 & 1 & 1 & 1 & -1 & 1 & -1 \\ 1 & 0 & 0 & -1 & 0 & 0 & 1 & 0 & 0 & 0 \\ 1 & 0 & 0 & 1 & 0 & 0 & 1 & 0 & 0 & 0 \\ 1 & 0 & 1.68 & 0 & 0 & 2.8224 & 0 & 0 & 0 & 0 \\ 1 & 0 & -1.68 & 0 & 0 & 2.8224 & 0 & 0 & 0 & 0 \\ 1 & -1 & 0 & 0 & 1 & 0 & 0 & 0 & 0 & 0 \\ 1 & 1 & 0 & 0 & 1 & 0 & 0 & 0 & 0 & 0 \end{bmatrix}$$

```
>Y:=matrix(18,1,[98.2743,98.4103,98.3869,98.4819,98.2782,98.0320,98.3174
,98.0505,98.6701,98.7184,82.0425,98.1998,98.0193,97.8809,98.0953,97.826
4,98.0534,98.3165]);
```

$$Y := \begin{bmatrix} 98.2743 \\ 98.4103 \\ 98.3869 \\ 98.4819 \\ 98.2782 \\ 98.0320 \\ 98.3174 \\ 98.0505 \\ 98.6701 \\ 98.7184 \\ 82.0425 \\ 98.1998 \\ 98.0193 \\ 97.8809 \\ 98.0953 \\ 97.8264 \\ 98.0534 \\ 98.3165 \end{bmatrix}$$

```
>XT:=transpose(X):
>XTX:=multiply(XT,X):
>invXTX:=inverse(XTX):
>XTY:=multiply(XT,Y):
>beta:=multiply(invXTX,XTY);
```

$$\beta := \begin{bmatrix} 98.65706792 \\ -1.478420000 \\ 1.285489857 \\ 1.555410000 \\ -.8689523 \\ -.296492263 \\ -1.1038023 \\ 2.150487500 \\ 2.089837500 \\ -2.011037500 \end{bmatrix}$$

```
>PE:=matrix(10,10,[0.007409,0,0,0,0,0,0,0,0,0,0.007409,0,0,0,0,0,0,0
,0,0,0.007409,0,0,0,0,0,0,0,0,0,0.007409,0,0,0,0,0,0,0,0,0,0.007409
,0,0,0,0,0,0,0,0,0,0.007409,0,0,0,0,0,0,0,0,0,0.007409,0,0,0,0,0,0,
0,0,0,0,0.007409,0,0,0,0,0,0,0,0,0,0.007409,0,0,0,0,0,0,0,0,0,0.007
409]):
>V(beta):=multiply(invXTX,PE);
```

$$V(\beta) := \begin{bmatrix} .001336351283 & 0. & 0. & 0. & -.0005744882988 & -.0003778404323 & -.0005744882988 & 0. & 0. & 0. \\ 0. & .0007409000000 & 0. & 0. & 0. & 0. & 0. & 0. & 0. & 0. \\ 0. & 0. & .0005429907364 & 0. & 0. & 0. & 0. & 0. & 0. & 0. \\ 0. & 0. & 0. & .0007409000000 & 0. & 0. & 0. & 0. & 0. & 0. \\ -.0005744882988 & 0. & 0. & 0. & .002392030040 & -.00003333221517 & -.001312469960 & 0. & 0. & 0. \\ -.0003778404323 & 0. & 0. & 0. & -.00003333221517 & .0005472980245 & -.00003333221517 & 0. & 0. & 0. \\ -.0005744882988 & 0. & 0. & 0. & -.001312469960 & -.00003333221517 & .002392030040 & 0. & 0. & 0. \\ 0. & 0. & 0. & 0. & 0. & 0. & 0. & .0009261250000 & 0. & 0. \\ 0. & 0. & 0. & 0. & 0. & 0. & 0. & 0. & .0009261250000 & 0. \\ 0. & 0. & 0. & 0. & 0. & 0. & 0. & 0. & 0. & .0009261250000 \end{bmatrix}$$

A 95% confidence interval for the true value of each parameter β_i was calculated as $\beta_i \pm t_{3,0.025} \times \sqrt{Var(\beta_i)}$, where $t_{3,0.025} = 3.182$. The result is

$$\beta_i \pm t_{3,0.025} \times \sqrt{Var(\beta_i)} = \begin{pmatrix} 98.66 \pm 0.12 \\ -1.48 \pm 0.09 \\ 1.29 \pm 0.07 \\ 1.56 \pm 0.09 \\ -0.87 \pm 0.16 \\ -0.30 \pm 0.07 \\ -1.10 \pm 0.16 \\ 2.15 \pm 0.10 \\ 2.09 \pm 0.10 \\ -2.01 \pm 0.10 \end{pmatrix}$$

All parameter estimates were retained and the total error SSR was

$$\text{SSR} = \sum_i (y_i - \hat{y}_i)^2 = 60.65 \text{ with } n - p = 8 \text{ degrees of freedom.}$$

and the pure error estimate was

$$\hat{\sigma}^2 = 0.0074 \text{ with } \nu_2 = m - 1 = 3 \text{ degrees of freedom.}$$

The lack of fit ratio is

$$R = \frac{\text{SSR} - \nu_2 \hat{\sigma}^2}{\nu_1 \hat{\sigma}^2} = 1637.$$

The model displayed lack of fit since $LFR >> F_{5,3,0.05} = 9.01$.

Appendix C Quantification of NP and NPnEO

NP and NPnEO were quantified based on HPLC analysis. NP analysis was based on an external standard method, whereby a series of dilutions of the standard was analyzed. Quantification of unknown NP amounts was based on the standard curve thus obtained. Routine analysis of standard samples indicated the NP peak shifted from time to time. In general, the retention time for the NP peak fell in the range of 5 – 6 minutes.

Peak identification for the different oligomers of NPnEO was based on results of Varineau and Charminski (1995). A chromatogram of Tergitol NP-4 standard is shown in Figure C–1. Peak area and identification are presented in Table C–1. Quantification of the various oligomer peaks was base on response factors reported by (Ahel and Giger, 1985) and the measured peak area for 100 mg/L NP standard. Good agreement between the calculated total concentration of all detectable peaks (4095 mg/L) to the concentration of the Tergitol NP-4 standard used (4080 mg/L) suggested that this quantification method was adequate.

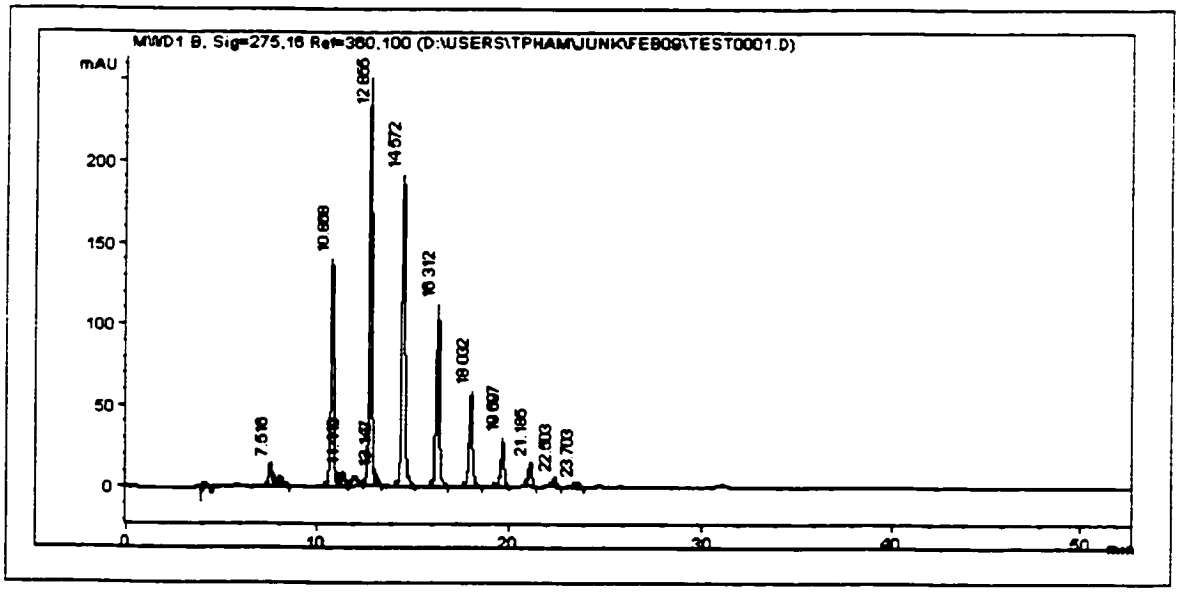

Figure C–1 HPLC chromatogram of 4080 mg/L Tergitol NP-4 standard sample.

Table C–1 Quantification of oligomer peaks for 4080 mg/L Tergitol NP-4 standard base on response factors reported by (Ahel and Giger, 1985).

Peak #	RT (min)	NPnEO n =	Peak Area (mAU*s)	Response Factor	Calculated Conc. (mg/L)
1	7.517	1	179.64	2.6	56.24
2	7.788	2	56.65	2.9	17.74
3	8.125	3	89.07	3.2	27.89
4	10.868	4	1597.61	3.5	557.85
5	11.250	5	77.02	4.0	26.89
6	11.449	6	95.77	4.2	33.44
7	12.051	7	153.65	4.6	53.65
8	12.855	8	2455.12	5.2	945.96
9	13.144	9	100.14	5.6	38.58
10	14.572	10	2121.29	5.9	893.97
11	16.312	11	1346.07	6.3	648.30
12	18.032	12	744.13	6.6	376.31
13	19.697	13	393.23	7.0	217.80
14	21.184	14	201.35	7.8	126.07
15	22.502	15	76.40	7.9	51.52
16	23.702	16	32.07	8.4	22.78
				Total:	4095.00

Appendix D Two-Tailed Paired-Sample *t* Test

Feed and effluent samples collected during the treatability study were analyzed for tolyltriazole content. A two-tailed paired-sample *t* test was carried out to determine whether differences between feed and effluent tolyltriazole concentrations were significant. For this test, the null hypothesis H_0: $\mu_d = 0$ is tested against the alternate hypothesis H_A: $\mu_d \neq 0$, where μ_d is the mean population difference.

The two-tailed paired-sample *t* test for the experimental data presented in Table 4–36 is as follows:

$n = 18$ $\qquad$ $\mathrm{DF} = n - 1 = 17$

$s_d^2 = \dfrac{\sum (d_i - \bar{d})^2}{n} = 0.00689$ $\qquad$ $\bar{d} = \dfrac{\sum d_i}{n} = -0.0329$

$s_{\bar{d}} = \dfrac{s_d}{\sqrt{n}} = 0.0196$ $\qquad$ $t = \dfrac{|\bar{d}|}{s_{\bar{d}}} = 1.68$

$t_{0.05(2),17} = 2.11$ $\qquad$ Do not reject H_0.

Where n is the number data points, DF is the degree of freedom, and d is the difference between feed and effluent tolyltriazole concentrations.

Appendix E Testing for Difference Among Regression Functions

Settling test results for the 23 run conditions in the treatability study were plotted. Linear regression equations were determined to describe the linear portion of the data sets. Based on these equations, upflow velocities resulting in 50% biomass washout (v_{50}) were interpolated. Differences among the 23 v_{50} values were determined by testing for differences among the slopes and elevations of the regression equations (Zar, 1999). The calculations required for this test are presented in Table E–1.

Table E–1 Calculations for test for difference among *k* linear regression equations (Zar, 1999).

	$\sum x^2$	$\sum xy$	$\sum y^2$	Residual SS	Residual DF
Regression 1 with n_1 data points	A_1	B_1	C_1	$SS_1 = C_1 - \frac{B_1^2}{A_1}$	$DF_1 = n_1 - 1$
Regression 2	A_2	B_2	C_2	$SS_2 = C_2 - \frac{B_2^2}{A_2}$	$DF_2 = n_2 - 1$
⋮	⋮	⋮	⋮	⋮	⋮
Regression *k*	A_k	B_k	C_k	$SS_k = C_k - \frac{B_k^2}{A_k}$	$DF_k = n_k - 1$
Pooled regression				$SS_p = \sum_{i=1}^{k} SS_i$	$DF_p = \sum (n - 2)$
Common Regression	$A_c = \sum_{i=1}^{k} A_i$	$B_c = \sum_{i=1}^{k} B_i$	$C_c = \sum_{i=1}^{k} C_i$	$SS_c = C_c - \frac{B_c^2}{A_c}$	$DF_c = \sum n - k - 1$
Total Regression	A_t	B_t	C_t	$SS_t = C_t - \frac{B_t^2}{A_t}$	$DF_t = \sum n - 2$

Test statistic for difference in slopes:

$$F = \frac{\left(\frac{SS_c - SS_p}{k-1}\right)}{\frac{SS_p}{DF_p}}$$

compared to $F_{0.05(1),k-1,DF_p}$

Test statistic for difference in elevations:

$$F = \frac{\left(\frac{SS_t - SS_c}{k-1}\right)}{\frac{SS_c}{DF_c}}$$

compared to $F_{0.05(1),k-1,DF_c}$

Appendix F The Tukey Test for Multiple Comparison Among Elevations

Multiple comparisons among elevations can be done when differences in slopes (performed as described in Appendix E) are not significant, but differences in elevations are significant. To determine between which elevations differences occurred, the Tukey test can be used, where the null hypothesis H_0: $\mu_A = \mu_B$ is tested against the alternate hypothesis H_A: $\mu_A \neq \mu_B$ for all possible pairs of elevations (Zar, 1999). For k elevations, there are $k\,(k-1)\,/\,2$ possible pairs. The null hypothesis is rejected if the probability (p) of committing a type I error where a true null hypothesis is falsely rejected is less than 0.05. The test statistic for the Tukey test with DF_p degrees of freedom (see Table E–1) is

$$q = \frac{\left|\left(\bar{Y}_A - \bar{Y}_B\right) - b_c\left(\bar{X}_A - \bar{X}_B\right)\right|}{SE}$$

where

$$b_c = \frac{\sum_{i=1}^{k}\left(\sum xy\right)_i}{\sum_{i=1}^{k}\left(\sum x^2\right)_i}$$

$$SE = \sqrt{\frac{\left(s^2_{Y\,X}\right)_c}{2}\left[\frac{1}{n_A} + \frac{1}{n_B} + \frac{\left(\bar{X}_A - \bar{X}_B\right)^2}{\left(\sum x^2\right)_A + \left(\sum x^2\right)_B}\right]}$$

Appendix G Analysis of Variance (ANOVA)

A single-factor ANOVA of the data presented in Tables 4–8 and 4–9 can be carried out. The null hypothesis being tested is H_0: $\mu_1 = \mu_2 = \cdots = \mu_k$, where k is the number of experimental groups or samples. The probability (p) of committing a type I error where a true null hypothesis is falsely rejected can be determined. The null hypothesis is rejected if $p < 0.05$. If H_0 is rejected, a Tukey test can be carried out to determine between which population means differences exist. Only comparisons involving controls were required since it was of interest to determine whether there is a significant difference between controls and test samples. A sample ANOVA for acetic acid consumption rates (see Table 4–8) is presented in Table G–1.

Table G–1 ANOVA and Tukey test for acetic acid consumption rates presented in Table 4–8.

Sample	Rate	dev	n	$s_i^2 = n(dev)^2$	$(n-1)s_i^2$	n(Rate)	$n(Rate)^2$	q
Control	-0.19	0.02	2	0.0005	0.0005	-0.3729	0.0695	-
0.5 DiMeBT	-0.15	0.01	2	0.0004	0.0004	-0.2912	0.0424	2.17
1.0 DiMeBT	-0.18	0.02	2	0.0007	0.0007	-0.3615	0.0654	0.30
1.5 DiMeBT	-0.17	0.02	2	0.0009	0.0009	-0.3491	0.0609	0.63
50 MeBT	-0.16	0.02	2	0.0006	0.0006	-0.3100	0.0481	1.67
100 MeBT	-0.18	0.02	2	0.0009	0.0009	-0.3536	0.0625	0.51
150 MeBT	-0.15	0.02	2	0.0005	0.0005	-0.3058	0.0468	1.79
50 BT	-0.15	0.02	2	0.0009	0.0009	-0.3027	0.0458	1.87
100 BT	-0.16	0.02	2	0.0006	0.0006	-0.3176	0.0504	1.47
150 BT	-0.14	0.01	2	0.0004	0.0004	-0.2859	0.0409	2.31
25 NP	-0.15	0.01	2	0.0004	0.0004	-0.2901	0.0421	2.20
50 NP	-0.12	0.01	2	0.0003	0.0003	-0.2346	0.0275	3.68
100 NP	-0.07	0.02	2	0.0006	0.0006	-0.1427	0.0102	6.13
50 NP-4	-0.18	0.02	2	0.0011	0.0011	-0.3629	0.0659	0.26
100 NP-4	-0.19	0.03	2	0.0019	0.0019	-0.3836	0.0736	0.29
300 NP-4	-0.18	0.02	2	0.0007	0.0007	-0.3594	0.0646	0.36

$$\text{error SS} = \sum_{i=1}^{k} (n_i - 1)s_i^2 = 0.0113 \qquad \text{groups SS} = \sum_{i=1}^{k} n_i \bar{X}_i^2 - \frac{\left(\sum_{i=1}^{k} n_i \bar{X}_i\right)^2}{\sum_{i=1}^{k} n_i} = 0.0278$$

$$\text{error DF} = \sum_{i=1}^{k} n_i - k = 16 \qquad \text{groups DF} = k - 1 = 15$$

$$F = \frac{(\text{groups SS} / \text{groups DF})}{(\text{error SS} / \text{error DF})} = 2.627 \qquad F_{0.05(1),15,16} = 2.352$$

Reject H_0 ($p = 0.0322$)

Tukey Test. H_0: $\mu_{\text{control}} = \mu_{\text{test}}$ where $q_{0.05,15,16} = 5.72$

$$\text{SE} = \sqrt{\frac{\text{error SS} / \text{error DF}}{n}} = 0.01878 \qquad q = \frac{(\bar{X}_{\text{control}} - \bar{X}_{\text{test}})}{\text{SE}}$$

$$q = \frac{(\bar{X}_{\text{control}} - \bar{X}_{100\,\text{NP}})}{\text{SE}} = 6.13 > q_{0.05,15,16} \qquad \text{Reject } H_0 : \mu_{\text{control}} = \mu_{100\,\text{NP}}$$

Appendix H Carbon Balance for EG Degradation

Table H–1 **Total carbon balance for test bottles during anaerobic degradation of EG at 35°C. Tests were done in duplicates.**

Test*	Total carbon (mM) at different sampling times											
	0 h	3 h	6 h	9 h	11 h	21 h	24 h	27 h	30 h	33 h	35 h	48 h
0.5 DiMeBT	101.6	80.9	61.6	53.8	46.6	23.8	20.0	16.8	14.6	10.4	9.5	1.7
Deviation	1.7	3.0	4.6	5.4	5.3	1.9	2.6	3.1	2.0	2.3	1.0	0.6
1.0 DiMeBT	98.6	80.5	63.6	52.2	46.2	24.5	18.4	15.9	13.6	9.8	7.9	1.1
Deviation	2.3	0.6	1.5	2.0	1.9	0.6	0.7	0.9	0.8	1.3	0.4	0.3
1.5 DiMeBT	103.0	82.8	65.9	56.1	49.3	27.0	22.1	19.5	16.5	12.7	11.0	2.6
Deviation	4.5	3.2	2.3	2.2	0.7	1.0	1.8	1.5	1.8	2.0	2.4	1.7
50 MeBT	103.2	78.7	60.9	54.5	47.0	22.5	20.6	18.5	15.9	10.9	9.0	2.2
Deviation	0.1	2.8	2.6	2.1	2.4	4.8	1.1	1.0	1.0	3.0	0.9	1.3
100 MeBT	101.5	75.0	58.5	50.1	40.3	24.9	19.7	17.5	14.7	10.7	8.6	1.7
Deviation	1.3	1.6	2.3	3.0	9.5	0.6	1.6	0.9	1.0	2.2	0.8	0.2
150 MeBT	102.3	76.3	58.7	54.4	48.0	27.7	21.7	19.0	17.9	13.2	10.1	3.3
Deviation	1.1	1.2	2.1	4.2	6.1	2.5	2.4	1.3	2.9	1.9	1.2	0.9
50 BT	106.8	80.3	61.2	53.2	47.7	25.4	19.7	17.6	14.7	11.3	9.3	2.0
Deviation	8.7	7.0	6.2	7.6	8.2	5.0	2.9	4.6	4.0	3.9	1.9	1.5
100 BT	105.1	79.9	61.6	56.1	46.4	21.1	19.9	15.5	12.8	8.0	8.0	0.6
Deviation	1.1	1.9	2.5	3.0	2.6	4.6	0.8	2.1	0.1	0.3	0.4	0.2
150 BT	101.4	78.4	61.1	53.4	44.9	19.3	17.3	14.8	12.0	9.1	7.7	1.0
Deviation	1.7	1.2	0.8	2.2	1.8	4.6	1.4	1.0	3.1	1.6	0.6	0.1
25 NP	103.3	83.6	66.3	55.4	44.8	21.2	21.2	18.7	17.0	11.7	12.3	2.9
Deviation	1.6	2.0	2.2	2.0	1.6	3.8	0.8	0.2	0.5	1.1	0.5	0.4
50 NP	104.6	81.0	64.3	54.5	45.4	25.1	22.8	19.8	18.4	13.9	13.8	6.1
Deviation	1.6	1.0	2.7	1.5	2.0	2.2	1.8	1.8	1.1	1.0	0.3	1.1
100 NP	102.3	80.8	66.0	53.6	45.8	25.7	25.0	22.8	20.9	17.4	16.7	14.5
Deviation	1.5	4.9	1.7	1.2	0.4	0.8	0.8	2.2	2.5	1.4	0.2	1.3
Control	101.8	82.8	68.0	54.4	42.7	21.3	17.5	14.8	10.4	7.5	7.1	0.5
Deviation	2.4	0.6	0.8	0.4	1.5	0.6	1.1	0.8	1.0	0.9	0.2	0.1
50 NP-4	101.9	84.6	68.8	55.7	44.1	23.8	20.3	15.4	13.6	10.2	8.9	0.8
Deviation	1.0	2.3	1.4	0.5	5.7	0.8	0.7	3.9	0.2	0.4	1.0	0.1
100 NP-4	100.0	79.5	64.9	53.2	44.0	22.2	18.7	14.9	11.6	9.2	7.8	0.5
Deviation	6.3	5.4	4.3	4.9	4.7	3.4	2.5	3.1	2.4	3.4	2.2	0.4
300 NP-4	103.2	83.1	67.5	55.3	46.4	24.7	21.7	17.2	14.1	11.4	10.6	1.7
Deviation	0.4	2.1	1.8	1.7	1.8	1.1	0.8	0.5	1.0	1.9	1.8	1.3

*Numbers represent concentration of the test chemical: e.g., 0.5 DiMeBT means 0.5 mg/L DiMeBT.

Appendix I Steady-state Data for ADF Treatment Study

A total of 23 experimental runs were conducted in bench-scale UASB reactors. Steady-state data for each experimental run is presented in Table I–1. After the completion of each steady state, the specific acetoclastic activity and settling velocity of the reactor biomass was determined and the results are presented in Table I–2.

Table I–1 Steady-state data for the 23 experimental runs conducted in bench-scale UASB reactors.

Run	Duration (d)	pH	Influent Total COD (g/L)	Flow Rate (L/d)	Effluent Total COD (mg/L)	Effluent Soluble COD (mg/L)	Effluent VSS[a] (mg/L)	CH_4 Produced (L/d)	Biogas CH_4 Content (%)	Biogas CO_2 Content (%)	Reactor Biomass (g VSS)	SRT (d)
1	11.0	7.48	9.2±0.2	4.1±0.1	250±44	170±19	307	14.7±0.4	63.4±2.2	34.7±2.3	203	58
2	9.8	7.49	9.1±0.2	4.0±0.1	260±60	161±39	111	14.3±0.5	62.2±0.9	36.0±0.4	203	55
3	9.8	7.50	9.0±0.2	3.9±0.2	281±79	164±40	86	13.5±0.5	62.7±0.7	35.8±0.7	203	47
4	9.8	7.50	9.1±0.2	3.6±0.3	255±54	155±40	130	13.2±1.0	62.0±1.4	35.9±0.5	203	57
5	9.9	7.53	6.2±0.3	2.7±0.1	139±40	106±19	166	6.5±0.2	64.3±1.5	33.0±0.5	101	144
6	9.9	7.54	6.2±0.3	3.0±0.1	183±43	121±14	126	6.5±0.2	64.7±0.8	33.9±0.3	203	173
7	11.0	7.53	6.3±0.3	5.8±0.5	157±22	105±28	139	13.4±0.9	63.6±0.4	34.6±0.4	103	70
8	10.8	7.50	6.2±0.3	5.9±0.2	198±40	119±19	182	15.3±0.5	63.9±0.7	34.3±0.5	203	94
9	10.1	7.46	11.4±0.5	2.9±0.1	259±22	151±13	137	12.9±0.4	61.7±0.3	36.4±0.3	117	147
10	10.1	7.45	11.4±0.5	3.1±0.1	238±60	143±13	129	12.5±0.3	62.0±0.3	36.5±0.3	234	141
11	5.0	7.21	11.3±0.4	6.0±0.1	2082±638	2032±616	83	19.9±2.2	59.3±7.5	38.9±7.7	119	76
12	10.1	7.43	11.4±0.5	6.1±0.1	318±31	204±12	127	29.4±0.8	61.6±0.4	37.0±0.4	237	100
13	13.1	7.40	8.4±0.6	4.3±0.3	280±84	164±34	245	12.4±0.8	59.2±0.8	38.8±0.4	107	60

Run	Duration (d)	pH	Influent Total COD (g/L)	Flow Rate (L/d)	Effluent Total COD (mg/L)	Effluent Soluble COD (mg/L)	Effluent VSS[a] (mg/L)	CH_4 Produced (L/d)	Biogas CH_4 Content (%)	Biogas CO_2 Content (%)	Reactor Biomass (g VSS)	SRT (d)
14	13.1	7.50	8.3±0.6	4.3±0.3	305±51	176±22	335	11.3±0.7	60.1±0.2	38.6±0.6	214	65
15	13.1	7.60	8.3±0.6	2.7±0.3	257±42	158±22	223	7.3±0.4	60.8±0.6	37.9±0.6	161	87
16	13.1	7.35	8.3±0.6	8.8±1.5	333±81	181±62	317	26.1±1.5	59.8±0.5	39.0±0.3	161	43
17	12.0	7.43	5.5±0.4	4.1±0.1	214±71	122±16	254	8.1±0.5	62.6±0.6	35.9±0.5	161	122
18	12.0	7.48	11.4±1.0	3.9±0.2	476±179	189±49	364	15.4±0.8	60.2±0.7	38.7±0.2	161	98
19	6.1	7.40	9.0±0.2	3.7±0.1	252±58	147±24	123	11.2±0.2	59.1±0.4	39.0±0.3	156	61
20	6.1	7.50	9.0±0.2	4.1±0.2	302±125	152±20	159	12.7±0.5	58.6±0.1	39.5±0.1	156	65
21	6.1	7.40	10.9±0.3	7.1±0.3	845±189	565±215	296	26.4±0.8	58.3±3.4	40.5±3.9	156	74
22	6.0	7.45	9.1±0.5	12.5±0.3	778±200	503±208	390	32.5±1.7	56.9±0.9	41.5±0.8	156	32
23	5.1	7.55	11.7±0.2	5.4±0.3	1160±565	466±147	1402	23.3±1.5	58.1±1.3	40.9±1.6	104	14

[a] VSS concentration was calculated as the total biomass weight divided by the total effluent volume for the run duration since day to day VSS concentration varied widely due to occasional washout of floating biomass.

Table I–2 **Specific acetoclastic activity for granular biomass after completion of an experimental run.**

Run	Design Conditions			Acetoclastic Activity[a] (g Ac/g VSS/d)
	ADF (%)	HRT (h)	[Biomass] (g VSS/L)	
1	1.2	36	27	0.42±0.02
2	1.2	36	27	0.40±0.02
3	1.2	36	27	0.43±0.02
4	1.2	36	27	0.42±0.01
5	0.8	48	18	0.46±0.01
6	0.8	48	36	0.44±0.03
7	0.8	24	18	0.55±0.03
8	0.8	24	36	0.50±0.02
9	1.6	48	18	0.41±0.01
10	1.6	48	36	0.42±0.02
11	1.6	24	18	0.39±0.01
12	1.6	24	36	0.38±0.01
13	1.2	36	18	0.28±0.02
14	1.2	36	36	0.35±0.01
15	1.2	56.1	27	0.34±0.02
16	1.2	15.8	27	0.34±0.01
17	0.8	36	27	0.46±0.01
18	1.6	36	27	0.35±0.02
19	1.2	36	27	0.25±0.01
20	1.2	36	27	0.23±0.01
21	1.6	20	27	0.24±0.01
22	1.2	12	27	0.31±0.03
23	1.6	24	18	0.28±0.01

[a] Specific acetoclastic activity determined at the end of each steady-state run.